FACULTE DES SCIENCES
Institut de Chimie thérapeutique
Groupe de Pharmacie galénique et Biopharmacie

Development of a hepatocyte hollow fiber bioreactor for the study of contrast agents by magnetic resonance imaging

THESE DE DOCTORAT

présentée à la
Faculté des Sciences de
l'Université de Lausanne

par

Corinne Planchamp Messeiller

Pharmacienne diplômée de la Confédération Hélvétique
Université de Lausanne

Jury

Prof. Giovanni Dietler, Président
Prof. Bernard Testa, Directeur de thèse
Prof. Luc Balant, Expert
Dr Sibylle Pochon, Expert
Dr Marianne Reist, Expert
Dr Jean-Paul Vallée, Expert

LAUSANNE
2002

Remerciements

Ce travail de thèse a été effectué de mars 1999 à octobre 2002, sous la direction du Docteur Joachim Mayer puis du Professeur Bernard Testa. Je tiens à remercier ici toutes celles et ceux qui ont collaboré à ce projet, ainsi que les personnes qui m'ont soutenues, d'une manière ou d'une autre, pendant ces années.

Je remercie le Docteur Joachim Mayer qui m'a accueillie dans son groupe. Je le remercie pour la confiance qu'il m'a accordée, pour tout ce qu'il m'a appris, pour ses encouragements, sa disponibilité et sa gentillesse. Il a suivi avec intérêt, pendant deux ans et demi de ma thèse, le développement de ce projet dont il était co-initiateur. Sa disparition tragique a laissé un grand vide. Merci à toutes celles et ceux qui m'ont aidée et soutenue dans ces moments difficiles.

J'exprime ma profonde gratitude au Professeur Bernard Testa qui a accepté de reprendre la direction de cette thèse et qui a fait en sorte que tout se passe au mieux pour sa continuation. En particulier, j'ai eu la chance de pouvoir profiter de ses conseils avisés pendant la phase de rédaction. Je lui adresse également mes chaleureux remerciements pour tout le soutien qu'il m'a témoigné lors de ce travail et pour mes projets futurs.

Un merci tout particulier au Docteur Marianne Reist qui a accepté de remplacer provisoirement le Docteur Joachim Mayer dans ses fonctions. Je la remercie pour l'intérêt qu'elle a porté à ce travail, pour sa grande compétence scientifique, sa disponibilité généreuse, son soutien et pour son amitié.

Je tiens à remercier également toutes les personnes du Département de Radiologie des Hôpitaux Universitaires de Genève qui ont participé activement à ce travail et qui m'ont accueillie chaleureusement dans leur groupe. Un grand merci au Professeur François Terrier pour avoir été à la base de ce projet avec Joachim et pour son grand enthousiasme communicatif. Merci au Docteur Jean-Paul Vallée pour son initiation à l'IRM, pour ses nombreuses idées, sa disponibilité. Je le remercie également d'avoir accepté de faire partie du jury. Un grand merci à Marko Ivancevic pour sa patience lors des longues soirées

d'acquisition de données et ses explications, ainsi que le Docteur Christophe Dornier pour les traitements d'image. Je joins à ces remerciements le Docteur Catherine Pastor, pour son aide, son soutien et son enthousiasme à toute épreuve.

Mes sincères remerciements au Professeur Luc Balant et à Marianne Gex-Fabry du Département de Psychiatrie des Hôpitaux Universitaires de Genève pour leur participation au projet. Je les remercie pour leur chaleureux accueil, leur générosité de temps et leurs compétences. Le savoir pharmacocinétique dont ils nous ont fait bénéficier a permis de donner une dimension supplémentaire à ce travail. Je remercie également Luc Balant d'avoir bien voulu faire partie du jury de cette thèse.

Mes remerciements vont également au Docteur Sibylle Pochon de Bracco Research S.A. pour avoir suivi le projet avec intérêt depuis le début, pour ses remarques et questions constructives et pour avoir bien voulu prendre la place de jury externe.

Merci au Professeur Giovanni Dietler de l'Université de Lausanne pour avoir accepté de présider le jury de thèse et d'y avoir participé activement.

Je remercie tous mes collègues du Groupe de Pharmacie galénique et Biopharmacie et de l'Institut de Chimie thérapeutique, en particulier Jean-Jacques Turban et Clotaire Ebring pour leur assistance technique, Gilles Boss pour ses conseils pratiques et pour son amitié, Sandrine pour ses recommandations, Pierre-Alain et Sébastien pour leurs compétences informatiques. Un merci tout particulier à Jérôme, fidèle compagnon d'étude puis de thèse, pour son amitié, son soutien, son humour et tous nos rires qui nous ont aidé à surmonter les moments difficiles.

Je ne saurais oublier ma famille, mes frères, mais surtout mes parents qui m'ont sans cesse encouragée et soutenue tout au long de mes études, en me laissant entièrement libre de mes choix. Enfin, une reconnaissance pleine de tendresse à Martial pour ses découragements de chaque instant.

A mes parents,

et à mes frères

A Martial

En souvenir de Joachim

Table of contents

Chapter 5: Development and validation of a hepatocyte hollow fiber bioreactor as a cellular model for the study of contrast agents by magnetic resonance imaging

Chapter 1
General introduction

1.1 Aim and scope of the thesis

Thanks to the continuous progress made in recent years, medical imaging has become an important tool in the diagnosis of various pathologies. In particular, magnetic resonance imaging (MRI) permits to obtain images with a remarkably high resolution without the use of ionizing radiation and is consequently widely applied for a broad range of conditions in all parts of the body.

Contrast agents are used in MRI to improve tissue discrimination. Different categories of contrast agents are clinically available, the most widely used being gadolinium chelates. One can distinguish between extracellular gadolinium chelates such as Gd-DTPA, and hepatobiliary gadolinium chelates such as Gd-BOPTA. The latter are able to enter hepatocytes from where they are partially excreted into the bile to an extent dependent on the contrast agent and animal species. Due to this property, hepatobiliary contrast agents are particularly interesting for the MRI of the liver. Actually, a change in signal intensity can result from a change in transport functions signaling the presence of impaired hepatocytes, e.g. in the case of focal (like cancer) or diffuse (like cirrhosis) liver diseases. Although the excretion mechanism into the bile is well known, the uptake mechanisms of hepatobiliary contrast agents into hepatocytes are still not completely understood and several hypotheses have been proposed. As a good knowledge of these transport mechanisms is required to allow an efficient diagnosis by MRI of the functional state of the liver, more fundamental research is needed and an efficient MRI compatible *in vitro* model would be an asset.

So far, most data concerning these transport mechanisms have been obtained by MRI with *in vivo* models or by a method of detection other than MRI with cellular or sub-cellular

models. Actually, no *in vitro* model is currently available for the study and quantification of contrast agents by MRI notably because high cellular densities are needed to allow detection, and no metallic devices can be used inside the magnet room, which is incompatible with most tissue or cell cultures that require controlled temperature and oxygenation.

The aim of this thesis is thus to develop an MRI compatible *in vitro* cellular model to study the transport of hepatobiliary contrast agents, in particular Gd-BOPTA, into hepatocytes directly by MRI. A better understanding of this transport and especially of its modification in case of hepatic disorder could permit in a second step to extrapolate this knowledge to humans and to use the kinetics of hepatobiliary contrast agents as a tool for the diagnosis of hepatic diseases.

1.2 Outline

This general introduction is followed by two theoretical chapters (chapters 2 and 3). The experimental work of this thesis is described in chapters 4 to 7 and finally, general conclusions are drawn and perspectives for future work are presented in chapter 8. Chapters 2, 5 and 7 are intended for publications.

Chapter 2 reviews the design, setup, validation and applications of the hepatocyte hollow fiber bioreactor (HFB). Special attention is paid on the culture conditions necessary to ensure a good cellular viability and functionality. This review also exposes the different tests that can be performed to control these parameters. Finally, the different uses of hepatocyte HFB are discussed, notably their use as a tool for the study of drug metabolism and transport.

Chapter 3 gives an overview of medical imaging, explains the principles of MRI and introduces the MRI contrast agents currently used, in particular for liver imaging. It intends to give the basic theory necessary for a good comprehension of the work described in this thesis. This chapter also reviews the present knowledge about the transporters known or suspected to play a role in the transport of MRI contrast agents in hepatocytes.

The isolation and preservation processes of rat hepatocytes are evaluated in chapter 4. A method to keep hepatocytes viable and functional for several hours is needed, as the MRI experiments cannot be performed immediately after hepatocyte isolation. The assessment of cryopreservation and cold preservation in the University of Wisconsin solution is described.

Chapter 5 is concerned with the development and validation of the MRI compatible hepatocyte HFB. A conventional HFB system, as described in chapter 2, is modified in order to be compatible with the magnetic field. This newly developed hepatocyte HFB is validated with an extracellular contrast agent, Gd-DTPA, and a hepatobiliary contrast agent, Gd-BOPTA, to check whether this cellular model can reveal a reproducible difference between the two types of contrast agents.

Three complementary studies performed to a) investigate the effect of contrast agent concentration on the MR signal, b) study a possible improvement of the MR signal analysis by the use of regions of interest or masks of the hollow fibers, and c) set up an additional in-line test for the evaluation of the viability of hepatocytes in the HFB, are reported in chapter 6.

Chapter 7 presents first the study of the expression of the receptors known or suspected to play a role in the transport of Gd-BOPTA in hepatocytes by Western blotting. The functionality of the transport mechanism assessed with an uptake study of Gd-BOPTA in freshly isolated rat hepatocytes in suspension is then described. Finally, the use of the MRI compatible hepatocyte HFB is extended to the study of the effect of Gd-BOPTA concentration on its uptake. A compartmental pharmacokinetic model is developed to describe the MRI data.

General conclusions on the work performed during this thesis are drawn and an outlook on further research is given in chapter 8. There follows a summary in English and French, a summary for the general public, and a list of the abbreviations currently used throughout this document.

Chapter 2
Hepatocyte hollow fiber bioreactors: design, setup, validation, and applications

2.1 Introduction

With its numerous different functions, the liver is one of the most important organs of the body. First, it plays a role in glucide metabolism, converting galactose and fructose to glucose which is particularly important for maintaining glycemia. Second, the liver is the main organ for lipid metabolism, being the major site of β-oxidation. It is also active in the metabolism of proteins, including urea formation to eliminate ammonia which is toxic for the central nervous system. Moreover, it has a secretory function, synthesizing bile acids for fat digestion and most of the plasma proteins like clotting factors and albumin. Finally, the liver plays also a key role in the metabolism of endogenous and exogenous substances in order to facilitate their excretion. These functions are carried out by the hepatocytes, epithelial cells that represent 80% of the liver volume. The remainder is constituted of at least four other types of cells, including endothelial cells, Kupffer cells, fat-storing cells and pit cells [1]. Methods routinely used to cultivate isolated hepatocytes include suspensions, adhesion on plates and more recently hollow fiber bioreactors (HFB).

HFB allow a dynamic three-dimensional mode of cell culture, which permits to restore a tissue-like cell density and interactions between cells, simulating physiological conditions. HFB have been used with different cell types to generate cell products like antibodies or hormones [2] and as artificial organs like bioartificial livers (BAL), pancreas, kidneys, and parathyroid glands [3]. In recent years, scientists have become increasingly interested in using hepatocyte HFB as a BAL to detoxify the blood of patients with acute liver failure (ALF).

The present chapter focuses on HFB as a liver model, i.e. containing primary hepatocytes or hepatocyte derived cell lines. It gives an overview of the different steps taking place in the setup of hepatocyte HFB and reviews notably drug metabolism studies performed with HFB. The aim is to provide the basic knowledge necessary to develop a hepatocyte HFB and to check its performance. First, generalities on HFB are exposed, including principles, transport phenomena, designs and cell culture conditions. Then, the tests which can be performed to assess the performance of the HFB, i.e. the viability and functionality of its cells, are discussed. Finally, possible uses of hepatocyte HFB are described. When reviewing the drug metabolism studies made with hepatocyte HFB, we have distinguished between metabolic studies performed to check hepatocyte viability and functionality in the HFB, and the studies pertaining to drug metabolism in the strict sense.

2.2 Principles and design of hepatocyte hollow fiber bioreactors

2.2.1 Principles

A HFB consists of a network of hollow fibers (HF) bundled together within a transparent plastic shell which defines two compartments, the extracapillary space (ECS) between the fibers and the plastic shell, and the intracapillary space (ICS) inside the fibers (figure 2.1). Although different kinds of HFB configurations exist, the principle of the perfusion system is similar for all of them. The basic system first described by Knazec et al. [4] comprises a culture medium reservoir, a pump, an oxygenation system and a HFB. It is a dynamic system where culture medium is continually pumped from a reservoir, charged with oxygen and carbon dioxide through silicone tubing, flows within the HF, diffuses radially through the semi-permeable membrane into the ECS and turns back to the reservoir. Under standard conditions, the entire system is placed in a 37°C CO_2 incubator.

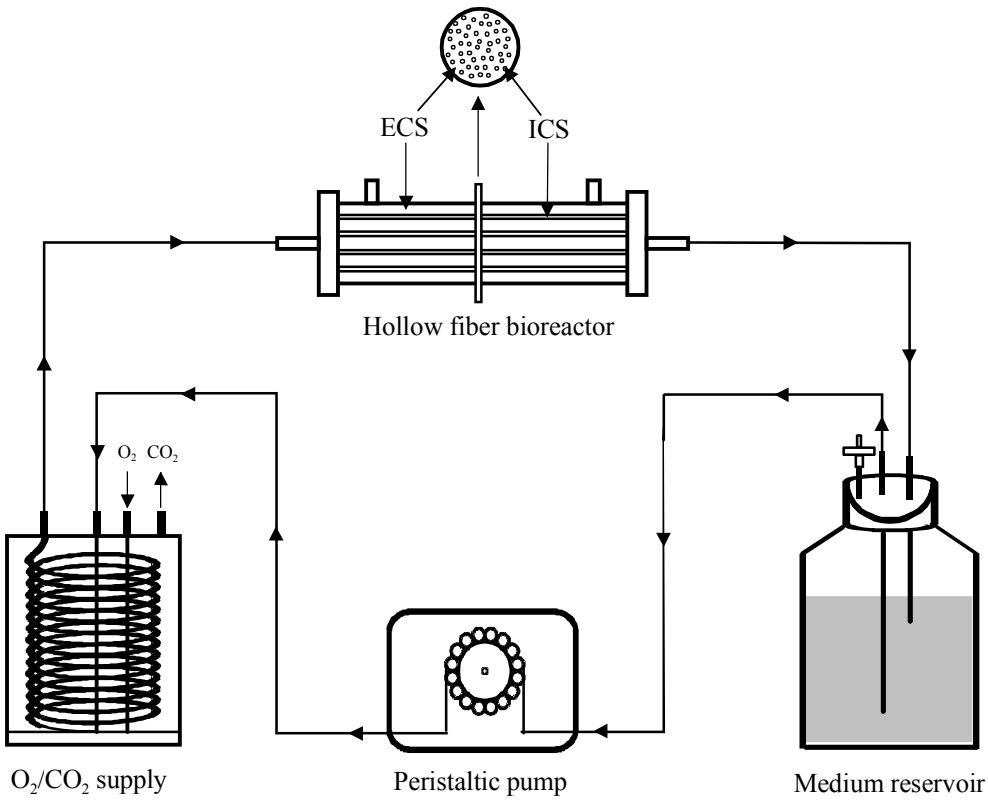

Figure 2.1: Schematic illustration of a hollow fiber bioreactor perfusion system. Culture medium is continually pumped from a reservoir, charged with oxygen and carbon dioxide, flows within the hollow fibers, diffuses radially through the semi-permeable membrane into the ECS and turns back to the reservoir. ECS: extracapillary space, ICS: intracapillary space.

Under these conditions the physiological environment is simulated and the HFB behaves like an organ. Indeed, HF act as blood vessels, with a culture medium oxygenated by an artificial lung (oxygenation system) replacing the blood, and the blood circulation is ensured by an artificial heart (pump).

2.2.2 Solute transport phenomena in hollow fiber bioreactors

Transport phenomena are of first importance since they affect directly cell viability and functionality and thus, the performance of the bioreactor. Fluid circulating within the HF brings oxygen and nutrients to cells and removes CO_2 and other waste products. Transport phenomena depend on the design of the HFB as on culture conditions.

In a HFB, one can distinguish at least three regions (figure 2.2): the medium (or blood/plasma in the case of BAL) compartment where culture medium (or blood/plasma) flows, the membrane compartment, and the cell compartment where cells are located [5]. In order to permit oxygen and nutrients to move from the culture medium to the cells, they must be transported:

- From the medium bulk to the medium-membrane interface. This occurs generally according to a diffusion-convection mechanism.
- Across the membrane wall. Mass transfer across semi-permeable membranes occurs by diffusion and/or convection in response to existing trans-membrane concentration or pressure gradients respectively. The porosity and the surface of the fibers, as well as the thickness of the membrane are important parameters which influence transport. Increasing pore size increases solute transport by both diffusion and convection, but also facilitates transport of immunogenic proteins in the case of BAL. Hence, membrane porosity is an important characteristic of HFB as it determines the size of the solutes able to cross the membrane.
- From the membrane surface through the cell mass. The presence of cells reduces solutes mobility in the cell compartment. Collagen or other extracellular matrix proteins often used to provide a substratum for cell attachment may also decrease solute mobility. Nyberg et al. [6] estimated the diffusion coefficient of oxygen in a collagen-hepatocyte gel being about 10% lower than that in water.

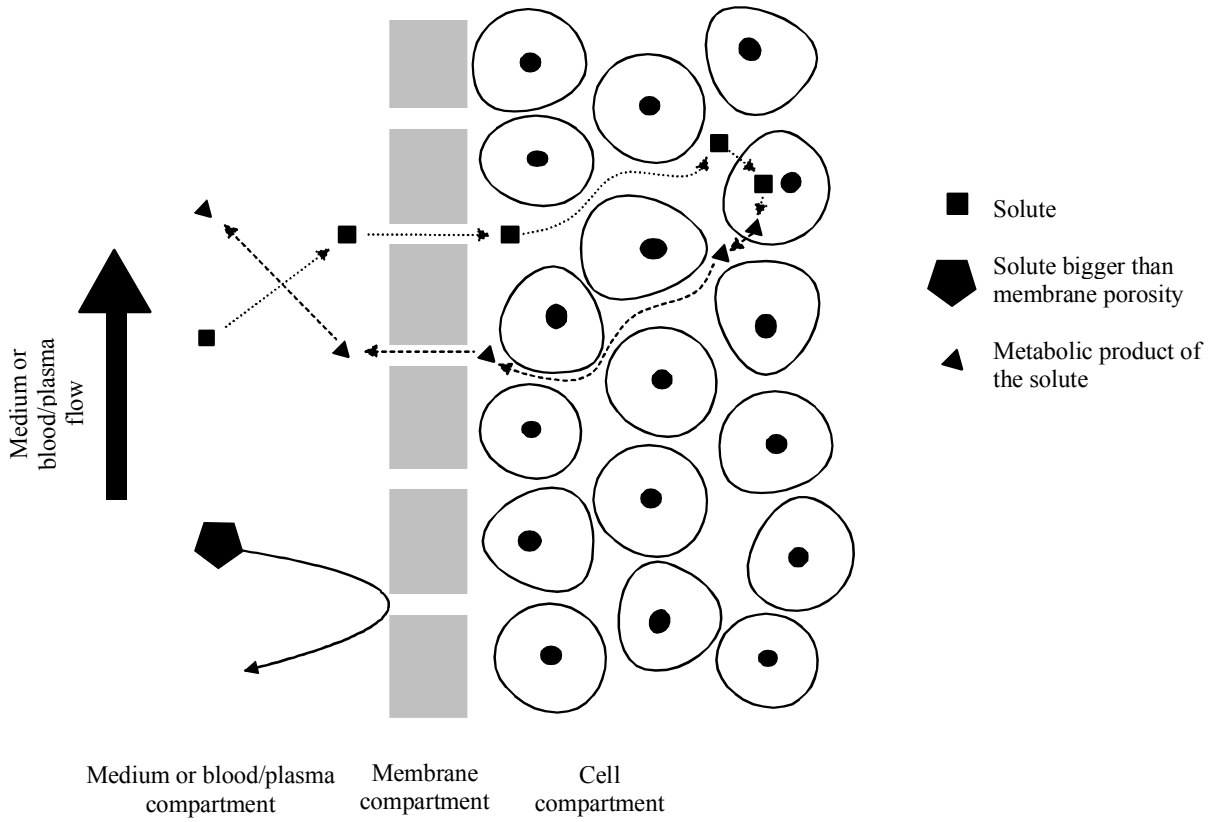

Figure 2.2: Illustration of mass transport phenomena in hollow fiber bioreactors (HFB). Membrane porosity is an important characteristic of HFB as it determines the size of the solutes able to cross the membrane.

In contrast to HFB, the transport in the liver is achieved primarily by convection along the sinusoid with a short diffusion distance (< 5 μm) across Disse space [7].

2.2.3 Designs of hollow fiber bioreactor

There are various configurations of HFB used for cell culture (figure 2.3). We distinguish here between single circuits where only the culture medium (or the blood/plasma in the case of BAL) is perfused through the HFB, and multiple circuits where two or more fluxes are present.

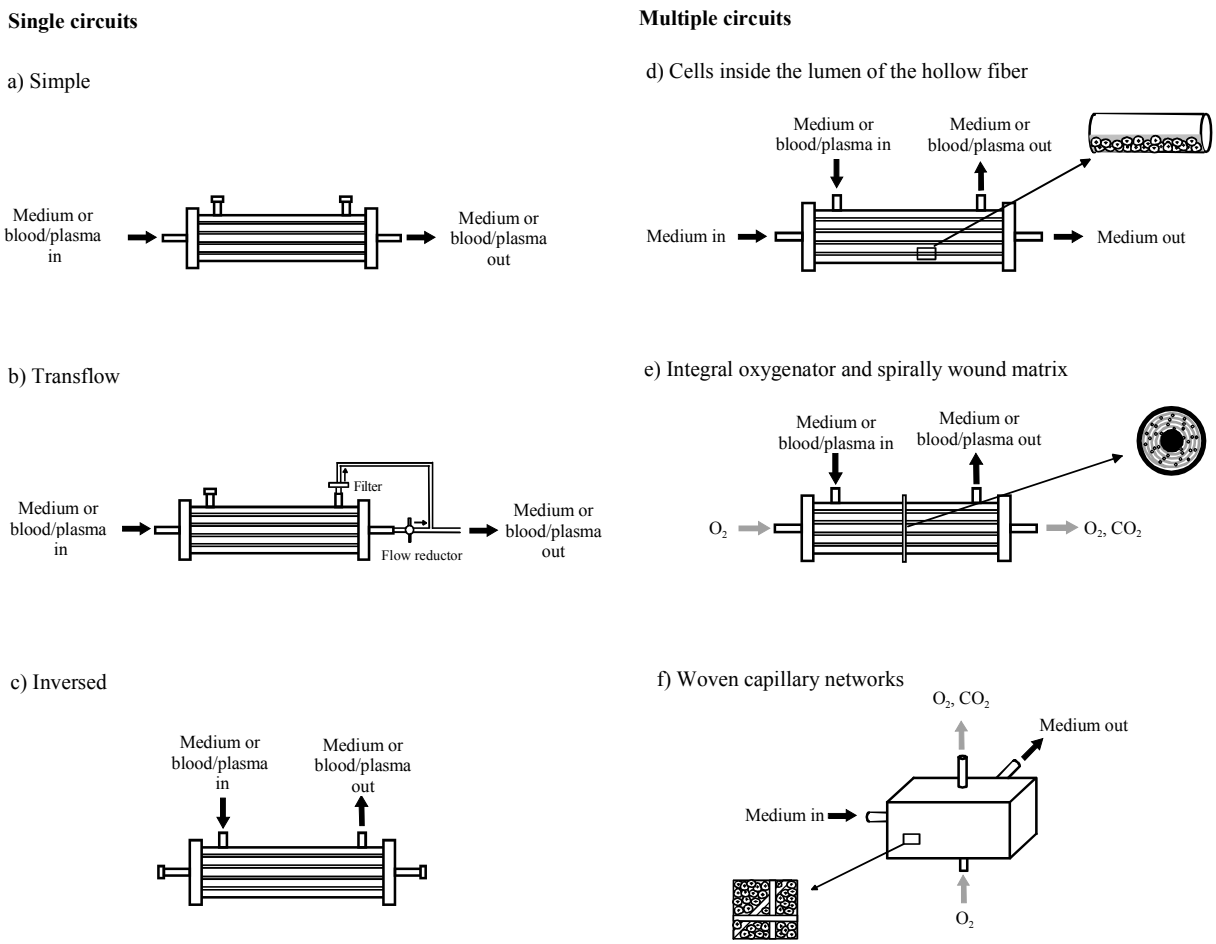

Figure 2.3: Current hepatocyte hollow fiber bioreactor (HFB) designs. In the single circuits, only the culture medium or the blood/plasma in the case of bioartificial livers is perfused through the HFB, while in multiple circuits two or more fluxes are present.

2.2.3.1 Single circuit systems

The simple mode (figure 2.3a) corresponds to the first model described by Knazek et al. [4]. Cells are cultivated outside the HF, while culture medium is perfused inside. It is the simplest and thus the most used system. In this model, the ECS pressure remains relatively constant along the length of the HFB, which is not the case for the ICS pressure. At the tube inlet, the ICS pressure is maintained above the ECS pressure. However, it decreases along the length of the HFB and can drop below the ECS pressure. Thus, while the initial convective trans-membrane flux is towards the ECS, it can be directed back into the ICS further down the axis [8]. Therefore, cells near the downstream section of the HFB can be under

nutrient-starvation conditions. This problem becomes more severe as the length of the HFB increases [2]. In the case of cell suspensions, this phenomenon may cause cells to be pushed and packed at the downstream end of the HFB [9].

To avoid the pressure drop along the HFB and thus the axial nutrient gradient, Rozga et al. [10] imagined a variant of the simple model (figure 2.3b). In his system the shell port downstream is open. Therefore, feed stream diffuses across the HF membrane and exits through the shell-side port. Unlike in the simple model, the tube-side pressure is always greater than the shell-side pressure but decreases linearly along the HFB. Thus, flow is always into the shell and solute appearance is faster than in the simple model [8]. A filter is set at the downstream side port to retain cells in the ECS.

Another single circuit has been described by Iwata et al. [11]. Compared to the simple model, the compartments are reversed, i.e. cells are cultivated in the ICS while the medium is perfused through the ECS (figure 2.3c). The advantage of this system is the short distance between the cells and the HF membrane. Consequently, even hepatocytes in the central part of the HF are well fed.

2.2.3.2 Multiple circuit systems

Unlike simple circuits, multiple circuit systems comprise more than one flux. Nyberg et al. [12-14] used a system where hepatocytes are entrapped in collagen gels inside the lumen of the HF. The medium circulates within the HF, over the gel-entrapped hepatocytes providing them with nutrients (figure 2.3d). A second flux, consisting of medium or blood/plasma in the case of BAL, flows in the ECS. The advantages of this design are the presence of a support for cell growth and the small diffusion distance for mass transfer of nutrients and waste products.

Flendrig et al. [15] built a HFB which delivers gases and liquid nutrients separately to the cells (figure 2.3e). It consists of a spirally wound non-woven polyester matrix which creates a three-dimensional framework for hepatocyte immobilization and aggregation, and of

integrated hydrophobic HF membranes for decentralized oxygen supply and CO_2 removal. Medium is perfused through the ECS and is therefore in direct contact with hepatocytes.

Gerlach et al. [16] used a HFB made of three discrete capillary systems, each serving a different purpose: one for plasma inflow, another for oxygenation and carbon dioxide removal, and the third for plasma outflow (figure 2.3f). The advantage of this system is the three-dimensional framework for decentralized cell perfusion with low metabolite gradients and decentralized oxygenation and CO_2 removal. Gerlach further improved the system by adding a fourth capillary system containing sinusoidal endothelial cells for co-culture [17].

2.3 Setup of hepatocyte hollow fiber bioreactors

2.3.1 Hepatocyte culture in hollow fiber bioreactors

Hepatocytes are anchorage-dependent epithelial cells which require a surface for attachment and proliferation. Recent advances in cell culture have evidenced the critical role of the microenvironment on cell activities. *In vivo*, cell microenvironment mainly consists of interactions between homotypic or heterotypic cells which affects the functional activity of cells and the cell shape and polarity [18]. The main progresses recently made in hepatocyte culture have been to define *in vitro* conditions which mimic *in vivo* situations. Schematically, three major strategies can be used: 1) providing hepatocytes with one of the several components that form the hepatic extracellular matrix (a complex mixture of collagens, non-collagenous proteins and carbohydrates) 2) using cell-cell contacts between hepatocytes 3) restoring cell-cell communications of hepatocytes with other liver cell types in co-culture.

In the case of HFB, several tools have been used to provide an attachment surface to the hepatocytes, including HF surface coating, attachment to microcarriers, and gel embedding. Figure 2.4 illustrates examples of hepatocyte culture in HFB.

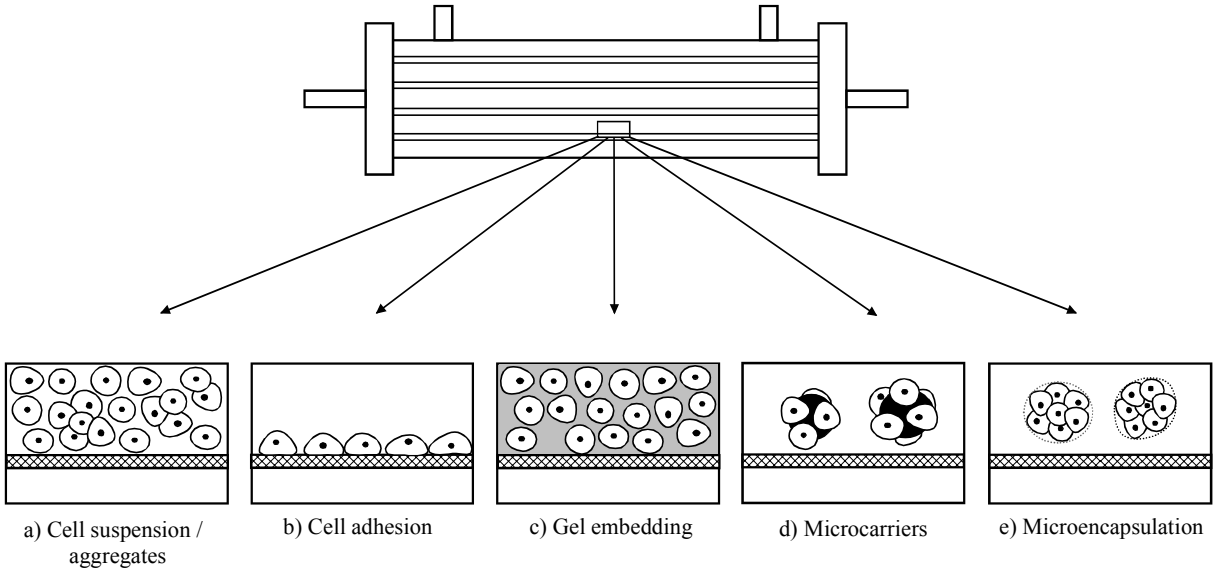

Figure 2.4: Hepatocyte culture in hollow fiber bioreactors (HFB). While the hepatocytes are simply loaded in the HFB in the case of suspensions, an attachment surface is present in the case of cell adhesion, gel embedding, microcarriers and microencapsulation.

2.3.1.1 Suspension of freshly isolated hepatocytes

Suspensions of freshly isolated hepatocytes (figure 2.4a) represent a quick, simple and reproducible manner of preparing a HFB. Furthermore, they permit to incorporate a large number of cells in a HFB, leading to an important cellular density. Suspensions have the advantage of representing a homogenous hepatocyte population with a cellular activity and function comparable to those present *in vivo*. Hepatocytes remain able to metabolize many compounds by phase I and II enzymes [19].

However, since hepatocytes are anchorage-dependent cells, their viability and functionality in suspension are limited to a few hours after their isolation, thus restricting extended experiments [20]. Prolonged survey of hepatocytes is only possible if they are maintained in culture attached to a support. Modification of the membrane architecture due to the isolation process is another disadvantage of freshly isolated hepatocytes in suspension. Cells loose their polarity, and structural and functional alterations can appear at the level of each

hepatocyte [21]. This has to be taken into account when such preparations are used as models of hepatic transport.

Nevertheless, an interesting aspect is that hepatocytes seem to spontaneously form aggregates when cultured at high density in suspension in bioreactors [15,16], restoring cell-cell interactions, leading to a better functionality and viability. Iwata et al. [11] prepared a BAL system by simply inoculating a porcine hepatocyte suspension into the ICS, medium being perfused through the ECS. They observed that hepatocytes formed aggregates spontaneously during perfusion, and exhibited tight cell-cell contact characteristics.

2.3.1.2 Adhesion on artificial membranes

As already discussed, the HF membrane separates cells from the perfusion medium. Its second role is to provide an attachment surface to hepatocytes (figure 2.4b), which improves their activity and viability. Hepatocytes are allowed to attach directly on the membrane or on a coated surface [22,23]. Immobilization and growth depend on the nature of the membrane as on the coating components. Substances often used to coat HF membranes include soluble basement membrane extracts (Matrigel®) [17], collagen (Vitrogen®) [24] and fibronectin [25].

Membranes with different chemical and physical properties have been used. Qiang et al. [26], compared growth and function of a human hepatoma cell line on six different membranes. Four of them were cellulose-based membranes, Cuprophan, Hemophan, Cellulose acetate, and Bioflux, two were synthetic polymers (SPAN and polysulphone). Polysulphone, SPAN and Hemophan appeared to be ideal membranes for hepatoma cells anchorage, while cells attached to cellulose acetate membrane to a lesser extend and failed to attach to Cuprophan and Bioflux. The cellular integrity was largely dependent on its attachment to the membrane, the best results being obtained with polysulphon. The intrinsic structure of membranes contributes highly to the differential behavior of hepatocytes on membranes. Although the precise mechanism of cellular attachment has not been elucidated, the importance of an electrically polar surface is recognized. Hemophan and cellulose actetate

are positively charged; polysulphone and SPAN are negatively charged. The unmodified cellulose membranes, Cuprophan and Bioflux remain electrically neutral. These results confirm that membranes that have hydrophilic groups on their surface enhance cell growth and functionality. A disadvantage of this mode of culture in HFB is the low cellular density achievable, as all hepatocytes have to be attached to the fiber membrane.

2.3.1.3 Gel embedding

Gel embedding of hepatocytes is represented in figure 2.4c. The gel matrix increases the surface area for cell support, yielding better cell viability and functionality. Hepatocytes can be entrapped in a collagen gel and cultured in the ECS [27,28] or in the ICS [12-14] of the bioreactor (figure 2.3d). Hepatocyte embedding in a collagen I gel at a concentration of about 0.2% is often used. A disadvantage of this design is that a steep concentration gradient of nutrients and oxygen may occur through the gel depth, resulting in either cell starvation or accumulation of toxic metabolites near the cells [5].

2.3.1.4 Microcarriers

Microcarriers (figure 2.4d) are artificial spherical bodies made from different materials including dextran, polystyrene, biologically modified polyhydroxymethylmethacrylate (poly-HEMA) or glass. Compared to membrane adhesion, microcarriers provide an increased surface area available for hepatocyte adhesion, increasing the cell density achievable in the HFB. Like HF membranes, microcarriers can be coated with different substances like chitosan [29], collagen [10,30-33] or fibronectin [34].

Dixit et al. [25] developed microcarriers with biologically modified poly-HEMA which yielded a higher hepatocyte immobilization than collagen-coated dextran microcarriers. Moreover, newly developed multiporous cellulose microcarriers are able to contain cells in their pores and may be more suitable than dextran microcarriers as a matrix for long-term, high-density culture of isolated hepatocytes [35]. The biopolymer chitosan is a suitable scaffold for the attachment of hepatocytes, because of its nontoxic and biocompatible nature

and its structure similar to that of glycosaminoglycans which are components of the liver extracellular matrix [36].

Furthermore, microcarriers are used to cryopreserve hepatocytes for the further preparation of the HepatAssist BAL (see §2.5.2), as microcarrier-attached hepatocytes are known to retain a good viability and functionality after thawing. Hepatocytes attached to collagen-coated dextran microcarriers have also been intraperitoneally injected into rats to treat liver insufficiency [37].

2.3.1.5 Microencapsulation

An example of microencapsulation is shown in figure 2.4e. Hepatocytes entrapped within a gel matrix of calcium alginate maintain their functionality *in vitro* [38-40], but difficulty has been experienced in terms of the permeability through the gel matrix of high-molecular weight substances such as secreted plasma proteins, although Tompkins et al. [41] showed that transport limitations do not occur in alginate droplets. In the case of BAL, encapsulation also permits to immunoisolate hepatocytes. As with microcarriers, hepatocytes retain their functional activity and metabolic capacity after cryopreservation in alginate droplets [42].

2.3.1.6 Co-culture

Co-culture means that two or more cell types are cultured together, resulting in a cell behavior and physiological responses which would not occur if the cell types were cultured alone. In the case of hepatocytes, co-culture with fibroblasts [43], endothelial cells [44] or with another epithelial cell type [45] improved hepatocytes functionality and life span in culture.

This technique has been applied notably by Gerlach et al. [17] who used a bioreactor made of four capillary systems, one being loaded with liver endothelial cells while the hepatocytes were cultured in the ECS.

2.3.2 Conditions of hollow fiber bioreactor culture

2.3.2.1 Culture medium

Optimization of the culture medium composition contributes to the long term maintenance of cell viability and functionality. Most authors use complete media containing amino acids and vitamins in addition to salts. The most common complete medium for hepatocytes culture is Williams'E medium [46], but media as Chee's essential medium [24] and Dubelcco's [31,47] are also cited. Simple balanced salt solutions (BSS) can be used such as Dubelcco's phosphate buffer saline or Hank's BSS. When performing metabolic studies, one should be aware that the more constituents in the culture media the higher the risks of interactions. Albumin or serum, growth factors and antibiotics are often included in the medium. In the case of BAL, medium is replaced by the patients or animals plasma or blood, although some authors keep in addition a culture medium stream flow to provide hepatocytes with specific nutrients and to eliminate hepatocyte waste products.

The presence of a carbonate buffer in the medium and 5% CO_2 in the incubator atmosphere ensures a pH around 7.4. If the CO_2 concentration in the gas phase increases, HEPES can be added to the medium to better stabilize the pH around 7.4. According to the human plasma osmolality, media osmotic pressure is usually set at 290 mOsm/kg. Slightly hypotonic media are sometimes used to compensate evaporation during long experiments. Upon exposure to anisotonic conditions most cells, including hepatocytes, initially change their volume according to the tonicity of the extracellular compartment [48]. In a second step, they are capable to actively restore their volume despite continuous hypotonic or hypertonic challenge, which is called regulatory volume decrease and regulatory volume increase, respectively.

2.3.2.2 Oxygenation

Special attention must be paid to optimal oxygenation of cells, since oxygen plays a key role in hepatocyte attachment and function [15]. Anoxia results in a gradual increase in

plasma membrane permeability, leading to the initiation of cell death. The capacity to supply the culture with oxygen is severely limited by the low solubility of oxygen in the medium (0.2 mmol O_2/liter at 37°C) and by the very high specific oxygen consumption rate of hepatocytes [2]. For this reason, oxygen is used as the limiting substrate in models of metabolite transport in HFB [49-51]. At high cell densities and low oxygen tensions, cells may change from aerobic metabolism to anaerobic glycolysis [2]. Macdonald et al. [52] determined in an MRI investigation that a diffusion distance between 200-500 μm is necessary to keep hepatocytes viable in a simple circuit bioreactor.

The first HFB oxygenation system described by Knazec et al. [4] consisted of silicone tubing through which O_2 and CO_2 (5% CO_2 in air) diffuse readily from the incubator atmosphere to the solution flowing inside the tubing. This oxygenation system is called indirect oxygenation as it is placed in series in the HFB system, oxygenating the circulating medium. On the other hand, the term of direct oxygenation is employed when the oxygenation system is included directly in the bioreactor. The later is the method used by Gerlach et al. [16,17,53] who found that during the first 24 hours of culture, hepatocytes in HFB reduced the ammonia content in the medium in the same range with direct and indirect oxygenation but that in longer term cultures the direct method resulted in enhanced cell metabolism. The composition of the feeding gas also influences the oxygen consumption. It was shown that the oxygen consumption rose with increasing oxygen tension [54].

2.3.2.3 Flow rate

High flow rates are often used to enhance in particular the amount of dissolved oxygen delivered to hepatocytes. Actually, the rate of solute appearance in the ECS is a function of the flow rate [8,10] and as oxygen is crucial for the maintenance of hepatocyte viability, its diffusion is much more critical than diffusion of other nutrients [55]. However, high flow rates are generally reluctantly selected because they increase hepatocyte shear stress and can cause an axial concentration gradient of cellular viability in spatial distribution.

2.3.2.4 Cellular density

The optimal hepatocyte density is the maximal one which permits to supply each cell with sufficient nutrients, including glucose and oxygen. It is reflected by the performances of the hepatocyte HFB: increasing cell mass must not alter cell functionality and viability. The optimal cellular density depends mainly on the HFB dimensions and on the mode of cell culture chosen. Actually, for cell suspensions, a tightly packed fiber bundle will support a high local density in the space between fibers, but the volume available for cells is reduced. Conversely, a large fiber spacing will afford a large volume for cells at a lower local density. Chresand et al. [50] proposed an equation to determine the maximal cell density achievable with a definite HFB based on nutrients consumption, oxygen being the limiting substrate, and on the HFB characteristics, i.e. the bioreactor and fiber dimensions, and the number of fibers.

Gerlach et al. [16] observed a different behavior of primary hepatocytes depending on their density in the HFB. When hepatocytes are seeded at low density between the HF, they adhere to the membrane surface and flatten. If they are seeded at high cellular densities, they attach to the membrane surface and additionally form aggregates in the ECS.

2.4 Validation of hepatocyte hollow fiber bioreactors

The validation of a HFB after its setup by checking its ability to sustain a good cellular viability and functionality is an important step, as the performances of the HFB directly depend on these factors. Most cellular viability tests rely on direct coloration of cells with dye (e.g. trypan blue, fluorescein). But such kind of tests cannot monitor cellular viability during HFB experiments as HFB are closed systems, impeding cell sampling. Consequently, other tests have to be used to quantify hepatocyte viability in HFB, as for example dosage of enzymes released, or evaluation of complex synthetic and metabolic activities.

For the validation procedure of HFB, we distinguish here between the evaluation of oxygen consumption and dosage of endogenous substances (e.g. enzymes, proteins), and the assessment of the metabolism of drugs and endogenous compounds.

2.4.1 Evaluation of the oxygen consumption and dosage of endogenous compounds

Oxygen consumption is currently used to assess cellular viability as it reflects the biochemical state of the cellular population. The consumption of insulin, which is sometimes added to the medium, is an indirect measure of hepatocytes growth as it stimulates hepatocytes proliferation. Dosage of liver specific proteins (e.g. albumin, fibrinogen, haptoglobin, creatinin, transferrin) reflects the synthetic capacity of hepatocytes associated with the preservation of a transcriptional activity.

Measurement of the specific release of intracellular enzymes (LDH, AST, ALT, GPT, GLDH, GGT and transaminases) due to membrane leakage acts as a criterion of cellular integrity. Some amino acids are sometimes dosed because they have long been suspected to be involved in hepatic encephalopathy, although their exact role has not been defined clearly [33].

2.4.2 Study of the metabolism of drugs and endogenous compounds

The term metabolism includes all the chemical reactions which modify molecules inside the body. It consists of the degradation or formation of complex substances and the use of nutrients to produce energy [56]. It includes also the modification of molecules to render them more hydrophilic to facilitate their elimination mainly through the kidneys which affects endogenous compounds and drugs. These reactions can be separated into phase I and phase II reactions. Phase I reactions involve the creation or modification of functional groups in a substrate molecule (i.e. oxidation, reduction and hydrolysis). Thus, phase I processes are often designated as functionalization reactions. In contrast, phase II reactions involve the

conjugation of an endogenous molecule or fragment to the substrate, yielding a metabolite known as a conjugate. Thus, phase II processes are often called conjugation reactions [57].

Table 2.1 presents different substances currently studied in hepatocyte HFB, either for the validation of the HFB or for the investigation of their metabolism.

2.4.2.1 Metabolic studies of endogenous compounds

The lactate/pyruvate ratio is an index of the functional state of cellular oxidation and aerobic metabolism [15]. Like oxygen consumption, the glucose depletion in the medium is an indicator of the biochemical state of the cells. The galactose elimination capacity has been used in clinical diagnosis as an indication of functional liver cell mass. In fact, galactose has first to enter cells by a carrier-mediated transport process, where it is then converted to glucose almost exclusively in the liver by enzymes involving galactokinase and uridyltransferase.

Ammonia elimination is a relevant metabolic reaction for BAL performance test as ammonia is one of the neurotoxic species related to hepatic encephalopathy [58]. Ammonia is detoxified by ureagenesis showing that hepatocytes retain the enzymes of the urea cycle. For *in vitro* tests, ammoniac elimination and urea synthesis are evaluated after administration of NH_4Cl. In the case of BAL tested with animals or humans, ammonia is naturally present in the blood as it results from the proteins degradation.

Bilirubin uptake, conjugation and excretion is a complex hepatic function [59]. Free bilirubin is conjugated with glucuronic acid by the hepatic enzyme uridine diphosphate-glucuronyltransferase, making it water soluble and thus excretable into the bile as the mono- and diglucuronide. It is an endogenous marker of phase II reactions. Finally, cytidine deamination to uridine by the enzyme cytidine deaminase indicates the functionality of cytosine arabinoside metabolism [22].

Table 2.1: Metabolic reaction, marker and analytical method of substances currently studied in hepatocyte hollow fiber bioreactors.

	Reaction	Marker	Analytical method	Reference
Endogenous compounds				
Ammonia	Ureagenesis	Ammonia	HPLC/UV	[12,60]
	Ureagenesis	Urea	UV	[15,22,61]
	Ureagenesis	Urea	HPLC/UV	[12]
Bilirubin	Glucuronidation	Mono- and di-glucuronide	HPLC/UV	[30]
Cytidine	Deamination	^{14}C-uridine	Radioactivity	[22]
Galactose	Conversion to glucose	Galactose	UV	[15,17,62]
Glucose	Glycolysis and gluconeogenesis	Glucose	Test strips	[15]
Exogenous compounds				
Diazepam	Oxidation	Diazepam	HPLC/UV	[24,54]
	Oxidation	Diazepam	Gaz-liquid chromatography	[22]
	Hydroxylation	Temazepam	HPLC/UV	[24,54]
	N-Demethylation	Nordiazepam	HPLC/UV	[24,54]
	Hydroxylation+N-demethylation	Oxazepam	HPLC/UV	[24,54]
Lidocaine	Oxidation	Lidocaine	GC	[29]
	Oxidation	Lidocaine	HPLC/UV	[11,12,15]
	Oxidation	Lidocaine	Immunoassays	[17,63]
	Oxidation	Lidocaine	Fluorescence polarization	[64]
	N-Dealkylation	MEGX	HPLC/UV	[11,12,15]
	N-Dealkylation	MEGX	Immunoassays	[17,63,65]
	N-Dealkylation	MEGX	Fluorescence polarization	[64]
	N-Dealkylation	GX	HPLC/UV	[12,15]
	Amide hydrolysis	Xylidine	HPLC/UV	[15]
	Hydroxylation	3-OH-Lidocaine	HPLC/UV	[12,65]
	N-Dealkylation + hydroxylation	3-OH-MEGX	HPLC/UV	[12]
Midazolam	Oxidation	Midazolam	Immunoassays	[17]
Cyclosporine	Hydroxylation	First-generation monohydroxylation products	HPLC/UV	[10]
	N-Demethylation	First-generation N-demethylation products	HPLC/UV	[10]
19-nortestosterone	Conjugation	19-Nortestosterone	GC/MS	[10]
	Isomerisation	19-Noreticholanolone	GC/MS	[10]
	Isomerisation	19-Norepiandrosterone	GC/MS	
PSP	Glucuronidation	PSP-glucuronide	UV	[24]
19-nortestosterone	Glucuronidation	19-Nortestosterone glucuronide	GC/MS	[10]
4-MU	Conjugation	4-MU	HPLC/UV	[12]
	Glucuronidation	MUG	HPLC/UV	[12]
	Sulfation	MUS	HPLC/UV	[12]

MEGX: monoethylglycinexylidide, GX: glycinexylidide, PSP: phenolsulfonphthalein, 4-MU: 4-methylumbelliferone, MUG: 4-methylumbelliferone glucuronide, MUS: 4-methylumbelliferone sulfate

2.4.2.2 Metabolic studies of drugs

Diazepam, an anxiolytic drug, and lidocaine, a local anesthetic and antiarrhythmic drug, are the most frequently used substrates to evaluate the metabolic function of hepatocytes. Their total metabolic activity reflects the status of the P450 pathway, indicating that hepatocytes have the capacity for oxidation and/or reduction of drugs. They can be considered as phase I markers. The scheme of diazepam metabolism is represented in figure 2.5.

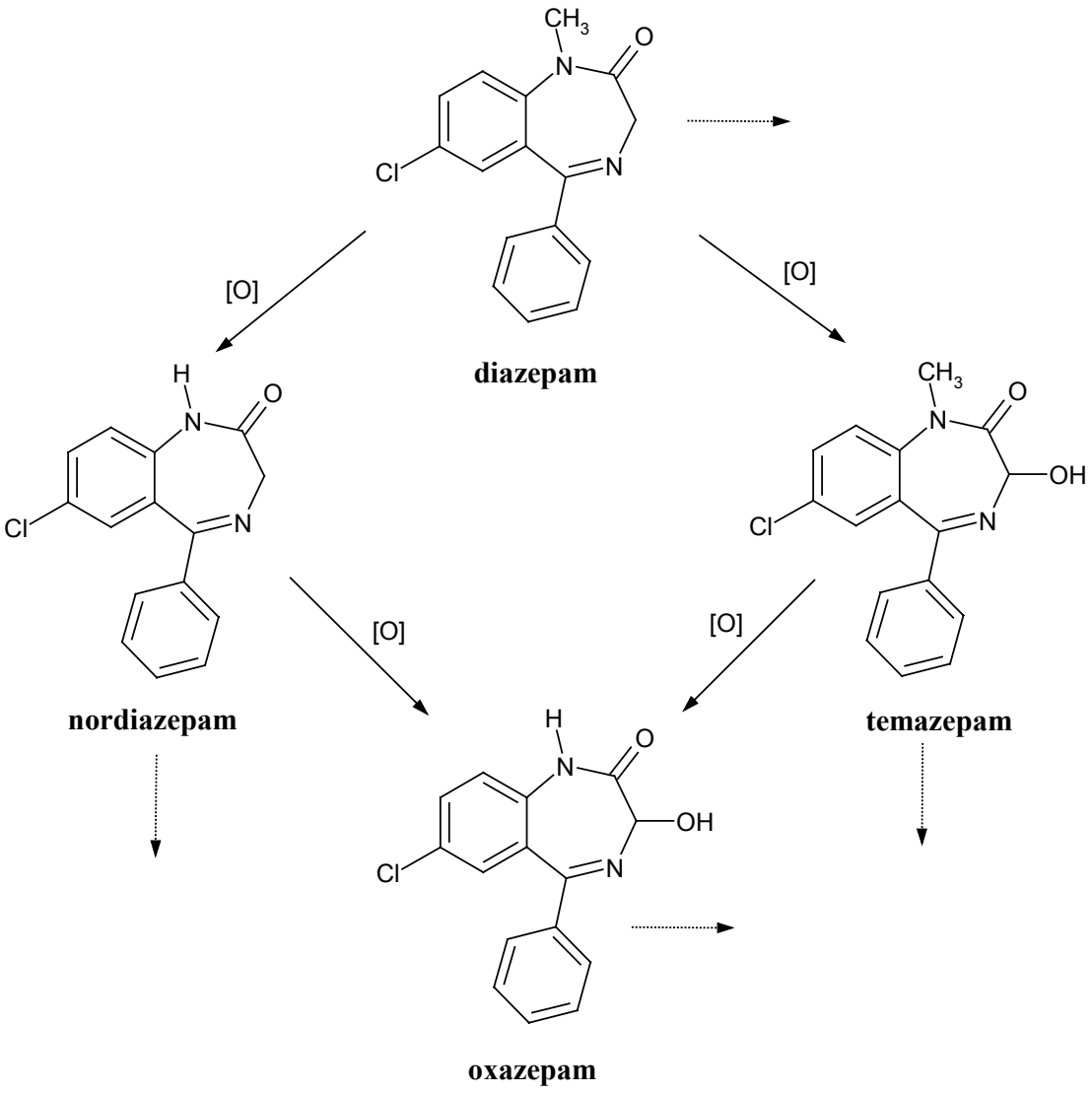

Figure 2.5: Oxidation of diazepam by cytochrome P450 to temazepam, nordiazepam and oxazepam.

Cyclosporine, an immunosuppressive agent, and midazolam, an anxiolytic compound, are also used as phase I markers. Although being a parent compound of the endogenous substance testosterone, 19-nortestosterone has been classified as a xenobiotic since it serves as an anabolic drug. Glucuroconjugation of 19-nortestosterone and 4-methylombelliferone, a spasmolytic and choleretic drug, are often used to evidence phase II drug metabolism.

2.5 Applications of hepatocyte hollow fiber bioreactors

Due to their conditions close to the physiological state, hepatocyte HFB are used for several purposes. Three main axes of use can be drawn: 1) for the synthesis of cellular products, 2) as artificial liver, and 3) as a tool for metabolic studies. Our aim here is not to provide an exhaustive list of the HFB uses but to give an overview of their possible applications.

2.5.1 Uses of hepatocyte HFB for the synthesis of cellular products

A significant part of the hepatocyte HFB used for the synthesis of cellular products is associated with tumor-derived cell lines. The advantages of cell lines over primary cell cultures are a continuous secretion, an easier purification and a better yield of cellular products. Moreover, cell lines are immortal, which facilitates cloning, their culture is easier and a higher cellular density is achievable.

For instance, purified hepatitis B surface antigen can be produced from Alexander hepatoma cells grown in HFB [66]. Today, human hepatitis B vaccines contain hepatitis B surface antigen obtained from plasma of humans infected with the hepatitis B virus. However, considering the risks linked to the use of human blood, the Alexander hepatoma cell line which carries the hepatitis B virus genome and secretes surface antigen of hepatitis B provides an interesting alternative antigen source for vaccine production.

Hep G2 cells, another human hepatoma cell line, are cultivated in HFB to produce Hep G2 crude conditioned medium (CCM) which contains high quantities of proteins, including the

endothelial cell growth factor and platelet-derived growth factor [67]. Hep G2 CCM was found to be comparable to or even better than fetal calf serum in supporting the growth of cells *in vitro*. Serum is traditionally added to cell cultures to provide nutrients, notably growth factors. But as the sources of serum are limited and its composition is subjected to variations, the development of serum substitutes is important and Hep G2 CCM seems to be a good candidate as a serum substitute.

2.5.2 The hepatocyte HFB as a bioartificial liver

Currently, the major application of hepatocyte HFB is as a BAL to serve as a bridge to transplantation for patients with acute liver failure (ALF). The use of BAL with patients suffering from ALF permit to increase their survival rate, as ALF is associated with a very high mortality rate. Symptoms of ALF include notably encephalopaty, reduced albumin synthesis, prolonged prothrombin time and elevated bilirubine and ALT levels [68]. Orthotopic liver transplantation is for the moment the treatment of choice for patients with ALF, but many of them are never transplanted because they do not survey until a donor organ becomes available.

Devices or techniques to support organisms suffering from ALF have been based primarily on extracorporeal blood processing, using physical or biological techniques. Physical techniques include dialysis, affinity chromatography, charcoal adsorption, and ion exchange. Biological techniques include extracorporeal perfusion of animal livers, cross-circulation with animals or cadavers, as well as simple exchange transfusion or plasmapheresis [59]. However, none of these therapeutic modalities has succeeded in gaining wide clinical application. The use of hepatic cells serves as an intermediate between physical and wholly biological techniques. Several BAL designs have been proposed, including direct hemoperfusion of microencapsulated hepatocytes in an extracorporeal chamber [40], plate dialyzer [69] and hollow fiber BAL systems, on which we focus hereinafter.

A BAL has to replace the multiple functions of the liver, including metabolic and secretory functions. All the information given in the previous sections is applied in the development of BAL to get an optimal functionality of the hepatocytes contained in the HFB. BAL functions are first investigated in a series of *in vitro* (table 2.2) and *in vivo* animal experiments (table 2.3) before being tested with humans (table 2.4). These tables list the characteristics of the HFB used, e.g. the ECS volume, the fiber porosity, the type of cells used and the way they are cultured. They also review the tests performed to check the viability and functionality of hepatocytes during BAL use. In addition to these tests, several examinations are performed on patients in clinical trials, including vital signs, neurological monitoring, whole blood cell counts, and coagulation tests.

A HFB used as a BAL (figure 2.6) brings hepatocytes or liver-derived cells from both human and animal origin into contact with patient whole-blood or plasma. Perfusing plasma through the HFB instead of whole blood eliminates problems linked to hemolysis, thrombocytopenia, clot formation, embolization and the need for heparinization [70], but the use of whole blood has the advantage of containing erythrocytes, which improves oxygen delivery to hepatocytes. A charcoal column is often included in the perfusion system before the HFB to adsorb part of the toxic compounds in the plasma [33,71]. The best procedure is to use primary human hepatocytes, but they are short in supply. Transformed human liver cells grow to high cellular density but are inferior to primary cells in accomplishing hepatic functions and bear the potential risk of tumor transmigration from the BAL into the patient's circulation [3,14]. Primary animal hepatocytes, on the other hand, have a limited life span *in vitro* and have the disadvantage of an increased risk of immunological complications and potential xenozoonosis. For clinical use, porcine hepatocytes are preferred to rodent hepatocytes because higher cell yields are obtained.

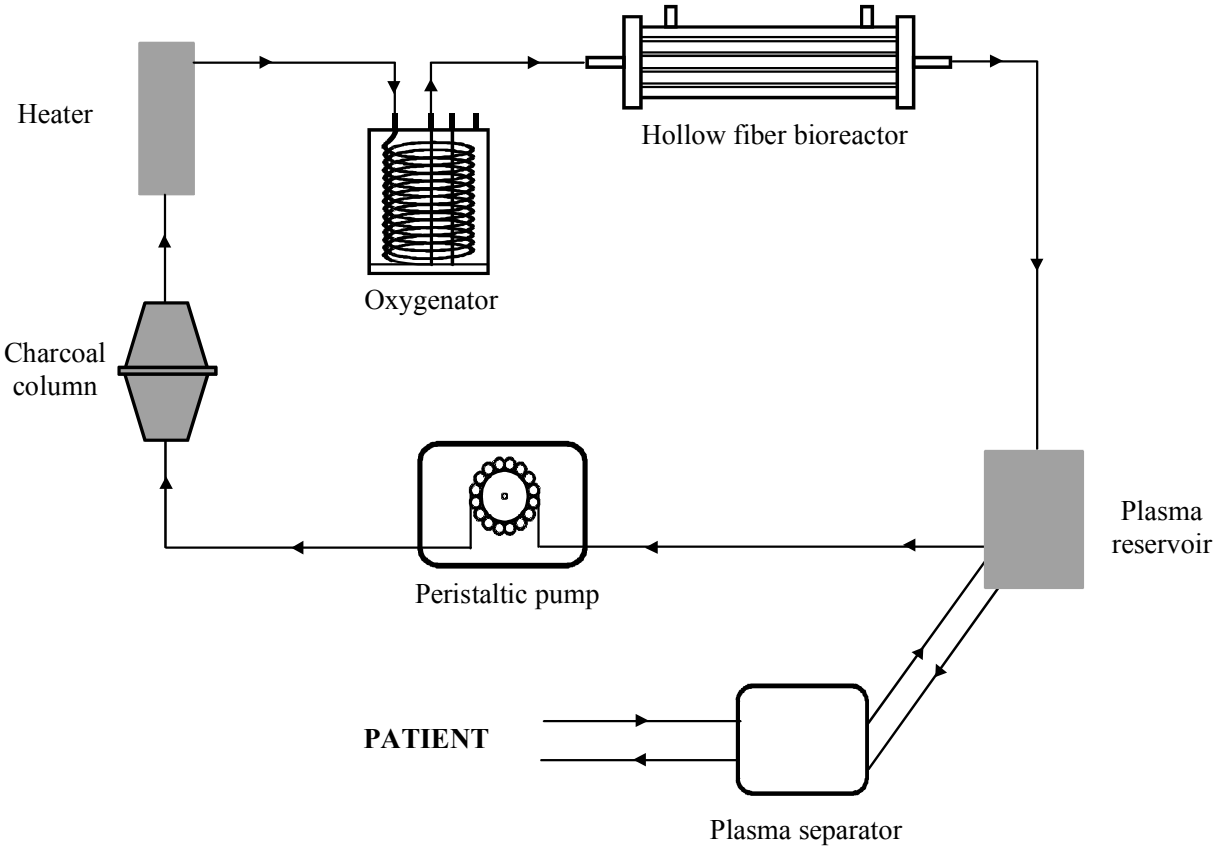

Figure 2.6: Schematic illustration of a hollow fiber bioartificial liver. The plasma separator is absent when whole blood is perfused through the system. Toxic compounds in patients whole blood or plasma are partially adsorbed on activated charcoal before being metabolized by the primary hepatocytes or liver-derived cells contained in the hollow fiber bioreactor.

Cellular immunologic isolation is important to reduce complications. However, it is difficult to determine the optimal molecular weight cut-off of HF membranes suitable for BAL. Actually, the smaller it is, the better it prevents immune reactions on both sides of the HF membrane, but the less it removes protein-bound toxins [72]. For example, HF membranes with a cut-off of 100 kD could act as impermeable barriers to immunoglobulins (~ 150 kD) and complement (> 200 kD) in the patient's blood and provide a barrier to transmission of pathogens, while allowing passage of soluble and albumin-bound toxins (albumin ~ 60 kD). In this point of view, the rather large HF porosity of 0.2 μm (0.1 μm ~ 1000 kD) of the porcine hepatocyte BAL HepatAssist can surprise. Its designers argued that the use of plasma perfusion (no direct contact between immune cells in the blood

and BAL cells), of purified isolated hepatocytes (no endothelial cells and other highly antigenic cells) and of HF with a large porosity (permeable to immunoglobulins but allowing excellent transport of molecules across the fibers) seemed to present a good compromise between the need for efficient function and prevention of immune reactions [70].

Despite the considerable number of *in vitro* experimental studies and animal models of ALF, only three systems have been recently assessed clinically, two of which in several studies (table 2.4). The Hepatix device uses a human hepatoblastoma cell line (C3A cells derived from the HepG2 cell line) in suspension within the ECS of the HFB, whole blood being used for the perfusion. The HepaAssist BAL utilizes cryopreserved porcine hepatocytes attached to collagen microcarriers contained within the ECS of the HFB. The treatment with hepatocyte hollow fiber BAL was well tolerated by all patients with evidence of clinical improvement. Patients were transplanted successfully after BAL treatments (6-7h), which shows that BAL can be used as a bridge to transplantation for patients with ALF. A few cases of spontaneous recovery without transplantation were even reported [73,74]. However, at the present time, no BAL device has received FDA approval for use in ALF.

Table 2.2: Bioartificial liver: *in vitro* tests.

Bioreactor design **Cartridge model** **Manufacturer**	**ECS vol** **Porosity**	**Type of cells** **Cell density or total cell number**	**Type of culture** **Treatment** **Inside/outside the fibers**	**Medium** **Flow rate**	**Hepatocyte function and viability tests**		**Ref**
					Exogenous compounds metabolism	**Endogenous compounds**	
Single circuit (fig 2.3a) Vitafiber Amicon, USA or Dowex cell culture tube c/HFBI-05 Bio Rad Lab, USA	ns 50 kD ns 30 kD	Rat hepatoma cell line H4-II-E ns	Adhesion (fig 2.4b) No treatment Outside the fibers	F12K 0.7-3.6 ml/min	ns	Bilirubin, glucose, LDH, AST, and GTP	Wolf 1975 [59]
Single circuit (fig 2.3a) Vitafiber XM50 Amicon, USA	ns 50 kD	Neonatal murine hepatocytes	Adhesion (fig 2.4b) No treatment Outside the fibers	Hams F12K 1 ml/min	Diazepam	Glucose, albumin, fibrinogen, transferrin, urea, cytidine	Hager 1983 [22]
Multiple circuits (fig 2.3d) H1P100 Amicon, USA	ns 100 kD	Primary rat hepatocytes ~ $5{\cdot}10^6$ cells/ml	Gel embedding (fig 2.4c) Collagen I 0.15% Inside the fibers	Williams' E SP: 30 ml/min FP: :9 ml/h	Lidocaine	Albumin, oxygen	Shatford 1992 [63,75]
Single circuit (fig 2.3b) Minikap 225 Microgon, USA	33.5 ml 0.2 μm	Primary rat hepatocytes $1{\cdot}10^6$ cells/ml	Microcarriers (fig 2.4d) Coated with collagen Outside the fibers	PBS 10, 30, 50 ml/min	Cyclosporine 19-nortestosterone	ns	Rozga 1993 [10]
Multiple circuits (fig 2.3d) H1P100 Amicon, USA	ns 100 kD	Primary rat hepatocytes or Hep G2 cells 5-$10{\cdot}10^6$ cells/ml	Gel embedding (fig 2.4c) Collagen I 0.15% Inside the fibers	Williams' E SP: 30 ml/min FP: 9 ml/h	Lidocaine 4-MU	Albumin, urea, lactate, glucose, insulin, aa and oxygen	Nyberg 1992 [13] 1994 [14]
Single circuit (fig 2.3a) ns Grace & Co, USA	7.2 ml ns	Primary rat hepatocytes $5.6{\cdot}10^6$ cells/ml	Adhesion (fig 2.4b) Fiber coating with collagen (Vitrogen®) Outside the fibers	Chee's EM 75 ml/min	Diazepam PSP	ns	Jauregui 1994 [24]
Multiple circuits (fig 2.3f) Home-made -	ns ns	Primary pig hepatocytes $2.5{\cdot}10^9$ total cells	Adhesion and aggregates (fig 2.4b) Fiber coating with collagen (Matrigel®) Outside the fibers	Williams' E 25 ml/min	Lidocaine Midazolam	Galactose, LDH, AST, GPT, GLDH, GGT, albumin	Gerlach 1994 [17]
Single circuit (fig 2.3a) Culture Flo G Asahi Medical, Japan	2 ml 0.4 μm	Primary rat hepatocytes $2{\cdot}10^7$ cells/ml	Gel embedding (fig 2.4c) Collagen I 0.2% Outside the fibers	Williams' E 1 ml/min	ns	Urea, albumin, ammonia, AST	Takeshita 1995 [27]
Single circuit (fig 2.3a) Cellmax Cellco, USA	ns 30 kD	Primary rat hepatocytes $1{\cdot}10^6$ cells/ml	Microcarriers (fig 2.4d) Coated with fructose-modified chitosan Outside the fibers	Williams' E 25 ml/min	Lidocaine	LDH, urea	Yagi 1997 [29]
Multiple circuits (fig 2.3e) Home-made Home-made	11 ml ns	Primary pig hepatocytes $2{\cdot}10^7$ cells/ml	Suspension / aggregates (fig 2.4a) No treatment Outside the fibers	Williams' E 30 ml/min	Lidocaine	Galactose, urea, protein, amino acids, lactate/ pyruvate, LDH, AST, GPT, glucose	Flendrig 1997 [15]
Multiple circuits (fig 2.3d) ns Althin Medical, USA	ns 100 kD	Primary porcine hepatocytes $3{\cdot}10^7$ cells/ml	Gel embedding (fig 2.4c) Collagen I 0.15% Inside the fibers	Williams' E SP: ns FP: 15 ml/h	ns	Urea, albumin, oxygen	Sielaff 1997 [61]
Single circuit (fig 2.3a) HepatAssist™ BAL2000 Circe Biomedical, USA	ns ns	Primary porcine hepatocytes ns	Microcarriers (fig 2.4d) No treatment Outside the fibers	Calf serum 100-600 ml/min	Diazepam	Oxygen	Custer 1998 [54]
Single circuit (fig 2.3c) Duo-Flux M170D JMS, Japan	145 ml ICS 99 ml 68 kD	Primary porcine hepatocytes $1{\cdot}10^8$ cells/ml	Suspension (fig 2.4a) No treatment Inside the fibers	80% Dubelcco + 20% human blood, 200 ml/min	Lidocaine	Urea, galacose	Iwata 1999 [11]

ns: non specified, LDH: lactate dehydrogenase, ALT: alanine aminotransferase, AST: aspartate aminotransferase, GPT: glutamic pyruvic transaminase, GLDH: glutamate dehydrogenase, GGT: γ-glutamyl transpeptidase, PSP: phenolsulphonphtalein, SP: shell perfusate, FP: fiber perfusate, 4-MU: 4-methylumbelliferone, ECS vol: extracapillary space volume, ICS: intracapillary space

Table 2.3: Bioartificial liver: *in vivo* animal tests.

Bioreactor design **Cartridge model** **Manufacturer**	**ECS vol** **Porosity**	**Animal model**	**Type of cells** **Cell density or total cell number**	**Type of culture** **Treatment** **Inside/outside the fibers**	**Medium** **Flow rate**	**Hepatocyte function and viability tests**		**Ref**
						Exogenous compounds metabolism	**Endogenous compounds**	
Single circuit (fig 2.3a) Vitafiber, Amicon, USA or Dowex cell culture tube c/HFBI-05 Bio Rad Lab, USA	ns 50 kD ns 30 kD	Rat	Rat hepatoma cell line H4-II-E ns	Adhesion (fig 2.4b) No treatment Outside the fibers	Blood 1 ml/min	ns	Bilirubin	Wolf 1975 [59]
Single circuit (fig 2.3a) Minipure ES 1-12 Microgon, USA	7 ml 0.2 μm	Rat	Primary rat hepatocytes $5.7 \cdot 10^6$ cells/ml	Microcarriers (fig 2.4d) Coated with collagen Outside the fibers	Blood 10 ml/min	ns	Bilirubin	Arnaout 1990 [30]
Single circuit (fig 2.3a) Cell-pharm 240-322 UniSyn Fibertec, USA	ns 70 kD	Dog	C3A cells ns	Suspension (fig 2.4a) No treatment Outside the fibers	Blood ns	ns	Albumin , ALT	Sussman 1992 [68]
Single circuit (fig 2.3b) Minikros M22M-030-01N Microgon, USA	33.5 ml 0.2 μm	Dog	Primary porcine and dog hepatocytes $1 \cdot 10^6$ cells/ml	Microcarriers (fig 2.4d) Coated with collagen Outside the fibers	Plasma 30 ml/min	ns	Glucose, lactate, LDH, AST	Rozga 1993 [10]
Single circuit (fig 2.3a) Z22M-060-01X Microgon, USA	177 ml 0.2 μm	Dog	Primary porcine hepatocytes $3.4 \cdot 10^6$	Microcarriers (fig 2.4d) Coated with collagen Outside the fibers	Plasma 200 ml/min	ns	Glucose, lactate, haptoglobin, fibrinogen , LDH, AST	Rozga 1993 [31]
Multiple circuits (fig 2.3d) H1P100 Amicon, USA	ns 100 kD	Rabbit	Primary rat hepatocytes $5\text{-}10 \cdot 10^6$ cells/ml	Gel embedding (fig 2.4c) Collagen I 0.15% Inside the fibers	Blood SP: 25 ml/min Williams' E FP: 9 ml/h	Lidocaine 4-MU	Albumin, ammonia, amino acids, lactate, oxygen, glucose	Nyberg 1993 [12]
Single circuit (fig 2.3a) ns ns	40 ml 0.15 μm	Rabbit	Primary rabbit hepatocytes $1.4 \cdot 10^7$ cells/ml	Adhesion (fig 2.4b) No treatment Outside the fibers	Blood 25 ml/min	Lidocaine, Diazepam	ALT, LDH, bilirubin, glucose, ammonia, creatinine	Jauregui 1995 [64]
Single circuit (fig 2.3a) Z22M-060-01ZX Microgon, USA	ns ns	Pig	Primary porcine hepatocytes ns	Microcarriers (fig 2.4d) Coated with collagen Outside the fibers	Plasma 30 ml/min	ns	Glucose, lactate, ammonia, urea, albumin, fibrinogen, creatinine, amino acids	Sheil 1996 [33]
Multiple circuits (fig 2.3f) Home-made -	ns ns	Pig	Primary pig hepatocytes $4 \cdot 10^{10}$ total cells	Adhesion and aggregates (fig 2.4b) ns Outside the fibers	Blood ns	ns	ns	Gerlach 1997 [76]
Multiple circuit (fig 2.3d) ns ns	ns 100 kD	Dog	Primary porcine hepatocytes ns	Gel embedding (fig 2.4c) Collagen I ns	Blood 100-500 ml/min	ns	ALT, AST, ammonia, lactate	Patzer 1999 [28]

ns: non specified, LDH: lactate dehydrogenase, ALT: alanine aminotransferase, AST: aspartate aminotransferase, SP: shell perfusate, FP: fiber perfusate, 4-MU:4-methylumbelliferone, ECS vol: extracapillary space volume

Table 2.4: Bioartificial liver: clinical studies.

Bioreactor design	Single circuit (fig 2.3a)	Single circuit (fig 2.3b)	Multiple circuits (fig 2.3f)
Cartridge model	Z22M-060-01X (HepatAssist)	Hepatix ELAD	Home-made
Manufacturer	Microgon, USA	ns	-
ECS vol	177 ml	125 ml	ns
Porosity	0.2 μm	70 kD	ns
Type of cell	Primary porcine hepatocytes	Human liver cell line (C3A)	Primary porcine hepatocytes
Cell density or total cell number	$5\text{-}30 \cdot 10^6$ cells/ml	$2 \cdot 10^8$ cells/ml	$4 \cdot 10^{10}$ total cells
Type of culture	Microcarriers (fig 2.4d)	Suspension (fig 2.4a)	Adhesion and aggregates (fig 2.4b)
Treatment	Coated with collagen	ns	ns
Inside/outside the fibers	Outside the fibers	Outside the fibers	Outside the fibers
Medium	Blood or plasma	Blood	Blood
Flow rate	40-400 ml/min	250-500 ml/min	ns
Exogenous compounds metabolism	ns	Lidocaine Caffeine	ns
Endogenous compounds	AST, ALT, LDH, ammonia, urea, bilirubin, glucose, lactate, amino acids, fibrinogen, transaminases and creatinine	Galactose, bilirubine, transaminases, lactate, ammonia, albumin, oxygen, coagulation factors, fibrinogen and antithrombin III	ns
Clinical procedure	1 to 3 treatments of 6 hours	Uninterrupted treatment for a mean of 62 hours	Uninterrupted treatment for 40 hours
Number of patients treated	~ 120	~ 30	1
Ref	Rozga 1993 [31], 1994 [77] Demetriou 1995 [70] Chen 1996 [32] Watanabe 1997 [71] Mullon 1999 [78] Didier 2002 [74]	Sussman 1994 [65,73] Ellis 1996 [62]	Gerlach 1997 [76]

ns: non specified, LDH: lactate dehydrogenase, ALT: alanine aminotransferase, AST: aspartate aminotransferase

2.5.3 The hepatocyte HFB as a tool for the study of drug metabolism and transport

Drug metabolism studies using hepatocyte HFB are essentially performed for two distinct reasons. One is to check the functionality and viability of the hepatocytes contained in the HFB, as already discussed (see §2.4.2). On the other hand, HFB can be used as a cellular model for the study of drug metabolism and transport. Table 2.5 summarizes the principle advantages and disadvantages of the use of HFB for these purposes. HFB have several benefits over plate or suspension cultures which are the most commonly used cellular model for drug metabolism investigations. In particular, HFB mimic more closely the *in vivo*

environment, and hepatocytes are continuously provided with nutrients and oxygen, permitting a prolonged duration of experiments. Moreover, HFB facilitate sampling, as perfusion solutions are already separated from cells by the semi-permeable membrane of the fibers. Another advantage of HFB is that they are dynamic culture systems, allowing continuous measurements and changes in perfusion conditions to study the influence of several different factors during a single experiment. This aspect enables for instance to perform a complete Michaelis Menten kinetic study and to investigate the effects of inhibition in a single HFB experiment.

Table 2.5: Advantages and disadvantages of HFB for the study of drug metabolism and transport.

Advantages	**Disadvantages**
– Long lasting experiments	– Complicated setup
– Study of slow metabolism	– High cost
– High cell density achievable	– Gradient of nutrients and cells
– Easy sampling	
– Continuous measurement	
– Study of different factors in the same experiments	

The equilibrium between the advantages and the disadvantages of HFB seem to be in favor of HFB to study drug metabolism and transport. Nevertheless and despite the numerous advantages cited, HFB are not currently used for that purpose probably because they are quite difficult to set up and expensive compared to suspensions and plate cultures.

The use of liver cell lines has to be avoided, as they are dedifferentiated cells which often lack important metabolic activities. For instance, the P450 and conjugation activities of HepG2 cells are more than 200, respectively 30 times lower than that of primary rat hepatocytes [14]. As high yields compensate low activities, these cells are nevertheless used in BAL.

In our laboratory, we use a HFB containing freshly isolated rat hepatocytes in suspension to study the metabolic chiral inversion of ibuprofen (figure 2.7) and the transport mechanism of magnetic resonance imaging (MRI) contrast agents (chapters 5 and 6). The use of a hepatocyte HFB to study the chiral inversion of R-ibuprofen permitted to prolong the duration of the experiment from 4 hours, as done for hepatocytes in conventional suspensions, to 10 hours. This increased duration of experiment, which allows to study the slow biotransformation reactions, is especially due to a better supply of the hepatocytes with nutrients and oxygen. It can even be prolonged over several days when hepatocytes are cultured in adhesion [17,24].

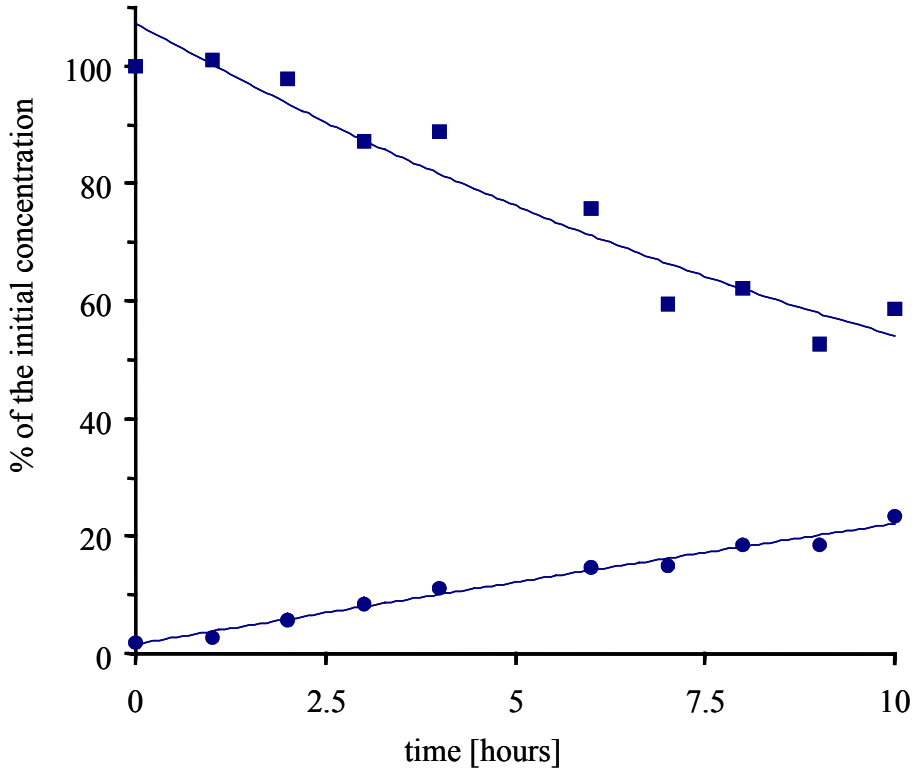

Figure 2.7: Incubation of (-)-*R*-ibuprofen 48,4 µM in a hollow fiber bioreactor (Minikros® Sampler M22M 030 01N, Spectrum, Rancho Dominguez, USA) containing $4 \cdot 10^7$ hepatocytes/ml: (-)-*R*-ibuprofen (■) and (+)-(S)-ibuprofen (●). Modified Hanks's solution was perfused through the hollow fiber bioreactor at a flow rate of 75 ml/min. Hepatocyte viability was checked during the experiment by the dosage of the enzymes AST and LDH released [79].

Hepatocyte HFB offer an interesting tool to study the transport mechanisms of contrast agents by MRI, because of the high cellular density achievable and the dynamic aspect of the system. Actually, HFB hepatocyte density can be sufficient to be detected by MRI. Moreover, the continuous perfusion of the HFB inside the MR magnet permits to continually supply hepatocytes with a 37°C oxygenated solution.

During a single experiment, solutions perfused through the HFB can be changed several times. Consequently, both uptake and excretion mechanisms of several contrast agents can be investigated successively with the same HFB, reducing the number of experiments and animals sacrificed. The uptake is observed during perfusion with a solution containing a contrast agent, while the excretion is studied during the following perfusion with a solution free of contrast agent.

2.6 Conclusion

HFB have several advantages compared to traditional cultures. The tri-dimensional matrix provides cells with an environment close to the physiological state. The continuous perfusion of a solution through the HFB continually supplies the cells with nutrients and oxygen. The semi-permeable membrane of the fibers, which separates physically cells and solution, protects them from a high shear stress and ensures a stable environment. The big surface of the fibers allows a high transfer of oxygen, which is particularly important for the survival of hepatocytes.

This chapter reviewed the design, setup, validation steps and uses of hepatocyte HFB. It provides future users with the basic knowledge necessary for the development of their own system. The different designs of HFB were first exposed. The concepts of these designs, in particular the multiple circuits systems, were developed to avoid the non-uniform cell and nutrient distribution observed with the simple design first described by Knazek et al. [4]. We then summarized the different ways of culturing hepatocytes in HFB. Long term culture can

be obtained when hepatocytes are attached to a support like the HF membrane, microcarriers or gel embedding, while suspensions of hepatocytes present the advantage of being the simplest method and yielding a higher cellular density. The importance of the experimental setup, in particular efficient oxygenation, was underlined. Several tests like the determination of nutrient consumption, the dosage of substances synthesized by the hepatocytes or the assessment of the metabolism of test compounds, can be applied to demonstrate that the developed HFB is able to sustain hepatocyte functionality and viability.

HFB containing immortalized cells derived from hepatocytes are used as culture device for the synthesis of cellular products like the surface antigen of hepatitis B for vaccine production or growth factors for the substitution of serum in cell culture solutions. However, the major use of hepatocyte HFB at the present time is as a BAL, to serve as a bridge to transplantation for patients suffering from ALF. Currently, several BAL devices including hollow fiber BAL are undergoing clinical evaluation. These studies suggest that they are safe and may be useful as a bridge to liver transplantation [32,65,70,71]. Finally, examples of the use of hepatocyte HFB as a tool for the investigation of drug metabolism were mentioned. Long lasting experiments can be performed, which permits the study of drugs with slow metabolism. Moreover, due to the dynamic aspect of the process, continuous measurement and changes in perfusion solutions become easy. Although having several interesting advantages, the high costs and the difficulty to set them up probably explain why HFB are not commonly used for drug metabolism studies.

Beside HFB, other kinds of hepatocyte bioreactors have been described such as multiplated hepatocyte monolayers, perfused beds containing suspensions of hepatocytes, microcarrier-attached or microencapsulated hepatocytes [7,80]. These systems can be used as the HFB but have the main disadvantage of exposing hepatocytes to high shear forces.

In summary, although being relatively difficult to set up, HFB represent a very attractive method to cultivate hepatocytes. An environment similar to the physiological one ensures an optimal viability and functionality of the hepatocytes. HFB can be used for several purposes,

e.g. for the synthesis of cellular products, as BAL, or as a tool for the study of drug metabolism and transport.

References

[1] Sasse D, Spornitz UM, and Maly IP, Liver architecture, *Enzyme*, 1992, **46**, 8-32.

[2] Tharakan JP, Gallagher SL, and Chau PC, Hollow-fiber bioreactor for mammalian cell culture, In 'Upstream Processes: Equipment and Techniques', Ed. Avshalom M, Alan R. Liss, New York, 1988, pp. 153-184.

[3] Nyberg SL, Peshwa MV, Payne WD, Hu W-S, and Cerra FB, Evolution of the bioartificial liver: the need for randomized clinical trials, *Am J Surg*, 1993, **166**, 512-521.

[4] Knazek RA, Gullino PM, Kohler PO, and Dedrick RL, Cell culture on artificial capillaries: an approach to tissue growth *in vitro*, *Science*, 1972, **178**, 65-67.

[5] Catapano G, Mass transfer limitations to the performance of membrane bioartificial liver support devices, *Int J Artif Organs*, 1996, **19**, 18-35.

[6] Nyberg SL, Santilli SM, Shatford RA, Cerra FB, Knighton DR, and Hu W-S, Microelectrode measurement of oxygen tensions in collagen-hepatocyte gels, *Biotechnol Tech*, 1991, **5**, 449-452.

[7] Allen JW, Hassanein T, and Bhatia SN, Advance in bioartificial liver devices, *Hepatology*, 2001, **34**, 447-455.

[8] Giorgio TD, Moscioni AD, Rozga J, and Demetriou AA, Mass transfer in a hollow fiber device used as a bioartificial liver, *ASAIO J*, 1993, **39**, 886-892.

[9] Tharakan JP, Operation and pressure distribution of immobilized cell hollow fiber bioreactors, *Biotechnol Bioeng*, 1986, **28**, 1064-1071.

[10] Rozga J, Williams F, Ro M-S, Neuzil DF, Giorgio TD, Backfisch G, Moscioni D, Hakim R, and Demetriou AA, Development of a bioartificial liver: properties and function of a hollow-fiber module inoculated with liver cells, *Hepatology*, 1993, **17**, 258-265.

[11] Iwata H, Sajiki T, Maeda H, Park YG, Zhu B, Satoh S, Uesugi T, Ikai I, Yamaoka Y, and Ikada Y, *In vitro* evaluation of metabolic functions of a bioartificial liver, *ASAIO J*, 1999, **45**, 299-306.

[12] Nyberg SL, Shirabe K, Peshwa MV, Sielaff TD, Crotty PL, Mann HJ, Remmel RP, Payne WD, Hu W-S, and Cerra FB, Extracorporeal application of a gel-entrapment, bioartificial liver: demonstration of drug metabolism and other biochemical functions, *Cell Transplant*, 1993, **2**, 441-452.

[13] Nyberg SL, Shatford RA, Peshwa MV, White JG, Cerra FB, and Hu W-S, Evaluation of a hepatocyte-entrapment hollow fiber bioreactor: a potential bioartificial liver, *Biotechnol Bioeng*, 1992, **41**, 194-203.

[14] Nyberg SL, Remmel RP, Mann HJ, Peshwa MV, Hu W-S, and Cerra FB, Primary hepatocytes outperform Hep G2 cells as the source of biotransformation functions in a bioartificial liver, *Ann Surg*, 1994, **220**, 59-67.

[15] Flendrig LM, La Soe JV, Jörning G.G.A., Steenbeek A, Karlsen OT, Bovée WMM, Ladiges NCJJ, te Velde AA, and Chamuleau RAFM, *In vitro* evaluation of a novel bioreactor based on an integral oxygenator and a spirally wound nonwoven polyester matrix for hepatocyte culture as small aggregates, *J Hepatol*, 1997, **26**, 1379-1392.

[16] Gerlach JC, Schnoy N, Smith MD, and Neuhaus P, Hepatocyte culture between woven capillary network: a microscopy study, *Artif Organs*, 1994, **18**, 226-230.

[17] Gerlach JC, Encke J, Hole O, Müller C, Ryan CJ, and Neuhaus P, Bioreactor for a larger scale hepatocyte *in vitro* perfusion, *Transplantation*, 1994, **58**, 984-988.

[18] Guguen-Guillouzo C, and Corlu A, Recent progresses on long-term hepatocyte primary cultures: importance of cell microenvironments, *Cytotechnology*, 1993, **11**, 3-5.

[19] Guillouzo A, Utilisation des hépatocytes isolés et en culture pour des études de métabolisme et de cytotoxicité des xénobiotiques, In 'Hépatocytes Isolés et en Culture', Eds. Guillouzo A and Guguen-Guillouzo C, INSERM/John Libbey Eurotext, Paris, 1986, pp. 327-346.

[20] Gerlach JC, Klöppel K, Schauwecker HH, Tauber R, Müller Ch, and Bücherl ES, Use of hepatocytes in adhesion and suspension cultures for liver support bioreactors, *Int J Artif Organs*, 1989, **12**, 788-792.

[21] Gebhardt R, Utilisation des hépatocytes isolés et en culture pour l'étude de la formation de la bile, In 'Hépatocytes Isolés et en Culture', Eds. Guillouzo A and Guguen-Guillouzo C, INSERM/John Libbey Eurotext, Paris, 1986, pp. 367-392.

[22] Hager JC, Carman R, and Porter LE, Neonatal hepatocyte culture on artificial capillaries: a model for drug metabolism and the artificial liver, *ASAIO J*, 1983, **6**, 26-35.

[23] Gerlach JC, Stoll P, Schnoy N, and Bucherl ES, Membranes as substrate for hepatocytes adhesion in liver support bioreactors, *Int J Artif Organs*, 1990, **13**, 436-441.

[24] Jauregui HO, Naik S, Santangini H, Pan J, Trenkler D, and Mullon C, Primary cultures of rat hepatocytes in hollow fiber chambers, *In Vitro Cell Dev Biol*, 1994, **30A**, 23-29.

[25] Dixit V, Development of a bioartificial liver using isolated hepatocytes, *Artif Organs*, 1994, **18**, 371-384.

[26] Qiang S, Yaoting Y, and Klinkmann H, Comparative evaluation of different membranes for the construction of an artificial liver support system, *Int J Artif Organs*, 1997, **20**, 119-124.

[27] Takeshita K, Ishibashi H, Suzuki M, Yamamoto T, Akaike T, and Kodama M, High cell-density culture system of hepatocytes entrapped in a three-dimensional hollow fiber module with collagen gel, *Artif Organs*, 1995, **19**, 191-193.

[28] Patzer II JF, Mazariegos GV, Lopez R, Molmenti E, Gerber D, Riddervold F, Khanna A, Yin W-Y, Chen Y, Scott VL, Aggarwal S, Kramer DJ, Wagner RA, Zhu Y, Fulmer ML, Block GD, and Amiot BP, Novel bioartificial liver support system: preclinical evaluation, *Ann New York Acad Sci*, 1999, **875**, 340-352.

[29] Yagi K, Michibayashi N, Kurikawa N, Nakashima Y, Mizoguchi T, Harada A, Higashiyama S, Murakana H, and Kawase M, Effectiveness of fructose-modified chitosan as a scaffold for hepatocyte attachment, *Biol Pharm Bull*, 1997, **20**, 1290-1297.

[30] Arnaout WS, Moscioni AD, Barbour RL, and Demetriou AA, Development of bioartificial liver: bilirubin conjugation in Gunn rats, *J Surg Res*, 1990, **48**, 379-382.

[31] Rozga J, Holzman MD, Ro M-S, Griffin DW, Neuzil DF, Giorgio TD, Moscioni AD, and Demetriou AA, Development of a hybrid bioartificial liver, *Ann Surg*, 1993, **217**, 502-511.

[32] Chen SC, Hewitt WR, Watanabe FD, Eguchi S, Kahaku E, Middleton Y, Rozga J, and Demetriou AA, Clinical experience with a porcine hepatocyte-based liver support system, *Int J Artif Organs*, 1996, **19**, 664-669.

[33] Sheil AG, Sun J, Mears DC, Waring M, Woodman K, Johnston B, Horvat M, Watson KJ, Koutalistras N, and Wang LS, Preclinical trials of a bioartificial liver support system in a porcine fulminant hepatic failure model, *Aust N Z Surg*, 1996, **66**, 547-552.

[34] Shnyra A, Bocharov A, Bochkova N, and Spirov V, Large-scale production and cultivation of hepatocytes on biosilon microcarriers, *Artif Organs*, 1990, **14**, 421-428.

[35] Kasai S, Sawa M, Tomita I, Hashimoto M, Nishida Y, Yamamoto T, and Mito M, Rat hepatocytes on a multiporous microcarrier for a hybrid artificial liver, *Artif Organs Today*, 1994, **3**, 217-225.

[36] Kawase M, Michibayashi N, Nakashima Y, Kurikawa N, Yagi K, and Mizoguchi T, Application of glutaraldehyde-crosslinked chitosan as a scaffold for hepatocyte attachment, *Biol Pharm Bull*, 1997, **20**, 708-710.

[37] Demetriou AA, Whiting JF, Feldman D, Levenson SM, Chowdhury NR, Moscioni AD, Kram M, and Chowdhury JR, Replacement of liver function in rats by transplantation of microcarrier-attached hepatocytes, *Science*, 1986, **233**, 1190-1192.

[38] Clément B, Desille M, Frémond B, Campion JP, Guguen-Guillouzo C, Bourel M, and Guillouzo A, Hépatocytes en thérapie cellulaire, *Transfus Clin Biol*, 1998, **5**, 80-87.

[39] Miura Y, Akimoto T, Kanazawa H, and Yagi K, Synthesis and secretion of protein by hepatocytes entrapped within calcium alginate, *Artif Organs*, 1986, **10**, 460-465.

[40] Dixit V and Gitnick G, The bioartificial liver: state-of-the-art, *Eur J Surg*, 1998, **Supplement**, 71-76.

[41] Tompkins RG, Carter EA, Carlson JD, and Yarmush ML, Enzymatic function of alginate immobilized rat hepatocytes, *Biotechnol Bioeng*, 1988, **31**, 11-18.

[42] Guyomard C, Rialland L, Fremond B, Chesne C, and Guillouzo A, Influence of gel entrapment and cryopreservation on survival and xenobiotic metabolism capacity of rat hepatocytes, *Toxicol Appl Pharmacol*, 1996, **141**, 349-356.

[43] Reid LM, and Jefferson DM, Culturing hepatocytes and other differentiated cells, *Hepatology*, 1984, **4**, 548-559.

[44] Morin O and Normand C, Long-term Maintenance of hepatocyte functional activity in co-culture: requirements for sinusoidal endothelial cells and dexamethasone, *J Cell Physiol*, 1986, **129**, 103-110.

[45] Begue J-M, Guguen-Guillouzo C, Pasdeloup N, and Guillouzo A, Prolonged maintenance of active cytochrome P-450 in adult rat hepatocytes co-cultured with another liver cell type, *Hepatology*, 1984, **4**, 839-842.

[46] Miyazaki M, Bai L, and Sato J, Selection of medium for serum-free culture of adult rat hepatocytes, *Acta Med Okayama*, 1990, **1**, 9-12.

[47] Ehrlich KC, Stewart E, and Klein E, Artificial capillary perfusion cell culture: metabolic studies, *In Vitro*, 1978, **14**, 443-450.

[48] Corasanti JG, Gleeson D, and Boyer JL, Effects of osmotic stresses on isolated rat hepatocytes. I. Ionic mechanisms of cell volume regulation, *Am J Physiol*, 1990, **258**, G290-G298.

[49] Hay PD, Veitch AR, Smith MD, Cousins RB, and Gaylor JDS, Oxygen transfer in a diffusion-limited hollow fiber bioartificial liver, *Artif Organs*, 2000, **24**, 278-288.

[50] Chresand TJ, Gillies RJ, and Dale BE, Optimum fiber spacing in a hollow fiber bioreactor, *Biotechnol Bioeng*, 1987, **32**, 983-992.

[51] Brotherton JD and Chau PC, Modeling of axial-flow hollow fiber cell culture bioreactors, *Biotechnol Prog*, 1996, **12**, 575-590.

[52] Macdonald JM, Grillo M, Schmidlin O, Tajiri DT, and James TL, NMR spectroscopy and MRI investigation of a potential bioartificial liver, *NMR in Biomedicine*, 1998, **11**, 55-66.

[53] Gerlach JC, Klöppel K, Stoll P, Vienken J, and Müller C, Gas supply across membranes in bioreactors for hepatocyte culture, *Artif Organs*, 1990, **14**, 328-333.

[54] Custer LM and Mullon C, Oxygen delivery to and use by primary porcine hepatocytes in the HepaAssist 2000 system for extracorporeal treatment of patients in end-stage liver failure, *Adv Exp Med Biol*, 1998, **454**, 261-271.

[55] Jensen MD, Production of anchorage-dependent cells-problems and their possible solutions, *Biotechnol Bioeng*, 1981, **23**, 2703-2716.

[56] Marieb EN, Anatomie et Physiologie Humaine, DeBoeck Université, Saint-Laurent, 1993.

[57] Testa B, The Metabolism of Drugs and Other Xenobiotics. Biochemistry of Redox Reactions, Academic Press, London, 1995.

[58] De Bartolo L, Catapano G, Della Volpe C, and Drioli E, The effect of surface roughness of microporous membranes on the kinetics of oxygen consumption and ammonia elimination by adherent hepatocytes, *J Biomater Sci Polymer Edn*, 1999, **10**, 641-655.

[59] Wolf CF and Munkelt BE, Bilirubin conjugation by an artificial liver composed of cultured cells and synthetic capillaries, *Trans Amer Soc Artif Int Organs*, 1975, **21**, 16-27.

[60] Nyberg SL, Payne WD, Amiot B, Shirabe K, Remmel RP, Hu W-S, and Cerra FB, Demonstration of biochemical function by extracorporeal xenohepatocytes in an anhepatic animal model, *Transplant Proc*, 1993, **25**, 1944-1945.

[61] Sielaff TD, Nyberg SL, Rollins MD, Hu MY, Amiot B, Lee A, Wu FJ, Hu W-S, and Cerra FB, Characterization of the three-compartment gel-entrapment porcine hepatocyte bioartificial liver, *Cell Biol Toxicol*, 1997, **13**, 357-364.

[62] Ellis AJ, Hughes RD, Wendon JA, Dunne J, Langley PG, Kelly JH, Gislason GT, and Sussman NL, Pilot-controlled trial of the extracorporeal liver assist device in acute liver failure, *Hepatology*, 1996, **24**, 1446-1451.

[63] Shatford RA, Nyberg SL, Meier SJ, White JG, and Payne WD, Hepatocyte function in a hollow fiber bioreactor: a potential bioartificial liver, *J Surg Res*, 1992, **53**, 549-557.

[64] Jauregui HO, Mullon C, Trenkler D, Naik S, Santangini H, Press P, Muller TE, and Solomon BA, *In vivo* evaluation of a hollow fiber liver assist device, *Hepatology*, 1995, **21**, 460-469.

[65] Sussman NL, Gislason GT, Colin CA, and Kelly JH, The Hepatix extracorporeal liver assist device: initial clinical experience, *Artif Organs*, 1994, **18**, 390-396.

[66] McAleer WJ, Markus HZ, Bailey FJ, Herman AC, Harder BJ, Wampler DE, Miller WJ, Keller PM, Buynak EB, and Hilleman MR, Production of purified hepatitis B surface antigen from Alexander hepatoma cells grow in artificial capillary units, *J Virol Meth*, 1983, **7**, 263-271.

[67] Liu JJ, Chen BS, Tsai TF, Wu YJ, Pang VF, Hsieh A, Hsieh JH, and Chang TH, Long term and large scale cultivation of human hepatoma Hep G2 cells in hollow fiber bioreactor, *Cytotechnology*, 1991, **5**, 129-139.

[68] Sussman NL, Chong MG, Koussayer T, He D-E, Shang TA, Whisennand HH, and Kelly JH, Reversal of fulminant hepatic failure using an extracorporeal liver assist device, *Hepatology*, 1992, **16**, 60-65.

[69] Cuervas-Mons V, Colas A, Rivera J, and Prados E, *In vivo* efficacy of a bioartificial liver in improving spontaneous recovery from fulminant hepatic failure: a controlled study in pigs, *Transplantation*, 2001, **69**, 337-344.

[70] Demetriou AA, Rozga J, Podesta L, LePage E, Morsiani E, Moscioni AD, Hoffmann A, McGrath M, Kong L, Rosen H, Villamil F, Woolf G, Vierling J, and Makowka L, Early clinical experience with a hybrid bioartificial liver, *Scand J Gastroenterol*, 1995, **208 (Suppl.)**, 111-117.

[71] Watanabe FD, Mullon CJ, Hewitt WR, Arkadopoulos N, Kahaku E, Eguchi S, Khalili T, Arnaout WS, Shackleton CR, Rozga J, Solomon BA, and Demetriou AA, Clinical experience with a bioartificial liver in the treatment of severe liver failure. A phase I clinical trial, *Ann Surg*, 1997, **225**, 484-491.

[72] Baur H, Kasperek S, and Pfaff E, Criteria of viability of isolated liver cells, *Hoppe-Seyler's Z Physiol Chem*, 1975, **356**, 827-838.

[73] Kelly JH and Sussman NL, The Hepatix extracorporeal liver assist device in the treatment of fulminant hepatic failure, *ASAIO J*, 1994, **40**, 83-85.

[74] Samuel D, Ichai P, Feray C, Saliba F, Azoulay D, Arulnaden J-L, Debat P, Gigou M, Adam R, Bismuth A, Castaing D, and Bismuth H, Neurological improvement during

bioartificial liver sessions in patients with acute liver failure awaiting transplantation, *Transplantation*, 2002, **73**, 257-264.

[75] Shatford RA, Nyberg SL, Payne WD, Hu W-S, and Cerra FB, A hepatocyte bioreactor as a potential bioartificial liver: demonstration of prolonged tissue-specific functions, *Surg Forum*, 1991, **42**, 54-56.

[76] Gerlach JC, Long-term liver cell cultures in bioreactors and possible application for liver support, *Cell Biol Toxicol*, 1997, **13**, 349-355.

[77] Rozga J, Podesta L, LePage E, Morsiani E, Moscioni AD, Hoffmann A, Sher L, Villamil F, Woolf G, McGrath M, Kong L, Rosen H, Lanman T, Vierling J, Makowka L, and Demetriou AA, A bioartificial liver to treat severe acute liver failure, *Ann Surg*, 1994, **219**, 538-546.

[78] Mullon C and Pitkin Z, The HepatAssist bioartificial liver support system: clinical study and pig hepatocyte process, *Exp Opin Invest Drug*, 1999, **8**, 229-235.

[79] Vu LT, Effets de substrats endogènes et exogènes sur l'inversion chirale de R-ibuprofène, *Thèse de doctorat*, Université de Lausanne, 1999

[80] Busse B and Gerlach JC, Bioreactors for hybrid liver support: historical aspects and novel designs, *Ann New York Acad Sci*, 1999, **875**, 326-339.

Chapter 3
Medical imaging, principles of magnetic resonance imaging (MRI), MRI of the liver, and MRI contrast agents

3.1 Introduction

During the last years, medical imaging has made incessant progresses. The details and the resolution which can be obtained permit to visualize the inside of the body with a remarkable precision. It enables both a better understanding of the anatomy and the detection of diseases. Hence, imaging is of great importance in the medical diagnostic.

The purpose of this chapter is to give an overview of magnetic resonance imaging (MRI), in particular at the level of the liver imaging and with a focus on contrast agents. It intends to give the basic knowledge necessary for a good comprehension of the experimental work described in this thesis consisting of the study of the mechanisms of MRI contrast agents towards hepatocytes.

The chapter begins with an outline of the techniques of medical imaging, including conventional radiography, computed tomography (CT), ultrasound (US) and the methods using nuclear medicine, such as scintigraphy and positron emission tomography (PET). The following section is dedicated to MRI. The principles of nuclear magnetism, relaxation and signal analysis, as well as the technical equipment and applications are described in more details. Then, emphasis is put on the MRI of the liver and on the contrast agents used to image this organ.

3.2 Medical imaging

Medical imaging is a diagnostic method which comprises different techniques of imaging. This section gives an overview of the basis of physics, of the technical aspects and of the diagnostic applications of the medical imaging techniques commonly used today [1,2]. The electromagnetic waves used in clinical imaging are presented in figure 3.1.

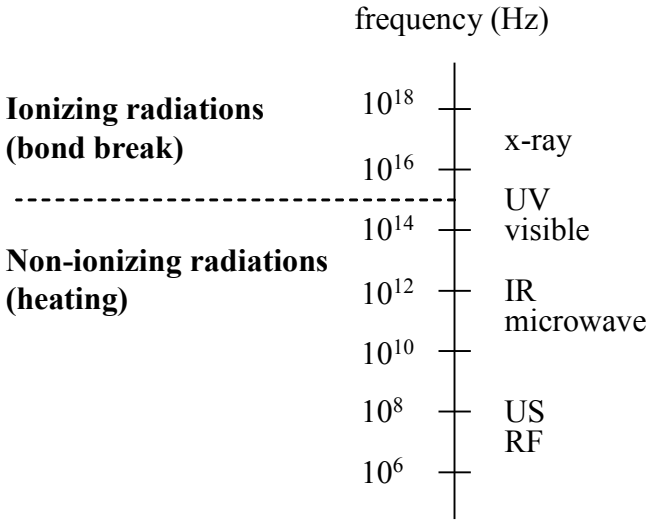

Figure 3.1: Electromagnetic spectrum showing the different waves used in clinical imaging. X-rays are used for conventional radiography and computed tomography (CT), ultrasound (US) waves are used for ultrasound imaging and radiofrequencies (RF) for magnetic resonance imaging (MRI).

As can be seen, conventional radiography and CT use ionizing radiations while US and MRI use non-ionizing radiations [3].

3.2.1 Conventional radiography

Conventional radiography, known to most people as X-ray, is the oldest and most frequently used technique of medical imaging. For nearly a century, diagnostic images have been created by passing small, highly controlled amounts of radiation through the body, capturing the resulting shadows and reflections on a photographic plate. Due to their calcium

content, bones are the most opaque and thus the most visible tissue on X-ray images. Soft tissues are less opaque than bones, but more opaque than adipose tissues. Air and gas are completely radio-transparent. Figure 3.2 shows an example of a conventional radiography.

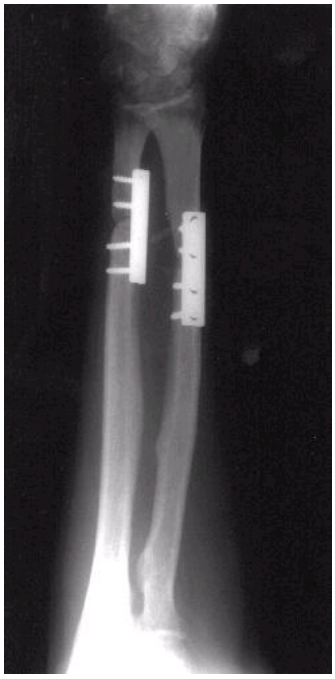

Figure 3.2: X-ray of an ulna fracture with subsequent immobilization.

A similar imaging method, called fluoroscopy, uses X-rays to capture a moving image of an organ while it is functioning. It is used in angiography (imaging of the blood vessels) for diagnostic and interventional procedure (use of imaging to guide percutaneous procedures).

Conventional radiography is the method of choice for the first line diagnostic of skeletal pathologies. It is also currently used for imaging lungs and breasts (mammography). The use of contrast agents, like barium and iodine salts, is often necessary when imaging soft tissues. For instance, barium sulfate, a non-toxic and very radio-opaque contrast agent administrated orally or in enema, is employed when imaging the gastrointestinal tract.

3.2.2 Computed tomography

Computed tomography (CT, “scanner X” in French) exists since 1975. It consists of a tube of X-rays which turns around the patient. The film of the regular radiography is replaced by numerical sensors and the image of cross-sections of body tissues and organs is built by computerized methods. CT scanning provides more detailed information than conventional radiography. It can show bone, soft tissues, and blood vessels in the same images with great differentiation and clarity (figure 3.3).

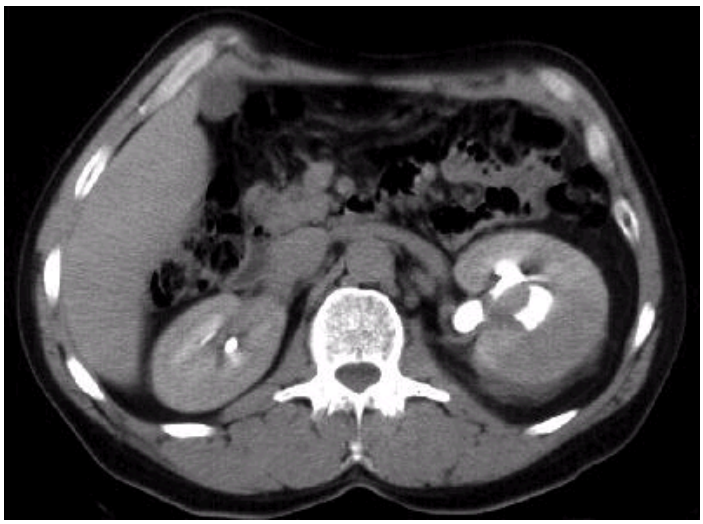

Figure 3.3: Computed tomography of a renal cell carcinoma.

Nowadays, CT encroaches on all fields of regular radiography, because of its better tissue differentiation. CT is widely used for imaging all the body parts. As for conventional radiography, the use of oral or rectal contrast agents, like barium and iodine salts, is necessary for imaging the gastrointestinal tract. Contrast agents can also be injected intravenously to increase the soft tissue differentiation. Despite its large medical applications, CT is now in competition with MRI.

3.2.3 Ultrasound

Ultrasound (US, sonography or ultrasonography) imaging appeared in the 60's. It is a method of imaging using high-frequency sound waves of frequencies ranging from 3 to 10 MHz. These waves are more or less reflected according to the different organic elements encountered and the sound waves reflected are recorded and displayed as a real-time image. No ionizing radiation is involved in ultrasound imaging.

US is a useful way of examining many of the body's internal organs, including the heart, liver, gallbladder, spleen, pancreas, kidneys, and bladder. And of course, pelvic ultrasound examinations of the uterus and fetus are the method of choice to detect eventual fetus malformations. Because US images are captured in real-time, they can show movement of internal tissues and organs, and enable physicians to see blood flow and heart valve functions. This can help to diagnose a variety of heart conditions and to assess damage after a heart attack or other illness. It is also used for interventional imaging. Ultrasound is now being used for abdominal imaging, to image the breasts and to guide biopsy of breast cancer. US interpretation is difficult and requires a good training, as can be seen in figure 3.4.

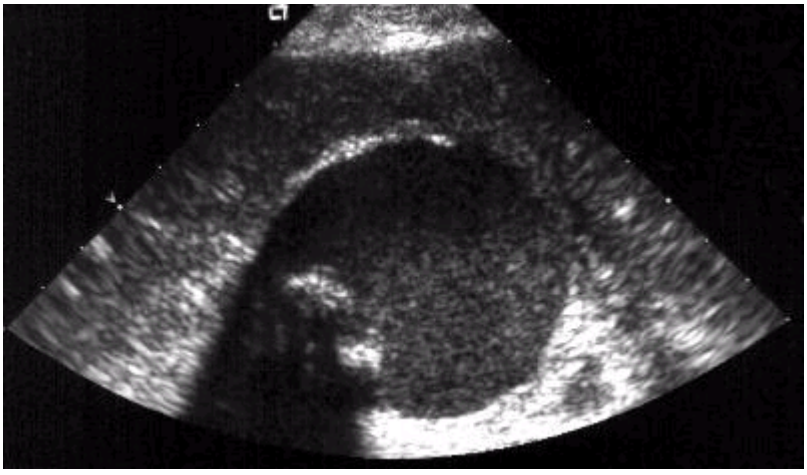

Figure 3.4: Ultrasound of the gallbladder with sludge and calculi.

Ultrasound waves are totally reflected by bones and gas. Thus US can not be used to image the adult skeleton or lungs. For the same reason, a gel is applied on the imaged area prior to apply the probe to avoid the presence of air bubbles.

Since the past decade, US contrast agents have been used to enhance ultrasonic signals. They improve the detection of flow within abnormal vessels, including tumor vascularization and stenotic vessels. They also hold promise for increasing the accuracy of US in the assessment of focal parenchymal disease [4]. At the present time, research is performed to allow detection of tissue enhancement similar to that obtained with CT or MRI.

3.2.4 Nuclear medicine

Nuclear medicine uses radioactive isotopes as a source of radiation. The medical applications of isotopes are based on the fact that biological systems, like the human body, do not distinguish between an isotope and a normal atom. Components marked with isotopes behave in the body like their natural equivalent, which permits to follow them with radiation detectors.

3.2.4.1 Scintigraphy

Scintigraphy (or gamma scintigraphy) uses radioactive isotopes which emit gamma rays. A gamma detector permits to follow the isotope transit in the body. Images obtained with scintigraphy have a low resolution but give useful functional information, in particular when a dynamic scintigraphy is performed.

The application of scintigraphy is large, its indications are notably the detection of tumors in the brain, the liver and the lungs. An example of scintigraphy is shown in figure 3.5.

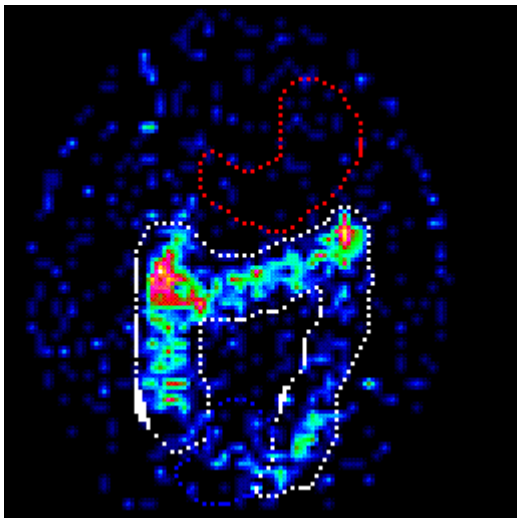

Figure 3.5: Scintigraphy of the gastrointestinal tract showing the gastrointestinal transit.

3.2.4.2 Positron emission tomography

Positron emission tomography (PET) is a diagnostic examination that involves the development of biologic images based on the detection of positrons. The positrons are emitted from a radioactive substance given to the patient. The subsequent views of the human body are used to quantitatively evaluate metabolic activities of different organs with a good resolution.

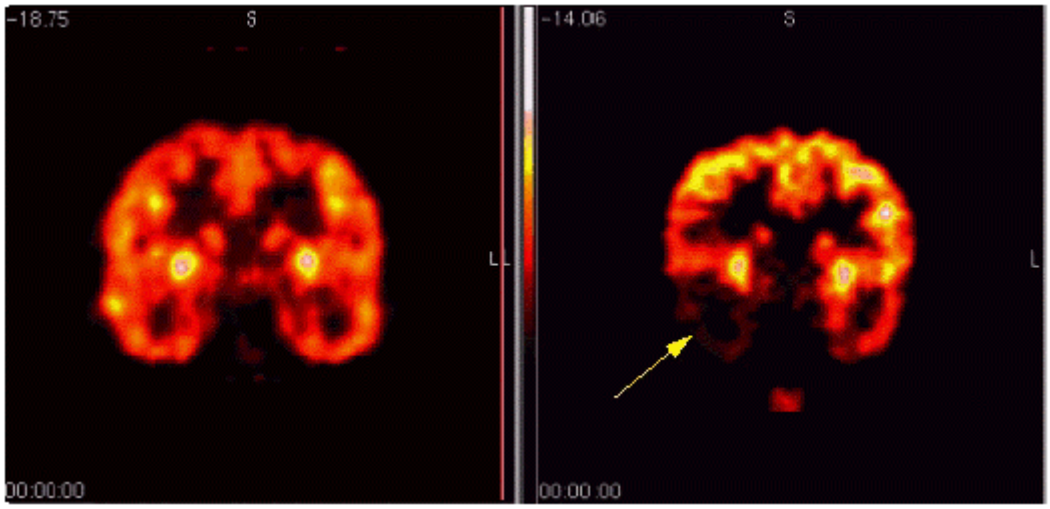

Figure 3.6: Positron emission tomography of a normal (left) and injured (right) brain.

Specifically, PET scans are used to detect cancer and to examine the effects of cancer therapy by characterizing biochemical changes with the cancer. These scans are performed on the whole body. PET scans of the heart can be used to determine the blood flow to the heart muscle and help to evaluate signs of coronary artery disease. Combined with a myocardial metabolism study, PET scans differentiate non-functioning heart muscle from heart muscle that would benefit from a procedure, such as angioplasty or coronary artery bypass surgery, which would re-establish adequate blood flow. PET scans of the brain (figure 3.6) are used to evaluate patients who have memory disorders of an undetermined cause; who have suspected or proved brain tumors; or who have seizure disorders that are not responsive to therapy, and therefore, are candidates for surgery.

PET units are one of the most expensive installations of imaging. The reconstruction of the image requires an electronic equipment of high performance and powerful computers, and a cyclotron is necessary to produce the radio-labeled substances.

3.3 Magnetic resonance imaging

In 1946, Block and Purcell received the Nobel Prize for their observations on nuclear magnetic resonance (NMR). NMR became a useful tool for the investigation of the structure of organic molecules. It is only in the 70's that, thanks to the computer science progress, NMR could be applied to the diagnostic imaging.

3.3.1 Principle

3.3.1.1 Nuclear magnetism

Certain atomic nuclei that have unpaired protons or neutrons possess an intrinsic spin, generating a small magnetic field, analogous to a microscopic bar magnet. The most abundant of the naturally spinning nuclei in the body is the hydrogen nucleus or proton, which represents 63% of the body atoms. Other nuclei that possess spin but are much less abundant include ^{23}Na, ^{31}P, and ^{13}C. If such randomly oriented spinning nuclei are placed within a static magnetic field B_0, they align parallel or antiparallel with the magnetic field. There is a small excess of protons which tend to align in the lower energy parallel orientation. This creates a resulting longitudinal magnetization in line with B_0, which can be represented by a magnetization vector M_0 (figure 3.7). It is upon this small excess that NMR signals depend. The spinning protons wobble about the axis of the main magnetic field at a rate given by the Larmor frequency. These two motions of the proton have different rates: the precessional motion is slow relative to the faster spinning motion.

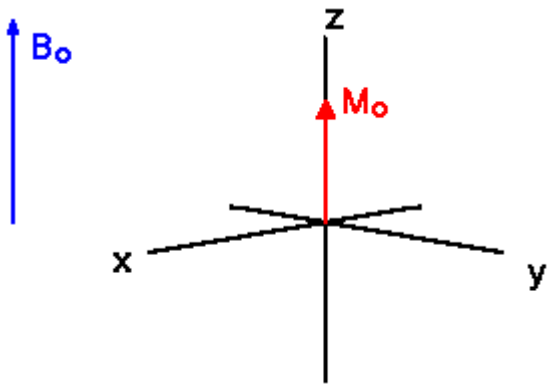

Figure 3.7: At equilibrium, the net magnetization vector lies along the direction of the applied magnetic field B_0 and is called the equilibrium magnetization M_0 [3].

3.3.1.2 Relaxation

When a radiofrequency (RF) field is applied perpendicular to B_0 at the same frequency as the precessing nuclei, it excites protons in the lower energy level into a higher energy state. The longitudinal magnetization is tipped out of its equilibrium position to a specific angle called flip angle (FA). Various flip angles can be obtained by varying the duration or the amplitude of the RF pulse. A 90° flip angle tips the longitudinal magnetization in the transverse plane. The energy adsorbed during this transition is subsequently released as electromagnetic waves to the environment as the protons relax back to their lower energy state and equilibrium (resonance phenomenon). This release of energy can be recorded as an electrical signal. The relaxation of the proton back to equilibrium is termed longitudinal relaxation. It is an exponential increase process and has a time constant referred to as T_1, which is the time needed by the magnetization to recover 63% of the longitudinal magnetization. Figure 3.8 describes the evolution of the magnetization after a 90° RF pulse. Immediately after the RF pulse is applied, the excited protons precess together, in phase with each other, at the resonant frequency. During relaxation, however, they quickly get out of synchronism due to small variations in local magnetic fields that results in energy dissipation between spins. This loss of phase is termed transverse relaxation. It is an exponential decay process and possesses the time constant T_2, which is the time needed for the dissipation of 63% of the transverse magnetization.

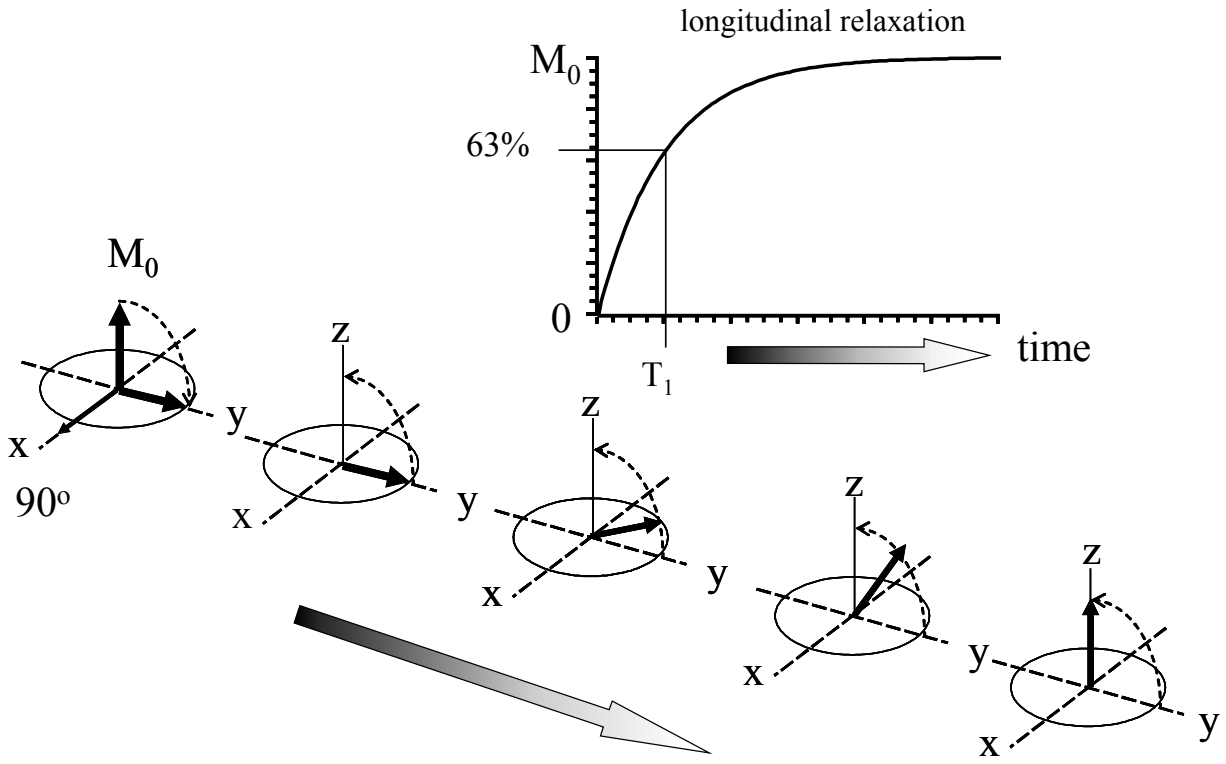

Figure 3.8: After a 90° RF pulse, the longitudinal magnetization M_0 is tipped in the transverse plane. The T_1 or longitudinal relaxation describes the evolution of the magnetization back towards M_0. T_1 is the time needed by the magnetization to recover 63% of M_0 [5].

3.3.1.3 Signal analysis

As the transmitted RF pulse and the MR signal take place at different times, the RF coil can act as both transmitter and receiver. The strength of radio waves or degree of whiteness or blackness (signal intensity) depends principally on four tissue factors, namely proton density, flow, T_1 and T_2 relaxation values as well as on pulse repetition time (TR), echo delay time (TE), and inversion time (TI) which are imaging parameters controlled by the operator. Proton density is the number of resonating hydrogen nuclei present in a particular volume of tissue following application of an RF pulse. In tissue, the concentration of such protons is related primarily to water content and secondarily to lipid content. Since signal intensity (SI) is directly proportional to the proton density, gas and cortical bone demonstrate extremely low SI (appearing black). Flow is a function of the speed at which hydrogen atoms move through the region being imaged, and the percentage of protons in the region that are moving. Flowing blood can appear black, white or any shade of gray depending on various factors. The relationship of these four factors to SI is simply described in table 3.1.

Table 3.1: Relationship of proton density, T_1, T_2 and blood flow to signal intensity [6].

Signal intensity	Proton density	T_1	T_2	Blood flow
High (white)	High	Short	Long	Stationary, slow
Low (black)	Low	Long	Short	Turbulent, fast

The conventional RF pulse sequences used in imaging are total or partial saturation recovery (SR), inversion recovery (IR), gradient echo (GRE) and spin echo (SE). These sequences give different weighting in the received signal to proton density, T_1 and T_2. SR gives a similar weight to these three parameters, while IR emphasizes T_1 [6]. According to the parameters TE and TR selected, GRE or SE images can be either proton density-weighted, T_1-weighted or T_2-weighted.

Magnetic resonance produces images of a slice through the human body. Each slice is composed of several volume elements or voxels. The volume of a voxel is approximately 3 mm^3. The magnetic resonance image is composed of several picture elements called pixels. The SI of a pixel is proportional to the SI of the contents of the corresponding voxel of the object being imaged.

A gradient system is used to generate small magnetic fields that are added to the main field to select slices and to localize the signal. Data analysis is made by a computer, using the Fourier transform.

3.3.1.4 Technical equipment

Magnetic resonance systems for clinical use include a magnet, RF coils, gradient coils, a computer, a display unit, and digital storage facilities.

The magnet produces the B_0 field for the imaging procedure. There are currently three main types of magnets used in MRI: permanent magnets, resistive magnets, and superconducting magnets. While the first two types of magnets can generate a maximum magnetic field of 0.3 to 1.0 Tesla (T), the super conducting magnet produces a higher field strength of 0.5 to 4 T. Such homogenous high field strength permits the production of high quality images, but requires liquid helium and nitrogen to keep the electric resistance near zero (4°K).

The RF coil produces the RF necessary to excite the protons in the body and also detects the signal from the spins within the body. There are two broad categories of RF coils used in imaging. The volume coils (e.g. body, head or wrist coils) are most commonly used. They completely surround the part of the body being imaged, and receive the same amount of signal from deep and superficial tissues. The second type consists of surface coils which are used to obtain high-resolution images of relatively superficial body structures.

The gradient system within the magnet consists of a set of gradient coils, covering each dimension. They are resistive electromagnets that can be switched on and off and varied

rapidly and precisely. This permits the selection of tissue slices in transverse, coronal, or sagittal planes.

The scan room is surrounded by an RF shield. The shield prevents the high power RF pulses from radiating out through the hospital. But it also prevents the various RF signals from television and radio stations to be detected by the imager. The heart of the imager is the computer, which controls all components on the imager.

3.3.2 Application and safety

Images obtained with MRI are remarkably good, as can be seen in figure 3.9. Tissue discrimination is superior with MRI than with CT and all planes can be imaged, while CT permits only to get transverse planes. MRI is widely applied, although the method is more limited for the imaging of moving regions because the acquisition of the image takes a few minutes. Nowadays, MRI is applied for a broad range of conditions in all parts of the body including the intestines, kidneys, liver, heart, vascular system, head, spinal cord, bones and joints. Contrast agents can be used to improve tissue discrimination. They are discussed in detail in section 3.4.

Figure 3.9: Magnetic resonance imaging of head and neck.

MRI is safe, as US it does not use ionizing waves. Nevertheless, MRI is unsuitable for some people who have metallic implants, or pacemakers, actually, the latter can act as a RF receptor or be unintentionally activated by the magnetic field.

The constraints to MRI are in particular financial, a MRI system costs about 3 millions CHF and an single exam about 800.- CHF, but also technical, as the system is heavy and needs a lot of place.

3.4 MRI of the liver

MRI is probably more advantageous to characterize hepatic lesions than CT scans, because of its lack of ionizing radiation, safety of gadolinium chelates in comparison to iodinated contrast agents and accuracy of the imaging. Nevertheless, CT remains the modality of choice at many institutions due to the speed of acquisition, good resolution and the clinical availability.

MRI enables an accurate evaluation of a wide variety of focal and diffuse hepatic diseases, although most imaging of the liver is performed to evaluate focal diseases.

3.4.1 Focal hepatic diseases

Liver cancers affect literally millions of people each year, hepatocellular carcinoma being one of the most frequent cancers worldwide. Additionally, the liver is the most common organ of the body to which cancer spreads from primary disease elsewhere. Accurate lesion detection and characterization is therefore necessary to ensure appropriate management of patients with liver cancer. One can distinguish two kinds of diagnoses: invasive and non-invasive procedures.

Invasive procedures include intraoperative ultrasonography, CT angio-portography, and CT after intra-arterial injection of iodized oil. These diagnostic methods are considered as having the highest sensitivity for the detection of focal liver lesions. Nevertheless, they are clinically limited, mainly because of the risk and cost induced by the invasiveness.

Most of the liver cancer patients undergo non-invasive diagnostic imaging, consisting of ultrasonography and CT, despite the fact that the false-negative rate of these methods is known to exceed 40% [7]. MRI is mostly applied as a diagnostic adjunct in cases where ultrasonography and CT do not clarify the situation thought it is reported to have a similar or even higher sensitivity for the detection of liver lesions. Unenhanced MRI also misses 35-40% of liver lesions, due to the fact that the liver and tumors within it often have similar signal intensity. The use of contrast agents can be used to increase the contrast difference between the liver and its lesions (figure 3.10).

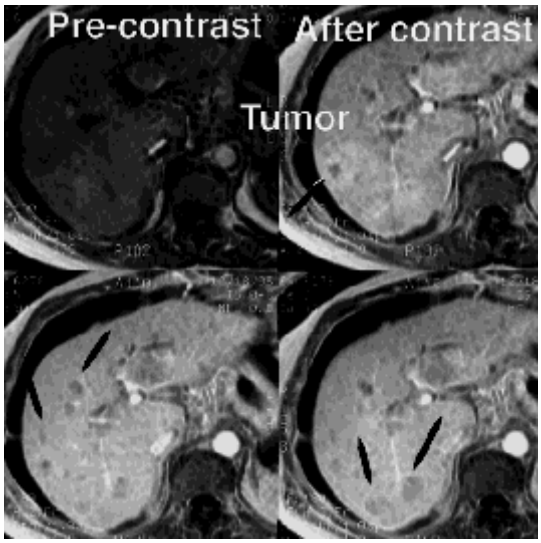

Figure 3.10: Magnetic resonance imaging of a liver with metastases. Above are shown multiple MR images after a contrast agent was injected (gadolinium based). Multiple small nodules are now seen diffusely throughout the liver, some of which are indicated by the lines.

3.4.2 Diffuse hepatic diseases

Nowadays, tests commonly used to assess liver function determine either the metabolic capacity of the liver with indocyanine green, galactose and lidocaïne as test compounds or the capacity of the liver to synthesize blood products, like cholinesterase, albumin, or coagulation factors [8].

MRI is used for the detection and characterization as well as follow-up of diffuse liver entities, such as fatty liver, hemochromatosis, and cirrhosis, obviating the need for biopsy in many cases. It allows the diagnosis of fatty liver, and the quantification of the hepatic fat content. This feature may be clinically useful in the evaluation of patients with metabolic and hepatotoxic conditions [9]. MRI is a sensitive and specific technique for identifying hepatic iron deposition, also allowing the characterization of its distribution. Patients with hemochromatosis or cirrhosis have an increased risk for hepatocellular carcinomas.

3.5 MRI contrast agents

MRI contrast agents are substances with magnetic properties which are used to improve tissue discrimination. They are intravenously administered to patients during the MRI exam. Their indication includes lesion characterization and detection as well as angiographic MR sequences. This section begins with the description of the effects of contrast agents on the MR signal. Then, the different categories of contrast agents used for MRI of the liver such as nonspecific extracellular gadolinium chelates, hepatobiliary and reticuloendothelial system (RES) contrast agents are discussed. Finally, the hepatic transporters suspected to play a key role in the transport of hepatobiliary contrast agents are introduced.

3.5.1 Effect of contrast agents on the MR signal

As already discussed in section 3.3.1.3, the contrast of MR images depends on the tissue characteristics (proton density, T_1 and T_2) and on the parameters of the sequences. The mechanism of action of MR contrast agents is indirect: they exert their effects by shortening the relaxation times T_1 and T_2 for protons that surround the molecule of the contrast agent. In other words, they increase the relaxation rates $1/T_1$ and $1/T_2$, which either enhances or diminishes the signal intensity.

The relaxation rates observed ($1/T_1$ and $1/T_2$) are the addition of the intrinsic rate of the tissues and of the rate due to the contrast agent, as expressed by equation 3.1 [10]:

$$1/T \text{ observed} = 1/T \text{ intrinsic} + 1/T \text{ contrast agent} \qquad \text{[Equation 3.1]}$$

3.5.1.1 Concentration of contrast agent and relaxation rate

The effect of the contrast agent on the relaxation rate is linearly correlated to its concentration, according to equations 3.2 and 3.3.

$$1/T_1 = 1/T_{1(0)} + (r_1 \cdot c) \qquad \text{[Equation 3.2]}$$

$$1/T_2 = 1/T_{2(0)} + (r_2 \cdot c) \qquad \text{[Equation 3.3]}$$

These relations permit to determine, under fixed conditions (magnetic field, temperature, dilution solution), the r_1 and r_2 relaxivities, defined as the slope of the straight lines obtained by plotting the relaxation rates $1/T_1$ and $1/T_2$ as a function of the concentration of contrast agent (figure 3.11).

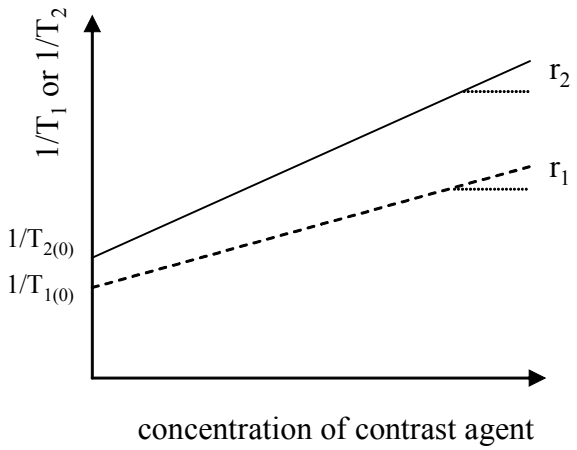

Figure 3.11: Plot of the relaxation rate $1/T_1$ and $1/T_2$ as a function of the contrast agent concentration.

3.5.1.2 Relaxation rates and contrast agent classes

Two classes of contrast agents are used: the paramagnetic and the superparamagnetic contrast agents. The effect of these two classes on the MR signal at usual doses is globally opposed.

A macroscopic magnetization appears when paramagnetic agents are placed in a magnetic field. They are composed of chelates of the paramagnetic metals gadolinium (Gd^{3+}) or manganese (Mn^{2+}). Chelation of Gd^{3+} and Mn^{2+} is necessary to decrease the high acute toxicity of the free metal ions. The r_1 and r_2 relaxivities of paramagnetic contrast agents are in the same range of values. Hence, they decrease both T_1 and T_2. As T_1 of the tissues is much higher than T_2 (about 10 times), the T_1 effect predominates the T_2 effect. The decrease of T_1 produces an enhancement of the MR signal intensity on T_1-weighted sequences. For this reason, these contrast agents are called positive or T_1-enhancing agents.

Superparamagnetic agents are substances which have a permanent macroscopic magnetization. They are composed of iron oxide nanoparticules [11]. As their r_2 relaxivity is very high and preponderant over the r_1 relaxivity, the T_2 effect predominates the T_1 effect. The decrease of T_2 diminishes the MR signal intensity on T_2-weighted but also to some extent on

T_1-weighted sequences. This class of contrast agents that decrease T_2 are called negative or T_2-enhancing agents.

3.5.1.3 Effect of the concentration of contrast agent on the MR signal

Although the relation between the relaxation rate and the concentration is linear, the MR signal is not linearly correlated to the concentration of contrast agent. Actually, the signal intensity is related to T_1, T_2 and the parameters of the data acquisition sequence by a nonlinear function. For instance the spin-echo sequence, which is commonly used in MRI, is described by equation 3.4, where s is a constant depending on the sensitivity of the signal detection of the scanner, ρ expresses the spin density, TR and TE are the repetition and echo times.

$$SI = s \cdot \rho \cdot (1-\exp(-TR/T_1)) \cdot \exp(-TE/T_2) \qquad \text{[Equation 3.4]}$$

In this sequence, the signal is weighted by T_1 and T_2 in an opposite manner. Thus, a decrease of T_1 induces an increase of SI as long as the decrease of T_2 is not too important to diminish considerably the signal intensity.

Hence, the conversion of the MR signal into contrast agent concentration, which is useful for the quantification of tissue perfusion or for a pharmacokinetic analysis, is not trivial. In the first step, the MR signal has to be converted into $1/T_1$ or $1/T_2$, which requires a signal calibration for each sequence used. In the second step, $1/T_1$ or $1/T_2$ has to be converted into the contrast agent concentration according to the linear relation existing between these parameters.

3.5.2 Contrast agents used for the MRI of the liver

Regarding their target tissue, contrast agents used for the MRI of the liver can be divided in two main categories: nonspecific extracellular and hepatospecific intracellular contrast agents. The later can be further subdivided in hepatobiliary and reticuloendotelial system

(RES) contrast agents. The different types of contrast agents and their distribution are presented schematically in figure 3.12.

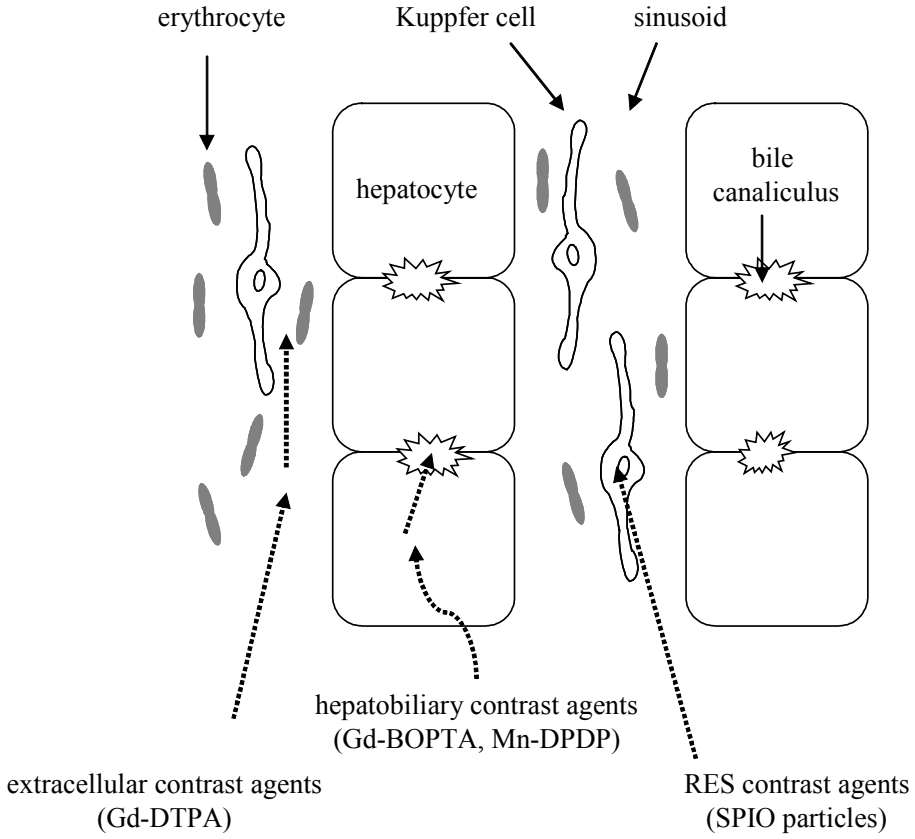

Figure 3.12: Hepatic distribution of the MRI contrast agents [11].

3.5.2.1 Nonspecific extracellular contrast agents

There are several nonspecific extracellular gadolinium chelates available on the market: Gd-DTPA, Gd-HP-DO3A, Gd-DOTA and Gd-DTPA-BMA, Gd-DTPA-BMEA, and Gd-DO3A-butriol. Their generic and trade names are listed in table 3.2. They are of relatively small molecular weight (<1000 Dalton) and follow the same kind of kinetics. They diffuse freely into and out of the interstitial space of the liver and are excreted exclusively by the kidneys. They improve tissue differentiation between normal parenchyma and tumors because of the differences in perfusion, capillary permeability and interstitial leakage of normal and

tumoral tissue [11]. They have no protein binding and are not metabolized [12]. Besides liver enhancement, gadolinium chelates are able to detect blood-brain barrier (BBB) defects, myocardial infarction and vascular disorders.

Table 3.2: Classification of some resonance magnetic contrast agents approved, or to be approved, for clinical use.

Short name	Generic name	Trade name	Firm
Extracellular contrast agents			
Gd-DTPA	Gadopentetate dimeglumine	Magnevist^{Ò}	Schering AG, Berlin, Germany
Gd-HP-DO3A	Gadoteridol	ProHance^{Ò}	Bracco SpA, Milan, Italy
Gd-DOTA	Gadoterate	Dotarem^{Ò}	Guerbet, Aulnay-sous-Bois, France
Gd-DTPA-BMA	Gadodiamide	Omniscan^{Ò}	Nycomed, Oslo, Norway
Gd-DTPA-BMEA	Gadoversetamide	Optimark^{Ò}	Mallinckrodt, St.Louis, USA
Gd-DO3A-butriol	Gadobutrol	Gadovist^{Ò}	Schering AG, Berlin, Germany
Reticuloendothelial system contrast agents			
AMI-25	Ferumoxides	Endorem^{â} / Feridex^{â}	Advanced Magnetics, Cambridge, USA
SH U 555	Ferucarbotran	Resovist^{â}	Schering AG, Berlin, Germany
AMI-227	Ferumoxtran	Sinerem^{â} / Combidex^{â}	Advanced Magnetics, Cambridge, USA
Hepatobiliary contrast agents			
Mn-DPDP	Mangafodipir trisodium	Teslascan^{â}	Nycomed, Oslo, Norway
Gd-BOPTA	Gadobenate dimeglumine	MultiHance^{â}	Bracco SpA, Milan, Italy
Gd-EOB-DTPA	Gadoxetic acid	Eovist^{â}	Schering AG, Berlin, Germany

3.5.2.2 Hepatospecific intracellular contrast agents

A variety of hepatospecific contrast agents have been developed for contrast-enhanced MR imaging of the liver. They have been targeted either to hepatocytes (hepatobiliary contrast agents) or to phagocytic reticuloendothelial system cells such as Kupffer cells (RES contrast agents) [13].

3.5.2.2.1 Reticuloendothelial system contrast agents

Reticuloendothelial system (RES) contrast agents consist of coated crystalline superparamagnetic iron oxide particles of 30 to 150 nm diameter, also called SPIO or MION particles. The coating of anchored surface molecules, usually a polysaccharide like dextran, stabilizes the particles in aqueous colloïdal solution.

Three iron oxide contrast agents have reached the commercial status:

AMI-25 is a SPIO colloid with low molecular weight dextran coating, resulting in a particle size of 50 ± 19 nm as determined by electron microscopy and 120 to 180 nm by photocorrelation spectroscopy.

SH U 555 is a SPIO colloid with carboxydextran coating, the resilatant microparticles having a mean hydrodynamic diameter of 61 nm and

AMI-227 is a USPIO (ultrasmall SPIO) consisting of a 5 nm-diameter iron oxide core covered with T10 dextran, yielding a particle with a mean diameter of 17 to 20 nm.

Their generic and trade names are listed in table 3.2.

RES contrast agents are cleared from the blood by phagocytosis by the reticuloendothelial system, so that uptake is observed in particular by Kupffer cells in the liver [11], but also in the spleen, lymph nodes, and bone marrow [9]. Iron oxide particles increase the sensitivity of MR imaging for the detection of lesions located in those tissues. Most focal liver lesions, particularly metastases, are composed of tissue without Kupffer's cells or without the capacity to take up particles. As a result, the contrast between lesion and liver is increased.

After the uptake of the RES contrast agents into phagocytic cells by receptor mediated endocytosis, they are transported to the lysosomal compartment where final breakdown appears to occur. From there, elemental iron is slowly released and subsequently used for hemoglobin synthesis [14].

3.5.2.2.2 Hepatobiliary contrast agents

Hepatobiliary contrast agents are soluble paramagnetic molecules taken up in hepatocytes and partially excreted into the bile. The property of being specifically taken up by functional hepatocytes gives these contrast agents a dual imaging capability: as extracellular agents, and as liver-specific agents whose properties permit an improved lesion to liver contrast.

Hepatocyte-directed MRI contrast agent enter the hepatocytes and generate a high and long lasting contrast-to-noise ratio that significantly increases the sensitivity of MRI for the detection of focal and diffuse liver impairment. As they are eliminated in part through the biliary system, they permit evaluation of hepatocyte function, of the liver excretory function and of the appearance and integrity of the biliary tree. Intracellular uptake is a specialized function of hepatocytes lacking in other tissues, such as metastases.

There are essentially two types of hepatobiliary agent: the manganese-based and the gadolinium-based agents. Generic and trade names are listed in table 3.2.

Manganese-based contrast agents

Mn-DPDP is the only commercially available example of a manganese-based contrast agent. The dissociation of Mn-DPDP to free manganese ions (Mn^{2+}) and free DPDP ligands occurs primarily in the liver, whereas a minor portion of the dissociated Mn^{2+} found in the liver comes from dissociation of the complex in the blood. Most of the dissociated Mn^{2+} in the liver becomes bound to macromecules and is responsible for the enhancement of the relaxivity observed with this agent [15].

The uptake mechanism of Mn-DPDP still remains unknown. Mn-DPDP is related synthetically to the vitamin B_6 analogue pyridoxal phosphate, a biochemical similarity that suggests that Mn-DPDP exploits the vitamin B_6 pathway of uptake into hepatocytes [16,17]. But other authors affirm that the vitamin B_6 carrier is not involved in the uptake of the paramagnetic complex [18,19]. The uptake of the free Mn^{2+} resulting from the minor decomplexation in the blood could be ascribed to the presence of a selective transporter for this cation. The uptake of the complex is hypothetical: passive diffusion through the membrane or nonspecific uptake by an anion transporter.

The amount of Mn^{2+} excreted into the bile represents 22-47% of the total dose in rats [20], and 50-60% [21] in humans, the remaining of the dose being excreted through the kidneys. None of the references cited mentioned the mechanisms involved in the excretion of Mn^{2+} into the bile.

Gadolinium-based contrast agents

There are two commercial examples of hepatobliary gadolinium-based contrast agents: Gd-BOPTA and Gd-EOB-DTPA. Both have the same basic Gd-DTPA structure into which a lipophilic moiety has been introduced (figure 3.13).

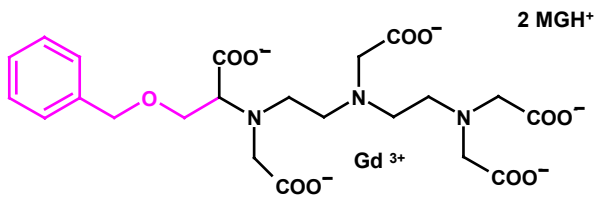

Gd-BOPTA

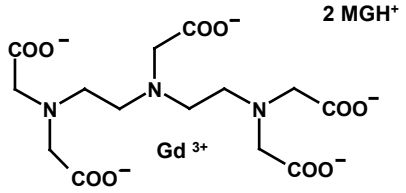

Gd-DTPA

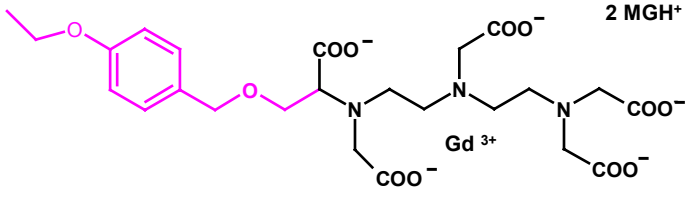

Gd-EOB-DTPA

Figure 3.13: Chemical structure of the extracellular MRI contrast agent Gd-DTPA, and the hepatospecific contrast agents Gd-BOPTA and Gd-EOB-DTPA.

An increased liver distribution space compared to that available for purely extracellular fluid contrast agents appears to be the main mechanism behind the enhancement of normal parenchymal signal intensity by hepatospecific gadolinium chelates. Microviscosity effects inside hepatocytes and, to a lesser extent, affinity for intracellular macromolecules may also add to their relaxation effectiveness. Gd-BOPTA and Gd-EOB-DTPA have a weak affinity for proteins [12,22,23] and undergo no biotransformation [23,24] .

The transport of the hepatospecific contrast agents Gd-BOPTA and Gd-EOB-DTPA into rat hepatocytes has not been fully elucidated (table 3.3). Some authors suggest a transport through passive diffusion [25], while others evoke that Gd-BOPTA is transported by the specific organic anion transporting polypeptide OATP1/oatp1 [26]. The possible inhibition by bromosulfophtalein (BSP) is debated, too.

Table 3.3: Study of the uptake mechanisms of Gd-BOPTA and Gd-EOB-DTPA.

Experimental models	Gd-BOPTA	Gd-EOB-DTPA	References
Rats	Partial inhibition by BSP	Not studied	De Haën, 1995 [27]
Phospholipid monolayers	No transport ⇒ No passive diffusion	No transport ⇒ No passive diffusion	Moncelli, 1998 [28]
Rat sinusoidal membrane vesicles	Passive diffusion Not inhibited by BSP	Passive diffusion Not inhibited by BSP	Pascolo, 1999 [25]
Oocytes transfected with human OATP cRNA	No transport	No transport	Pascolo, 1999 [25] Van Montfoort, 1999 [26]
Oocytes transfected with rat oatp1 cRNA	Not studied	Oatp1 mediated transport inhibited by BSP, taurocholate rifamycin and rifampicin	Van Montfoort, 1999 [26]

Table 3.4: Summary of the properties and pharmacokinetic parameters of the different categories of contrast agents used for MRI of the liver [17].

	Extracellular Gd^{3+} chelates	RES contrast agents	Hepatobiliary contrast agents		
			Gd-BOPTA	Gd-EOB-DTPA	Mn-DPDP
Target tissue	Blood / interstitial space	RES	Hepatocytes	Hepatocytes	Hepatocytes
Typical dose [μmol/kg]	100	10-15	50-500	30-100	3-10
Uptake transport	No	Phagocytosis	OATP1/oatp1?	OATP1/oatp1?	Vitamin B6 transporter ?
Excretion transport	No	No	MRP2/mrp2	MRP2/mrp2	?
Plasma half-life [min]	10	10	15	10	120
Elimination route	100% renal	100% iron metabolism	Hepatobiliary: Rat: 44 - 52% Human: 2-7%	Hepatobiliary: Rat: 63-80% Human: 50%	Hepatobiliary: Rat: 22-47% Human: 50-60%
Protein binding	No	Nf	Weak affinity for albumin	10-17% to plasma proteins	Mn^{2+} complexes: no Mn^{2+}: yes
Biotransformation	No	Iron metabolism	No	No	*In vivo* dissociation to Mn^{2+} and DPDP
Imaging properties	T_1 enhancement	T_2, T_1 enhancement	T_1 enhancement	T_1 enhancement	T_1 enhancement

References are found in the text related to each contrast agent (? = not fully understood, Nf = not found in the literature)

The excretion of Gd-BOPTA and Gd-EOB-DTPA into the bile occurs via the multidrug resistance-associated protein MRP2/mrp2 at the canalicular side of the hepatocyte [22,29-31] and is highly dependant on the species. In the rat, 44-52% of the dose of Gd-BOPTA is excreted into the bile, whereas this percentage is only 2-7% in humans [24,25] . In the case of Gd-EOB-DTPA, 63-80% of the dose is excreted in the bile in rats [20] and about 50% in humans [16].

To summarize, table 3.4 provides a comparative compilation of properties and pharmacokinetics of the different categories of contrast agents used for MRI of the liver.

3.5.3 Hepatic transporters

The liver plays the principal role in the clearance and metabolism of endogenous and xenobiotic substances. Following uptake into the hepatocytes, compounds undergo biotransformation and are subsequently eliminated from the liver cell via excretion into the bile or via transport back to the sinusoid (figure 3.12). Thus, there are several kinds of transporters present in the hepatocyte membrane. In this section, we will focus on the transporters involved in the transport of bile acids, in particular the OATP and MRP families, as they are known or suspected to play a key role in the transport of hepatobiliary contrast agents.

Table 3.5 summarizes the OATP/oatp and MRP/mrp transporters expressed in the liver, with respect to their tissue distribution, function, substrates and modulation of their expression. As a convention, capital and small letters are used when referring to human and rat, respectively. Differences between species exist in terms of the amino acid sequence of transporters. Some transporters have their orthologue in rats and in humans, others not.

Table 3.5: Characteristics of OATP/oatp and MRP/mrp transporters of the hepatocyte membrane [32,33].

Transporter	Tissue distribution	Function and substrates	Expression
Rat			
oatp1	liver (sinusoidal), kidney, brain	entry of bile acids and organic anions, BSP, steroids, ouabain, temocaprilat, Gd-BOPTA?, Gd-EOB-DTPA?	↓ cholestase
oatp2	liver (sinusoidal), kidney, brain	entry of bile acids, digoxin, T4, temocaprilate	
oatp3	liver, brain, kidney	entry of bile acids	
oatp4	liver (sinusoidal)	entry of bile acids, bilirubin monoglucuronide, conjugated steroids, T4, peptides	
mrp1	liver (sinusoidal)	export of organic anions and di-anionic bile salts, glucuronide and glutathione conjugates	↑ endotoxaemia
mrp2	liver (canalicular), kidneys	export of glucuronide and glutathione conjugates, Gd-BOPTA, Gd-EOB-DTPA	
mrp3	liver (sinusoidal), cholangiocytes	export of organic anions and di-anionic bile salts, monovalent bile acids, glucuronide and glutathione conjugates	↑ in EHBR (mrp2 defect) and cholestasis
Human			
OATP-A	liver (sinusoidal?), lung, kidney	entry of bile acids and organic anions	
OATP-C	liver (sinusoidal)	entry of bile acids and organic anions, bilirubin monoglucuronide, conjugated steroids, T4, peptides	
OATP-8	liver (sinusoidal)	entry of bile acids and organic anions, BSP, digoxin	
MRP1	liver (sinusoidal)	export of organic anions and di-anionic bile salts, glucuronide and glutathione conjugates	↑ in proliferation cells
MRP2	liver (canalicular), kidneys	export of conjugated bile acids, conjugated bilirubin, and organic anions, glucuronide and glutathione conjugates, Gd-BOPTA, Gd-EOB-DTPA	
MRP3	liver (sinusoidal), cholangiocytes, enterocytes	export of conjugated bile acids, glucuronide and glutathione conjugates	↑ in Dubin-Johnson syndrome (MRP2 defect) and cholestasis

BSP: bromosulfophtalein, T4: thyroxine, EHBR: Eisai hyperbilirubinaemic rats, ?: not fully understood

3.5.3.1 Organic anion-transporting polypeptide

The organic anion-transporting polypeptides are members of a growing family that mediates the Na^+-independent uptake of many amphiphatic compounds, including conjugated and unconjugated bile acids [34]. Other substrates include cardiac glycosides, steroids, peptides, and selected organic cations [33].

At the present time, four rat oatps (oatp1, oatp2, oatp3 and oatp4) and 3 human OATPs (OATP-A, OATP-C, and OATP-8) have been localized in the liver for which bile salts are substrates. Beside their expression in the liver, some of them are found in other tissues. OATPs/oatps can function as bidirectional transporters [32]. Under these conditions, they could take part in the efflux of bile salts at the sinusoidal membrane when accumulation occurs in hepatobiliary diseases [33]. The hepatobiliary MRI contrast agents, Gd-BOPTA and Gd-EOB-DTPA, appear to be specific oatp1 substrates [26].

3.5.3.2 Multidrug resistance proteins

Multidrug resistance proteins are "Traffic ATPases" belonging to a superfamily of proteins found in all cellular organisms and characterized by an ABC (ATP-binding cassette) in their primary structure.

The first member of the MRP family, MRP1, was cloned from a multidrug resistant human lung cancer cell line. Since then, at least five further members have been identified. MRP2 is localized at the canalicular domain of hepatocytes and exports a range of organic anions. That is why it is also called canalicular multispecific organic anion transporter (cMOAT). A mutation in the *MRP2* gene is the basis of the Dubin-Johnson syndrome, a liver disorder characterized by chronic conjugated hyperbilirubinemia. Eisai hyperbilirubinaemic rats (EHBR) have an equivalent mrp2 defect. A third MRP member, MRP3/mrp3, is found in the liver. Both MRP1/mrp1 and MRP3/mrp3 are expressed at the basolateral surface of normal hepatocytes, but at very low levels. They are able to export bile acids at the basolateral

surface of hepatocytes. Gd-BOPTA and Gd-EOB-DTPA are known to be excreted into the bile via mrp2 [29,30] .

3.5.3.3 Expression in injured livers

Some diseases can modify the expression of certain hepatic transporters (table 3.5). For instance, oatp1 is down regulated in experimental cholestasis, induced either by a bile duct ligation or by endotoxin [32]. MRP1 is upregulated in the endotoxaemic rat liver. MRP3 is induced in patients with the Dubin-Johnson syndrome and in primary biliary cirrhosis. Rat mrp3 is similarly induced in livers of EHBR rats and in experimental cholestasis. The inducible nature of MRP1 and MRP3 and their location at the basolateral surface of hepatocytes may explain the shift towards renal excretion as the major mechanism for bile acid elimination in patients with some forms of cholestasis.

According to these changes in the expression of receptors induced by definite diseases, hepatospecific contrast agents are expected to modify their distribution in the presence of hepatic diseases. The resulting change in the liver MRI signal enhancement has a potential to evaluate the hepatic function.

3.6 Conclusion

This chapter underlines the fact that powerful techniques of medical imaging are now available. These techniques permit to get very useful information about the inside of the body and to distinguished pathologies, which could otherwise not be detected. In particular, MRI enables to obtain a very high degree of anatomic precision without the use of ionizing radiation and, despite a high cost, its use is now spreading over the world.

The section dealing with the contrast agents used for MRI of the liver emphasizes that the mechanisms of action of some contrast agents, in particular hepatobiliary contrast agents, are still not fully understood. A better understanding of the mechanisms of action of these

contrasts agents as well as how these mechanisms are altered in focal and diffuse hepatic diseases could constitute a supplementary useful tool in MRI diagnostics. These reflections were taken as a basis for the initiation of the project of this thesis and thus, the experiments described in the following chapters.

References

[1] Csillag A, Introduction, In 'Atlas d'imagerie médicale', Ed. Könemann Verlaggesellschaft, Vince Books, Cologne, 2000, pp. 13-32.

[2] Internet Communication, Radiological Society of North America and American College of Radiology, Radiology info, http://192.203.125.55/

[3] Internet Communication, Hornak J-P, The basics of MRI, http://www.cis.rit.edu/htbooks/mri/

[4] Correas J-M, Bridal L, Lesavre A, Méjean A, Claudon M, and Hélénon O, Ultrasound contrast agents: properties, principles of action, tolerance, and artifacts, *Eur Radiol*, 2001, **11**, 1316-1328.

[5] Vallée J-P, Tissue perfusion quantification using magnetic resonance imaging and contrast media, *Thèse de doctorat*, Université de Genève, 1999

[6] Takayasu K, and Okuda K, Magnetic resonance imaging (MRI), In 'Imaging in liver disease', Oxford University Press, 1997, pp. 448-450.

[7] Bartolozzi C and Spinazzi A, MultiHance: help or hype?, *J Comput Assist Tomogr*, 1999, **23 (suppl. 1)**, S151-S159.

[8] Schmitz SA, Mühler A, Wagner S, and Wolf K-J, Functional hepatobiliary imaging with gadolinium-EOB-DTPA. A comparison of magnetic resonance imaging and 153gadolinium-EOB-DTPA scintigraphy in rats, *Invest Radiol*, 1996, **31**, 154-160.

[9] Taylor HM and Ros PR, Hepatic imaging, *Radiol Clin North Am*, 1998, **36**, 237-245.

[10] Internet Communication, Université de Rennes, http://www.med.univ-rennes1.fr/cerf/edicerf/BASES/BA002_cv_rb_21.html

[11] Clément O, Siauve N, Cuénod C-A, Vuillemin-Bodaghi V, Leconte I, and Frija G, Mechanisms of action of liver contrast agents: impact for clinical use, *J Comput Assist Tomogr*, 1999, **23**, S45-S52.

[12] Cavagna FM, Maggioni F, and Castelli PM, Gadolinium chelates with weak binding to serum proteins. A new class of high-efficiency, general purpose contrast agents for magnetic resonance imaging, *Invest Radiol*, 1997, **32**, 780-796.

[13] Reimer P, Bader A, and Weissleder R, Application of a stable cell culture assay for the functional assessment of novel MR contrast agents, *Eur Radiol*, 1997, **7**, 527-531.

[14] Schulze E, Ferrucci JT, Poss K, Lapointe L, Bogdanova A, and Weissleder R, Cellular uptake and trafficking of a prototype magnetic iron oxide label *in vitro*, *Invest Radiol*, 1995, **30**, 604-610.

[15] Gallez B, Bacic G, and Swartz HM, Evidence for the dissociation of the hepatobiliary MRI contrast agent Mn-DPDP, *Magn Reson Med*, 1996, **35**, 14-19.

[16] Hahn PF and Saini S, Liver-specific MR imaging contrast agents, *Radiol Clin North Am*, 1998, **36**, 287-297.

[17] Semelka RC and Helmberger TKG, Contrast agents for MR imaging of the liver, *Radiology*, 2001, **28**, 27-38.

[18] Colet J-M, Elst LV, and Muller RN, Dynamic evaluation of the hepatic uptake of manganese-based MRI contrast agents: a 31P NMR study on the isolated perfused rat liver, *JMRI*, 1998, **8**, 663-669.

[19] Gallez B, Baudelet C, Adline J, Charbon V, and Lambert DM, The uptake of Mn-DPDP by hepatocytes is not mediated by the facilitated transport of pyridoxine, *Magn Reson Imaging*, 1996, **14**, 1191-1195.

[20] Mühler A, Clément O, Vexler V, Berthezène Y, Rosenau W, and Brasch RC, Hepatobiliary enhancement with Gd-EOB-DTPA: comparison of spin-echo and STIR imaging for detection of experimental liver metastases, *Radiology*, 1992, **184**, 207-213.

[21] Wang C, Gordon PB, and Hustvedt O, MR imaging properties and pharmacokinetics of Mn-DPDP in hepathy volunteers, *Acad Radiol*, 1997, **38**, 665-676.

[22] De Haën C, La Ferla R, and Maggioni F, Gadobenate dimeglumine 0.5 M solution for injection (Multihence) as contrast agent for magnetic resonance imaging of the liver: mechanistic studies in animals, *J Comput Assist Tomogr*, 1999, **23 (Suppl. 1)**, S169-S179.

[23] Schuhmann-Giampieri G, Frenzel T, and Schmitt-Willich H, Pharmacokinetics in rats, dogs and monkeys of a gadolinium chelate used as a liver-specific contrast agent for magnetic resonance imaging, *Drug Res*, 1993, **43 (II)**, 927-931.

[24] Lorusso V, Arbughi T, Tirone P, and De Haën C, Pharmacokinetics and tissue distribution in animals of gadobenate ion, the magnetic resonance imaging contrast enhancing component of gadobenate dimeglumine 0.5 M solution for injection (MultiHance), *J Comput Assist Tomogr*, 1999, **23 (Suppl. 1)**, 181-194.

[25] Pascolo L, Cupelli F, Anelli PL, Lorusso V, Visigalli M, Uggeri F, and Tiribelli C, Molecular mechanisms for the hepatic uptake of magnetic resonance imaging contrast agents, *Biochem Biophys Res Commun*, 1999, **257**, 746-752.

[26] Van Montfoort JE, Stieger B, Meijer DKF, Weinmann H-J, Meier PJ, and Fattinger KE, Hepatic uptake of the magnetic resonance imaging contrast agent gadoxetate by the organic anion transporting polypeptide Oatp1, *J Pharmacol Exp Ther*, 1999, **290**, 153-157.

[27] Freshney RI, Specialized cells, In 'Culture of Animal Cells', Ed. Freshney RI, Alan R. Liss, New York, 2000, pp. 345-384.

[28] Moncelli MR, Becucci L, De Haën C, and Tirone P, Interactions between magnetic resonance imaging contrast agents and phospholipid monolayers, *Bioelectrochem Bioenerg*, 1998, **46**, 205-213.

[29] Pascolo L, Petrovic S, Cupelli F, Bruschi CV, Anelli PL, Lorusso V, Visigalli M, Uggeri F, and Tiribelli C, ABC protein transport of MRI contrast agents in canalicular rat liver plasma vesicles and yeast vacuoles, *Biochem Biophys Res Commun*, 2001, **282**, 60-66.

[30] De Haën C, Lorusso V, and Tirone P, Hepatic transport of gadobenate dimeglumine in TR- rats, *Acad Radiol*, 1996, **3**, 452-454.

[31] Lewin M, Clément O, Belguise-Valladier P, Tran L, Cuénod C-A, Siauve N, and Frija G, Hepatocyte targeting with Gd-EOB-DTPA, *Invest Radiol*, 2001, **36**, 9-14.

[32] Kullak-Ublick GA, Regulation of organic anion and drug transporters of the sinusoidal membrane, *J Hepatol*, 1999, **31**, 563-573.

[33] St-Pierre MV, Kullak-Ublick GA, Hagenbuch B, and Meier PJ, Transport of bile acids in hepatic and non-hepatic tissues, *J Exp Biol*, 2001, **204**, 1673-1686.

[34] Kullak-Ublick GA, Beuers U, Fahney C, Hagenbuch B, Meier PJ, and Paumgartner G, Identification and functional characterization of the promoter region of the human organic anion transporting polypeptide gene, *Hepatology*, 1997, **26**, 991-997.

Chapter 4
Isolation and preservation of hepatocytes

4.1. Introduction

The aim of this work was to define a procedure to enable us to keep freshly isolated hepatocytes alive, without loss of viability and function, for a long period of time. Actually, it is difficult to maintain durably the viability and functionality of freshly isolated hepatocytes. Hepatocytes maintained in suspensions are known to have a survival span of only about 4 hours [1]. To perform experiments with hepatocyte hollow fiber bioreactors (HFB), a large supply of hepatocytes was needed, which implied more than one liver isolation procedure and preservation of hepatocytes since experiment could not be performed immediately after isolation. Hence, it was imperative to have a means to preserve hepatocytes, without loss of integrity. To this end, we tested different methods with a view to preserve hepatocytes for periods up to 48 hours.

Techniques currently used to preserve cells include cryopreservation and preservation at 4°C. The danger of hepatocyte cryopreservation is a considerable loss of viability and metabolic activity after thawing [2,3], although some authors succeeded in freezing hepatocytes with very good efficiency [4-7]. It has also been reported that isolated hepatocytes could be stored at 4°C for several days in organ preservation solutions, such as the University of Wisconsin (UW) solution, without loss of viability and transport functions [8-10].

The steps to isolate rat hepatocytes are described below. Freshly isolated hepatocytes were cryopreserved for 10 days and their viability assessed after thawing and incubation at 37°C. In addition, isolated hepatocytes were used to evaluate the potential of different solutions for the preservation of hepatocytes at 4°C and for the subsequent incubation at 37°C.

4.2 Materials and methods

4.2.1 Chemicals

Bovine serum albumin (BSA, fraction V, 97%) and ethyleneglycol-O,O'-bis(2-aminoethyl)-N,N,N',N'-tetraacetic acid (EGTA) were purchased from Fluka. Collagenase from Clostridium histolicum type IV (collagen digestion activity: 295 U/mg solid), fetal calf serum (FCS), Williams E medium, and bovine pancreas insulin were obtained from Sigma Chemical (St-Louis, MO, USA). Trimetazidine (TMZ) was generously donated by Servier, Institut de Recherche International, France. All other chemicals were of analytical grade.

4.2.2 Animals

Adult male Sprague-Dawley rats (250 to 350 g) came from Charles River Lab (Iffa Credo, L'Arbresle, France). They were maintained in cages in an air-conditioned room (21-25°C, 50% humidity) with circadian day/night rhythm of 12 hours. Standard lab chow (n° 950.9, Protector S. A., Lucens, Switzerland) and water were given ad-libitum. The protocol of these studies was approved by the Cantonal Veterinary Service (authorization n° 1313).

4.2.3 Isolation of hepatocytes

Hepatocytes were isolated by a two-step collagenase perfusion of the liver first described by Seglen et al. [11]. The rats were anesthetized by an intraperitoneal injection of sodium pentobarbital (80 mg/kg). The rat abdomen was opened, a cannula (1.7 mm, 5.1 cm) was inserted into the portal vein and fixed with two silk threads (3 m, 2/0 USP, B. Braun Melsungen AG, Switzerland), as seen in figure 4.1. Simultaneously with opening the vena cava in its abdominal part, perfusion of the liver was started with preperfusion solution (isolation buffer containing 0.50 mM EGTA, adjusted to pH 7.4, 37°C). Perfusion started with a flow rate of 5 ml/min and was then progressively increased over 1 minute to 30 ml/min; perfusion was maintained at this flow rate during 10 minutes. The perfusion was then switched over to perfusion solution (isolation buffer containing 0.05% collagenase and 2.00 mM $CaCl_2$, adjusted to pH 7.55, 37°C). The composition of the isolation buffer was the following: 151 mM NaCl, 5.37 mM KCl, 0.63 mM Na_2HPO_4, 0.44 mM KH_2PO_4, 4.2 mM $NaHCO_3$, 5.55 mM glucose.

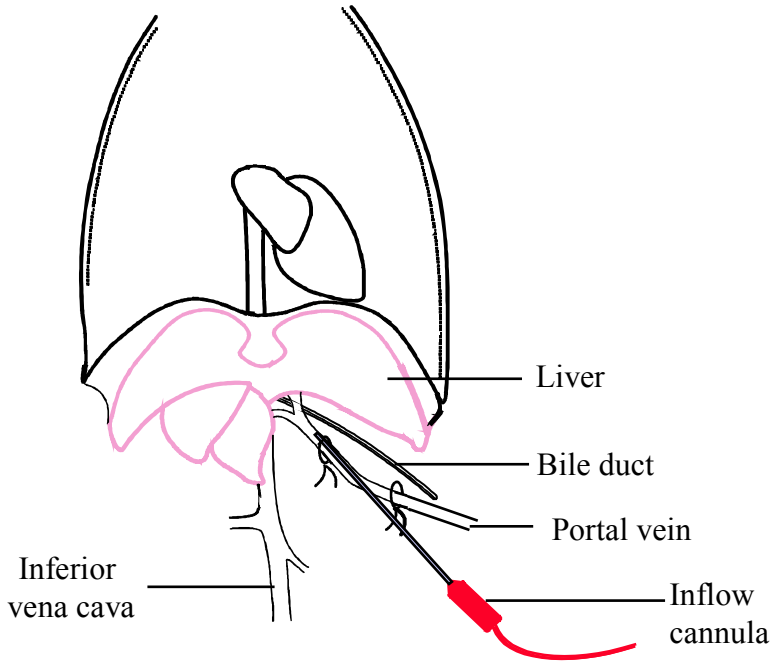

Figure 4.1: Scheme of the liver perfusion for hepatocyte isolation. The rat abdomen was opened, a cannula was inserted in the portal vein and fixed with threads.

After 10 minutes perfusion at a flow rate of 30 ml/min, the tissue was very swollen and tended to fall apart; sometimes, perfusion had to be stopped before 10 minutes. The liver was removed and transferred to an ice cold wash solution (isolation buffer containing 0.5% BSA and 0.41 mM $MgSO_4$, adjusted to pH 7.4). The hepatocytes were released by gentle shaking after disruption of the Glisson capsule (figure 4.2). The resulting cell suspension was filtered through 100 µm nylon mesh. The viable cells were allowed to sediment and the supernatant containing debris and dead cells was discarded. Cell viability was assessed by trypan blue exclusion, according to equation 4.1.

$$\text{viability}\,[\%] = \frac{\text{number of living cells}}{\text{total number of cells}} \cdot 100 \qquad \text{[Equation 4.1]}$$

The cells were washed one more time with the wash solution followed by slow centrifugation (50 g, 2 min, 4°C) to remove collagenase, damaged cells, and non-parenchymal cells. The remaining cell pellet was used to perform the experiments of cryopreservation and cold preservation at 4°C.

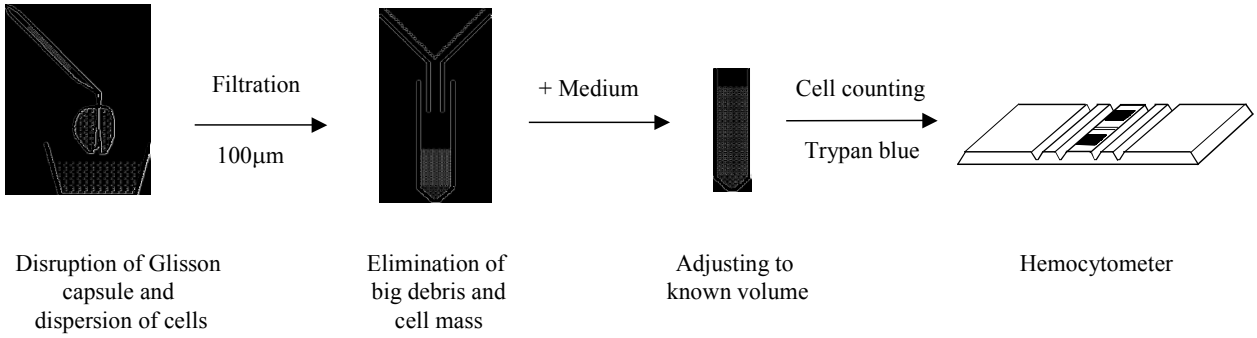

Figure 4.2: Diagram of the hepatocyte isolation procedure after perfusion with collagenase. The liver was removed from the rat abdomen, and hepatocytes were released in ice cold solution after disruption of the Glisson capsule. Cells were filtered and viability was assessed with trypan blue.

4.2.4 Cryopreservation

Two freshly isolated hepatocyte suspensions were prepared in modified Hanks's solution, with a hepatocyte density of $2 \cdot 10^6$ and $1 \cdot 10^7$ cells/ml. The composition of the modified Hanks's solution is given in table 4.1. The samples to be frozen were prepared by mixing 0.5 ml of each suspension with 0.5 ml of freezing solution in freezing tubes of 1.8 ml. Two freezing solutions were tested. Both consisted of Hanks's solution supplemented with 10% dimethylsulfoxide (DMSO), one additionally containing 10% FCS. The tubes were wrapped in padding and introduced in an expended polystyrene box, which was then placed in a –80°C freezer for 4 hours. The tubes were then rapidly transferred to liquid nitrogen, where they were kept for 10 days.

After cryopreservation, cells were thawed by rapid immersion of the freezing tubes in a water bath at 37°C. When thawing had started, the tubes were placed in ice. Hanks's solution at 4°C was added to the hepatocytes drop by drop to a volume of 1.8 ml. The suspensions were transferred in 15 ml centrifuge tubes and the addition of Hanks's solution was continued to reach 10 ml. Hepatocyte viability and recovery were immediately assessed by trypan blue exclusion, according to equations 4.1 and 4.2 respectively.

$$\text{recovery}[\%] = \frac{\text{total number of cells before freezing}}{\text{total number of cells after freezing}} \cdot 100 \qquad \text{[Equation 4.2]}$$

Cell suspensions were centrifuged (50 g, 2 min, 4°C) and the supernatant was removed to eliminate the freezing solution and damaged cells. To wash the cells, 10 ml of Hanks's solution were added to the cell pellets and the hepatocyte suspensions were centrifuged again. The cell pellets were suspended in Hanks's solution to obtain a final density of $2 \cdot 10^5$ cells/ml. To check the evolution of the viability of hepatocytes after cryopreservation and thawing, the hepatocyte suspensions were incubated (37°C, shaking, 5% CO_2 in air atmosphere) in an incubator (EG 110IR, Société Juan, Saint Herblain, France) for 3 hours. A control experiment was carried out by incubating suspensions of freshly isolated hepatocytes. Cell viability was checked every hour by trypan blue exclusion test.

4.2.5 Preservation at 4°C

Samples for the preservation of hepatocytes at 4°C were prepared by mixing $5 \cdot 10^7$ freshly isolated hepatocytes with 5 ml preservation solution in a 15 ml centrifuge tube. The tested preservation solutions were: modified Hanks's solution with or without 5% of polyethyleneglycol (PEG), modified UW solution, and Williams E medium with or without 5% of PEG, the solutions were supplemented with 0.5% of BSA and 280 U/l insulin; pH was adjusted to 7.4. The detailed composition of these solutions is given in table 4.1. The tubes were kept at 4°C in the fridge for 4, 20 or 24 hours. During the preservation at 4°C, the hepatocyte viability was assessed every hour by trypan blue.

Table 4.1: Composition of the solutions used for the preservation and incubation of hepatocytes.

		modified Hanks's		modified UW		Williams E	
Component	Mol wt.	g/l	mM	g/l	mM	g/l	mM
Inorganic salts							
$CaCl_2$	111	0.222	2.00			0.265	2.39
KCl	74.55	0.40	5.4			0.4	5.4
K_2HPO_4	136.1	0.06	0.44	3.402	25.00		
$MgCl_2 \cdot 6\ H_2O$	203.3						
$MgSO_4 \cdot 7\ H_2O$	246.5	0.10	0.41	1.232	5.000	0.0977	0.396
NaCl	58.44	7.365	126.0			6.8	116.4
$NaHCO_3$	84.01	1.5	17.9				
$Na_2HPO_4 \cdot 2\ H_2O$	177.99	0.112	0.629			0.122	0.685
$Na_2HPO_4 \cdot 7\ H_2O$	268.1						
NaOH	40			1.00	25.0		
KOH	56.1			3.09	~55		
Energy metabolism							
Glucose	180.2	1.5	8.3			2.0	11.1
Sodium pyruvate	110					0.025	0.227
Other components							
Lactobionic acid	358.3			28.664	80.0		
Raffinose	594.5			7.835	30.0		
Allopurinol	136.1			0.136	1.0		
PEG 8000	8000			50	6.25		
Phenol red	376					0.0107	0.0285
Nucleosides, etc.							
Adenosine	267.2			1.336	5.0		
Trace elements							
$CuSO_4 \cdot 5\ H_2O$	160					1E-07	6.E-07
$Fe(NO_3)_3 \cdot 9\ H_2O$	404					1E-07	2.E-07
$MnCl_2 \cdot 4\ H_2O$	125.8					1E-07	8.E-07
$ZnSO_4 \cdot 7\ H_2O$	288					2E-07	7.E-07
Antioxidants							
Glutathione red.	307					0.00005	0.0002
Lipids and precursors							
Linoleic acid methyl esther	280					0.00003	0.0001
Amino acids							
L-alanine	89					0.09	1.01
L-arginine	211					0.05	0.24
L-asparagine	132					0.02	0.15
L-aspartic acid	133					0.03	0.23
L-cysteine	176					0.04	0.23
L-cystine	240					0.02	0.08
L-glutamic acid	147					0.0445	0.3027

L-glutamine	146	0.292	2.000
Glycine	75	0.05	0.67
L-histidine	210	0.015	0.071
L-isoleucine	131	0.05	0.38
L-leucine	131	0.075	0.573
L-lysine HCl	183	0.08746	0.47792
L-methionine	149	0.015	0.101
L-phenylalanine	165	0.025	0.152
L-proline	115	0.03	0.26
L-serine	105	0.01	0.10
L-threonine	119	0.04	0.34
L-tryptophane	204	0.01	0.05
L-tyrosine	181	0.05045	0.27873
L-valine	117	0.05	0.43
Vitamins			
Ascorbic acid Na	176	0.00227	0.01290
D-biotin	244	0.0005	0.0020
Calciferol	300	0.0001	0.0003
Choline chloride	140	0.0015	0.0107
Folic acid	441	0.001	0.002
Myo-inositol	180	0.002	0.011
Menadione	172	0.00001	0.00006
Niacinamide	122	0.001	0.008
DL-pantothenic acid	238	0.001	0.004
Pyridoxal HCl	204	0.001	0.005
Retinol acetate	329	0.0001	0.0003
Riboflyavin	376	0.0001	0.0003
Thiamine HCl	337	0.001	0.003
DL-α-tocopherol	430	0.00001	0.00002
Vitamin B12	1355	0.0002	0.0001

After cold preservation, the viability of hepatocytes was immediately evaluated by trypan blue exclusion. The tubes were then centrifuged (50 g, 2 min, 4°C), and the supernatant was removed to eliminate the preservation solution. The cell pellets were washed once more with 10 ml incubation solution. The cell pellets were mixed with 10 ml incubation solution at 4°C. The resulting suspensions were poured in Erlenmeyers of 500 ml and 90 ml of incubation solution at 37°C were added to each suspension. To assess the evolution of the viability of hepatocytes after preservation at 4°C, the hepatocyte suspensions were incubated at 37°C for 2 hours. The tested incubation solutions were modified Hanks's solution with or without

TMZ 10^{-6} M and Williams E medium, the solutions were supplemented with 0.5% of BSA and 280 U/l insulin, pH 7.2. A control experiment was carried out by incubating suspensions of freshly isolated hepatocytes. The viability of hepatocytes was checked at 30 minutes intervals by trypan blue exclusion.

4.3 Results

4.3.1 Isolation of hepatocytes

The isolation procedure by a two-step collagenase perfusion resulted in a yield of 4-6·10^8 hepatocytes per liver. Cell viability was routinely greater than 90% as assessed by trypan blue exclusion. The criterion for positive trypan blue staining was a visible blue nucleus, while living cells were smaller, round and yellow. The hepatocytes were purified from cell debris, dead cells and other smaller cells of the liver by slow centrifugation.

The isolation procedure was initiated by a perfusion of a calcium-free EDTA buffer. EDTA is a Ca^{2+} and K^+ chelator, which weakens the intercellular bonds and thus facilitates the action of collagenase, perfused in a second time. Calcium is necessary for collagenase action and was added to the collagenase solution.

4.3.2 Cryopreservation

To assess the viability and recovery of isolated hepatocytes after cryopreservation, suspensions of hepatocytes at densities of 1·10^6 and 5·10^6 cells/ml in freezing solutions containing 10% DMSO with or without FCS were kept in liquid nitrogen for 10 days. Their viability and recovery immediately after thawing as determined by trypan blue exclusion are depicted in figure 4.3.

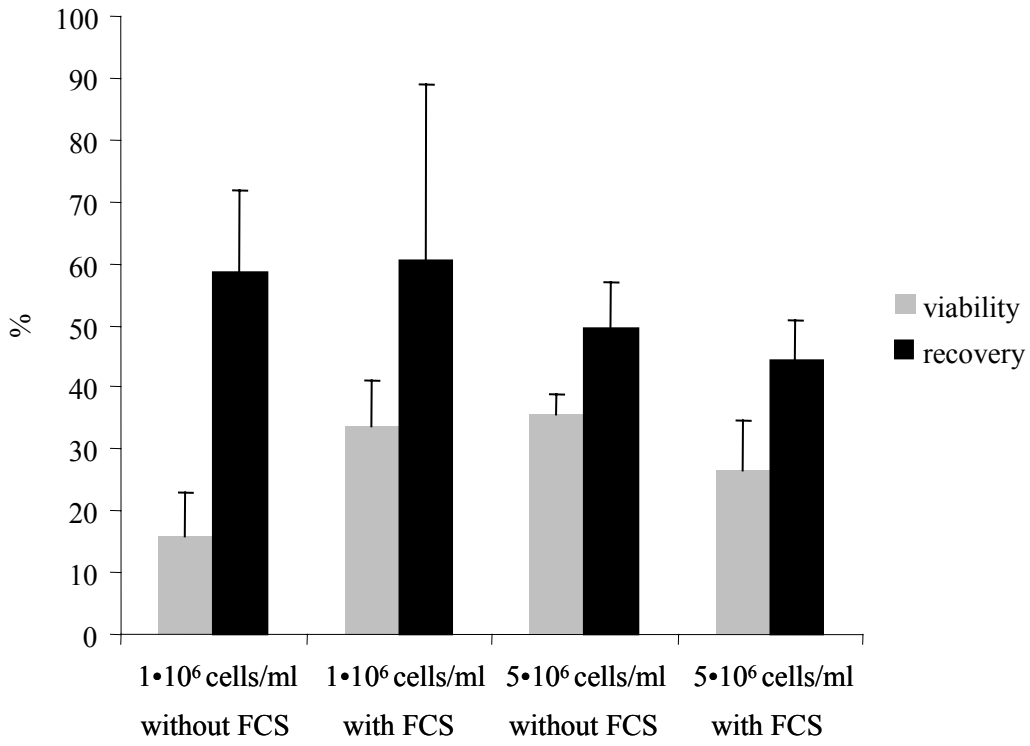

Figure 4.3: Viability and recovery of hepatocytes after thawing of suspensions containing $1 \cdot 10^6$ and $5 \cdot 10^6$ cells/ml in freezing solution with or without FCS, kept in liquid nitrogen for 10 days (n = 3).

Cell recovery indicates the amount of hepatocytes still detectable with trypan blue after freezing. It is expressed as a percentage of the number of cells detectable before freezing. Thus, it includes viable and dead cells, as classified according to the blue or yellow coloration of the hepatocytes by trypan blue. The measure of viability takes into account the viable cells only and is expressed as a percentage of the total number of cells detectable after freezing. Recovery after freezing was about 50-60%, as seen in figure 4.4. These results indicate that about 30-40% of the hepatocytes were totally disintegrated during cryopreservation. Among the 50-60% of hepatocytes recovered after thawing, viability assessment indicated that only about 20-30% were viable. Thus, only about 15% of the total number of cryopreserved hepatocytes were viable after 10 days of cryopreservation and thawing. Cell density and FCS had no considerable effect on cell recovery.

The evolution of viability of cryopreserved hepatocytes in suspension incubated at 37°C for 3 hours is shown in figure 4.4.

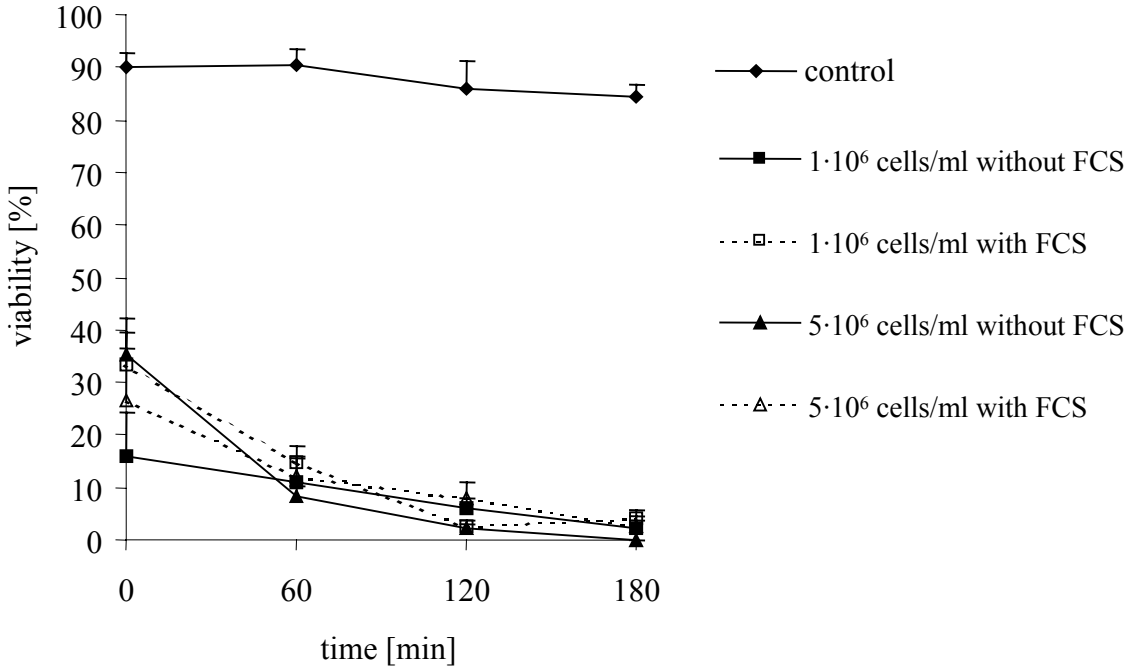

Figure 4.4: Evolution of viability of hepatocytes incubated in suspension for 3 hours after 10 days of cryopreservation. The legend indicates the freezing conditions. Hepatocytes were frozen at a density of $1 \cdot 10^6$ or $5 \cdot 10^6$ cells/ml in freezing solution containing 10% DMSO, with or without FCS (n = 3).

As can be seen, the already low viability of hepatocytes immediately after thawing dramatically fell to less than 10% after 2 hours when these cryopreserved hepatocytes were further incubated at 37°C. This indicates that, although the hepatocytes were classified as viable by trypan blue exclusion, they were not in a good state for further incubation at 37°C. A control experiment showed that the viability of freshly isolated hepatocytes in suspension remained near 90% during 3 hours of incubation.

As already seen immediately after thawing, none of the different freezing conditions did significantly improve the viability of cryopreserved hepatocytes incubated in suspension after thawing. In summary, the results presented here show that cryopreservation of hepatocytes is not a good method of preservation.

4.3.3 Cold preservation

The effect of the composition of the preservation solution on the viability of hepatocytes maintained at 4°C for 20 hours is shown in figure 4.5.

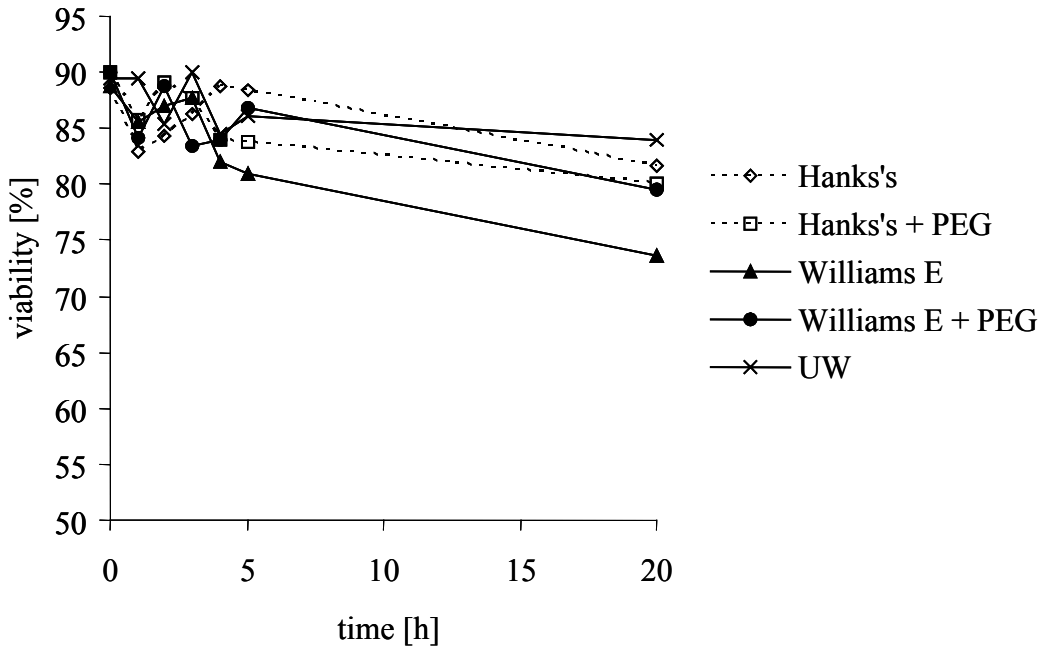

Figure 4.5: Evolution with time of the viability of hepatocytes conserved at 4°C for 20 hours in different solutions (n = 1).

After 5 hours, all investigated solutions maintained a hepatocyte viability of nearly 85%, although Williams E medium seemed to be slightly less efficient. Viability decreased slightly between 5 and 20 hours of preservation at 4°C, the decline being more pronounced with Williams E medium. The results further show that PEG had no effect on cell viability. Indeed, Williams E medium with additional PEG gave a better viability than Williams E medium alone, but Hanks's solution alone gave better results than Hanks's supplemented with PEG.

The morphological examination of the cells showed an alteration of the cell shape when hepatocytes were preserved in Hanks's solution, Hanks's solution + PEG, Williams E medium,

and Williams E medium + PEG. Processes of vacuolisation and cell swelling were observed, the phenomenon becoming more pronounced with time. Only hepatocytes preserved in UW solution retained a stable round shape. To summarize, the best results were obtained with a UW solution which maintained a cell viability of 85% after 20 hours of preservation at 4°C, without loss of membrane integrity. With all other preservation solutions a cell viability of about 80% could be ensured after 20 hours of storage at 4°C and alterations of the membrane were observed.

The evolution of the viability during incubation at 37°C after cold preservation was also assessed. Figure 4.6 presents the effect of the preservation solution, in which hepatocytes were kept at 4°C for several hours, and the effect of the incubation solution, in which hepatocytes were incubated for 2 hours at 37°C after the cold storage.

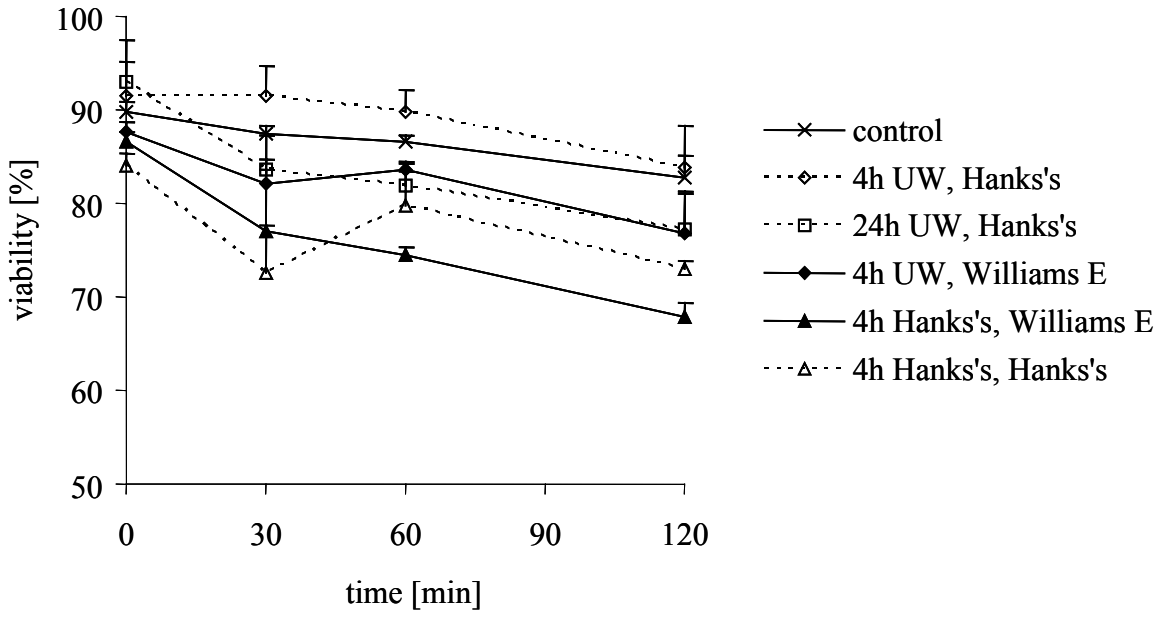

Figure 4.6: Evolution with time of the viability of hepatocytes incubated at 37°C for 2 hours in Williams E or Hanks's solution after preservation at 4°C for 4 or 24 hours in UW or Hanks's solution. In the legend, the first name indicates the preservation solution and the second, the incubation solution. A control experiment was performed by incubating suspensions of freshly isolated rat hepatocytes without cold preservation (n = 3).

The viability at time zero indicates the viability after the period of preservation at 4°C. After 4 and 24 hours of preservation at 4°C in UW and Hank's solutions, the viability of hepatocytes was better than 85%, as already seen in figure 4.5.

For all investigated incubation conditions, hepatocytes viability decreased slightly during the 2 hours of incubation at 37°C. Better viabilities during incubation were obtained when the hepatocytes had been preserved at 4°C in UW solution. Hence, the preservation solution influenced not only the viability during cold storage, but also the viability during incubation at 37°C. When looking more closely at the effect of the incubation solution, it can be observed that hepatocytes incubated in Hanks's solution had a better viability than those incubated in Williams E medium. Hence, the best results were obtained when hepatocytes were preserved at 4°C in UW solution and incubated at 37°C in Hanks's solution. Under these conditions, hepatocytes could be kept 24 hours at 4°C and incubated for 2 hours without a significant loss of viability.

To investigate the possible effect of TMZ on the cold preservation of hepatocytes, TMZ was added to the UW solution at a concentration of 10^{-6} M. Figure 4.7 shows the evolution of the viability of hepatocytes incubated in suspension in Hanks's solution at 37°C for 2 hours, after preservation at 4°C for 24 or 48 hours in UW solution with or without TMZ.

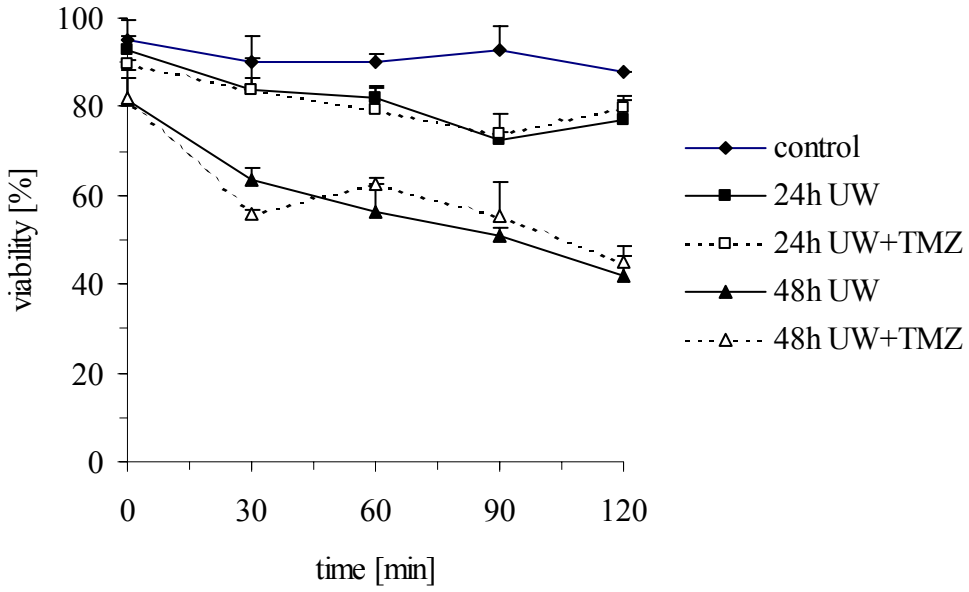

Figure 4.7: Evolution with time of the viability of hepatocytes incubated at 37°C for 2 hours in Hanks's solution after preservation at 4°C for 24 or 48 hours in UW solution with or without 10^{-6} M TMZ. A control experiment was performed by incubating suspensions of freshly isolated rat hepatocytes without cold preservation (n = 3).

As can be seen, TMZ had no positive effect on the viability of hepatocytes during cold preservation. The evolution of the viability of hepatocytes with time during incubation at 37°C was the same after cold preservation in the presence or absence of TMZ in the UW solution. It could also be seen that the duration of cold preservation influenced both the viability of hepatocytes immediately after the time of preservation at 4°C and the decline of viability during 2 hours of incubation at 37°C. Actually, the initial viability of hepatocytes after 24 hours of preservation in UW solution was 90%, while it dropped to 80% when hepatocytes were stored during 48 hours in the same solution. Moreover, the viability of hepatocytes kept 48 hours at 4°C decreased more rapidly during incubation than that of cells preserved only 24 hours at 4°C. These observations are in good agreement with the results shown above (figure 4.6): the poorer the initial viability after cold preservation, the more rapid the decline of viability during incubation.

4.3 Discussion

On average, 4 to $6 \cdot 10^8$ cells were obtained from the two-step collagenase isolation procedure of the liver, which represented about 50% of the total hepatocyte population of the liver [12]. Cell viability was routinely greater than 90% as assessed by trypan blue exclusion. The yield values found in the literature with the same isolation procedure range from to 2 to $6 \cdot 10^8$ cells, with a cell viability average of 85-90% [12-14]. The first techniques to obtain hepatocytes used mechanical methods, such as forcing the tissue through stainless steel screens or cheesecloth, then chelators such as citrate or EDTA to neutralize Ca^{2+} and K^+ ions which play a key role in intercellular bonds, and finally enzymes, such as trypsin, papain, lysozym, neuraminidase, or pepsin. With all these techniques, the cell yield did not exceed 5% of the total population of hepatocyte and the functional properties of most cells were lost [13]. An important step in the preparation of intact hepatocytes was made by the introduction of collagenase. Berry and Friend set up the basic protocol of the *in situ* two-step collagenase perfusion of the liver, which was further modified by Seglen [11].

Centrifugation permitted to separate the hepatocytes (sediment) from cell debris, dead cells and other smaller cells of the liver (supernatant). Other techniques exist to obtain pure hepatocyte suspensions, but they are more sophisticated. For instance, hepatocytes can be purified by Percoll density gradient separation [4,15,16]. This procedure results in the separation of single and viable parenchymal cells from cell aggregates, debris, and nonparenchymal cells, based on the density of the different elements.

The fine structure of isolated hepatocytes is comparable to the one of cells *in vivo* [13], the functionality of the cytochromes P450 is similar in the entire liver and in the freshly isolated hepatocytes [17], but membrane polarity is altered during isolation [18]. *In vivo*, the hepatocyte is a polar cell with two different surfaces, which are in contact with two different compartments: the sinusoidal cell membrane is in contact with the blood while the canalicular membrane is in contact with the bile. Microscopic observation of freshly isolated hepatocytes shows a spherical shape of the cells with a uniform membrane, and recognition of the

different poles of the membrane is no longer possible. Hence freshly isolated cells have altered cell surface receptors for attachment and/or binding of xenobiotics and endogenous toxic products [19,20], although isolated hepatocytes exhibit transport characteristics similar to those of livers *in vivo* [21,22]. Nevertheless, on must be aware of this problem when using freshly isolated hepatocytes to study drug transport or/and metabolism.

The preservation of primary cells, especially hepatocytes, is difficult and there are different points to respect. First, the cellular density has to be adequate. Freshly isolated hepatocytes are usually suspended at $1 \cdot 10^6$ to $2 \cdot 10^7$ cells/ml. Powis et al. [4] found that freezing with densities of 10^8 cells /ml was unsuccessful. When the number of hepatocytes was decreased to 10^6 cells/ml, cell recovery was increased. Second, the freezing solution must contain a preservative such as DMSO, glycerol or propyleneglycol at a final concentration of 5 – 10%, 10% serum is sometimes added, too. DMSO has been shown to give a better cell recovery than propyleneglycol [4]. Third, the freezing process must be slow and controlled. The use of the expended polystyrene box allowed a slow freezing of about 1°C per minute. And finally, after cryopreservation, cells have to be thawed rapidly, for instance by immersion in a water bath at 37°C.

Our experiments showed that only about 20% of freshly isolated hepatocytes were viable after cryopreservation, and that they did not survive when incubated at 37°C. We used only trypan blue exclusion to measure cell viability. Dye exclusion tests are approximate measure of viability, and functional viability tests such as metabolic studies could give better results. Some authors found that cryopreservation produces altered cells [2], while others reported that hepatocytes were normal after cryopreservation [4]. As hepatocytes are anchorage-dependent cells, better results can be obtained when hepatocytes are bound to a surface. For instance, microcarrier-attached hepatocytes [5,6] and hepatocytes immobilized in calcium-alginate beads [7] have shown to have a good recovery after thawing.

To avoid the inevitable hazard of freezing and thawing, short-term cold storage of hepatocytes was also investigated. All solutions used for preservation maintained a good hepatocyte viability of about 85% after 4 hours of storage at 4°C, Williams E medium gave

the worst results and UW solution the best. The protective capacity of UW solution for cold storage was particularly evident when hepatocytes were incubated at 37°C after a longer period of cold preservation, i.e. 24 hours. Actually, hepatocytes preserved for 24 hours at 4°C in UW solution had a viability after preservation identical to that before cold preservation (90%), and when incubated at 37°C they kept a viability greater than 85% after 2 hours of incubation.

The loss of viability during cold preservation is mainly due to cell swelling [23]. Cooling lowers the rate of chemical reactions and thus has a general depressive effect on metabolism. A disturbance in the maintenance of the intracellular ionic composition may occur. Passive fluxes tend to be less affected by temperature than energy-dependent pumps and the rate of ion pumping at hypothermia is unable to match passive ion flux. The net result is an intracellular gain of Na^+ and Cl^- which draws in water by osmosis and leads to cell swelling [24].

The UW solution was originally developed for pancreas preservation [25] and has now become the standard cold storage preservative for most organs, including the kidney, liver, pancreas, and heart [25,26]. Different UW solutions have been described, all deriving from the original one. UW solutions contain agents to suppress hypothermic cell swelling (lactobionic acid, raffinose, hydroxyethyl starch, PEG), a hydrogen ion buffer (phosphate), and other agents that may be beneficial (gluthathione, adenosine, allopurinol, magnesium). In our studies, we did not observe any effect of PEG when added to the cold preservation solution (figure 4.6). UW solutions have a high concentration of potassium, which is thought to suppress the efflux of potassium from cold-stored cells. Calcium appears to play a role in the suppression of cell swelling as well as maintenance of mitochondrial function. Amino acids are important in preventing loss of viability and maintaining respiratory activity [27]. Glutahthione (GSH) is often omitted because it is unstable. The autooxidation of GSH produces H_2O_2, shortens the shelf life and reduces the antioxidant capacity of organ storage solutions since it can act simultaneously as an antioxidant and prooxidant [28].

UW is now used by numerous workers to preserve hepatocytes for long periods of time without loss of viability and transport function [8-10]. Hepatocytes can be preserved for 22 hours in UW at 0°C without significant loss of viability and transport function, but in Krebs-Henseleit buffer, viability and transport function of hepatocytes deteriorate after 22h [29,30]. Krebs-Henseleit buffer is a balanced salt solution (BSS) like Hanks's solution, whose protective properties were found to be inferior to UW solution (figure 4.6). Thus, our results obtained with different preservation solutions are in good agreement with the literature. However, this is not quite the case with the tested incubation solutions. Marsh et al. [31] showed that the viability of rewarmed hepatocytes was more reduced upon incubation with BSS than with tissue-culture media. In contrast, we observed that hepatocytes incubated after cold preservation with Hanks's solution remained more viable than hepatocytes incubated in Williams E, a complete tissue-culture medium (figure 4.7), although the difference was slight. Although Williams E medium is a complete medium, including notably amino acids and vitamins (table 4.1), we did not observe any viability improvement during incubation after cold preservation. Williams E medium was used because it is a medium currently employed for hepatocyte culture [32,33-36].

Hepatocytes tolerate a wide range of pH values in the storage solution (7.0 to 8.0) [37]. Mamprin et al. [38] analyzed the effect of different pH of resuspension solutions on the viability of hepatocytes preserved for 96 hours in UW solution. The viability was significantly higher for cells incubated at pH 7.2. The importance of the pH was not studied here. However, this information was taken into account when preparing preservation and incubation solutions. The pH of the incubation solutions was adjusted to 7.2 instead of a usual 7.4.

We did not detect any positive effect of TMZ on the cold preservation of hepatocytes. The addition of TMZ to the UW solution did not improve viability of hepatocytes during the period of cold preservation, or during incubation. The concentration of TMZ added was 10^{-6} M, which is the concentration usually described in the literature [39-43]. During preliminary studies, TMZ was tested at a concentration of 10^{-5} M without producing any

beneficial effect. In further studies, TMZ could be added at lower concentrations or directly to the solutions used to isolate hepatocytes.

TMZ has shown a beneficial effect on the viability of transplanted organs such as kidney [40-44], intestines [45], heart [39], and liver [46], when added to the organ preservation solution at a concentration of 10^{-6} M. The mechanism of action of TMZ is not fully understood but could be a protection against ischemia/reperfusion injury.

4.4 Conclusion

The viability of cryopreserved hepatocytes dramatically dropped after thawing and incubation at 37°C. According to these results, cryopreservation does not appear appropriate to preserve hepatocytes when large numbers of viable cells are needed for the preparation of a hepatocyte HFB. Even if the procedure was improved, it would require a very large number of freezing tubes, due to the low density of cells during freezing, and this would complicate the preparation of the HFB.

Conversely, the cold preservation of hepatocytes in UW solution appears suitable for our purpose. It preserves hepatocytes during 24 hours at 4°C without significant loss of viability during cold preservation and subsequent incubation in Hanks's solution at 37°C for 2 hours. These results provide a framework for the future preparation and perfusion of the hepatocyte HFB. If several rat livers have to be used to isolate a sufficient number of hepatocytes, cells resulting from the first liver isolation procedures can be kept at 4°C in UW solution, until enough cells are isolated to load the HFB. Further, if the experiment can not be performed immediately after hepatocyte isolation, the HFB containing hepatocytes in suspension in UW solution can be kept at 4°C. The cells can be preserved 24 hours without loss of viability, meaning that the HFB experiment could be performed 24 hours after hepatocyte isolation. Hanks's solution can be used to perfuse the HFB, as it was shown to be a suitable solution to sustain hepatocytes during incubation at 37°C after cold preservation. TMZ did not

demonstrate any additional beneficial effect on hepatocytes viability during cold preservation, when added to UW solution at a concentration of 10^{-6} M.

References

[1] Freshney RI, Specialized cells, In 'Culture of Animal Cells', Ed. Freshney RI, Wiley-Liss, New York, 2000, pp. 345-384.

[2] Koebe H-G, Pahernik SA, Thasler WE, and Schildberg F-W, Porcine hepatocytes for biohybrid artificial liver devices: a comparison of hypothermic storage techniques, *Artif Organs*, 1996, **20**, 1181-1190.

[3] Guillouzo A, Rialland L, Fautrel A, and Guyomard C, Survival and function of isolated hepatocytes after cryopreservation, *Chem-Biol Inter*, 1999, **121**, 7-16.

[4] Powis G, Santone KS, Melder DC, Thomas L, Moore DJ, and Wilke TJ, Cryopreservation of rat and dog hepatocytes for studies of xenobiotic metabolism and activation, *Drug Metab Dispos*, 1987, **15**, 826-832.

[5] Rozga J, Williams F, Ro M-S, Neuzil DF, Giorgio TD, Backfisch G, Moscioni D, Hakim R, and Demetriou AA, Development of a bioartificial liver: properties and function of a hollow-fiber module inoculated with liver cells, *Hepatology*, 1993, **17**, 258-265.

[6] Arnaout WS, Moscioni AD, Barbour RL, and Demetriou AA, Development of bioartificial liver: bilirubin conjugation in Gunn rats, *J Surg Res*, 1990, **48**, 379-382.

[7] Guyomard C, Rialland L, Fremond B, Chesne C, and Guillouzo A, Influence of gel entrapment and cryopreservation on survival and xenobiotic metabolism capacity of rat hepatocytes, *Toxicol Appl Pharmacol*, 1996, **141**, 349-356.

[8] Sandker GW, Weert B, Slooff MJH, and Groothuis GMM, Preservation of isolated rat and human hepatocytes in UW solution, *Transplant Proc*, 1990, **22**, 2204-2205.

[9] Sandker GW, Weert B, Merema M, Kuipers W, Slooff MJH, Meijer DKF, and Groothuis GMM, Maintenance of viability and transport function after preservation of isolated rat hepatocytes in various simplified University of Wisconsin solutions, *Biochem Pharmacol*, 1993, **46**, 2093-2096.

[10] Groothuis GMM and Meijer DKF, Drug traffic in the hepatobiliary system, *J Hepatol*, 2001, **24**, S3-S28.

[11] Seglen O, Preparation of isolated rat liver cells, In 'Methods in Cell Biology', Ed. Prescott DM, Academic Press, New York, 1976, Vol. 13, pp. 29-83.

[12] Quistorff B, Dich J, and Grunnet N, Preparation of isolated rat liver hepatocytes, In 'Animal Cell Culture', Eds. Pollard JW and Walker JM, Humana press, Clifton, 1989, Vol. 5, pp. 151-160.

[13] Guguen-Guillouzo C, and Guillouzo A, Méthodes de préparation d'hépatocytes adultes et foetaux, In 'Hépatocytes Isolés et en Culture', Eds. Guillouzo A and Guguen-Guillouzo C, INSERM/John Libbey Eurotext., Paris, 1986, pp. 1-12.

[14] Shatford RA, Nyberg SL, Meier SJ, White JG, and Payne WD, Hepatocyte function in a hollow fiber bioreactor: a potential bioartificial liver, *J Surg Res*, 1992, **53**, 549-557.

[15] Kreamer BL, Staeker JL, Sawada N, Sattler GL, Hsia MT, and Pitot HC, Use of a low speed, isodensity percoll centrifugation method to increase the viability of isolated rat hepatocyte preparations, *In Vitro Cell Dev Biol*, 1999, **22**, 201-211.

[16] Aiken J, Cima L, Schloo B, Mooney D, Johnson L, Langer R, and Vacanti JP, Studies in rat liver perfusion for optimal harvest of hepatocytes, *J Pediatr Surg*, 1990, **25**, 140-145.

[17] Guillouzo A, Utilisation des hépatocytes isolés et en culture pour des études de métabolisme et de cytotoxicité des xénobiotiques, In 'Hépatocytes Isolés et en Culture', Eds. Guillouzo A and Guguen-Guillouzo C, INSERM/John Libbey Eurotext, Paris, 1986, pp. 327-346.

[18] Gebhardt R, Utilisation des hépatocytes isolés et en culture pour l'étude de la formation de la bile, In 'Hépatocytes Isolés et en Culture', Eds. Guillouzo A and Guguen-Guillouzo C, INSERM/John Libbey Eurotext, Paris, 1986, pp. 367-392.

[19] Jauregui HO, and Gann KL, Mammalian hepatocytes as a foundation for treatment in human liver failure, *J Cell Biochem*, 1991, **45**, 359-365.

[20] Bader A, Reimer P, Knop E, Böker K, Christians U, Weissleder R, and Sewing K-F, An organotypical *in vitro* model of the liver parenchyma for uptake studies of diagnostic MR receptor agents, *Magn Reson Imaging*, 1995, **13**, 991-1002.

[21] Schwenk M, Transport systems of isolated hepatocytes, *Arch Toxicol*, 1980, **44**, 113-126.

[22] Miyauchu S, Sawada Y, Iga T, Hanano M, and Sugiyama Y, Comparison of the hepatic uptake clearences of fifteen drugs with a wide range of membrane permeabilities in isolated rat hepatocytes and perfused rat livers, *Pharm Res*, 1993, **10**, 434-440.

[23] Marsh DC, Lindell S, Fox LE, Belzer FO, and Southard JH, Hypothermic preservation of hepatocytes. I. Role of cell swelling, *Cryobiology*, 1989, **26**, 524-534.

[24] Armitage WJ, Preservation of viable tissue for transplantation, In 'Clinical Application of Cryobiology', Eds. Fuller BJ and Grout BWW, CRC Press, Boca Raton, 1991, pp. 169-189.

[25] Jamieson NV, Sundberg R, Lindell S, Claesson K, Moen J, Vreugdenhil PK, Wight DGD, Southard JH, and Belzer FO, The 24- to 48-hour preservation of canine liver by simple cold storage using UW lactobionate solution, *Transplant Proc*, 1989, **21**, 1292-1293.

[26] D'Alessandro AM, Southard JH, Love RB, and Belzer FO, Organ preservation, *Surg Clin North Am*, 1994, **74**, 1083-1095.

[27] Umeshita K, Monden M, Fujimori T, Sakai H, Gotoh M, Okamura J, and Mori T, Extracellular calcium protects cultured rat hepatocytes from injury caused by hypothermic preservation, *Cryobiology*, 1988, **25**, 102-109.

[28] Gnaiger E, Kuznetsov AV, Königsrainer A, and Margreiter R, Autooxidation of glutathione in organ preservation solutions, *Transplant Proc*, 2000, **32**, 14-14.

[29] Olinga P, Merema M, Slooff MJH, Meijer DKF, and Groothuis GMM, Influence of 48 hours cold storage in University of Wisconsin organ preservation solution on metabolic capacity of rat hepatocytes, *J Hepatol*, 1997, **27**, 738-743.

[30] Sandker GW, Slooff MJH, and Groothuis GMM, Drug transport, viability and morphology of isolated rat hepatocytes preserved for 24 hours in University of Wisconsin solution, *Biochem Pharmacol*, 1992, **43**, 1479-1485.

[31] Marsh DC, Hjelmhaug JA, Vreugdenhil PK, Kerr JA, Rice MJ, Belzer FO, and Southard JH, Hypothermic preservation of hepatocytes. III. Effects of resuspension media on viability after up to 7 days of storage, *Hepatology*, 1990, **13**, 500-508.

[32] Shatford RA, Nyberg SL, Payne WD, Hu W-S, and Cerra FB, A hepatocyte bioreactor as a potential bioartificial liver: demonstration of prolonged tissue-specific functions., *Surg Forum*, 1991, **42**, 54-56.

[33] Nyberg SL, Remmel RP, Mann HJ, Peshwa MV, Hu W-S, and Cerra FB, Primary hepatocytes outperform Hep G2 cells as the source of biotransformation functions in a bioartificial liver, *Ann Surg*, 1994, **220**, 59-67.

[34] Gerlach JC, Encke J, Hole O, Müller C, Ryan CJ, and Neuhaus P, Bioreactor for a larger scale hepatocyte *in vitro* perfusion, *Transplantation*, 1994, **58**, 984-988.

[35] Takeshita K, Ishibashi H, Suzuki M, Yamamoto T, Akaike T, and Kodama M, High cell-density culture system of hepatocytes entrapped in a three-dimensional hollow fiber module with collagen gel, *Artif Organs*, 1995, **19**, 191-193.

[36] Sielaff TD, Nyberg SL, Rollins MD, Hu MY, Amiot B, Lee A, Wu FJ, Hu W-S, and Cerra FB, Characterization of the three-compartment gel-entrapment porcine hepatocyte bioartificial liver, *Cell Biol Toxicol*, 1997, **13**, 357-364.

[37] Fox LE, Marsh DC, Southard JH, and Belzer FO, The effect of pH on the viability of hypothermically stored rat hepatocytes, *Cryobiology*, 1989, **26**, 186-190.

[38] Mamprin ME, Rodriguez JV, and Guibert EE, Importance of pH in resuspension media on viability of hepatocytes preserved in University of Wisconsin solution, *Cell Transplant*, 1995, **4**, 269-274.

[39] Kay L, Finelli C, Aussedat J, Guarnieri C, and Rossi A, Improvement of long-term preservation of the isolated arrested rat heart by TMZ: effect of the energy state and mitochondrial function, *Am J Cardiol*, 1995, **76**, 45B-49B.

[40] Hauet T, Baumert H, Amor IB, Gibelin H, Tallineau C, Eugene M, Tillement J-P, and Carretier M, Pharmacological limitation of damage to renal medulla after cold storage and tranplantation by trimetazidine, *J Pharmacol Exp Ther*, 2000, **292**, 254-260.

[41] Hauet T, Mothes D, Goujon JM, Germonville T, Caritez JC, Carretier M, and Tillement J-P, Trimetazidine reverses deleterious effects of ischemia-reperfusion in the isolated perfused pig kidney model, *Nephron*, 1998, **80**, 296-304.

[42] Baumert H, Goujon JM, Richer JP, Lacoste L, Tillement J-P, Carretier M, and Hauet T, Renoprotective effects of trimetazidine against ischemia-reperfusion injury and cold storage preservation: a preliminary study, *Transplantation*, 1999, **68**, 300-303.

[43] Hauet T, Goujon JM, Vandewalle A, Baumert H, Lacoste L, Tillement J-P, and Carretier M, Trimetazidine reduces renal dysfunction by limiting the cold ischemia/reperfusion injury in autotransplanted pig kidneys, *J Am Soc Nephrol*, 2000, **11**, 138-148.

[44] Richer JP, Gibelin H, Tallineau C, Ben Amor I, Hebrard W, Carretier M, and Hauet T, Limitation of lipid peroxidation and renal medullary cell injury of the kidney after 48- and 72-hour cold storage in University of Wisconsin solution: effect of trimetazidine, *Transplant Proc*, 2000, **32**, 46-46.

[45] Tetik C, Ozden A, Calli N, Bilgihan A, Bostanci B, Yis O, and Bayramoglu H, Cytoprotective effect of trimetazidine on 60 minutes of intestinal ischemia-reperfusion injury in rats., *Transplant International*, 1999, **12**, 108-112.

[46] Tsimoyiannis EC, Moutesidou KJ, Moschos CM, Karayianni M, Karkabounas S, and Kotoulas OB, Trimetazidine for prevention of hepatic injury induced by ischemia and reperfusion in rats, *Eur J Surg*, 1993, **159**, 89-93.

Chapter 5
Development and validation of a hepatocyte hollow fiber bioreactor as a cellular model for the study of contrast agents by magnetic resonance imaging

5.1 Introduction

Magnetic resonance imaging (MRI) is a non-invasive and safe method for the detection and characterization of a wide variety of diffuse (e.g. fatty liver, hemochromatosis, and cirrhosis) and focal (e.g. cancers) hepatic diseases. It has become an important tool in the clinical routine of liver imaging to evaluate focal diseases. The most commonly used contrast agents are the nonspecific extracellular gadolinium (Gd^{3+}) chelates, like Gd-DTPA. Indeed, they are inexpensive, safe, well-tolerated, and allow to detect and characterize a wide range of hepatic diseases. However, as a method for assessing liver function, MRI is still at a research stage, but it has a great potential thanks to hepatobiliary contrast agents, such as the gadolinium-based Gd-BOPTA or the manganese-based Mn-DPDP. They distribute initially into the interstitial space, as the nonspecific extracellular contrast agents do, but are also taken up specifically by hepatocytes and are partially excreted into the bile. Because the uptake of these contrast agents relies on the functional state of the hepatocytes, they could be used to obtain quantitative information on the functional state of the liver. However, before MRI can be used clinically as a routine tool for this purpose, more research is needed to elucidate the mechanisms by which these hepatobiliary contrast agents interact with hepatocytes, and how these mechanisms are disturbed or altered in different liver diseases. *In vitro* cellular models are of great value for the study of such mechanisms.

Methods currently used for contrast agent detection with *in vitro* cellular models include radioactivity measurements of radio-labeled contrast agents, ^{31}P NMR spectroscopy in the

case of Mn-DPDP, and fluorescence for iron oxide particle-based contrast agents. MRI is not currently used as an analytical tool for the study and quantification of contrast agents *in vitro*, due to the low MRI resolution achievable with the current MR systems, the difficulty to obtain reproducible results, and the impossibility to use metallic devices inside the magnet room. The latter point is incompatible with most tissue or cell cultures, which require controlled temperature and oxygenation. Nevertheless, MRI has an interesting advantage over the quantification techniques cited above: it can detect not only one specific but all kinds of MRI contrast agents without the need of radio-labeled molecules.

The aim of this work was to develop a MRI compatible cellular *in vitro* model containing freshly isolated rat hepatocytes, where the effects of contrast agents could be directly measured by MRI. A dynamic perfusion system including a hollow fiber bioreactor (HFB), and a system of circulation, heating, and oxygenation, was set up according to the difficulty due to the magnetic field. The system was validated by measuring the signal intensity of the hepatocyte bioreactor during perfusion of an extracellular (Gd-DTPA) and a hepatobiliary contrast agent (Gd-BOPTA). The system permitted to evidence a reproducible difference between both contrast agents, due to the uptake of Gd-BOPTA into hepatocytes.

5.2 Materials and methods

5.2.1 Chemicals

Solution of Gd-BOPTA 0.5 M was generously provided by Bracco Research S.A. (Geneva, Switzerland). A commercially available solution of Gd-DTPA 0.5 M (Magnevist®, Schering, Germany) was used. Bovine serum albumin (BSA, fraction V, 97%) and ethyleneglycol-O,O'-bis(2-aminoethyl)-N,N,N',N'-tetraacetic acid (EGTA) were purchased from Fluka. Collagenase from Clostridium histolicum type IV (collagen digestion activity: 295 U/mg solid) and bovine pancreas insulin were obtained from Sigma Chemical (St-Louis, MO, USA). All other chemicals were of analytical grade.

5.2.2 Set up of the MRI compatible perfusion system

The MRI compatible perfusion system comprised a solution circulation system, a heating system, an oxygenation system, a bubble trap and a HFB. A schematic drawing of the perfusion system is presented in figure 5.1.

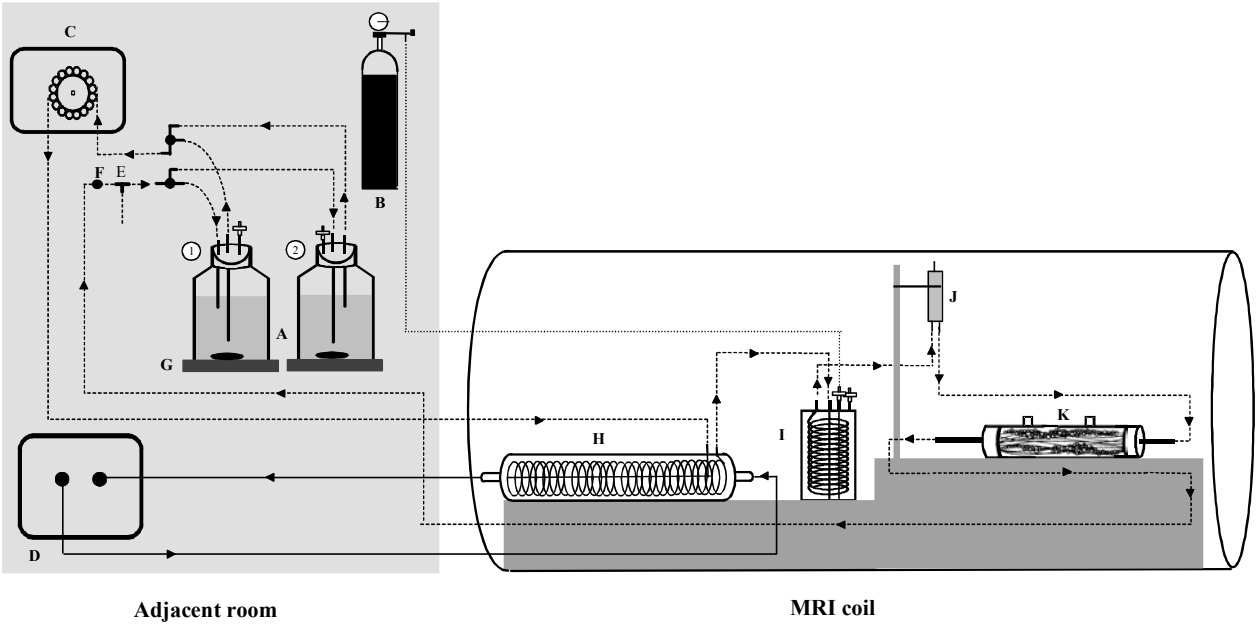

Figure 5.1: Schematic drawing of the hollow fiber bioreactor perfusion system. The system was composed of solution reservoirs φ and κ (A), a gas bottle (B), a peristaltic pump (C), a heating

circulator (D), a sampling port (E), a temperature probe (F), a magnetic stirrer (G), a refrigerant (H), an oxygenator (I), a bubble trap (J) and a hollow fiber bioreactor (K). Elements A to G were placed in a room adjacent to the magnet room.

To avoid interference with the magnetic field, all material used in the magnet room was exempt of any metallic piece and made of plastic and glass; the heating system, the gas bottle and the pump were installed in an adjacent room. All elements inside the magnet were fixed to a PVC support. The dimensions of the magnet were measured and the PVC support was built so that the HFB could be fitted at the exact isocenter of the magnet.

5.2.2.1 Solution circulation system

The solution was contained in glass bottles closed with a three-way cap, one for solution outlet, one for solution inlet and one for venting (figure 5.1). A 0.22 μm filter (Millex® FG, Millipore Co., Bedford, MA, USA) was set on the venting outlet in order to prevent microbiological contamination of the system. The installation included two solution reservoirs, which permitted to switch perfusion solution during experiment. Magnetic agitation ensured good homogeneity of the solutions. Solution bottles were connected to the HFB by 15 meters of tubing (Tygon® 2257, ID 1/8", OD 3/16", and Pharmed® 65, ID 1/4", OD 3/8", Saint-Gobain Performance Plastics Co., Akron, Ohio, USA). The tubing was chosen in order to minimize adsorption phenomena. A peristaltic pump (ISM 915, Ismatec SA, Glattbrugg-Zürich, Switzerland) continually circulated the solution into the system. To avoid gas bubbles getting through the HFB a plastic bubble trap was installed just before its inlet. A sampling port allowed sampling for analysis during the experiment. The different elements of tubing were connected to each other with nylon luer and Kent® fittings (Value Plastics®, Fort Collins, CO, USA).

5.2.2.2 Heating system

The solution was heated by circulation through a glass spiral of a refrigerant while warm water from the heating circulator (Haake N6, Karlsruhe, Germany) flowed outside the spiral. The refrigerant was installed in the magnet, just before the oxygenator system.

Temperature measurements were made using a thermocouple thermometer (Extech Instruments Corp., n° 422315, Waltham, MA, USA) with two Kapton® insulated probes type T (Physitemp Instruments Inc., Clifton, NJ, USA). The probes were hermetically fixed to luer fittings in order to be included in the perfusion system.

The relation between the water temperature in the heating circulator, the temperature in the inlet, the temperature inside the HFB, and in the outlet tubing near the solution reservoir was determined in preliminary studies. To avoid interference with the magnetic signal, only the temperature probe in the outlet near the solution reservoirs was fitted during MRI experiments.

5.2.2.3 Oxygenation system

An efficient oxygenation was assured by a silicone membrane oxygenator [1] which consisted of 7 meters of thin-walled silicone tubing (Silastic®, ID 0.132", OD 0.183", Dow Corning Co., Midland, MI, USA) permeable to oxygen and carbon dioxide and coiled in a plastic box. It was fed with a mix of oxygen (95%) and carbon dioxide (5%), at the minimal rate which saturated it with oxygen. The oxygenator box comprised four apertures: one for unoxygenated solution entrance, one for oxygenated solution exit, one for gas inlet, and one for gas outlet, the later two being connected to a 0.22 μm filter (Millex® FG, Millipore Co., Bedford, MA, USA) in order to prevent microbiological contamination of the system.

To investigate possible adsorption in the silicone tubing of the contrast agents, one liter of 0.2 mM Gd-BOPTA or Gd-DTPA solution was recirculated through the perfusion system and its UV absorbance at 210 or 190 nm respectively was regularly measured with a spectrophotometer UV (1601, Shimadzu Co., Kyoto, Japan).

5.2.2.4 Hollow fiber bioreactor

The HFB consisted of a network of semi-permeable artificial capillaries bundled together within a transparent plastic shell (figure 5.2). The HFB was composed of two compartments separated by a porous membrane, the intracapillary space (ICS) and the extracapillary space (ECS). The perfusion solution, continually pumped from a reservoir, oxygenated and heated, flowed within the capillaries from where it diffused through the semi-permeable membrane into the ECS.

The used HF devices (Minikros® Sampler, Spectrum, Rancho Dominguez, CA, USA) were made of hydrophilic polyethersulfone fibers, with a diameter of 0.5 mm and had a length of 15 cm and an ECS volume of 25 ml. Module 1 (product n° M15E 220 01N) had a fiber surface area (FSA) of 140 cm^2 and a porosity of 0.5 µm, module 2 (product n° M15E 260 01N) had a FSA of 420 cm^2 and a porosity of 0.5 µm and module 3 (product n° M12E 220 01N) had a FSA of 140 cm^2 and a porosity of 0.2 µm. During perfusion, the HFB was surrounded by an Armaflex® jacket for thermal insulation.

Figure 5.2: Picture of the hollow fiber module 1 made of hydrophilic polyethersulfone fibers with a diameter of 0.5 mm, ECS volume of 25 ml, fiber surface area of 420 cm^2 and porosity of 0.5 µm. The hollow fibers are bundled together within a transparent plastic shell.

5.2.3 Preparation of the hepatocyte HFB

5.2.3.1 Isolation of hepatocytes

Hepatocytes were isolated from adult male Sprague-Dawley rats (250 to 350 g) by a two-step collagenase perfusion of the liver first described by Seglen [2] and described in detail in chapter 4.

An average of $5 \cdot 10^8$ hepatocytes were obtained from the isolation procedure of one rat liver, with a cell viability greater than 90% as assessed by trypan blue exclusion. The suspension of freshly isolated hepatocytes obtained after the isolation process was centrifuged (50 g, 2 min, 4°C) and the cell pellet was mixed with 30 ml of ice cold modified University of Wisconsin (UW) solution containing 80 mM lactobionic acid, 30 mM raffinose, 25 mM KH_2PO_4, 25 mM NaOH, 10 mM glycine, 5 mM $MgSO_4$, 5 mM adenosine, 1 mM allopurinol, 165,700 U/l Penicillin G, 5% PEG 800, and 0.5% BSA; pH was adjusted to 7.3 with KOH 2.5 N (~55 mM). The UW solution was filtered aseptically before use (Millex® GS, 0.22 μm, Millipore Co., Bedford, Massashuset, USA). This suspension was kept at 4°C till the loading of the bioreactor.

5.2.3.2 Loading of the bioreactor

The HF module 2 was first rinsed by flowing 1l of high purity water in a single pass through the fibers with a flow rate of 50 ml/min. The HF module was then autoclaved by a 30-minute cycle at 121°C (Varioclav® 300 E, H+P Labortechnik AG, Oberschleissheim / München, Germany).

Just before the inoculation of hepatocytes, the ECS and ICS of the HFB were filled with UW solution, taking care not to introduce air bubbles. The hepatocytes suspended in UW solution were (50 g, 5 min, 4°C) centrifuged to decrease the volume of the cell suspension. Supernatant was removed and the remaining hepatocyte suspension was inoculated into the ECS of the sterile HF module through the ECS port as depicted in figure 5.3. The hepatocyte suspension was gently poured in a sterile 50 ml luer-lock syringe without piston which was fixed to a ECS port. Cells were aspirated in the ECS by another syringe fixed to the second ECS port. The bioreactor was preserved at 4°C for up to 4 hours till experiment.

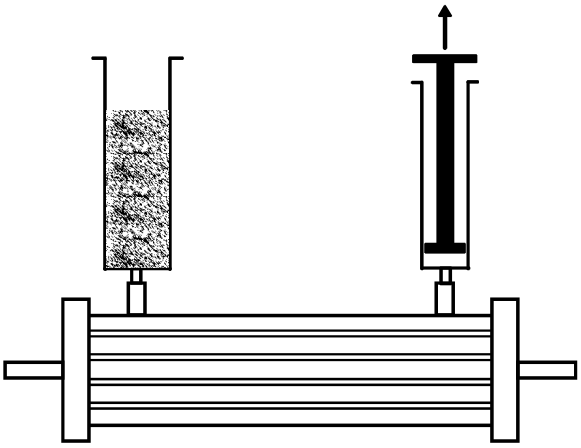

Figure 5.3: Preparation of the hepatocyte hollow fiber bioreactor (HFB). Hepatocytes suspended in the University of Wisconsin solution were inoculated in the extracapillary space of the HFB using a system of two syringes.

5.2.4 Viability assessment of hepatocytes

During HFB perfusion experiments cell viability was checked by dosing the cytosolic enzyme lactate dehydrogenase (LDH) and the mitochondrial enzyme aspartate aminotransferase (AST) released in the perfusate (UV kits n° 1442616 and 1442490 respectively, Roche Diagnostics, Rotkreuz, Switzerland) and by determining oxygen consumption (ABL 500, Radiometer Copenhagen, Brunson, DK) of hepatocytes.

Amounts of LDH and AST released in the perfusion solution were expressed as percentage of the total amount of LDH and AST contained in the hepatocytes. Total quantities of LDH and AST were obtained by determining the quantity of enzymes released after cellular lysis with Triton X-100 [3]. Briefly, 0.5 ml of freshly isolated hepatocyte suspension containing $5 \cdot 10^6$ cells were mixed with 9.5 ml of Triton X-100 solution 0.1% and agitated for 1 hour. The mixture was centrifuged (400 g, 4 min), the supernatant was removed and LDH and AST were dosed by UV. This permitted to calculate the total quantity of LDH and AST contained in a million hepatocytes. For the bioreactor experiments, the percentage of enzymes released was calculated as the activity in the perfusion solution compared to the total activity contained in a million hepatocytes multiplied by the total million number of cells in the HFB.

PO_2 determination of samples taken simultaneously at the bioreactor inlet and outlet, as well as the perfusate flow rate were used to calculate the oxygen consumption of the bioreactor. Oxygen consumption (ΔO_2) by the hepatocytes in the HFB was determined with the following equation [4]:

$$\Delta O_2 = S(O_2) \cdot [P_{in} - P_{out}] \cdot Q_E \qquad \text{[Equation 5.1]}$$

where P_{in} and P_{out} are the oxygen tensions (kPa) in the HFB inlet (solution from bubble trap) and outlet (solution from sampling port) respectively, Q_E is the flow rate (ml/h), and $S(O_2)$ is the oxygen solubility in water at 37°C ($9.68 \cdot 10^{-6}$ mol O_2/ml/kPa).

5.2.5 HFB perfusion conditions

The perfusion system was first sterilized by circulating ethanol 70% V/V for 15 minutes. The system was then emptied, rinsed with 1l sterile water and emptied again. After this sterilization step the perfusion system was filled with perfusion solution contained in reservoir 1, which had the following composition: 76.0 mM NaCl, 5.37 mM KCl, 0.63 mM Na_2HPO_4, 0.44 mM KH_2PO_4, 17.9 mM $NaHCO_3$, 2.00 mM $CaCl_2$, 0.41 mM $MgSO_4$, 40.0 mM HEPES Na, 5.55 mM glucose, 99420 U/l Penicillin G, 77700 U/l streptomycin sulfate, 280 U/l insulin and 0.5% BSA, pH was adjusted to 7.2. Perfusion solutions were aseptically filtered before use (Millex® GP_{50}, 0.22 μm, Millipore Co., Bedford, Massashuset, USA) and kept at 4°C in sterile glass bottles till experiment. The first 50 ml were discarded to eliminate residual water from the previous washing step. Solution was recirculated in the perfusion system till the required temperature was obtained. At that time, the HFB was introduced in the perfusion system. When desired, the solution was switched to solution with contrast agent contained in reservoir 2.

Solution sterility following experiment was evaluated by incubation on agar-agar (Biotest Hycon GK-A/HS, Biotest AG, Dreieich, Germany) at room temperature for 3 days.

5.2.5.1 Determination of the optimal concentration of hepatocytes

To determine the optimal concentration of hepatocytes in HF module 2 hepatocyte densities of $2 \cdot 10^7$ and $4 \cdot 10^7$ cells/ml were compared in terms of cellular viability. HFB were perfused during 4 hours with a solution free of contrast agent at a solution and gas flow rate of 100 ml/min and 4 l/min respectively. Samples were taken every hour and checked for their content of LDH and AST.

5.2.5.2 Choice of the hollow fiber module

To choose the hollow fiber module, diffusion in the extracapillary space of Gd-DTPA 2 mM was assessed by MRI in HF modules 1, 2 and 3 free of hepatocytes, with a flow rate of 100 ml/min. Each module and the perfusion system were first separately filled with perfusion solution without contrast agent. The first module was then introduced in the perfusion system, in the wrist coil, and imaged. Perfusion with solution free of contrast agent for 15 seconds was followed by perfusion with Gd-DTPA 2 mM for 10 minutes. The same procedure was repeated with the two other modules.

5.2.5.3 Optimization of the flow rate

The effect of flow rate on the time to reach contrast agent equilibrium between ICS and ECS was also measured in the absence of hepatocytes by MRI. HFB filling with Gd-DTPA 0.2 mM at flow rates of 50, 75 and 100 ml/min was studied with module 2 following the same protocol as already described for the choice of the HF module.

5.2.5.4 Validation of the hepatocyte hollow fiber bioreactor

The developed HFB system was validated by perfusion of HF module 2 containing $4 \cdot 10^7$ hepatocytes/ml with solutions of Gd-DTPA and Gd-BOPTA at different concentrations. Each perfusion with contrast agent was followed by a washing period with solution free of contrast agent. The perfusion and the following washing period lasted 20 minutes each when

Gd-DTPA and 30 minutes when Gd-BOPTA was perfused. Solution and gas flow rate were 100 ml/min and 4 l/min respectively.

5.2.6 Magnetic resonance imaging

The wrist coil - HFB system was laid on a plastic support built so that the middle of the HFB was exactly in the isocenter of the magnet. During perfusion, eight cross sections of the HFB inlet tubing, reference vials containing 0.5, 2 and 4 mM of Gd-DTPA, and the HFB were imaged on an Eclipse 1.5 T MR system (Philips Medical Systems Inc., Cleveland, OH, USA).

Dynamic T_1-weighted imaging was performed using fast gradient echo sequence FAST [5] with the following imaging parameters: 90°-180° magnetization preparation, TI/TR/TE 28/10.52/4 ms, FA 90°, FOV 10 cm, matrix size 256 x 256, slice thickness 5 mm. The inter-image delay was 2.5 seconds for the choice of the HFB and 20 seconds for all other experiments. Results were expressed as the mean SI of a cross-section as a function of time. Bioreactor SI - time curves obtained with different experiments were compared after normalization with the SI values of the 4 mM reference vial obtained during the experiment and corrected for the baseline.

A high resolution image was taken after each perfusion using a T_1-weighted spin echo sequence with the following imaging parameters: TR/TE 400/20 ms, bandwidth 20.83 kHz, slice thickness 5 mm, matrix size 512 x 512, number of averages 2, slices 8.

5.2.7 Kinetic modeling

For the choice of the HF module and flow rate, MR signal intensities (SI) of a HFB cross-section by respect to time were submitted to compartmental analysis using the software MicroPharm (version 4.0, 1995, Inserm, France). Equation 5.2 described the one-compartment model while the two-compartment model was described by equation 5.3, where k1 and k2 are the rate constants of phase 1 and 2 respectively.

$$SI = A \cdot \left[1 - e^{-k \cdot t} \right] \qquad \text{[Equation 5.2]}$$

$$SI = A \cdot \left[1 - e^{-k_1 \cdot t}\right] + B \cdot \left[1 - e^{-k_2 \cdot t}\right]$$ [Equation 5.3]

The relationship between the rate constant (k) and the half-life ($t_{½}$) is given by equation 5.4:

$$t_{1/2} = \frac{\ln 2}{k}$$ [Equation 5.4]

5.3 Results and discussion

5.3.1 Set up of the MRI compatible perfusion system

The major challenge was to build a MRI compatible perfusion system which did not contain any metallic piece inside the magnet room. This was possible by using only plastic and glass materials and by installing the heating system, the gas bottle and the pump in an adjacent room. A picture of the MRI part of the perfusion system is shown in figure 5.4.

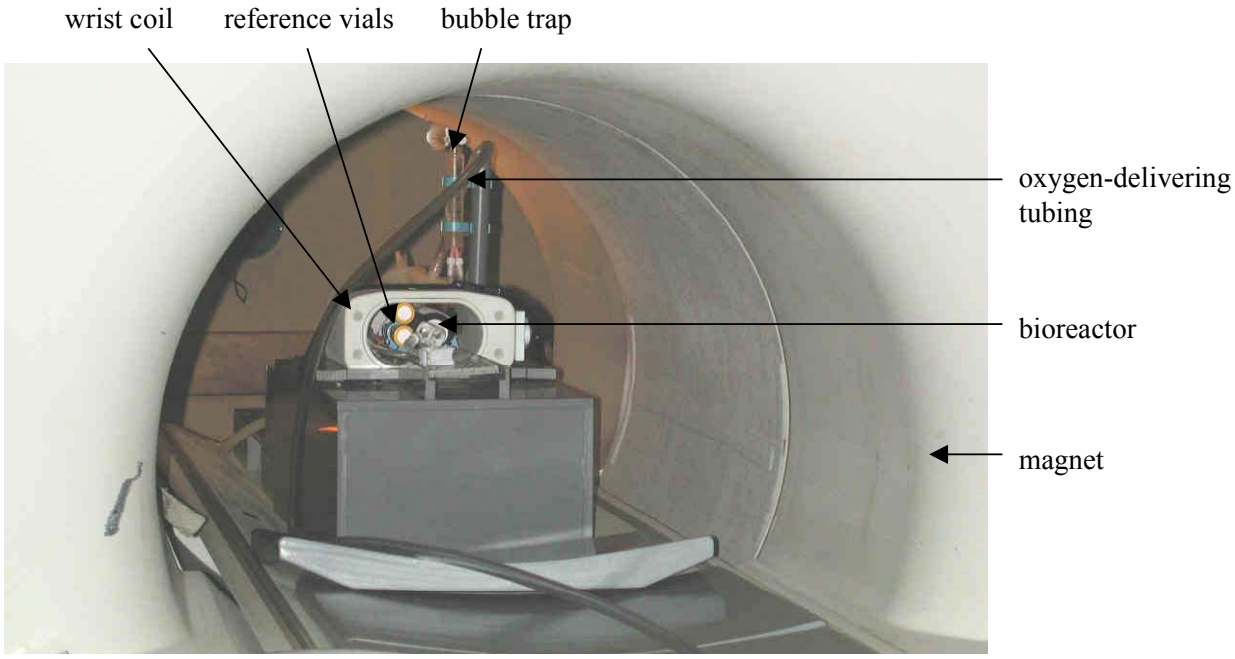

Figure 5.4: Picture of the MRI part of the perfusion system. The hollow fiber bioreactor was located in the isocenter of the magnet and wrist coil to have the best MRI resolution. The bioreactor was surrounded by the reference vials. The picture also shows the bubble trap and the oxygen-delivering tubing.

The HFB was imaged with the wrist coil because its size best suited for imaging the HFB. Strongest MR signal is obtained when imaging an object with a coil adapted to the size of the object and the wrist coil was the smallest coil available for the HFB.

5.3.1.1 Solution circulation system

The solution pH was adjusted to 7.2 during preparation. It rose and stabilized at pH 7.4 in the perfusion system, because of the increased oxygen concentration. HEPES enabled to stabilize the pH around 7.4, which was not possible with a bicarbonate buffer alone. Antibiotics were added to ensure sterility.

Long tubing was necessary to connect the different elements of the perfusion system, as they were located in two different rooms; the total dead volume was 275 ml. Hence, an efficient control was required to ensure a temperature of 37°C in the hepatocyte HFB.

5.3.1.2 Heating system

The temperature recommended for most human and warm-blooded animal cells is 37°C, close to body heat. It was set a little lower for safety reasons, as overheating is a more serious problem than underheating [6].

In order to have a culture temperature of 36.5°C inside the HFB the heating circulator temperature had to be set at 38.6°C. The corresponding temperature indicated by the probe at the outlet of the HFB near the reservoir was 32.0°C. During HFB perfusion experiments, only this latter temperature was continually checked, because of the risk of causing interferences with the magnetic signal if a probe was set at the HFB inlet, in the magnet. A reproducible temperature control of 32.0 ± 0.1 °C was obtained and considered as acceptable. Long tubing and big dead volumes explain the temperature decrease observed between the heating circulator, the HFB and the reservoir.

The refrigerant was installed in the magnet, just before the oxygenator system and the HFB. This avoided bubble formation due to temperature elevation, as oxygen solubility

decreases when temperature increases. Actually, if the solution had been oxygenated prior to heating, it would have produced bubbles.

5.3.1.3 Oxygenation system

As hepatocytes do consume a lot of oxygen, an improved oxygenation had to be ensured. This required the use of an artificial lung. We used a silicone membrane oxygenator similar to the one first described by Knazek et al. [7]. It consisted of silicone tubing through which O_2 and CO_2 can diffuse readily.

A gas flow rate of 3 l/min was found to be the minimal one which saturated the solutions with oxygen. For more security, the flow rate was fixed to 4 l/min during experiments. Actually, oxygen plays a key role in hepatocyte function and anoxia may lead to cell death [8]. An insufficient oxygenation of the system would cause a poor hepatocyte function and viability.

When using silicone tubing, one must be aware of possible adsorption phenomena of solutes contained in the perfusion solution. In our lab, we saw 7-ethoxycoumarin (7-EC) adsorption in the oxygenator. The evolution of Gd-BOPTA and Gd-DTPA concentrations in the perfusion solution with time during perfusion of the whole system is shown in figure 5.5. The adsorption of 7-EC in the system, was added to the graph for comparison.

In contrast to 7-EC, no adsorption of Gd-BOPTA or Gd-DTPA in the perfusion system was detected. The absence of adsorption of Gd-DTPA and Gd-BOPTA was also confirmed during MRI experiments by measuring the inlet tubing signal intensity during HFB perfusion which stayed stable during the whole period of perfusion with Gd-DTPA and Gd-BOPTA. Like 7-EC, other drugs are also adsorbed by silicone, e.g. antibiotics [9] or fentanyl [10]. Nevertheless, silicone tubing is used to improve oxygenation in various cell culture systems, and in particular for HFB [11].

Other kinds of oxygenators have been described, mainly polypropylene-based oxygenators, which are less susceptible to drug adsorption [10]. For instance, Gerlach et al. [12] developed

an HFB with a direct oxygenation of the hepatocytes. The system was composed of a separate network of HF which did not contained the perfusion solution but oxygen. Polypropylene hollow fibers are also used clinically for blood oxygenation during cardiopulmonary bypass [13,14].

As the simple and good value silicone membrane oxygenator allowed an improved oxygenation of the hepatocytes without adsorbing the investigated contrast agents Gd-BOPTA and Gd-DTPA, it was further used in the MRI perfusion experiments.

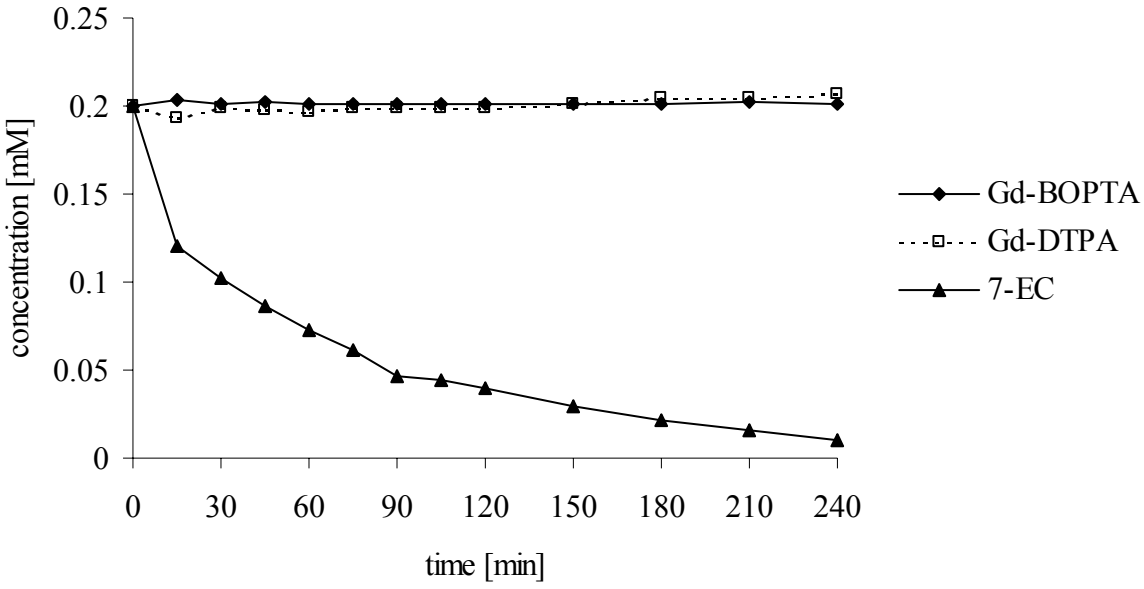

Figure 5.5: Adsorption in the perfusion system of Gd-BOPTA, Gd-DTPA and 7-ethoxycoumarin (7-EC).

5.3.2 Determination of the optimal hepatocyte concentration in the HFB

The hepatocyte concentration in the HFB is a crucial point as it must be as large as possible to mimic liver cellular density and permit MRI detection. However, it should avoid

causing cellular toxicity due to density and a minimum of animals should be sacrificed. Two different cellular densities were compared: $2 \cdot 10^7$ and $4 \cdot 10^7$ cells/ml.

According to the literature [15-17], the mean hepatocyte diameter is estimated at 25 μm, which gives a mean hepatocyte volume of 8181 μm^3. It is assumed that the total hepatocyte volume represents 80-85% of the liver volume and hepatocyte density is 10^8 cells/cm^3. In comparison, with a cell density in our HFB of $2 \cdot 10^7$ cells/ml, the volume occupied by hepatocytes is only about 20% of the ECS of the HFB (25 ml). This volume is about 40% when the cell density in the HFB is $4 \cdot 10^7$ cells/ml. A density of $2 \cdot 10^7$ cells/ml corresponds to 500 millions of hepatocytes inoculated in the 25 ml ECS of the bioreactor. This quantity was isolable from a single rat liver. On the other hand, $4 \cdot 10^7$ cells/ml was achievable with hepatocyte extraction of two rat livers, which could be made in less than 8 hours. While extracting cells from the second liver, hepatocytes already isolated from the first liver were kept in ice-cold UW solution. Hepatocytes preserved at 4°C in this solution remain functional and viable for several hours [18-21] without deterioration of transport functions, as shown in chapter 4.

The percentage of LDH and AST released in the perfusion solution as a function of time was used as a toxicity index to validate the optimal HFB cellular density. The percentage of LDH and AST released in the perfusion solution was calculated as the percentage of LDH and AST activity in the perfusion solution compared to the total LDH and AST activity contained in hepatocytes. The total activity of enzymes contained in hepatocytes determined after disruption of the membrane with Triton X-100 was 6.46 ± 0.73 U/10^6 cells for LDH and 2.55 ± 0.26 U/10^6 cells for AST (n = 18).

Figure 5.6 shows the evolution of LDH and AST release in the solution as a function of time of perfusion. These results suggest that increasing the HFB hepatocyte density from $2 \cdot 10^7$ cells/ml to $4 \cdot 10^7$ cells/ml did not result in increased cellular toxicity. Actually, AST and LDH activity in the perfusion solution showed similar progressions, the curves obtained with $4 \cdot 10^7$ cells/ml rose a little more than the curves obtained with $2 \cdot 10^7$ cells/ml, but the

difference was not significant. After 4 hours of perfusion, about 16% of total intracellular LDH and about 5% of total intracellular AST were released in the perfusion solution.

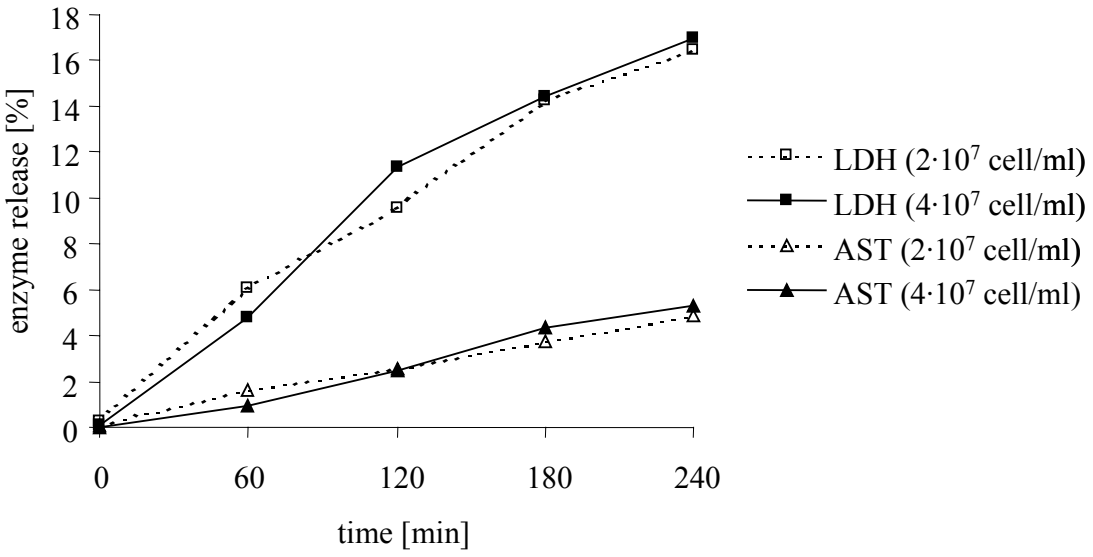

Figure 5.6: Evolution of LDH and AST release in the solution as a function of time of perfusion, expressed as percentage of the total LDH and AST activity contained in hepatocytes.

Most cell viability tests rely on direct coloration with dye (e.g. trypan blue, fluorescein). These tests could not be applied to monitor cell viability during our experiments as HFB are closed systems, rendering cell sampling impossible. The methods currently used to quantify cell vitality in HFB perfusion systems include oxygen consumption, enzyme release, and evaluation of complex synthetic and metabolic activities [22]. The concentration of intracellular enzymes released due to membrane leakage (e.g. LDH, AST, ALT, GPT, GLDH, GGT and transaminases) is used as a criterion of cellular integrity and quality [23]. The percentage of LDH liberation observed is more important than that of AST because LDH is located in the cytosol, while AST is found in the mitochondria. When cell death begins, the cell membrane is damaged first, leading to LDH release, and the mitochondrial membrane is affected only later, with its consequent AST liberation. Among all enzymes, LDH is the most sensitive marker of cell damage [23]. Baur et al. [22] observed a correlation between the

percentage of total cells stainable by trypan blue and the percentage of total LDH release; LDH release was even a little more sensitive than the trypan blue exclusion test. Using LDH release as a cellular viability marker, our results suggest that hepatocyte viability was about 85% after 4 hours of perfusion.

It is difficult to compare our results of total enzyme activities in hepatocytes with values from the literature, as they vary markedly among authors. For instance, Chao et al. [24] found that fresh hepatocytes treated with 0.1% Triton X-100, yielded 3500-4500 U LDH/10^6 cells. Baur et al. [22] demonstrated that a liver with a fresh weight of 12 g corresponded to a total LDH activity of 4200 U. Considering that liver density is 1 g/ml and hepatocyte density 10^8 cells/cm^3 [15], this gives a total LDH activity of 3.5 U/10^6 hepatocytes. Thus, our result of the total activity of LDH, 6.5 U/10^6 hepatocytes, is situated close to the value of Baur et al.

To summarize, increasing the HFB hepatocyte density from $2 \cdot 10^7$ cells/ml to $4 \cdot 10^7$ cells/ml did not increase cellular toxicity, and the higher the cellular density, the better it will mimic the physiological state. Hence, a cellular density of $4 \cdot 10^7$ cells/ml was used for further MRI experiments. This represents a cellular density in the ECS of 40%, which allows a good compromise between cellular toxicity, animal sacrifice, and physiological state, where the hepatocyte density is about 80%. A picture illustrating HFB before and after inoculation of $4 \cdot 10^7$ cells/ml in the ECS is presented in figure 5.7.

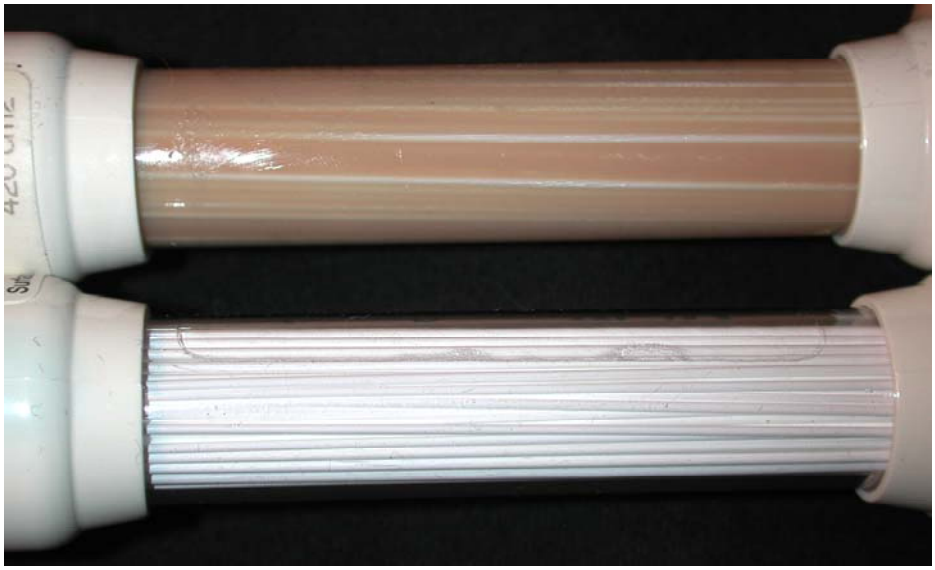

Figure 5.7: Hollow fiber bioreactor before (at the bottom) and after inoculation of $4 \cdot 10^7$ cells/ml (in the top) in the extracapillary space.

5.3.3 MRI of the bioreactor

SI was maximal in the zone situated in the middle of the HFB which corresponded to the isocenter of the magnet. As seen in figure 7.8, this zone corresponded to the 4th and 5th of the eight cross-sections measured. The value of the maximal SI decreased as the slices moved away from the isocenter. Indeed, the SI of the second and 7th slice were lower than the one of the 4th and 5th. The very low SI of the first cross-section may suggest that it was situated outside the HFB.

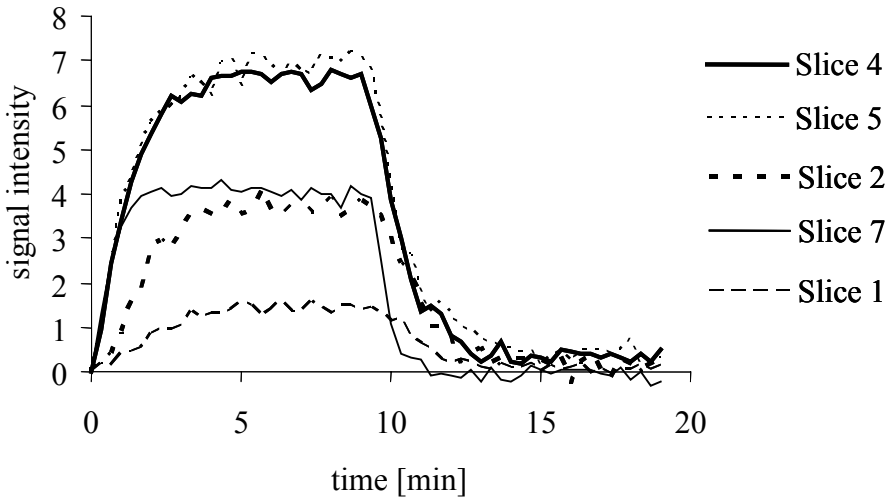

Figure 7.8: Evolution of MR signal intensity with time of a hollow fiber bioreactor perfused with solution + Gd-DTPA 0.2 mM for 10 minutes and with solution free of contrast agent for 8 minutes. The SI obtained with different slices were corrected for the baseline. Only 5 of the 8 cross-sections measured were represented for a better legibility of the graph.

Consequently, the 4th slice was taken for the different calculations and interpretations made with the HFB. Results of dynamic imaging were expressed as signal intensity - time curves.

An example of a high resolution image of a typical experiment at the level of the 4th slice of the HFB is depicted in figure 5.8. This image represents a cross section of the elements located in the wrist coil. The hollow fibers and packs of hepatocytes could be observed inside the bioreactor, which was not possible by dynamic imaging. Reference vials and HFB inlet and outlet tubing were surrounding the HFB.

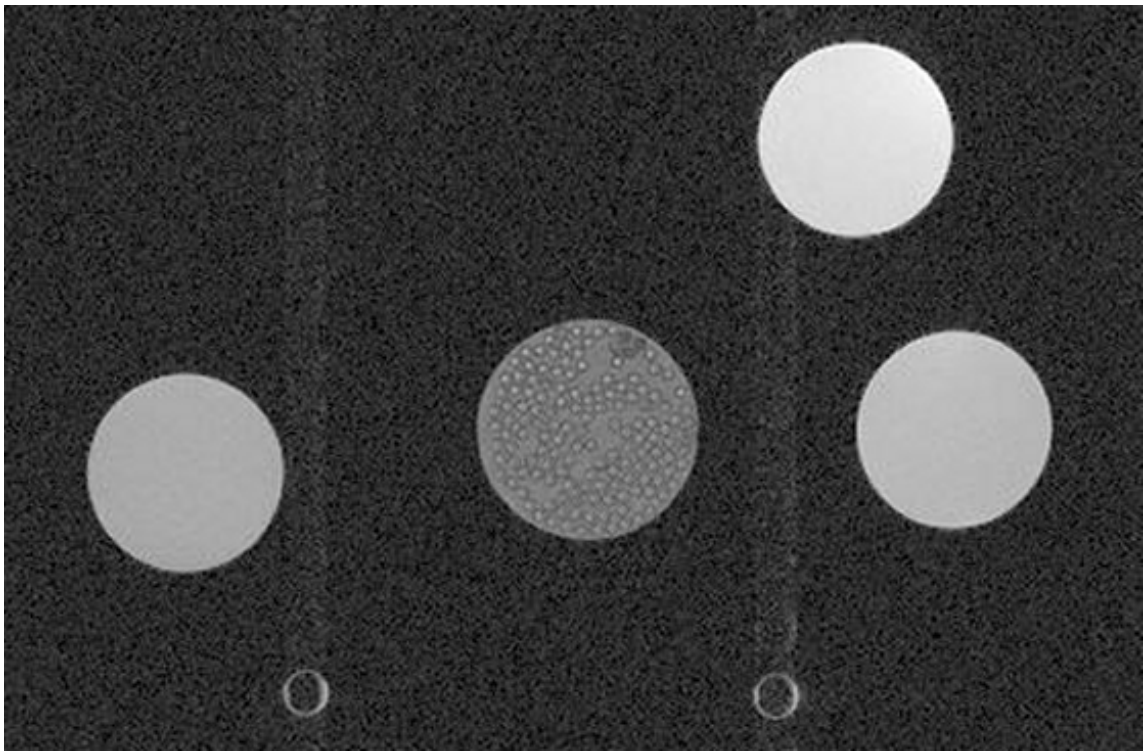

Figure 5.8: High resolution image (spin echo sequence, TR/TE 400/20 ms, bandwidth 20.83 kHz, slice thickness 5 mm, matrix size 512 x 512) of the hepatocyte hollow fiber bioreactor (HFB). The HFB (in the middle) was surrounded by three reference vials containing 0.5 (at the bottom left), 2 (at the bottom right) and 4 mM (at the top right) of Gd-DTPA, and by HFB inlet and outlet tubing (at the bottom). Hollow fibers were distinguishable inside the bioreactor.

5.3.3.1 Choice of the hollow fiber module

There are many kinds of HFB modules available on the market, but we decided to test only a small number of HF modules which corresponded to our criteria, namely:

Large fiber porosity to have a maximal exchange rate between the ICS and the ECS, i.e. to rapidly obtain contrast agent concentration equilibrium, and to provide hepatocytes with maximal nutrients and oxygen;

HF module diameter large enough to allow MRI analysis, and

Length short enough to get an important cell density.

The three modules tested differed from each other by fiber surface area (FSA) and porosity: module 1 had a FSA of 140 cm^2 and a porosity of 0.5 μm, module 2 had a FSA of 420 cm^2 and a porosity of 0.5 μm and module 3 had a FSA of 140 cm^2 and a porosity of 0.2 μm.

The diffusion of Gd-DTPA 2 mM into the ECS of the three different HF modules tested at a flow rate of 100 ml/min is depicted in figure 5.9. HFB were first perfused with a solution without contrast agent, and after 15 seconds with a solution containing 2 mM Gd-DTPA.

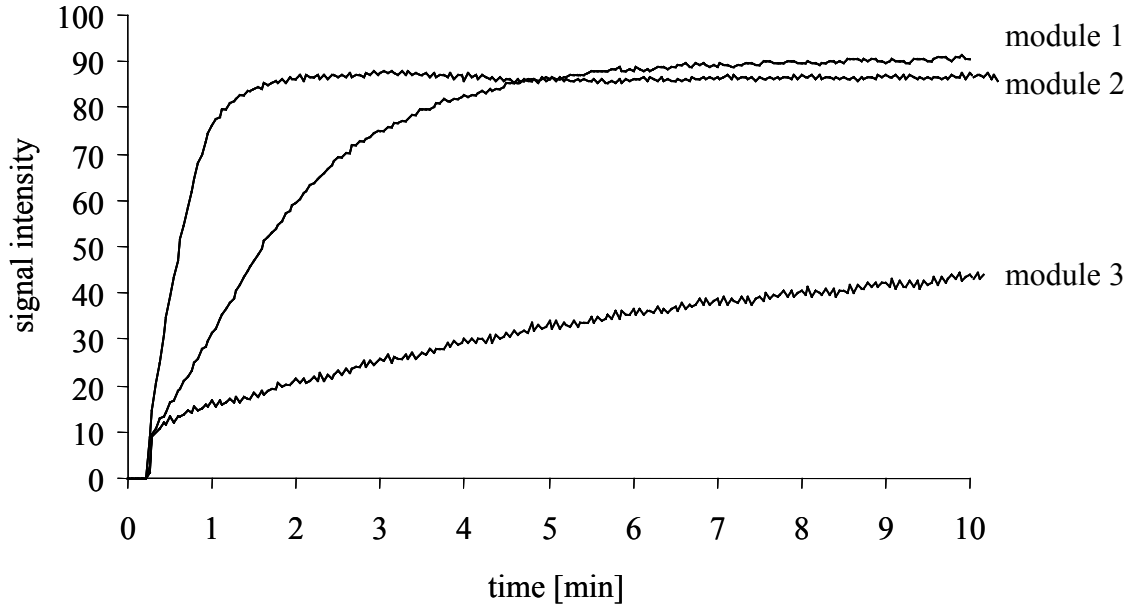

Figure 5.9: Normalized MRI signal intensity – time curves of hollow fiber bioreactor (HFB) filling with Gd-DTPA 2 mM, flow rate = 100 ml/min, module 1 = 0.5 μm, 140 cm^2, module 2 = 0.5 μm, 420 cm^2, module 3 = 0.2 μm, 140 cm^2. HFB were first perfused with a solution without contrast agent, and after 15 seconds with a solution containing 2 mM Gd-DTPA for 10 minutes.

As shown in figure 5.9, steady-state was rapidly reached with modules 1 and 2. On the contrary, with module 3 steady-state was not reached after 10 minutes.

SI – time curves were analyzed according to equations 5.1 and 5.2. Results of the kinetic compartmental analysis are given in table 5.1.

Table 5.1: Results of the kinetic compartmental analysis of the SI - time curves.

	Kinetic model	t ½ phase 1	t ½ phase 2
Module 1	1 compartment	1.19 ± 0.01 min	-
Module 2	1 compartment	0.29 ± 0.00 min	-
Module 3	2 compartments	0.06 ± 0.01 min	4.56 ± 0.13 min

Compartmental kinetic analysis enabled to quantify the filling process of the HFB with contrast medium. While the filling process of modules 1 and 2 followed a one-compartment model, the one of module 3 corresponded to a two-compartment model (table 5.1).

These results suggest that in the case of modules 1 and 2, both fiber filling with Gd-DTPA and its diffusion through the fibers in the ECS were so rapid as not to be distinguishable. The filling of Gd-DTPA was more rapid with module 2 than with module 1, as shown by the half-lives of 0.3 and 1.3 minutes respectively. Generally, it is considered that 4 half-lives are necessary to reach 90 % of the steady-state. Consequently, one can estimate that module 1 was completely filled with Gd-DTPA after 4.8 minutes while it took only 1.2 minutes for module 2. These results are in good agreement with the curves depicted in figure 5.9.

In contrast, for module 3 the filling of the fibers with contrast solution and the diffusion process in the ECS showed different rate constants. The first phase, characterized by a short half-life of 0.1 minute corresponded to the filling of the hollow fibers with Gd-DTPA, whereas the second phase corresponded to the diffusion of contrast medium through the fibers in the ECS as it was observed on the images obtained during the dynamic imaging of the HFB. The latter was slow and was the limiting step of HFB filling. It had a half-life of 4.6 minutes, which means that 18.4 minutes were necessary to reach 90 % of the steady-state. Indeed, one can observe in figure 5.9 that steady-state was not obtained after 10 minutes perfusion with Gd-DTPA.

The slow diffusion of Gd-DTPA observed with module 3 was probably due to the smaller pore size of 0.2 μm compared to 0.5 μm. Module 2 filling was faster than the one of module 1 because of its larger fiber surface area of 420 cm^2, whereas it was only 140 cm^2 for module 1.

Module 2 was used for further hepatocyte HFB experiments as it permitted to reach the steady-state after the shortest time period (1.2 minutes).

5.3.3.2 Optimization of the flow rate

Figure 5.10 shows the influence of the perfusion solution flow rate on the diffusion of Gd-DTPA 0.2 mM in module 2, as a function of time. The three different flow rates tested were 50, 75 and 100 ml/min. The HFB was first perfused with solution without contrast agent and after 3 minutes with a solution containing 0.2 mM Gd-DTPA.

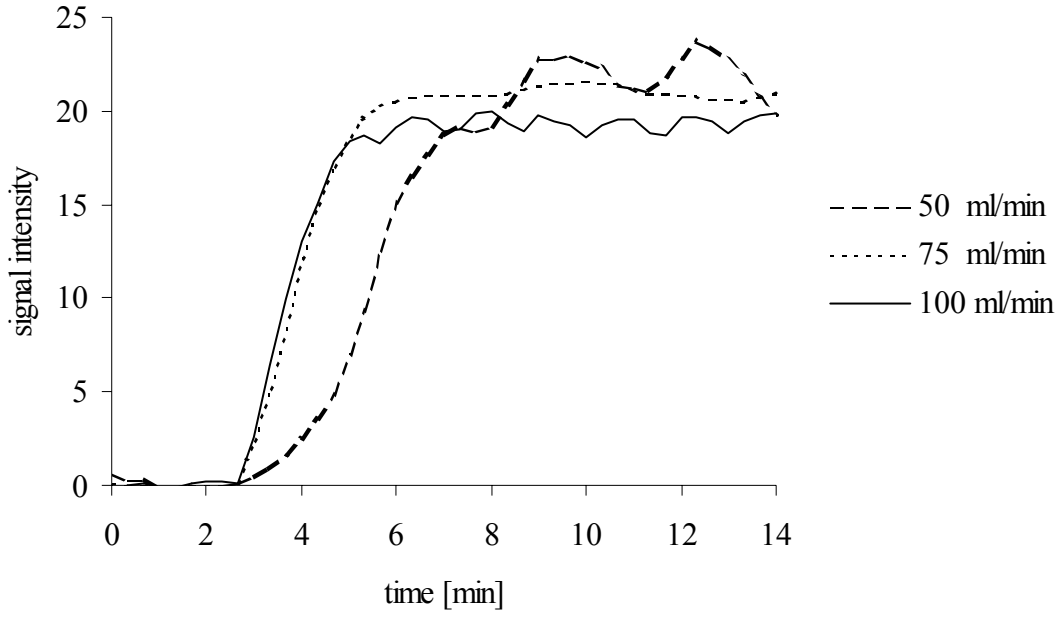

Figure 5.10: Normalized MRI signal intensity – time curves of hollow fiber bioreactor (HFB) filling (module 2, 0.5 μm, 420 cm^2) with Gd-DTPA 0.2 mM, at three different flow rates (50, 75 and 100 ml/min). HFB was first perfused with solution without contrast agent and after 3 minutes with a solution containing 0.2 mM Gd-DTPA.

The results presented in figure 5.10 clearly indicate that the steady-state was obtained with the three flow rates tested, but with different velocities. Whereas the steady-state was obtained rapidly and almost at the same time with flow rates of 75 and 100 ml/min, diffusion of Gd-DTPA in the ECS of the HF module was slower with a flow rate of 50 ml/min.

Kinetic analysis enabled to measure the diffusion difference between flow rates of 75 and 100 ml/min. The two curves were well described by a one-compartment model, with half-lives of 1.00 ± 0.05 and 0.82 ± 0.04 minutes respectively. Hence, diffusion of contrast medium through the HF membrane in the ECS was more rapid with a flow rate of 100 ml/min, although the difference with diffusion at a flow rate of 75 ml/min was slight. The relation between the rate of solute appearance in the ECS and the flow rate has also been observed by other authors [25,26].

One could have tested greater flow rates. Based on the previously shown results, the greater the flow rate, the more rapid the diffusion. However, diffusion did not accelerate significantly when increasing the flow rate from 75 to 100 ml/min. This suggests that increasing the flow rate over 100 ml/min would not have considerably changed diffusion, but it could have improved oxygenation and oxygen is the most important nutrient for hepatocytes [11]. On the other hand, increasing the flow rate also increases cell shear stress when hepatocytes are present in the HFB extracapillary space, which is prejudicial. Thus, a compromise between optimal diffusion, oxygenation and minimal cell shear stress was chosen and the flow rate was fixed to 100 ml/min for the hepatocyte HFB experiments.

A closer look at figure 5.10 shows that signal intensity did not remain stable after having reached the steady-state. Signal intensity oscillations were greater with flow rates of 50 and 100 ml/min than with a flow rate of 75 ml/min. The source of these SI oscillations is still unknown, but they seem to be related to the flow rate. Indeed, oscillation period and amplitude looked like being two times greater with a flow rate of 50 ml/min than with a flow rate of 100 ml/min. These oscillations were maybe due to a kind of resonance phenomenon in the perfusion system. This aspect will be investigated in a near future.

5.3.3.3 Validation of the hepatocyte hollow fiber bioreactor

To validate our *in vitro* model, we studied the behavior of an extracellular contrast agent (Gd-DTPA) and an intracellular contrast agent (Gd-BOPTA) by MRI during perfusion of the HFB with the two contrast agents. Typical rough SI - time curves are presented in figure 5.11.

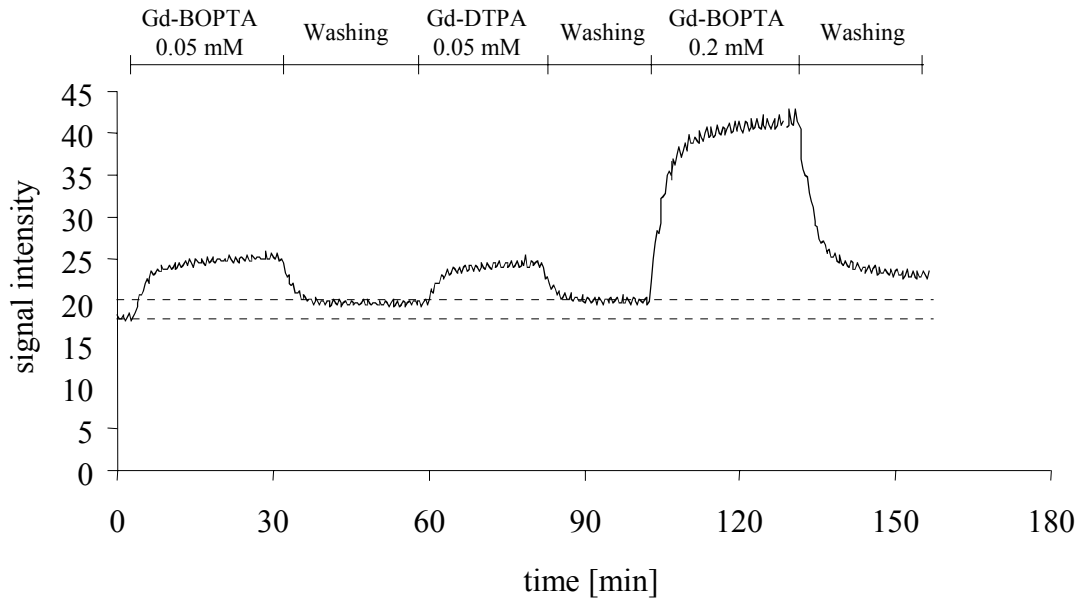

Figure 5.11: Evolution of MR signal intensity with time in a hollow fiber bioreactor (HFB) containing $4 \cdot 10^7$ hepatocytes/ml. The HFB was perfused with a solution + 0.05 mM Gd-BOPTA for 30 minutes, with a solution free of contrast agent for 30 minutes, with a solution + 0.05 mM Gd-DTPA for 20 minutes, with a solution free of contrast agent for 20 minutes, with a solution + 0.2 mM Gd-BOPTA for 30 minutes, and finally with a solution free of contrast agent for another 30 minutes. Dashed lines indicate the baselines.

These results indicate that the hepatocyte HFB system was able to show differences between Gd-DTPA and Gd-BOPTA. As can be seen in figure 5.11, at the beginning of the perfusion with Gd-BOPTA 0.05 mM the SI rapidly increased, followed by a slower increase. During the washing step, SI decreased rapidly to a value different from the one before the perfusion. Beyond that point, SI remained stable or very slightly decreased but without returning to the baseline. The subsequent perfusion of the hepatocyte HFB with Gd-DTPA 0.05 mM showed that the SI rapidly reached a steady-state and returned to the value of the

residual SI observed before the initiation of the perfusion with Gd-DTPA when the perfusion was switched to solution without contrast agent. This indicates that the residual amount of Gd^{3+} resulting from the first perfusion with Gd-BOPTA remained in the bioreactor or at least was released so slowly that the decrease was not detectable during the time period of the experiment. Consequently, it was possible to continue with an additional perfusion using the same hepatocytes in the same HFB by simply taking into account this new baseline. In the case presented in figure 5.11, the HFB was further perfused with a solution containing Gd-BOPTA 0.2 mM. The shape of the SI-time curve was similar to the one obtained with Gd-BOPTA 0.05 mM but with a higher SI. This procedure allowed to use the same hepatocyte HFB for up to three consecutive experiments, which represented a gain in time and animals. Indeed, the preparation of the hepatocyte HFB is time-consuming and a reduced number of sacrificed animals is an advantage from an ethical and economic point of view.

The rapid and reversible evolution of SI obtained with the extracellular contrast agent Gd-DTPA can be explained as follows: Gd-DTPA rapidly diffused from the ICS through the hollow fibers and filled the ECS of the bioreactor, i.e. the space between hepatocytes. When perfusion was changed to solution without contrast agent, Gd-DTPA completely disappeared from the HFB. During perfusion of the intracellular contrast agent Gd-BOPTA, the same observable processes of diffusion and filling occurred, but with a supplementary phenomenon: Gd-BOPTA had an additional distribution space, as it can penetrate hepatocytes, and this was the rate-limiting step. After 30 minutes perfusion with solution free of contrast medium, Gd-BOPTA was not completely washed out from the bioreactor. A residual SI was observed (figure 5.11), indicating that a part of the Gd-BOPTA remained in the hepatocytes. Actually, this residual SI could not be due to adsorption of Gd-BOPTA anywhere in the bioreactor as no adsorption of Gd-BOPTA was detected by fluorescence and MRI in the whole perfusion system (5.3.1.3).

The reproducibility of the method was assessed with two additional experiments in which solutions of Gd-BOPTA 0.2 mM were perfused in the hepatocyte HFB (figure 5.12).

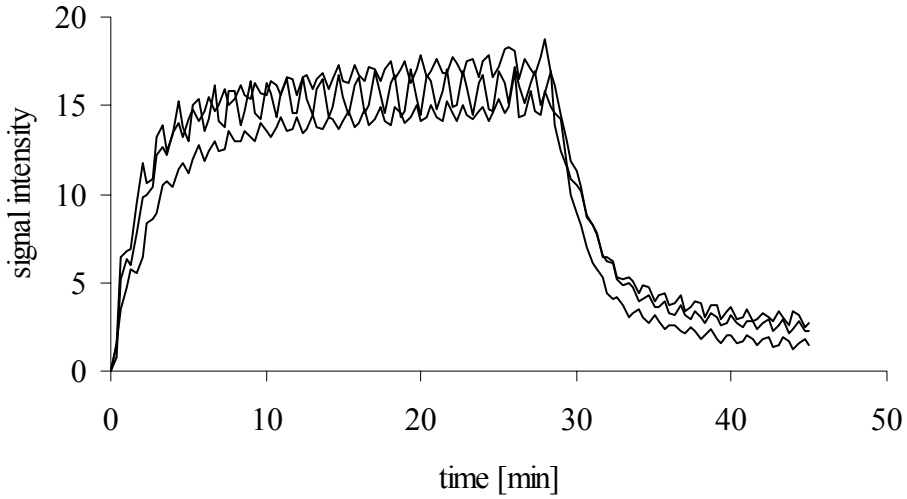

Figure 5.12: Evolution of normalized MRI signal intensity with time in three hollow fiber bioreactors containing $4 \cdot 10^7$ hepatocytes/ml. Bioreactors were perfused with solution + 0.2 mM Gd-BOPTA for 30 minutes, and then with solution exempt of contrast agent for 15 minutes. SI were first corrected to zero and then normalized according to the SI of reference vials.

These results indicate that reproducible SI - time curves were obtained with Gd-BOPTA perfusion during different experiments, after normalization according to SI values of the 4 mM reference vial and correction to zero. Actually, the SI obtained after 30 minutes of perfusion with Gd-BOPTA 0.2 mM with three experiments are the same (15.1 ± 0.9; 16.1 ± 0.8; 17.1 ± 1.2). The same reproducibility was obtained with perfusion of Gd-DTPA (data not shown). Correction to zero was necessary as SI obtained with a solution free of contrast agent had a positive initial SI value. MRI does not give identical SI from one experiment to the other. Therefore, normalization with reference vials was crucial. Indeed, uncorrected SI - time curves obtained during diverse experiments performed under identical experimental conditions (e.g. concentration of contrast agent, etc.) could differ from each other by more than 50%.

The cellular viability during experiments was checked by determination of the oxygen consumption and release of intracellular enzymes, AST and LDH. As seen in table 5.2, the oxygen consumption was about 1000 μM/h after 3 hours of experiment; it did not decline with time but seemed to have an upward trend. The viability of hepatocytes, based on the

amount of AST and LDH released was routinely greater than 90% after 3 hours of experiment. These results confirm that the perfusion system was able to ensure a good cellular viability.

Table 5.2: Cell viability monitoring with oxygen consumption and LDH and AST release (n = 3).

time [min]	0	30	60	90	120	150	180
O_2 consumption [μM/h]	0.0 ± 0.0	700.0 ± 35.6	626.5 ± 8.2	908.3 ± 105.1	1068.1 ± 61.7	1025.1 ± 203.2	1017.6 ± 144.2
LDH release [%]	0.0 ± 0.0	1.1 ± 0.4	2.0 ± 0.2	3.6 ± 0.4	5.6 ± 0.2	6.5 ± 0.1	8.3 ± 0.8
AST release [%]	0.0 ± 0.0	0.2 ± 0.1	0.6 ± 0.1	0.8 ± 0.2	1.3 ± 0.2	1.9 ± 0.2	2.2 ± 0.4

No bacterial growth was observed in agar-agar cultures, indicating that the perfusion system remained sterile during the whole experiment.

5.4 Conclusion

The purpose of this work was to develop and to validate a MRI compatible *in vitro* cellular model permitting the study of contrast agents. The cell culture device consisted of a HFB containing freshly isolated rat hepatocytes. The HFB perfusion system was set up according to the MRI requirements, in particular the absence of metallic components in the MRI room. The elements located in the magnet room were made of plastic or glass material, and the equipment containing metal pieces was set in an area adjacent to the magnet room.

The perfusion system developed was able to supply hepatocytes contained in the ECS of the HFB with a thermoregulated and oxygenated solution. The use of a silicone membrane oxygenator alimented with a mix of oxygen (95%) and carbon dioxide (5%) at a flow rate of 4 l/min resulted in a good oxygenation without adsorption of the investigated contrast agents. Perfusion experiments were performed using a HF module with a porosity of 0.5 μm, which was the biggest porosity available on the market, and a surface area of 420 cm^2. These

characteristics, together with the use of a high flow rate of 100 ml/min permitted to rapidly reach a concentration equilibrium between the intra- and the extracapillary space of the bioreactor. Rapid and total diffusion of contrast agents was very important as we wanted to see their behavior towards hepatocytes; rapid diffusion of oxygen and other nutrients is also crucial for the maintenance of hepatocytes viability. As a result, we obtained a good cellular viability during perfusion experiments; based on LDH release, one can estimate that hepatocyte viability was greater than 85% after 4 hours perfusion. HFB hepatocyte density was $4 \cdot 10^7$ cells/ml. This density did not cause cellular toxicity and did not require an excessive sacrifice of animals, but permitted to obtain a hepatocyte density close to the half of the *in vivo* hepatocyte density.

Normalization of the SI – time curves by means of reference vials allowed the comparison of results generated by different experiments and it was shown that the results were reproducible. These results also demonstrated that the *in vitro* model developed permitted to differentiate the behavior of the intracellular contrast agent Gd-BOPTA and the extracellular contrast agent Gd-DTPA, the contrast agents being directly measured by MRI. Moreover, the consecutive perfusion of a single hepatocyte HFB with up to three different solutions of contrast agent was a procedure which represented an important gain in time and animals.

In summary, we succeeded in developing an *in vitro* cellular model for the study of MRI contrast agents, where the effects of the contrast agents investigated were directly measured by MRI. We offer a tool to better understand the mechanisms of hepatobiliary contrast agents both in healthy and diseased hepatocytes.

References

[1] Hamilton RL, Berry MN, Williams MC, and Severinghaus EM, A simple and inexpensive membrane "lung" for small organ perfusion, *J Lipid Res*, 1974, **15**, 182-186.

[2] Seglen O, Preparation of isolated rat liver cells, In 'Methods in Cell Biology', Ed. Prescott DM, Academic Press, New York, 1976, Vol. 13, pp. 29-83.

[3] Mamprin ME, Rodriguez JV, and Guibert EE, Importance of pH in resuspension media on viability of hepatocytes preserved in University of Wisconsin solution, *Cell Transplant*, 1995, **4**, 269-274.

[4] Nyberg SL, Remmel RP, Mann HJ, Peshwa MV, Hu W-S, and Cerra FB, Primary hepatocytes outperform Hep G2 cells as the source of biotranformation functions in a bioartificial liver, *Ann Surg* , 1994, **220**, 59-67.

[5] Gyngell ML, The application of steady-state free precession in rapid 2DFT NMR imaging: FAST and CE-FAST sequences, *Magn Reson Imaging*, 1988, **6**, 415-419.

[6] Freshney RI, Media, In 'Culture of Animal Cells', Ed. Freshney RI, Wiley-Liss, New York, 2000, pp. 89-104.

[7] Knazek RA, Gullino PM, Kohler PO, and Dedrick RL, Cell culture on artificial capillaries: an approach to tissue growth *in vitro*, *Science*, 1972, **178**, 65-67.

[8] Flendrig LM, La Soe JV, Jörning GGA, Steenbeek A, Karlsen OT, Bovée WMM, Ladiges NCJJ, te Velde AA, and Chamuleau RAFM, *In vitro* evaluation of a novel bioreactor based on an intgral oxygenator and a spirally wound nonwoven polyester matrix for hepatocyte culture as small aggregates, *J Hepatol*, 1997, **26**, 1379-1392.

[9] Mizutani T, Adsorption of some antibiotics and other drugs on silicone-coated glass surfaces, *J Pharm Pharmacol*, 1982, **34**, 608-609.

[10] Rosen DA, Rosen KR, and Silvasi DL, *In vitro* variability in fentanyl absorption by different membrane oxygenators, *J Cardiothoracic Anesth*, 1990, **4**, 332-335.

[11] Tharakan JP, Gallagher SL, and Chau PC, Hollow-fiber bioreactor for mammalian cell culture, In 'Upstream Processes: Equipment and Techniques', Ed. Avshalom M, Alan R. Liss, New York, 1988, pp. 153-184.

[12] Gerlach JC, Encke J, Hole O, Müller C, Ryan CJ, and Neuhaus P, Bioreactor for a larger scale hepatocyte *in vitro* perfusion, *Transplantation*, 1994, **58**, 984-988.

[13] Funakubo A, Sakuma I, Fukui Y, and Kawamura T, Development of a compact extracorporeal membrane oxygenation (ECMO) system, *Artif Organs*, 1991, **15**, 56-65.

[14] Niimi Y, Yamane S, Yamaji K, Tayama E, Sueoka A, and Nosé Y, Protein adsorption and platelet adhesion on the surface of an oxygenator membrane, *ASAIO J*, 1997, **43**, M706-M710.

[15] Greengard O, Federman M, and Knox WE, Cytomorphology of developing rat liver and its application to enzyme differentiation, *J Cell Biol*, 1972, **52**, 261-272.

[16] Sasse D, Spornitz UM, and Maly IP, Liver architecture, *Enzyme*, 1992, **46**, 8-32.

[17] Weibel ER, Staubli W, Gnagi HR, and Hess FA, Correlated morphometric and biochemical studies on the liver cell, *J Cell Biol*, 1969, **42**, 68-91.

[18] Sandker GW, Weert B, Slooff MJH, and Groothuis GMM, Preservation of isolated rat and human hepatocytes in UW solution, *Transplant Proc*, 1990, **22**, 2204-2205.

[19] Olinga P, Merema M, Slooff MJH, Meijer DKF, and Groothuis GMM, Influence of 48 hours cold storage in University of Wisconsin organ preservation solution on metabolic capacity of rat hepatocytes, *J Hepatol*, 1997, **27**, 738-743.

[20] Sandker GW, Slooff MJH, and Groothuis GMM, Drug transport, viability and morphology of isolated rat hepatocytes preserved for 24 hours in University of Wisconsin solution, *Biochem Pharmacol*, 1992, **43**, 1479-1485.

[21] Hammond AH and Fry JR, Maintenance of xenobiotic metabolism and toxicity in rat hepatocyte cultures after cell preservation at 4°, *Biochem Pharmacol*, 1993, **46**, 333-335.

[22] Baur H, Kasperek S, and Pfaff E, Criteria of viability of isolated liver cells, *Hoppe-Seyler's Z Physiol Chem*, 1975, **356**, 827-838.

[23] Kardassis D, Busse B, Besseling A, Kraemer M, Puhl G, Spatkowski G, Holland G, Schnoy N, Mueller C, Neuhaus P, and Gerlach JC, Enzyme release in hybrid liver support systems: marker for quality prior to clinical application, *Transplant Proc*, 1999, **31**, 668-669.

[24] Chao ES, Dunbar D, and Kaminski LS, Intracellular lactate dehydrogenase concentration as an index of cytotoxicity in rat hepatocytes primary culture, *Cell Biol Toxicol*, 1988, **4**, 1-11.

[25] Rozga J, Williams F, Ro M-S, Neuzil DF, Giorgio TD, Backfisch G, Moscioni D, Hakim R, and Demetriou AA, Development of a bioartificial liver: properties and function of a hollow-fiber module inoculated with liver cells, *Hepatology*, 1993, **17**, 258-265.

[26] Giorgio TD, Moscioni AD, Rozga J, and Demetriou AA, Mass transfert in a hollow fiber device used as a bioartificial liver, *ASAIO J*, 1993, **39**, 886-892.

Chapter 6
Complementary studies: effect of contrast agent concentration on the MR signal, image analysis and metabolism study

In the previous chapter, we described the development of a magnetic resonance imaging (MRI) compatible hepatocyte hollow fiber bioreactor (HFB) for the study of MRI contrast agents. It was shown that the system allowed to distinguish in a reproducible manner between the behavior towards hepatocytes of the hepatobiliary contrast agent Gd-BOPTA and the one of the extracellular contrast agent Gd-DTPA. In the present chapter, we investigated whether there was a domain of linearity between the MR signal intensity and the concentration of contrast agents. This linear correlation is important for further investigation of contrast agent mechanisms using the MRI compatible HFB. Hence, in the first part of this chapter, we studied the relation between the concentration of contrast agent and the signal intensity (SI) of tubes containing solutions of Gd-DTPA and Gd-BOPTA.

Another objective was to study a possible improvement of the MR image analysis. Two different approaches of image treatment were applied to improve the quality of the results by focusing on the effects due to hepatocytes. Unfortunately neither the delimitation of regions of interest (ROI) nor the creation of a mask of the fibers improved the results and will thus not be used for further experiments.

Finally, we tried to set up an additional test for the evaluation of the viability of hepatocytes contained in the HFB consisting of a continuous in-line assessment of the metabolic functions of the cells. Due to important adsorption phenomena of the substrate in the HFB perfusion system, it was not possible to perform this test to detect a metabolic reaction.

6.1 Effect of contrast agent concentration on the MR signal

As already mentioned in chapter 3, the MR signal depends on the characteristics of the object imaged, such as the proton density, on the relaxation times T_1 and T_2, and on the parameters of the data acquisition sequence. The signal intensity depends on these factors in a nonlinear way. On the other hand, the decrease of the relaxation times T_1 and T_2 by contrast agents is linearly correlated to their concentration but depends on various factors such as the temperature and the composition of the solution containing the contrast agents.

The present study aimed at an improved quantification of the MR signal. The influence of the concentration of Gd-DTPA and Gd-BOPTA on the signal intensity with tubes containing concentrations of contrast agent ranging from 0 to 50 mM was studied. Actually, to investigate the mechanisms of contrast agents in our future experiments, we would like to study the effect of the concentration of contrast agent perfused through the hepatocyte HFB, and this implies that the signal intensity is linearly correlated with the contrast agent concentration so that the results can be compared to each other.

6.1.1 Materials and methods

6.1.1.1 Chemicals

Solution of Gd-BOPTA 0.5 M was generously donated by Bracco Research S.A. (Geneva, Switzerland). A commercially available solution of Gd-DTPA 0.5 M (Magnevist®, Schering, Germany) was used. Bovine serum albumin (BSA, fraction V, 97%) was purchased from Fluka. All other chemicals were of analytical grade.

6.1.1.2 Preparation of the tubes and measurement of the signal intensities

Solutions of Gd-DTPA and Gd-BOPTA with concentrations ranging from 0 to 50 mM were prepared by diluting the concentrated solutions of Gd-DTPA and Gd-BOPTA in purified water and in modified Hanks's solution with or without 0.5% BSA. The solutions were filtered aseptically (Millex® GS, 0.22 μm, Millipore Co., Bedford, Massashuset, USA) in

plastic tubes of 50 ml and kept at 4°C till magnetic resonance imaging. The tubes were imaged using the same dynamic T_1-weighted sequence as for the HFB experiments described in chapter 5 but with the head coil instead of the wrist coil.

6.1.2 Results and discussion

Tubes containing solutions of Gd-DTPA and Gd-BOPTA in water with concentrations ranging from 0 to 50 mM were imaged in order to see the relation between signal intensity and the concentration of contrast agent (figure 6.1).

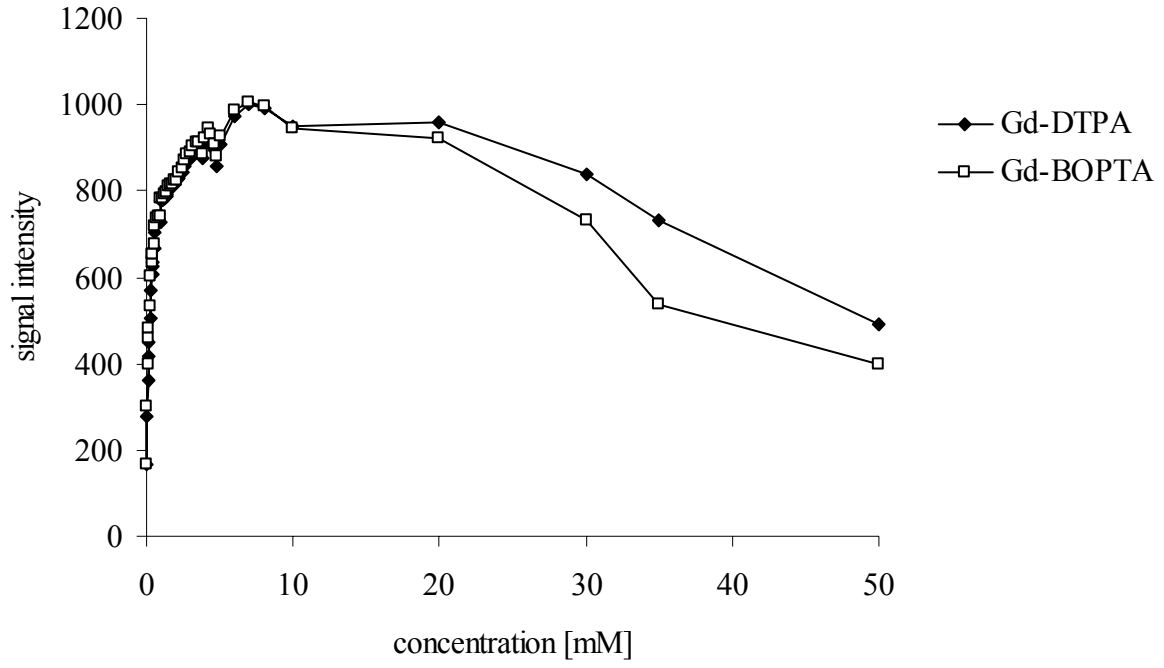

Figure 6.1: Plots of the signal intensity of tubes containing 0 to 50 mM of Gd-BOPTA and Gd-DTPA in water as a function of the contrast agent concentration.

When increasing the concentration of contrast medium from 0 to 7 mM, SI increased, too, but with a saturation of the signal intensity. Beyond 7 mM, SI declined with the increase of concentration, due to the growing importance of the T_2 effect. Hence, the SI of tubes

containing solutions of contrast agents ranging from 0 to 50 mM was not linearly correlated with concentration.

However, there seemed to be a linear correlation between SI and low concentrations of Gd-BOPTA and Gd-DTPA. Thus, we tested low concentrations of the two contrast agents to see whether there was a domain of linearity. We also studied the influence of the presence of 0.5% BSA as this is the amount of protein present in the modified Hanks's solution used for the HFB experiments.

The imaging of tubes containing solutions of Gd-DTPA and Gd-BOPTA with or without 0.5% of BSA showed that SI was linearly correlated to the concentration of contrast agent up to 0.4 mM (figure 6.2). Parameters of the linear regressions are compiled in table 6.1.

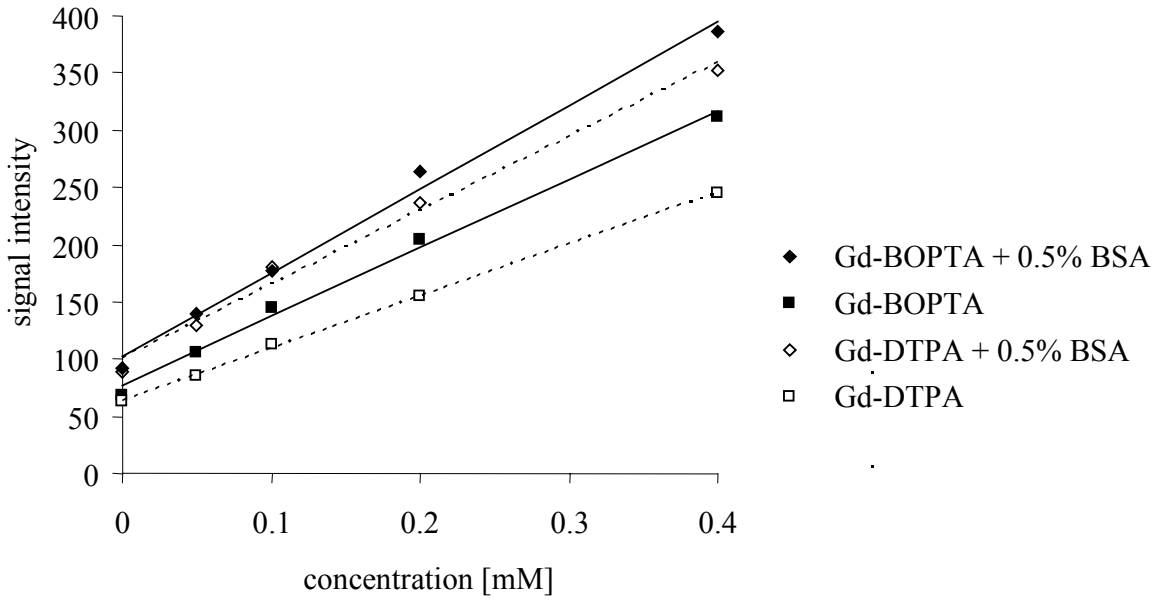

Figure 6.2: Plot of the signal intensity of tubes containing 0 to 0.4 mM of Gd-BOPTA and Gd-DTPA in Hanks's solution with or without 0.5% albumin as a function of the contrast agent concentration.

Table 6.1: Linearity between the signal intensity and the concentration of contrast agent (0 - 0.4 mM).

	Regression parameters					
	slope	Y-intersept	n	r^2	s	F
Gd-DTPA	455.2 ± 6.905	63.71 ± 1.424	5	0.999	2.184	4346
Gd-DTPA + 0.5% BSA	647.1 ± 40.69	100.4 ± 8.388	5	0.988	12.87	252.9
Gd-BOPTA	600.2 ± 26.56	77.03 ± 5.475	5	0.994	8.398	510.8
Gd-BOPTA + 0.5% BSA	733.6 ± 37.07	101.5 ± 7.641	5	0.992	11.72	391.7

BSA: bovine serum albumin, r^2: squared correlation coefficient, s: standard deviation of the residuals, F: Fisher test for significance of the equation

As the SI changed linearly with the concentration of Gd-DTPA and Gd-BOPTA up to 0.4 mM, with and without BSA in the Hanks's solution, this range of concentrations will be used for the further experiments performed with the HFB. Actually, within this range signal intensities obtained with different concentrations of contrast agent can be directly compared to each other. However, the linear regressions obtained cannot be used to convert signal intensities to concentrations in HFB perfusion experiments and the SI-time curves obtained from MR images of the HFB cannot be compared to dynamic concentration-time curves. In fact, the linear relationships obtained were observed in static tubes, while a flux is present in the HFB and flux is known to influence the SI. Moreover, when hepatocyte HFB were perfused with a solution containing Gd-BOPTA, the contrast agent was partially taken up by the hepatocytes. As the composition of the intracellular fluid is not identical to the one of the solution perfused, in particular richer in macromolecules which are known to change the relaxivity of several contrast agents, including Gd-BOPTA and Gd-DTPA, relaxivities are different in the intracellular fluid and the perfusion solution [1]. Hence, the non-homogeneity of the different compartments contained in the hepatocyte HFB impede the conversion of SI to concentration of contrast agent, at least at the present time where more research is needed to permit a better calibration of the MR signal.

As also shown in figure 6.2, the presence of albumin increased the SI by about 10% for Gd-BOPTA and Gd-DTPA. It is known that contrast agents have in general higher relaxivities in protein solutions than in water or saline. This has been attributed to so-called microviscosity effects [2]. Published values of the r_1 relaxivities of Gd-BOPTA are 4.4 $mM^{-1}s^{-1}$ in protein-free aqueous solution and ~8.0 $mM^{-1}s^{-1}$ in 4% BSA solution, while these values are 3.8 $mM^{-1}s^{-1}$ and ~4.3 $mM^{-1}s^{-1}$ respectively for Gd-DTPA [1,2]. Hence, the improvement of Gd-BOPTA relaxivity in the presence of 4% albumin is reported to be about two times higher than in saline solution, whereas the one of Gd-DTPA is more moderate. This is explained by the weak binding of Gd-BOPTA to albumin [3], while Gd-DTPA does not bind to albumin at all [1]. In our case, the increase of the SI of Gd-BOPTA in the presence of albumin was not so important (figure 5.9), probably because there was only 0.5% of albumin in the solutions. We investigated a concentration of 0.5% of albumin because it was the concentration used for the hepatocyte HFB experiments. Nevertheless and contrary to the literature, we observed that the SI of Gd-DTPA was even slightly more sensitive to the presence of 0.5% BSA than Gd-BOPTA.

At the same concentration, Gd-BOPTA gave a SI about 10% higher than the one of Gd-DTPA, with and without 0.5% BSA in the Hanks's solution. This will have to be taken into account when interpreting the signal intensities obtained with the hepatocyte HFB. Indeed, differences in SI were also observed when perfusing a bioreactor free of hepatocytes with Gd-BOPTA and Gd-DTPA 0.1 mM, as presented in figure 6.3. Thus, a higher SI observed when perfusing a hepatocyte HFB with Gd-BOPTA, compared to Gd-DTPA, can not simply be interpreted as being the consequence of the uptake of Gd-BOPTA in the hepatocytes. In fact, at least a part of this increase of SI is due to the higher relaxivity of Gd-BOPTA.

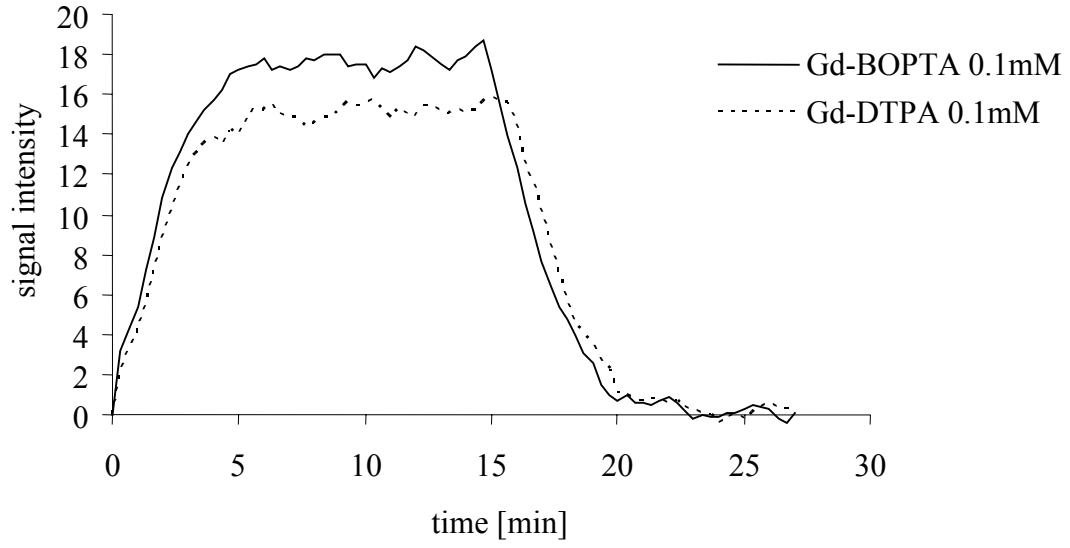

Figure 6.3: Evolution of the signal intensity with time in a hollow fiber bioreactor free of hepatocytes. The bioreactor was perfused with Hanks's solution + 0.1 mM of Gd-DTPA or Gd-BOPTA for 15 min, and washed with solution free of contrast agent for 15 min. SI was first corrected to zero to facilitate comparison.

6.1.3 Conclusion

The MRI of tubes containing increasing concentrations of contrast agents indicated that SI was linearly correlated to the concentration of Gd-DTPA and Gd-BOPTA as long as the concentration did not exceed 0.4 mM, in presence and in absence of albumin. According to these results, this range of concentrations will be used for further hepatocyte HFB experiments. Within this range, SI obtained with different concentrations of Gd-BOPTA and Gd-DTPA can be directly compared to each other.

At the same concentrations, with and without albumin, the signal intensities obtained with Gd-BOPTA were a little higher than with Gd-DTPA. Furthermore, the presence of 0.5% albumin slightly increased the SI for both of them. The higher SI of Gd-BOPTA compared to Gd-DTPA will have to be considered when interpreting results obtained with the hepatocyte HFB.

6.2 Approaches to improve the hollow fiber bioreactor image analysis

6.2.1 Introduction

In chapter 5, the MRI results obtained with the HFB were expressed as the mean SI of a cross section with time. Thus, the SI included the contribution of at least three elements: the fibers, the hepatocytes and the extracellular space surrounding the hepatocytes outside the fibers.

In this section, we tried different approaches of image treatment to see if it was possible to improve the quality of the results by focusing on the effects due to hepatocytes. The first approach was to see whether more information could be obtained from the SI generated by regions of interest (ROI) defined in the extracapillary space (ECS) of the bioreactors, and centered on hepatocytes. Secondly, we investigated the contribution of the intracapillary space (ICS) of the fibers to the signal intensity of the total cross section of the HFB and tried to eliminate it by building a mask of the fibers.

6.2.2 Materials and method

6.2.2.1 Chemicals

Solution of Gd-BOPTA 0.5 M was generously donated by Bracco Research S.A. (Geneva, Switzerland). A commercially available solution of Gd-DTPA 0.5 M (Magnevist®, Schering, Germany) was used. Bovine serum albumin (BSA, fraction V, 97%) was purchased from Fluka. All other chemicals were of analytical grade.

6.2.2.2 Isolation of hepatocytes, preparation of the bioreactor, and perfusion of the system

Hepatocytes were isolated from two rat livers by a two-step collagenase perfusion as described in chapter 4 and loaded in a HFB (Minikros® Sampler M15E 260 01N, Spectrum, Rancho Dominguez, CA, USA) at a final density of $4 \cdot 10^7$ cells/ml. The hepatocyte HFB was set in the wrist coil, and perfused with a 37°C oxygenated Hanks's solution containing

0.5% BSA with or without contrast agent at a flow rate of 100 ml/min. The viability of the hepatocytes was greater than 85% after 4 hours of experiment as assessed by the release of lactate dehydrogenase (LDH) and aspartate aminotransferase (AST) in the perfusate and by determining the oxygen consumption of hepatocytes. The setup of the whole procedure was described in detail in chapter 5.

6.2.2.3 Magnetic resonance imaging

Cross sections of the HFB were imaged with high resolution and dynamic sequences, as already described in chapter 5. The image treatments were based on the 4th slice of the HFB. High resolution images were used to define ROI in the extracapillary space of the HFB and to build a mask to remove the signal intensity coming from the hollow fibers. ROI were delimited by drawing a region in the ECS by hand. The construction of the mask began with the subtraction of two high resolution images, one with a flux of solution in the fibers and the other without flux, by stopping the peristaltic pump at the end of the experiment. This permitted to separate the fibers from the remaining of the section thanks to a threshold of SI. The images coming from the dynamic sequences were then reanalyzed considering only the signal intensity of the ROI or the signal intensity of the whole cross section without the fibers.

6.2.3 Results and discussion

6.2.3.1 Regions of interest

Figure 6.4 shows a high resolution image of a cross section of the HFB which served to delimitate a ROI in the extracapillary space of the hepatocyte HFB, where hepatocytes were located and where cell packs could be seen.

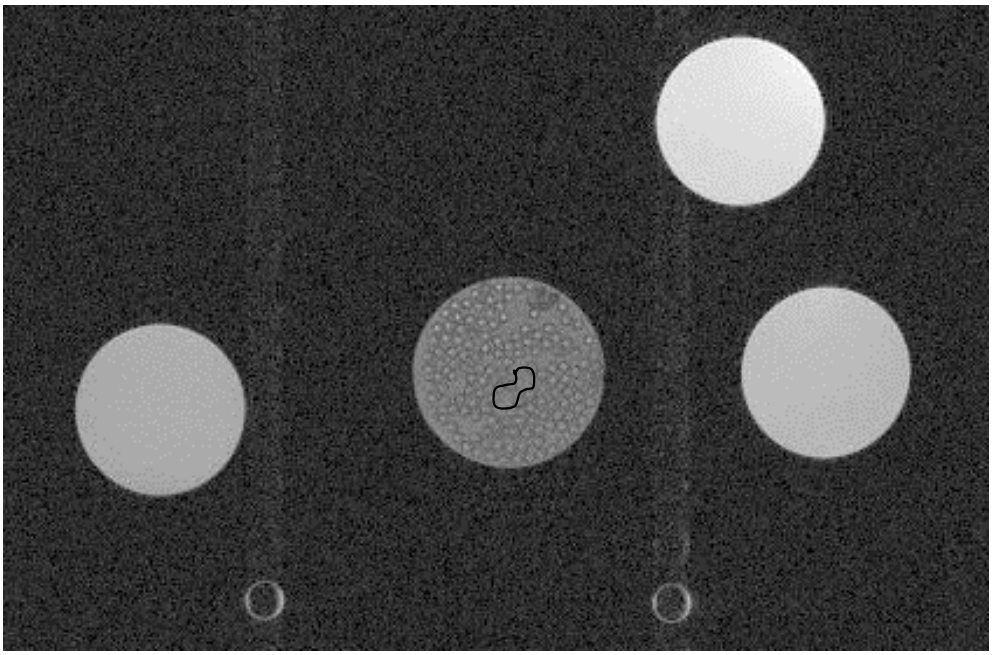

Figure 6.4: High resolution image of the hepatocyte hollow fiber bioreactor (HFB) with a delimitation of a region of interest (ROI). The ROI was drawn inside the bioreactor (in the middle) which was surrounded by three reference vials containing 0.5, 2 and 4 mM of Gd-DTPA, and by HFB inlet and outlet tubing (at the bottom). Hollow fibers were distinguishable inside the bioreactor.

After their creation in the high resolution images, ROI were applied to the whole dynamic imaging sequences during the hepatocyte HFB perfusion with Gd-DTPA and Gd-BOPTA. The evolution of the signal intensity in two different ROI and in the whole section of the HFB during the perfusion of Gd-DTPA and Gd-BOPTA 0.1 mM is shown in figure 6.5.

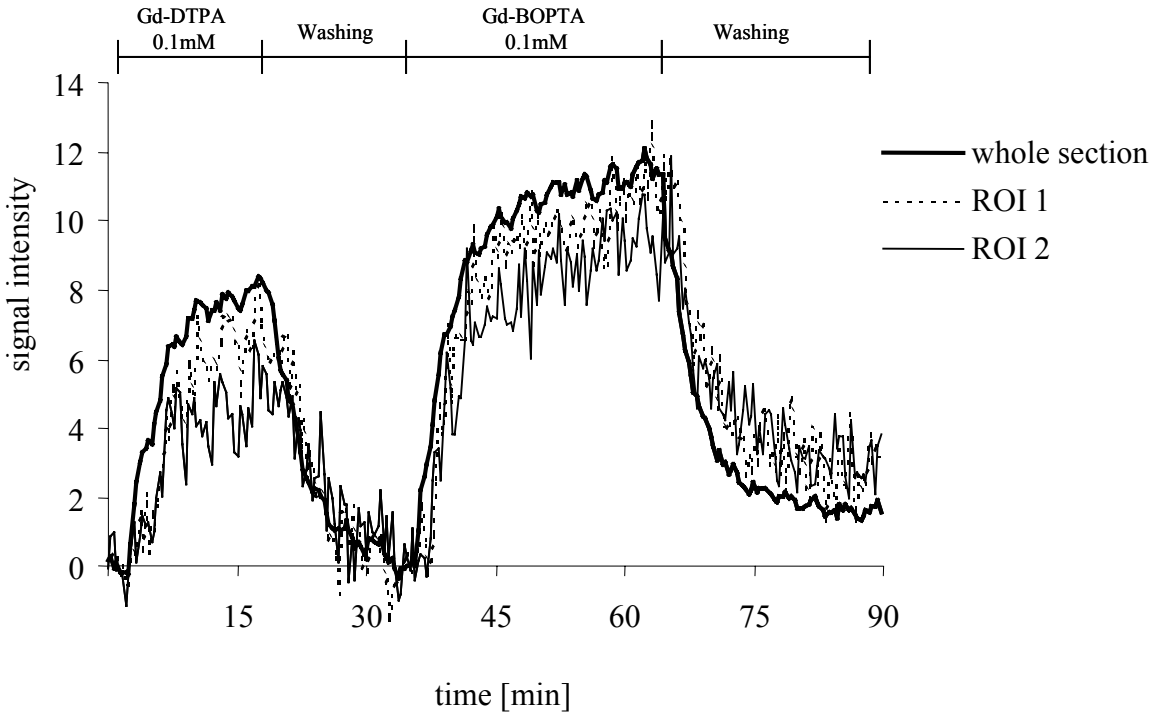

Figure 6.5: Evolution of MRI signal intensity with time in two different regions of interest delimited in the extracapillary space of a bioreactor containing $4 \cdot 10^7$ hepatocytes/ml. The bioreactor was perfused with Hanks's solution + 0.1 mM Gd-DTPA for 15 minutes, solution without contrast agent for 15 minutes, solution + 0.1 mM Gd-BOPTA for 20 minutes, and finally solution without contrast agent for 20 minutes. SI was corrected to zero for a better legibility of the figure.

The curves obtained with the ROI reached maxima which were lower than the one of the whole cross section of the HFB, while the residual SI observed after the perfusion with Gd-BOPTA were slightly higher. The difference between the SI of the whole section of the HFB and the ROI is due to the fact that ROI were drawn in the ECS in places where packs of hepatocytes could be seen. Thus, ROI permitted the withdrawal of regions in the ECS free of hepatocytes but also filled with contrast agent and to concentrate on the cells. As seen in chapter 5, the effect due to the cells is reflected by the residual SI. ROI permit to decrease the effect of the extracellular area, which was expressed as an inferior maximum of SI, while increasing the effect of hepatocytes, which was expressed as an amplified residual SI.

The fluctuations of SI obtained with ROI were larger than the ones obtained with the whole cross section of the HFB. These high fluctuations impeded the quantitative analysis of

the ROI SI-time curves. Results of only two ROI were presented here, although we assayed a larger number of them. Some ROI could not be used because of a huge fluctuation of SI and an absence of the characteristic shape of the curves. This illustrates the poor reproducibility of the results obtained with ROI, which can be explained by their location in spaces with more or less hepatocytes, or even with a piece of fiber. The high resolution images were of good quality, nevertheless, the determination by hand of ROI free of fiber pieces was not easy.

Though being an interesting approach, the use of ROI did not seem to be a useful way to analyze our results, considering the impossibility to perform quantitative analysis of the ROI SI-time curves and the complexity of the delimitation of ROI. Thus, it will not be applied in future experiments.

6.2.3.2 Mask of the fibers

High resolution images were used to build a mask which permitted to eliminate the signal intensity coming from the hollow fibers. The progression of the signal intensity of the whole cross section of the HFB with or without the contribution of the SI due to the fibers is shown in figure 6.6.

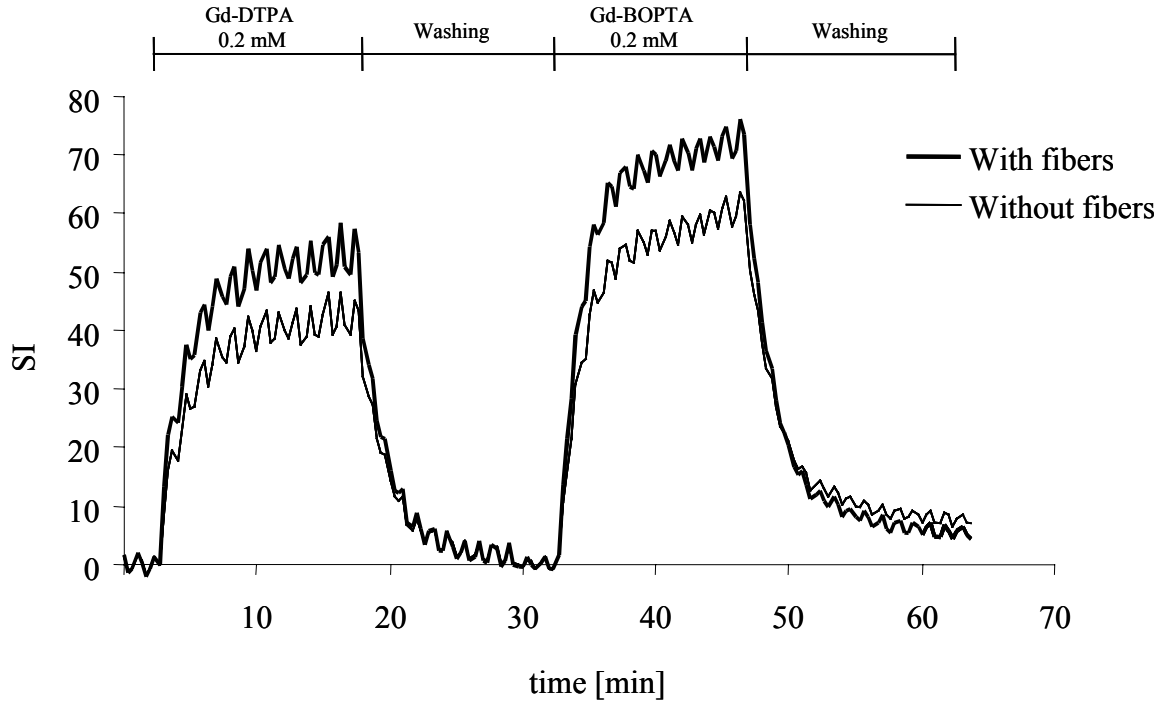

Figure 6.6: Progression of the MRI signal intensity of a cross section of a bioreactor containing $4 \cdot 10^7$ hepatocytes/ml with or without the contribution of the hollow fibers. The bioreactor was perfused with Hanks's solution + 0.2 mM Gd-DTPA for 20 minutes, solution without contrast agent for 15 minutes, solution + 0.2 mM Gd-BOPTA for 20 minutes, and finally solution without contrast agent for 15 minutes. SI was corrected to zero for a better legibility.

The curves obtained with the cross section of the HFB without the contribution of the fibers reached maxima which were lower than the ones of the whole cross section of the HFB. This difference can be totally assigned to the effect of the fibers. The fluctuations of the SI with or without fibers were similar. The residual SI visible after the perfusion with Gd-BOPTA were comparable, though being very slightly greater when the contribution of the fibers was eliminated.

The quantitative analysis of the SI-time curves with and without fibers indicated that both had the same rate constant. Since it did not confirm our expectations of getting improved results and as it is a rather complicated and long lasting technique, we will neither use masks of the fibers nor ROI in the future.

6.2.4 Conclusion

Two approaches to improve image analysis of the HFB, delimitation of ROI and building of a mask of the fibers, were compared in terms of SI to the standard image analysis, which considered the whole cross section of the HFB. Both approaches were interesting but none brought new information, as compared to the total section of the HFB. Moreover, the reproducibility of results obtained with ROI was not satisfactory. As they were time-consuming and did not bring new elements, we decided not to pursue these methods for the analysis of future HFB experiments. Only the treatment of the SI coming from the whole cross section of the HFB will be taken into account for future experiments.

6.3 Metabolism study

6.3.1 Introduction

The evaluation of the metabolic activity is a possibility to quantify the viability and functionality of isolated hepatocytes. Other tests, like coloration of cells with dye, quantification of enzymes released, and evaluation of the synthesis of endogenous compounds, and the consumption of nutrients, are often used for the same purpose.

Throughout the development of the MRI compatible bioreactor (chapter 5), the viability of hepatocytes during the HFB experiments was assessed by the determination of oxygen consumption and the enzymes LDH and AST released in the perfusion medium. The aim of the present study was to set up a metabolic test with continuous in-line detection, which would complete the evaluation of the viability of hepatocytes contained in HFB.

We used the substrate 7-ethoxycoumarin (7-EC) which is transformed to 7-hydroxycoumarin (7-HC) by cytochrome P450 1A1 as presented in figure 6.6. 7-EC was chosen because it can be analyzed by fluorimetry directly in the solution used for the

bioreactor perfusion [4,5]. Furthermore, the method could have been adapted in a second time so that the solution perfused went through a small fluorimetric cell allowing a continuous measurement of the fluorescence during the HFB experiments.

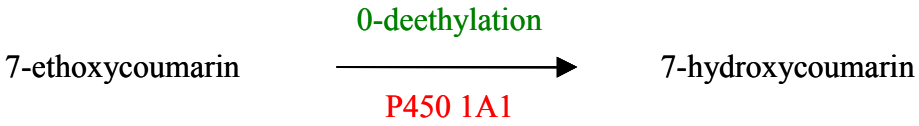

Figure 6.6: Biotransformation of 7-ethoxycoumarin to 7-hydroxycoumarin by cytochrome P450 1A1.

First the analytical conditions permitting the dosage of 7-EC and 7-HC were determined. Then, the feasibility of the method was assessed by performing a blank experiment, i.e. with the whole system including a HFB but free of hepatocytes.

6.3.2 Materials and methods

6.3.2.1 Chemicals

7-ethoxycoumarin and 7-hydroxycoumarin were obtained from Sigma Chemical (St-Louis, MO, USA). All other chemicals were of analytical grade.

6.3.2.2 Set up of the analytical method

7-EC and 7-HC were dissolved in acetonitrile at a concentration of 25 mM. The concentrated stock solutions were diluted with a modified Hanks's solution of the following composition: 76.0 mM NaCl, 5.37 mM KCl, 0.63 mM Na_2HPO_4, 0.44 mM KH_2PO_4, 17.9 mM $NaHCO_3$, 2.00 mM $CaCl_2$, 0.41 mM $MgSO_4$, 40.0 mM HEPES Na, 5.55 mM glucose, 99420 U/l Penicillin G, 77700 U/l streptomycin sulfate, 280 U/l insulin and 0.5% BSA, pH 7.4. Fluorimetric assays of diluted solutions of 7-EC and 7-HC were performed with a spectrofluorimeter (LS 50 B, Perkin Elmer Instruments, USA), with a bandwidth of 2.5 nm and an integration time of 1 second. Determination of the maximal wavelengths of excitation

and emission of 7-EC and 7-HC was made using the "scan" mode of the fluorimeter with 10 µM solutions. Fluorescence intensities at fixed wavelengths were obtained with the "read" mode. The linearity field was determined with solutions of 7-EC and 7-HC at 20°C and at concentrations ranging from 1.25 to 50 µM at the maximal wave lengths of excitation and emission determined before. The stability of the concentrated and diluted solutions was checked by measuring the fluorescence at 20°C before and after 12 days of preservation at 4°C. The effect of a slight change in pH was assessed by measuring the fluorescence 10 µM solutions of 7-EC and 7-HC diluted from the concentrated stock solutions with Hanks's solution at pH 7.3 and 7.5. The effect of temperature was tested by measuring the fluorescence of a 10 µM solutions of 7-EC and 7-HC at 4°C and 20°C.

6.3.2.3 Adsorption of 7-ethoxycoumarin in the HFB perfusion system

The HFB perfusion system comprised a solution reservoir, a peristaltic pump, a heating circulator, a refrigerant, an oxygenator, a bubble trap and a HFB (Minikros® Sampler M12E 220 01N, Spectrum, Rancho Dominguez, CA, USA). These elements were connected to each other by 15 meters of Tygon® tubing. The peristaltic pump continually circulated the solution in the system at a flow rate of 100 ml/min. The solution was heated by circulation through the glass spiral of the refrigerant while warm water from the heating circulator flowed outside the spiral tubing. The oxygenator consisted of 7 meters of thin-walled silicone tubing permeable to oxygen and carbon dioxide and coiled in a plastic box [6]. The system is described in detail in chapter 5.

The adsorption of 7-EC was assessed by circulating 1l of Hanks's solution containing 15 µM of 7-EC at 20°C or 37°C for 75 minutes in the whole system or in the system without oxygenator or bioreactor. Samples were taken every 15 minutes, diluted if necessary, and analyzed by fluorimetry to determine the concentration of 7-EC at the maximal wave lengths of excitation and emission determined before.

To investigate whether the adsorption followed a saturable and irreversible process, 1l of Hanks's solution containing 230 µM of 7-EC was circulated in the whole system at 37°C for

4 hours. After 4 hours, the solution containing 7-EC was replaced by 1l of Hanks's solution free of 7-EC. This solution was circulated through the system during 90 minutes and then substituted with 1l of ethanol 96% which was circulated for another 90 minutes. Samples were taken every 15 minutes, diluted if necessary, and analyzed by fluorimetry to determine their concentration of 7-EC.

6.3.3 Results

6.3.3.1 Set up of the analytical method

7-EC and 7-HC were dissolved in acetonitrile because this solvent was shown not to interfere with cytochromes P450, in contrast to other solvents like methanol or DMSO [7]. Excitation and emission spectra of 7-EC and 7-HC are presented in figure 6.7.

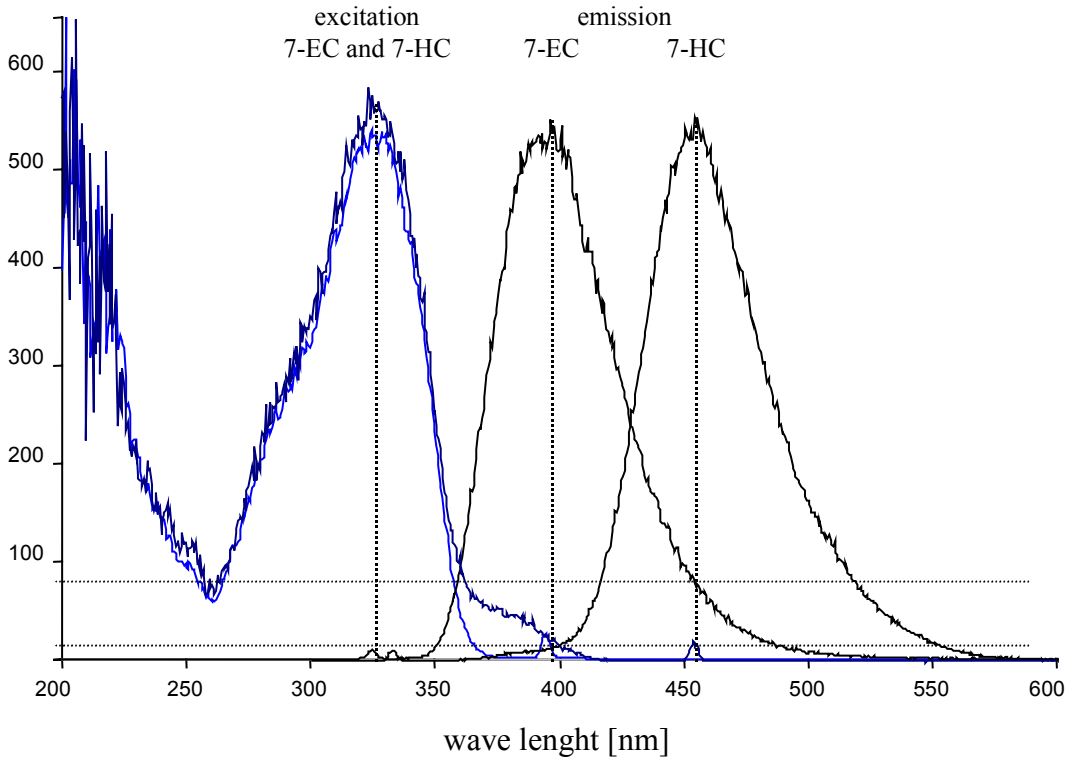

Figure 6.7: Excitation and emission fluorescence spectra of solutions containing 10 μM of 7-ethoxycoumarin (7-EC) and 7-hydroxycoumarin (7-HC).

As can be seen, both 7-EC and 7-HC had the same maximal wavelength of excitation of 333 nm, and the maximal wave lengths of emission were 394 and 454 nm respectively. Compared to the maximum fluorescence of about 520, the fluorescence of 7-HC at 394 nm, equal to 15, represented 3% of the total fluorescence, which is sufficiently low as to be neglected. In contrast, the fluorescence of 7-EC at 454 nm, equal to 80, represented 15% of the total fluorescence, which is significant. Hence, the 7-EC concentration was calculated from the emission at 394 nm while the concentration of 7-HC was determined by subtraction of the contribution of 7-EC calculated from the emission at 394 nm from the total fluorescence obtained at 454 nm.

A good linearity was found for 7-EC at 394 nm and 454 nm and for 7-HC at 454 nm as long as concentrations did not exceed 10 μM, as shown in table 6.2.

Table 6.2: Linearity between the fluorescence and the concentration of 7-ethoxycoumarin and 7-hydroxycoumarin (0 - 10 μM).

	Regression parameters					
	slope	Y-intercept	n	r^2	s	F
7-EC, 394 nm	29.5 ± 1.3	18.8 ± 8.5	5	0.994	9.854	459.9
7-EC, 454 nm	4.48 ± 0.22	4.1 ± 1.4	5	0.993	1.595	405.0
7-HC, 454 nm	46.5 ± 1.3	11.5 ± 6.9	5	0.998	10.39	1205

7-EC = 7-ethoxycoumarin, 7-HC = 7-hydroxycoumarin, r^2: squared correlation coefficient, s: standard deviation of the residuals, F: Fisher test for significance of the equation

The fluorescence of solutions of 7-EC and 7-HC at a concentration of 10 μM at 20°C were identical before and after 12 days of conservation at 4°C, as well as the one of solutions of 10 μM prepared with the concentrated stock solutions after their preservation for 12 days at

4°C. This indicates that both concentrated and diluted solutions of 7-EC and 7-HC could be stored at 4°C during 12 days without loss of stability.

We also showed that a small variation of pH did not influence the fluorescence reading. Indeed, the fluorescence of 10 µM solutions of 7-EC and 7-HC at 20°C were identical at pH 7.3 and 7.5. This slight variation of pH is the one observed with the samples of the perfusion solution taken during the HFB experiments. In practice, this means that within a pH range of 7.3 to 7.5 the fluorescence of samples can be compared to each other. As the samples were kept in the fridge till analysis, we wondered if the temperature had an influence on the fluorescence, and we found that the fluorescence of 10 µM solutions of 7-EC and 7-HC was about 10% higher at 4°C than at 20°C. Thus, all samples had to be at the same temperature when measuring their fluorescence.

6.3.3.2 Adsorption of 7-ethoxycoumarin in the HFB perfusion system

The adsorption of 7-EC in the HFB perfusion system at 20°C or 37°C, with or without oxygenator, is shown in figure 6.8. The complete system consisted of Tygon® tubing, oxygenator, HFBfree of hepatocytes, and bubble trap.

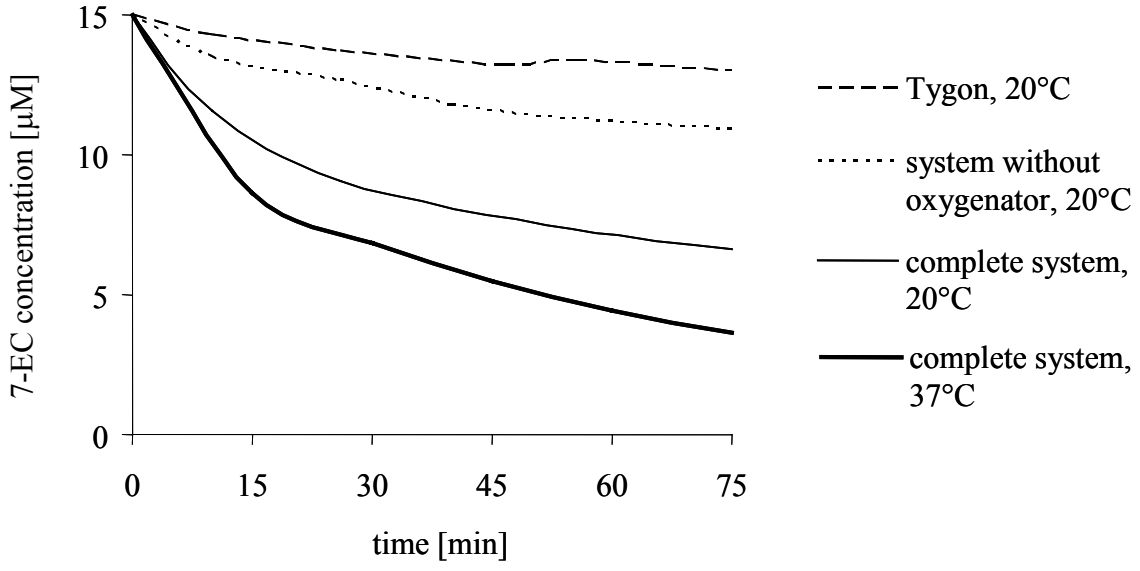

Figure 6.8: Adsorption of 7-ethoxycoumarin (7-EC) in the Tygon® tubing, in the HFB perfusion system without oxygenator, or in the complete system at 20°C or 37°C.

The concentration of 7-EC remaining in solution after 75 minutes of perfusion of the different elements present in the system are shown in table 6.3.

Table 6.3: Remaining concentration of 7-ethoxycoumarin (7-EC) in solution after 75 minutes of perfusion. The initial concentration of 7-EC was 15 μM.

Conditions	Concentration of 7-EC [μM]	Remarks
Complete system, 37°C	3	Huge adsorption
Complete system, 20°C	6	Temperature ↓ ⇒ adsorption ↓
Complete system without HFB, 20°C	6	No adsorption in the HFB
System without oxygenator, 20°C	11	Oxygenator responsible for the adsorption of 5 μM
Tygon®, 20°C	13	Tygon® responsible for the adsorption of 2 μM

These results indicate that only a small amount of 7-EC was adsorbed to Tygon® tubing. Actually, the concentration of 7-EC in the solution only decreased from 15 to 13 μM after 75 minutes of circulation at 20°C, which is in good agreement with the manufacturer's indications. The kind of Tygon® tubing used was chosen because it was known to minimize adsorption phenomena. Withdrawal of the bioreactor did not change the adsorption profile, indicating that no adsorption of 7-EC occurred in the bioreactor. The content of 7-EC in the solution decreased from 15 to 6 μM after 75 minutes of circulation in the whole system. The comparison between the adsorption of 7-EC in the whole system and in the system without oxygenator indicates that the oxygenator was responsible for the adsorption of 5 μM of 7-EC. As already seen, 2 μM were adsorbed to Tygon® tubing and another 2 μM were adsorbed elsewhere in the system, for instance in the bubble trap. Hence, more than 50% of the total

amount of 7-EC adsorbed was lost in the oxygenator. As the oxygenator is an indispensable element of the perfusion system, due to the requirement of a good oxygenation of hepatocytes, it cannot be omitted and an important 7-EC adsorption cannot be avoided. Perfusion experiments of the whole system at 37°C showed that the adsorption of 7-EC was even more pronounced at this physiological temperature.

The saturability and the reversibility of the adsorption of 7-EC were assessed by circulating a solution containing 230 μM of 7-EC in the whole system at 37°C for 4 hours, followed by washing with Hanks's solution free of 7-EC for 90 minutes and ethanol for 75 minutes. The concentration-time profiles obtained are sown in figure 6.9.

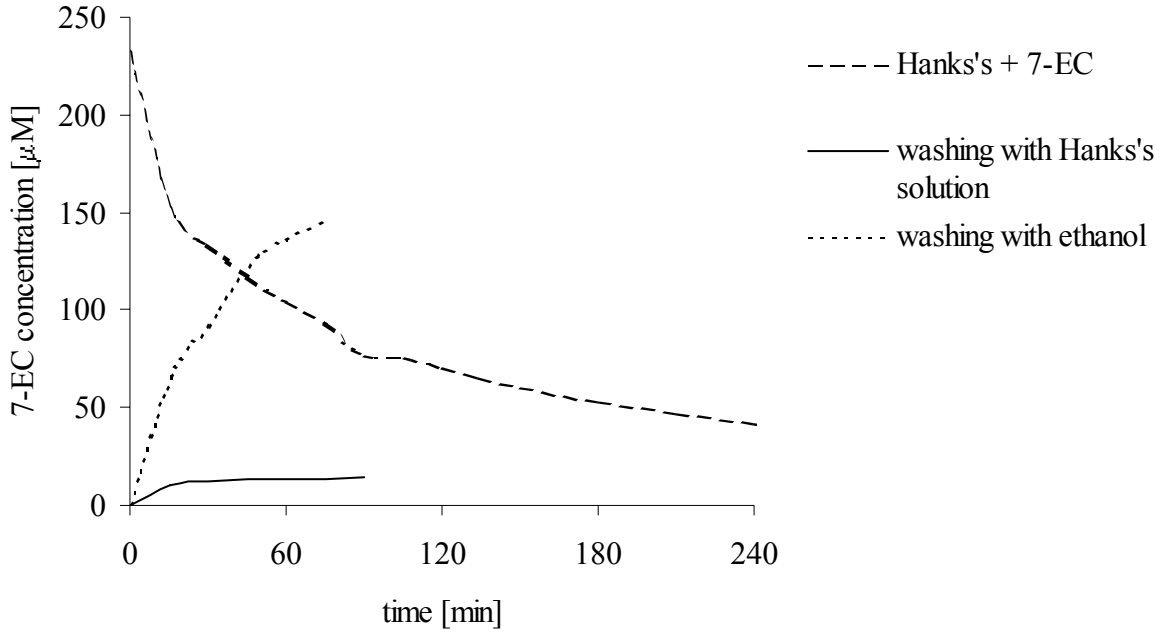

Figure 6.9: Assessment of the saturability and reversibility of 7-ethoxycoumarin (7-EC) adsorption at 37°C. A Hanks's solution containing 230 μM of 7-EC was circulated in the whole system for 4 hours. The system was then washed with Hanks's solution free of 7-EC for 90 minutes and finally with ethanol for 90 minutes.

These results suggest that the adsorption of 7-EC was a non-saturable process. The concentration of 7-EC in the solution was increased from 15 to 230 µM, as compared to the previous experiment. But even with this about 20 times higher concentration, no saturation of the adsorption was observed. The results further show that the adsorption was a reversible process. 7-EC was slowly released into Hanks's solution free of 7-EC, and readily released into ethanol. Indeed, 14 µM of 7-EC were liberated in Hanks's solution after 90 minutes and this quantity was increased to 145 µM after the circulation of ethanol for 90 minutes (figure 6.9). This is easily explained by the low, respectively high solubility of 7-EC in water and in ethanol.

Hence, 7-EC would not be a good substrate to assess the functionality of hepatocytes in our HFB. Actually, 7-EC was adsorbed in the perfusion system in a huge quantity, moreover, the adsorption was not saturable and reversible. This means that, in the presence of hepatocytes, it would be difficult to differentiate between the decrease of 7-EC due to metabolism and the decrease due to adsorption. Furthermore, one could imagine that the amount of 7-EC metabolized would be compensated by a release of 7-EC adsorbed, and this could totally mask the biotransformation of 7-EC. The dosage of the 7-HC produced would neither be suitable, as Sakai et al. [5] showed that the concentration of 7-HC detectable in the solution after 8 hours was only about 1% of the initial concentration of 7-EC. 7-HC is probably immediately further metabolized.

The high adsorption of 7-EC in the oxygenator can be explained by its silicone composition. Like 7-EC, other drugs are also adsorbed by silicone, e.g. antibiotics [8] or fentanyl [9]. Nevertheless, silicone tubing is often used to improve oxygenation in various cell culture systems, and in particular for HFB [10].

6.3.4 Conclusion

A good analytical method was set up for the dosage of 7-EC and 7-HC by fluorimetry. But a blank experiment performed with the whole system without hepatocytes in the HFB

demonstrated that 7-EC was readily adsorbed in the system, and that the adsorption process was neither saturable, nor irreversible. Hence, 7-EC is not a suitable substrate to assess the functionality of hepatocytes in our HFB perfusion system. These results illustrate that adsorption which could take place in silicone membrane oxygenators is a problem that cannot be neglected.

The same study could be done with other fluorescent substrates to find one which would not be adsorbed to silicone tubing. Another solution would be to use a system of oxygenation that does not include silicone, for instance polypropylene-based oxygenators, which are less susceptible to drug adsorption [9]. Nevertheless, we decided not to pursue this project because of lack of time. We will satisfy ourselves with the dosage of LDH and AST and the determination of the oxygen consumption, which have shown to be totally reliable for the assessment of the hepatocyte viability (chapter 5).

References

[1] Cavagna FM, Maggioni F, and Castelli PM, Gadolinium chelates with weak binding to serum proteins. A new class of high-efficiency, general purpose contrast agents for magnetic resonance imaging, *Invest Radiol*, 1997, **32**, 780-796.

[2] De Haën C, Cabrini M, Akhnana L, Ratti D, Calabi L, and Gozzini L, Gadobenate dimeglumine 0.5M solution for injection (Multihance): pharmaceutical formulation and physicochemical preoperties of a new magnetic resonance imaging contrast medium, *J Comput Assist Tomogr*, 1999, **23**, S161-S168.

[3] De Haën C, La Ferla R, and Maggioni F, Gadobenate dimeglumine 0.5 M solution for injection (Multihence) as contrast agent for magnetic resonance imaging of the liver: mechanistic studies in animals, *J Comput Assist Tomogr*, 1999, **23** (Suppl. 1), S169-S179.

[4] Sakai Y, Ichikawa K, Sakoda A, and Suzuki M, Quantitative comparison of rat hepatocyte functions in two improved culture systems with or without rat liver epithelial cell line, *Cytotechnology*, 1996, **21**, 243-252.

[5] Sakai Y, Naruse K, Nagashima I, Muto T, and Suzuki M, A new bioartificial liver using porcine hepatocyte spheroids in high-cell-density suspension perfusion culture: *in vitro* performance in synthesized culture medium and in 100% human plasma, *Cell Transplant*, 1999, **8**, 531-541.

[6] Hamilton RL, Berry MN, Williams MC, and Severinghaus EM, A simple and inexpensive membrane "lung" for small organ perfusion, *J Lipid Res*, 1974, **15**, 182-186.

[7] Easterbrook J, Lu C, Sakai Y, and Li AP, Effects of organic solvents on the activities of cytochrome P450 isoforms, UDP-dependent glucuronyl transferase, and phenol sulfotransferase in human hepatocytes, *Drug Metab Dispos*, 2001, **29**, 141-144.

[8] Mizutani T, Adsorption of some antibiotics and other drugs on silicone-coated glass surfaces, *J Pharm Pharmacol*, 1982, **34**, 608-609.

[9] Rosen DA, Rosen KR, and Silvasi DL, *In vitro* variability in fentanyl absorption by different membrane oxygenators, *J Cardiothoracic Anesth*, 1990, **4**, 332-335.

[10] Tharakan JP, Gallagher SL, and Chau PC, Hollow-fiber bioreactor for mammalian cell culture, In 'Upstream Processes: Equipment and Techniques', Ed. Avshalom M, Alan R. Liss, New York, 1988, pp. 153-184.

Chapter 7
Study of Gd-BOPTA transport in freshly isolated rat hepatocytes and pharmacokinetic analysis of MRI data obtained with a hepatocyte hollow fiber bioreactor

7.1 Introduction

Gd-BOPTA is a hepatobiliary MRI contrast agent which is taken up specifically by hepatocytes and partially excreted into the bile. Due to these properties, Gd-BOPTA has a dual imaging capability: on the one hand it can be used as an extracellular agent for the MRI of diverse parts of the body, and on the other hand it can be used for the MRI of the liver to facilitate the MRI detection of hepatic diseases. In this organ it distributes not only in the extracellular space but also enters hepatocytes.

As already discussed in chapter 3, the transport of Gd-BOPTA into hepatocytes is not fully understood and different hypotheses have been proposed. Moncelli et al. [1] found that Gd-BOPTA did not diffuse through phospholipid monolayers and therefore concluded that the uptake of Gd-BOPTA was not due to free diffusion of the contrast agent through the lipidic membrane. They suggested the presence of a specific transport system which allows Gd-BOPTA to enter hepatocytes. Conversely, Pascolo et al. [2] observed that the uptake of Gd-BOPTA in rat sinusoidal membrane vesicles occurred by passive diffusion. They also found that Gd-BOPTA was not taken up into oocytes transfected with human OATP cRNA. This latter result is in good agreement with the one of Van Montfoort et al. [3] who showed that Gd-EOB-DTPA, a hepatobiliary contrast agent related to Gd-BOPTA, was not transported into oocytes transfected with human OATP cRNA, while they observed that it was taken up into oocytes transfected with rat oatp1 cRNA according to a saturable mechanism, which may indicate that there is a difference between species. The possible

inhibition of the transport of Gd-BOPTA into hepatocytes by bromosulfophthalein (BSP) is also debated. De Haën et al. [4] observed a partial inhibition of the uptake of Gd-BOPTA by BSP in rat liver, while Pascolo et al. [2] found that the passive diffusion of Gd-BOPTA through rat sinusoidal membrane vesicles was not inhibited by BSP. On the other hand, the excretion mechanism of Gd-BOPTA into the bile is known, it occurs via the multidrug resistance-associated protein MRP2/mrp2 (capital letters refer to the human protein) at the canalicular side of the hepatocyte [5-7].

As seen in the previous paragraph, there are different techniques available to study the hepatobiliary transport of drugs, ranging from the intact liver *in vivo* to the isolated perfused liver, isolated hepatocytes, liver slices, membrane vesicles and transport proteins [8]. *In vivo* studies provide useful general data related to the transport mechanisms of drugs, but there are numerous factors that cannot be controlled, which complicates the interpretation of the results. The isolated perfused liver has the advantage of eliminating the extrahepatic influences while keeping the liver architecture intact. Liver slices offer the possibility to perform many experiments with a single liver. Freshly isolated hepatocytes showed to have similar transport characteristics to those of the liver *in vivo* and the isolated perfused liver [9], despite of the loss of their membrane polarity. Moreover, they are superior as a model for drug transport than cultured hepatocytes or hepatocyte derived cell lines, which have deficient transport functions [10]. Plasma membrane vesicles can be separately prepared from the sinusoidal and canalicular membranes, but the integrity of the transport proteins is hard to assess. Liver slices, isolated hepatocytes, and plasma membrane vesicles can be obtained also from human source. So far numerous transport proteins have been isolated and characterized, notably thanks to molecular biology.

The aim of this work was to study the transport of Gd-BOPTA in freshly isolated rat hepatocytes. As the isolation process is rather aggressive and results in hepatocytes that have lost their membrane polarity, we first assessed the expression of the transporters known or suspected to play a role in the transport of Gd-BOPTA and compared it to the one of an entire liver. In a second step, we checked the functionality of the uptake mechanisms by incubating

hepatocyte suspensions with Gd-BOPTA. Finally, we studied the uptake of different concentrations of Gd-BOPTA into hepatocytes by means of the MRI compatible hepatocyte hollow fiber bioreactor (HFB) developed in chapter 5. In this last step, particular attention was paid to the development of a compartmental pharmacokinetic model to describe the MRI data.

7.2 Materials and methods

7.2.1 Chemicals

Solution of Gd-BOPTA 0.5 M was generously donated by Bracco Research S.A. (Geneva, Switzerland). A commercially available solution of Gd-DTPA 0.5 M (Magnevist®, Schering, Germany) was used. Bovine serum albumin (BSA, fraction V, 97%) and ethylene glycol-O,O'-bis(2-aminoethyl)-N,N,N',N'-tetraacetic acid (EGTA) were purchased from Fluka. Collagenase from Clostridium histolicum type IV (collagen digestion activity: 295 U/mg solid), bovine pancreas insulin, 4-(2-aminoethyl) benzenesulfonyl fluoride hydrochloride (AEBSF), aprotinin, leupeptin, bestatin, pepstatin A and N-(trans-epoxysuccinyl)-L-leucine 4-guanidinobutylamide (E-64) were obtained from Sigma Chemical (St-Louis, MO, USA). The rabbit polyclonal antibodies against rat-oatp1, rat-oatp2, rat-oatp4 and rat-mrp2 were kindly provided by Dr B. Stieger (University Hospital, Zurich, Switzerland) [11-15]. All other chemicals were of analytical grade.

7.2.2 Isolation of hepatocytes

Hepatocytes were isolated from adult male Sprague-Dawley rats (250 to 350 g) by a two-step collagenase perfusion of the liver first described by Seglen et al. [16] and described in detail in chapter 4. An average of $5 \cdot 10^8$ hepatocytes were obtained from the isolation

procedure of one rat liver, with a cellular viability greater than 90% as assessed by trypan blue exclusion.

7.2.3 Determination of the expression of hepatic transporters by Western blotting

Cell samples containing $5 \cdot 10^7$ freshly isolated hepatocytes were introduced in 1.5 ml "Eppendorf" tubes, frozen in liquid nitrogen and kept at -80°C until use. The expression of the transporters was evaluated with hepatocytes resulting from the separate isolation procedure of three rat livers and compared to the one of an entire rat liver.

Liver tissue or, alternatively, cell samples were homogenized in a potter with ice-cold Tris buffer (100 mM Tris-HCl, pH 7.6) containing protease inhibitors, AEBSF, Aprotinin, Leupeptin, Bestatin, Pepstatin A and E-64. The homogenates were centrifuged at 10 000 g for 10 minutes at 4°C. This first supernatant was used for the detection of oatp1 and oatp4. The extraction of the two transporters was quantitative because they could not be detected in the pellet. On the other hand, no mrp2 was present in the first supernatant. Therefore the pellet was homogenized with the same buffer containing 1% Triton X-100. After centrifugation at 10 000 g for 10 minutes at 4°C, this second supernatant was used for the detection of mrp2. To better extract oatp2 a different Tris buffer was used [17]; it contained 50 mM Tris-HCl, 0.1 mM EGTA, 0.1 mM ethylenedinitrilo tetraacetic acid (EDTA), 0.1% sodium dodecyl sulfate (SDS), 0.1% deoxycholic acid, 1% Triton X-100, pH 7.5. Protein concentrations were determined according to Bradford [18] (Bio-Rad, Glattbrugg, Switzerland). The supernatants were stored at –70°C until use.

Sodium dodecyl sulfate polyacrilamide gel electrophoresis (SDS-PAGE) and Western blotting were performed according to standard procedures [19-21]. 100 µg of protein extracts were separated on a 7.5% polyacrylamide gel. Then the gel was transferred to a polyvinylidene difluoride membrane (Millipore, Switzerland). The membrane was blocked for 1 hour at room temperature with 5% nonfat dry milk in phosphate buffered saline (PBS) and incubated with the specific antibodies. Staining with Ponceau red before blocking

assessed that equal quantities of proteins were loaded on each line. The membrane was then incubated over-night at 4°C with anti-oatp1 (1:1 000), anti-oatp2 (1:5 000), anti-oatp4 (1:2 000) or anti-mrp2 (1:2 000) antibody in PBS containing 5% nonfat dry milk. The membrane was washed four times with PBS-0.2% Tween-20 and incubated for 1 hour with an alkaline phosphatase-conjugated goat anti-rabbit IgG antibody at 1:5 000 (Stressgen, Victoria, Canada). Then the membrane was washed four times with PBS-Tween buffer. Development was performed using an Immune-Star chemiluminescent protein-detection system (Bio-Rad) according to the manufacturer's instructions. Molecular weight markers and controls were included in each experiment.

7.2.4 Uptake of Gd-BOPTA by hepatocytes in suspension

Suspensions containing $5 \cdot 10^7$ freshly isolated hepatocytes were introduced in centrifuge tubes of 15 ml (figure 7.1) and gently mixed with 10 ml of ice cold incubation solution which had the same composition than the perfusion solution used for the bioreactor experiments (chapter 5), namely 76.0 mM NaCl, 5.37 mM KCl, 0.63 mM Na_2HPO_4, 0.44 mM KH_2PO_4, 17.9 mM $NaHCO_3$, 2.00 mM $CaCl_2$, 0.41 mM $MgSO_4$, 40.0 mM HEPES Na, 5.55 mM glucose, 99420 U/l Penicillin G, 77700 U/l streptomycin sulfate, 280 U/l insulin and 0.5% BSA, pH 7.2. The tubes were then centrifuged (50 g, 2 min, 4°C) and supernatant was removed. Cell suspensions were prepared by suspending the cell pellet in 100 ml of incubation solution supplemented with 0.2 mM of Gd-BOPTA or Gd-DTPA. Hepatocyte suspensions were incubated (37°C, shaking, 5% CO_2 in air atmosphere) in an incubator (EG 110IR, Société Juan, Saint Herblain, France) for 60 minutes. Control experiments were performed under the same experimental conditions but without contrast agent in the incubation solution. Cell viability was checked every 30 minutes by trypan blue exclusion. After incubation, hepatocytes were centrifuged, the supernatant was removed, and the cell pellets were washed twice with ice cold incubation solution free of contrast agent. The cell pellets were kept at -80°C till analysis by inductively coupled plasma atomic emission spectrometry (ICP-AES) to determine their levels of gadolinium (Gd^{3+}). The intracellular

concentration of Gd^{3+} was calculated from this value considering that the cell pellets contained $5 \cdot 10^7$ hepatocytes having a mean volume of 8181 μm^3 [22-24].

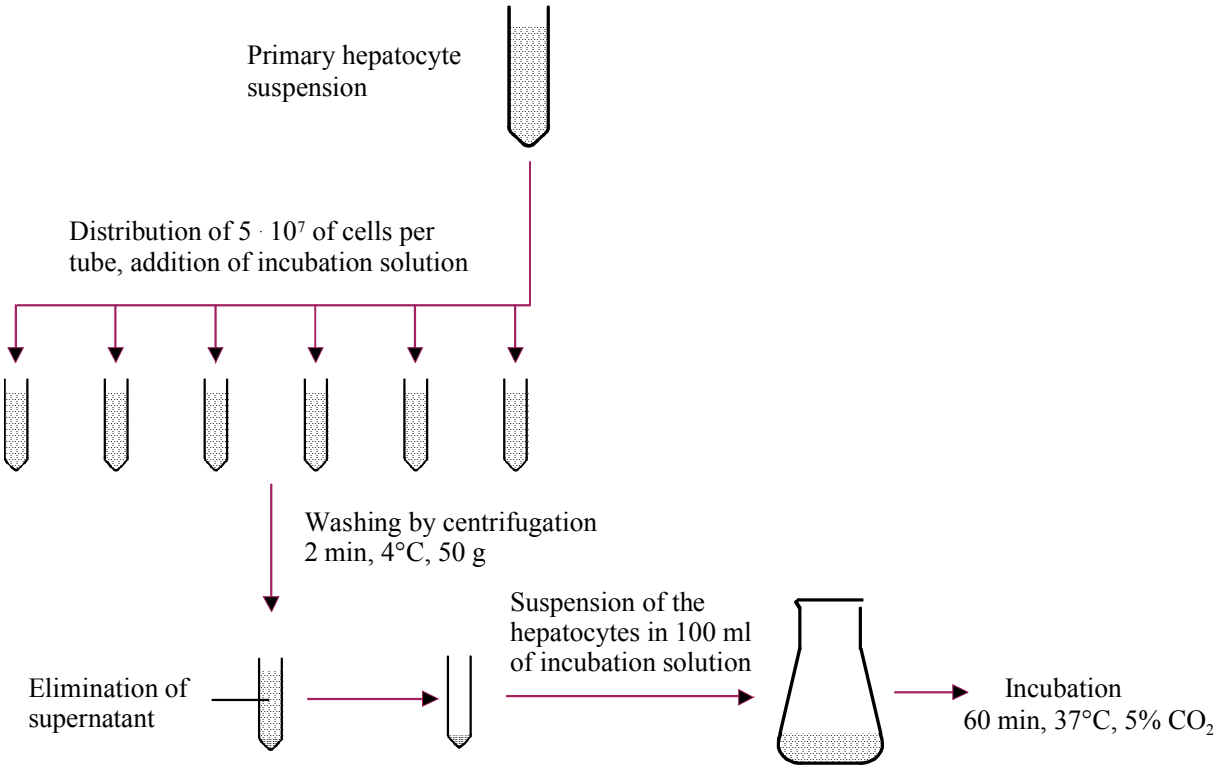

Figure 7.1: Preparation of the hepatocyte suspensions. The hepatocytes were incubated 60 minutes (37°C, 5% CO_2) in incubation solution containing either 0.2 mM Gd-DTPA, 0.2 mM Gd-BOPTA or no contrast agent.

7.2.5 Transport of contrast agents in hepatocytes within a MRI compatible bioreactor

The whole procedure for the preparation of the hepatocyte HFB was described in detail in chapter 5. Briefly, a suspension containing $1 \cdot 10^9$ freshly isolated hepatocytes obtained after the isolation processes of two livers was centrifuged (50 g, 2 min, 4°C) and the cell pellet was mixed with ice-cold modified University of Wisconsin solution. The resulting cell suspension was inoculated in a HFB (Minikros® Sampler M15E 260 01N, Spectrum, Rancho Dominguez, CA, USA) and the bioreactor was preserved at 4°C till MRI experiment.

For the MRI experiment, the hepatocyte HFB was set in the wrist coil and perfused with a 37°C oxygenated perfusion solution with or without contrast agent at a flow rate of 100 ml/min. Experiments were carried out with contrast agent concentrations of 0.05, 0.1, 0.2 and 0.4 mM. Inhibition experiments were performed by perfusing the HFB first with a solution containing 0.1 mM Gd-BOPTA alone and then with a solution containing 0.1 mM Gd-BOPTA and 0.1 mM BSP. The experiment was repeated with 0.4 mM solutions of Gd-BOPTA and BSP. The viability of hepatocytes was greater than 85% after 4 hours of experiment as assessed by the release of lactate dehydrogenase (LDH) and aspartate aminotransferase (AST) in the perfusate and by determining the oxygen consumption of hepatocytes.

Results were based on the signal intensity (SI) of the 4^{th} cross section of the HFB during dynamic sequences, as already described in chapter 5. The SI-time curves obtained were submitted to a compartmental pharmacokinetic analysis after normalization with reference vials and correction for the baseline.

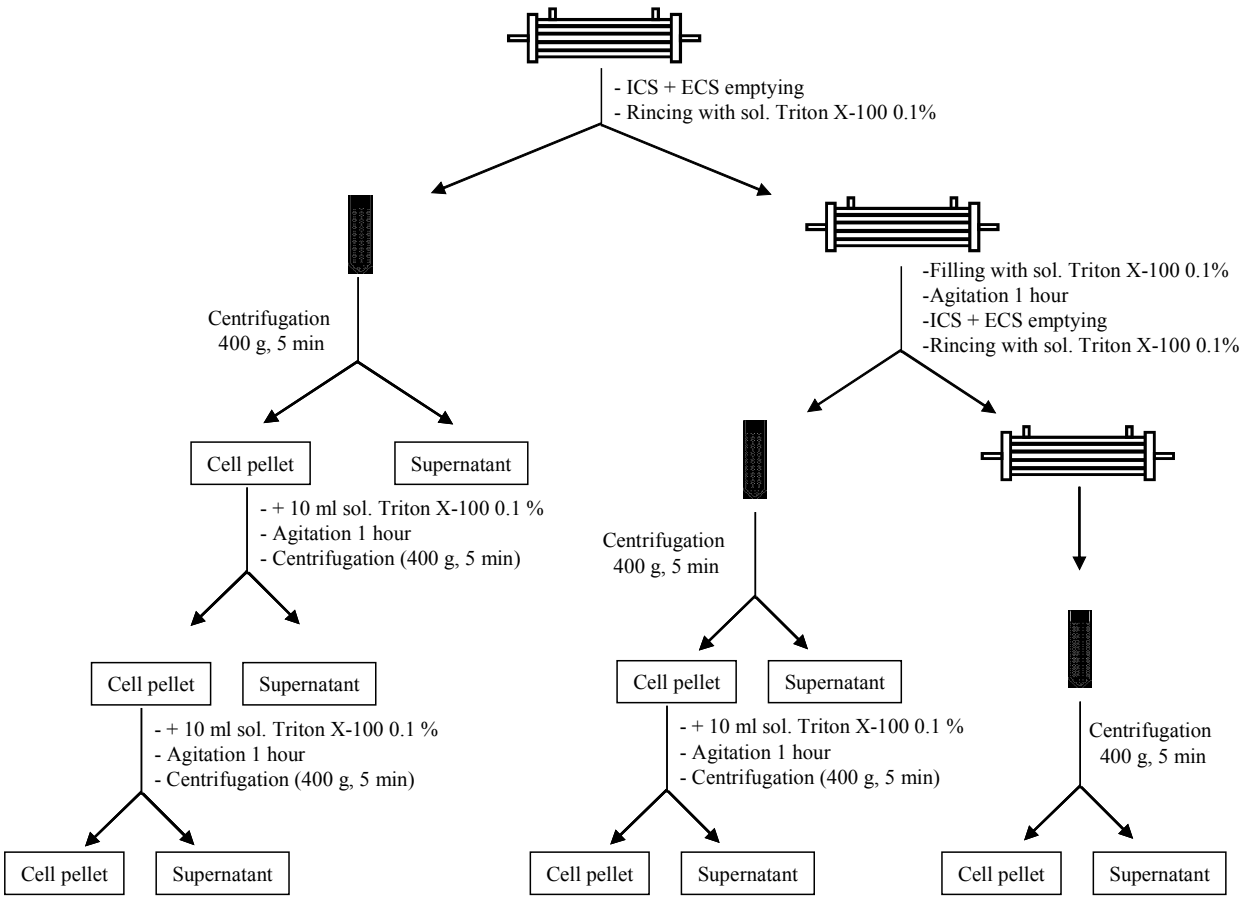
- ICS + ECS emptying
- Rincing with sol. Triton X-100 0.1%
Centrifugation
400 g, 5 min
-Filling with sol. Triton X-100 0.1%
-Agitation 1 hour
-ICS + ECS emptying
-Rincing with sol. Triton X-100 0.1%
Cell pellet
Supernatant
- + 10 ml sol. Triton X-100 0.1 %
- Agitation 1 hour
- Centrifugation (400 g, 5 min)
Centrifugation
400 g, 5 min
Cell pellet
Supernatant
- + 10 ml sol. Triton X-100 0.1 %
- Agitation 1 hour
- Centrifugation (400 g, 5 min)
Centrifugation
400 g, 5 min
Cell pellet
Supernatant
Cell pellet
Supernatant
- + 10 ml sol. Triton X-100 0.1 %
- Agitation 1 hour
- Centrifugation (400 g, 5 min)
Cell pellet
Supernatant
Cell pellet
Supernatant

Figure 7.2: Scheme of hepatocytes extraction and lysis with a solution of Triton-X 100 0.1% after the MRI experiment. Supernatants were put together, weighted and measured by ICP-AES for the determination of the Gd^{3+} content.

After the MRI experiments, the hepatocytes were extracted from the bioreactor and lysed with a solution of Triton X-100 0.1% as illustrated in figure 7.2. Three consecutive extractions of the HFB were made. The extracts were centrifugated, the supernatants collected, and the cell pellets further lysed with Triton X-100. All supernatants were put together, weighted and analyzed by ICP-AES to determine their levels of gadolinium (Gd^{3+}). The intracellular concentration of Gd^{3+} was calculated from this value considering that the HFB contained $1 \cdot 10^9$ hepatocytes having a mean volume of 8181 μm^3 [22-24].

7.2.6 Development of a compartmental pharmacokinetic model to describe the MRI data

SI-time curves normalized with reference vials and corrected for the baseline were submitted to compartmental analysis using the software NONMEM (Version V, University of California, San Francisco, USA).

A compartmental model uses compartments to describe the different parts of the organism. Compartment 1 is frequently called the central compartment because drug is administered into and distributed from it. The drug distributes between this central compartment and peripheral compartments composed of tissues into which distribution is slower. Figure 7.3 illustrates a two-compartment model where elimination occurs only from the central compartment and where the drug distributes into a peripheral compartment. A two-compartment model can adequately describe a biexponential curve of drug increase or decay. Movements of drug between the two compartments can be characterized by transfer rate constants, where k_{12} denotes the rate constant associated with passage from compartment 1 into compartment 2, and k_{21} is the rate constant associated with the reverse process. The rate constant k_{10} is associated with loss from compartment 1 by metabolism and/or excretion.

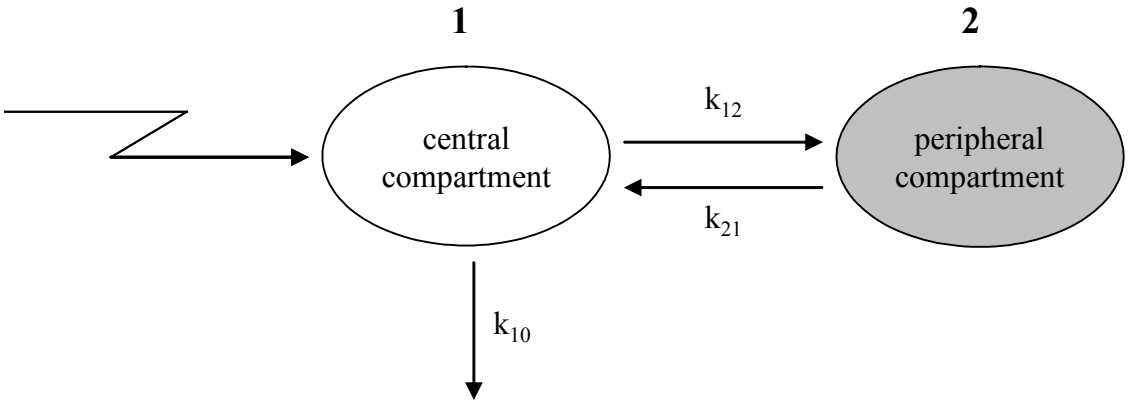

Figure 7.3: Schematic representation of a two-compartment open model. Drug is administered and eliminated from compartment 1 (central compartment) and distributes between compartment 1 and 2 (peripheral compartment). The rate constants for the processes are indicated.

In a two-compartment model, the concentration-versus-time curve of a drug during infusion is described by equation 7.1, whereas equation 7.2 describes the curve during the washing phase, after having stopped drug administration [25].

$$C(t \le T) = \frac{K_0}{V \cdot k_{10}} \left[1 + \frac{k_{10} - \alpha}{\alpha - \beta} \cdot e^{-\beta \cdot t} - \frac{k_{10} - \beta}{\alpha - \beta} \cdot e^{-\alpha \cdot t} \right] \quad \text{[Equation 7.1]}$$

$$C(t > T) = \frac{K_0}{V \cdot k_{10}} \left[\frac{k_{10} - \beta}{\alpha - \beta} \cdot (1 - e^{-\alpha \cdot T}) \cdot e^{-\alpha (t-T)} - \frac{k_{10} - \alpha}{\alpha - \beta} \cdot (1 - e^{-\beta \cdot T}) \cdot e^{-\beta (t-T)} \right] \quad \text{[Equation 7.2]}$$

where K_0 is the infusion rate, T is the duration of infusion, V is the volume of the central compartment, α and β are rate constants defined by equations 7.3 and 7.4.

$$\alpha = \frac{1}{2} \left[(k_{12} + k_{21} + k_{10}) + \sqrt{(k_{12} + k_{21} + k_{10})^2 - 4 k_{21} k_{10}} \right] \quad \text{[Equation 7.3]}$$

$$\beta = \frac{1}{2} \left[(k_{12} + k_{21} + k_{10}) - \sqrt{(k_{12} + k_{21} + k_{10})^2 - 4 k_{21} k_{10}} \right] \quad \text{[Equation 7.4]}$$

The half-life $t_{1/2(k)}$ of a process characterized by a rate constant k is calculated using equation 7.5.

$$t_{1/2(k)} = \frac{\ln 2}{k} \qquad \text{[Equation 7.5]}$$

Implementation of the model in NONMEM proceeded through the use of the ADVAN3 and TRANS1 subroutines. Observations were assumed to reflect the sum of predictions in the central and peripheral compartments plus an additive error term, according to the following equation:

$$C_{observed} = C_{predicted,\ central} + C_{predicted,\ peripheral} + \varepsilon \qquad \text{[Equation 7.6]}$$

where ε is the residual error normally distributed with mean 0 and constant variance σ^2.

Alternatively, an exponential error model identical to a constant CV model was considered:

$$C_{observed} = (C_{predicted,\ central} + C_{predicted,\ peripheral}) \cdot \exp(\varepsilon) \qquad \text{[Equation 7.7]}$$

Primary parameters to be estimated were k_{10}, k_{12}, k_{21}, V and σ^2. Secondary parameters (i.e. calculated on the basis of primary parameters) were α, β and the corresponding half-lives $t_{1/2\alpha}$ and $t_{1/2\beta}$. NONMEM provided information about precision of the estimates through standard errors and correlation matrix of parameter estimates. Goodness of fit was assessed through analysis of residuals and graphical techniques.

In the present case, the concentration was replaced by the signal intensity and the volume of distribution reflected a proportionality constant relating the signal to the infusion rate. The baseline SI at the time point immediately preceding SI increase was determined visually and manually to be the starting value of the perfusion with contrast agent for pharmacokinetic data analysis and the SI at the time point immediately preceding SI decrease was determined visually and manually to be the end of the perfusion of contrast agent and the starting value of the washing phase.

7.3 Results and discussion

7.3.1 Determination of the expression of hepatic transporters by Western blotting

The transport of the hepatobiliary contrast agents Gd-BOPTA and Gd-EOB-DTPA into rat hepatocytes is not yet fully elucidated. Some authors suggest a transport through passive diffusion [2], while others believe that Gd-BOPTA is transported by the specific organic anion transporting polypeptide OATP1/oatp1 (capital letters refer to the human protein) [3]. On the other hand, the excretion of Gd-BOPTA and Gd-EOB-DTPA into the bile is known to occur via the multidrug resistance-associated protein MRP2/mrp2 at the canalicular side of the hepatocyte [5-7,26]. Taking these observations into account, we studied the expression of the transporters of the oatp family and mrp2 in isolated rat hepatocytes. We checked that these transporters were not altered during the isolation procedure of the liver, and as a consequence that isolated rat hepatocytes can be used as a cellular model to study the transport of Gd-BOPTA.

Figure 7.4 shows the Western blot with the expression of the hepatic transporters oatp1, oatp2, oatp4 and mrp2 in isolated hepatocytes obtained with three different rats (lanes 1-3) and in a control liver extract (C).

The hepatic transporter oatp1 had the same expression in freshly isolated hepatocytes and in a control liver extract, oatp2 seemed to be lower in isolated hepatocytes and oatp4 was no longer expressed in hepatocytes after the isolation procedure (figure 7.4). Mrp2 also seemed to have a similar expression in isolated hepatocytes than in the entire liver, although the expression in the isolated hepatocytes coming from rat 3 seemed to be lower.

It is important to check the presence of transporters in the isolated hepatocytes, as they can be lost during the isolation process [27,28]. Indeed, beside the direct aggressive effect of collagenase on hepatocyte membranes, membrane polarity is altered. Microscopic observation of freshly isolated hepatocytes reveals a spherical shape of the cells with a uniform

membrane, such that one can no longer recognize the different poles of the membrane present *in vivo*, where the hepatocyte membrane is in contact with three different compartments, namely the perisinusoidal space (37% of the membrane area), the biliary capillaries (13%), and the neighboring hepatocytes (50%) [24]. Isolated cells in suspension are no more surrounded by different compartments, but only by the culture solution. Nevertheless, freshly isolated hepatocytes were found to be more suitable to evaluate the uptake of ligands by multispecific anion transporter systems than primary hepatocyte cultures that maintain membrane polarity [29].

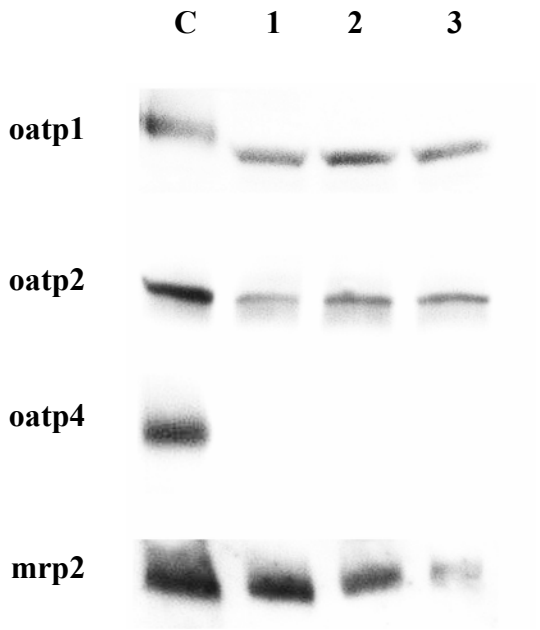

Figure 7.4: Western blot showing the expression of oatp1, oatp2, oatp4 and mrp2 proteins in isolated rat hepatocytes coming from 3 rat livers (lanes 1-3) compared to a control liver extract (C).

To sum up, one can say that the expression of the transporters oatp1, oapt2 and mrp2 was slightly or not changed during the isolation procedure of the liver, in contrast to oatp4. Hence, these results suggest that freshly isolated hepatocytes can be used as a cellular model to study the transport of drugs which imply the presence of oatp1, oapt2 and mrp2, although a Western blot only tells whether the transporters are expressed, not whether they are functional.

Therefore the functionality should be investigated in additional experiments, for instance with specific substrates.

7.3.2 Uptake of Gd-BOPTA by hepatocytes in suspension

The intracellular concentration of gadolinium (Gd^{3+}) in hepatocytes incubated 60 minutes with Gd-BOPTA 0.2 mM was 32.6 ± 4.6 µM, i.e. 16.3 ± 2.3% of the concentration in the incubation solution (figure 7.5). A much lower concentration of Gd^{3+}, namely 4.9 ± 0.3 µM, was observed after incubation with 0.2 mM Gd-DTPA, the extracellular contrast agent. This amount represented 2.4 ± 0.2% of the initial concentration in the incubation solution. There was no Gd^{3+} detectable in control hepatocytes incubated in solution free of contrast agent.

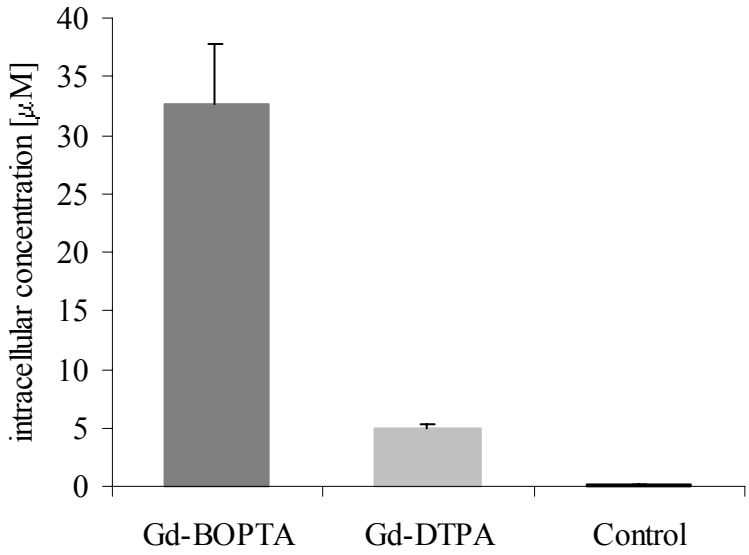

Figure 7.5: Intracellular content of contrast agent in hepatocytes incubated 60 minutes with 0.2 mM Gd-BOPTA, 0.2 mM Gd-DTPA or without contrast agent (n = 3).

The intracellular concentration of Gd^{3+} measured after incubation with Gd-DTPA may be due to contrast agent sticking to the cell surface, indicating that two washing cycles were not sufficient to eliminate all traces after incubation. Actually, it is known that Gd-DTPA is not

taken up by hepatocytes, explaining why it is classified among the extracellular contrast agents. Thorsternsen et al. [30] found that freshly isolated rat hepatocytes in suspension approximately took up 0.8% of the total extracellular Gd-DTPA .

These results clearly demonstrate that freshly isolated hepatocytes in suspension were able to take up the hepatobiliary contrast agent Gd-BOPTA. Actually, hepatocytes incubated in 0.2 mM solutions took up about 16% of the total extracellular concentration. These observations indicate that the uptake transport of Gd-BOPTA was not only present but also functional and that freshly isolated hepatocytes could be further used as a cellular model for the uptake study of Gd-BOPTA.

7.3.3 Perfusion of a MRI compatible hepatocyte bioreactor with contrast agents: pharmacokinetic analysis of the MRI data and transport studies

7.3.3.1 Development of a compartmental pharmacokinetic model to describe the MRI data

Unlike with most of the conventional software used for pharmacokinetic analysis, with NONMEM it is possible to define the compartment which is monitored as being the sum of all compartments present, i.e. the central and the peripheral compartments. Actually, the particularity of the results obtained by MRI is that the SI measured is the mean of the element imaged (in the present case a cross section of the HFB); hence, it includes the SI coming from all compartments present. This situation is different from the one found in conventional pharmacokinetics where the sampling is made in the central compartment (generally blood).

The pharmacokinetic analysis was first done on the curves obtained with the hepatobiliary contrast agent Gd-BOPTA with a proportional constant CV error model according to equation 7.7. Although appropriate for Gd-BOPTA, this error model was found to be unsuitable to treat the curves obtained with the extracellular contrast agent Gd-DTPA, because some of the points were equal or close to 0 and the SI fluctuations were similar over the whole curve, i.e. for the higher values of SI as well as for the SI values near 0. As the

additive error model (equation 7.6) best fitted the Gd-DTPA curves and also suited for the analysis of the curves obtained with Gd-BOPTA, it was further used for all the modeling.

Figure 7.7 shows an example of SI-time curves of Gd-BOPTA and Gd-DTPA after normalization with reference vials and correction for the baseline together with the predicted curves resulting from pharmacokinetic analysis. One can see that the predicted curve for the whole system fitted very well the experimental data for the two contrast agents investigated. The SI-time curves of Gd-BOPTA were fitted successfully with a two-compartment model and these of Gd-DTPA with a one-compartment model. Indeed, during the perfusion with Gd-BOPTA (figure 7.7a), the SI increased rapidly at the beginning of the perfusion and then increased more slowly. During the initiation of the washing step, SI decreased rapidly to a value different from the one before the perfusion. Beyond that point, SI remained stable or decreased very slightly but without returning to the baseline. These observations were described correctly by a two-compartment model. During the perfusion with Gd-DTPA (figure 7.7b), the SI increased and rapidly reached a steady-state. During washing, the inverse process occurred and the SI returned to the same value as before the perfusion with Gd-DTPA. These observations fitted well with a one-compartment model. We also tried to apply a two-compartment model to the data of Gd-DTPA, but the resulting estimation error on k_{12} and k_{21} was more than 100% and the correlation matrix of estimates showed that these parameters were correlated, indicating that the two-compartment model was too complex to describe the data.

The graphs of residuals show that they were well distributed around 0. However, higher residuals were observed at times corresponding to the beginning and end of the perfusion with the contrast agent (about 30 minutes for Gd-BOPTA and 15 minutes for Gd-DTPA). This indicates that the visual determination of the beginning and end of the perfusion might not be an adequate technique. For Gd-DTPA, an additional remark has to be done concerning the last points. Actually, as the software does not allow negative values, all the negative values were changed to 0, which explains the slightly positive residuals of the last points of the Gd-DTPA curve.

In addition to the fitting of the observations coming from the whole system, the two-compartment model enables to estimate the SI due to Gd-BOPTA in the central and peripheral compartment. The evolution of the SI in the central compartment is similar to the one observed with Gd-DTPA. SI rapidly reached steady-state during the perfusion of Gd-BOPTA and quickly returned to baseline during washing. On the other hand, in the peripheral compartment SI rose regularly and less intensely during the perfusion and did not or only slightly diminish over the period of washing. The comparison between the one-compartment model describing the behavior of the extracellular contrast agent Gd-DTPA and the two-compartment model describing the one of the hepatobiliary contrast agent Gd-BOPTA suggests that the peripheral compartment of Gd-BOPTA may represent the hepatocytes in which Gd-BOPTA distributed. Considering the evolution of the SI in the peripheral compartment, i.e. in the hepatocytes, one can see that Gd-BOPTA entered hepatocytes regularly over the period of perfusion but did not exit at the same rate. In fact, Gd-BOPTA stayed in the hepatocytes or was only slightly released back in the central compartment during washing. Moreover, when considering the composition of the HFB itself, one remarks that it consists of two compartments, the intracapillary space (ICS) and the extracapillary space (ECS). Nevertheless, the filling process of the HFB with Gd-DTPA followed a one-compartment model, which signifies that fiber filling with Gd-DTPA and its diffusion through the fibers in the ECS were not distinguishable processes. This was already observed during the choice of the HFB in chapter 5.

In most cases, the pharmacokinetic models described observations very well, but there were some exceptions. Figure 7.8 illustrates a case where k_{21} had to be fixed to 0 to fit the experimental data and a case where the model was less adapted to the experimental observations. In both cases, the fluctuation of the SI was reflected in the distribution of residuals. In the example of Gd-BOPTA 0.2 mM (figure 7.8 a), the model was not good when we allowed the software to choose the k_{21} value freely. Fixing of k_{21} to 0 improved considerably the quality of the estimate. The k_{21} value was in fact not fixed strictly to 0 because the software does not accept 0, but to 1.00E-06. In the example of Gd-BOPTA

0.4 mM (figure 7.8b), the estimated curve did not strictly fit the observations, especially for the first points, where the SI of the experimental points rose more rapidly than the estimate.

a) Gd-BOPTA 0.2 mM

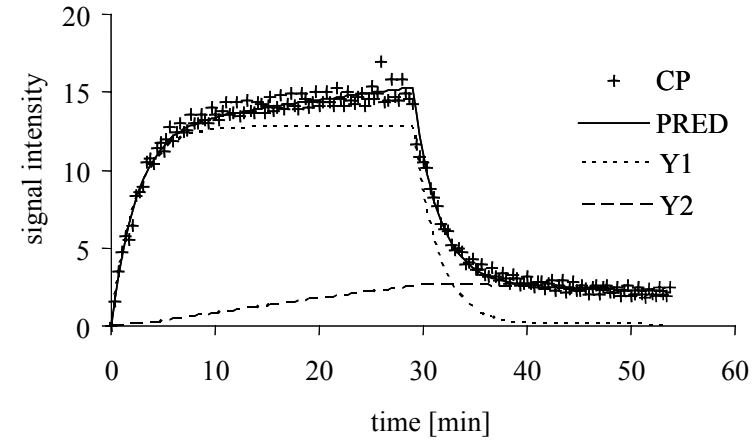

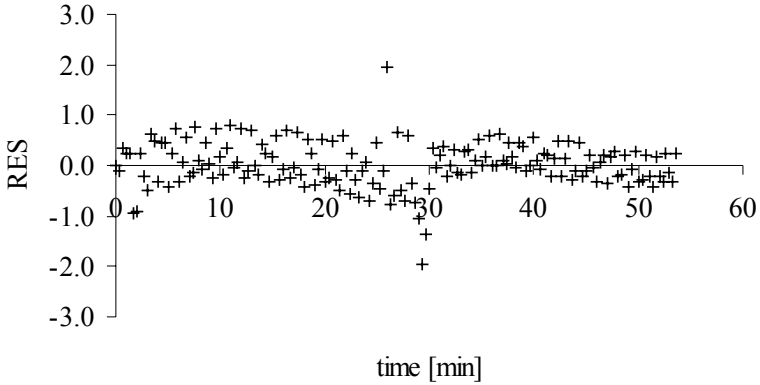

b) Gd-DTPA 0.2 mM

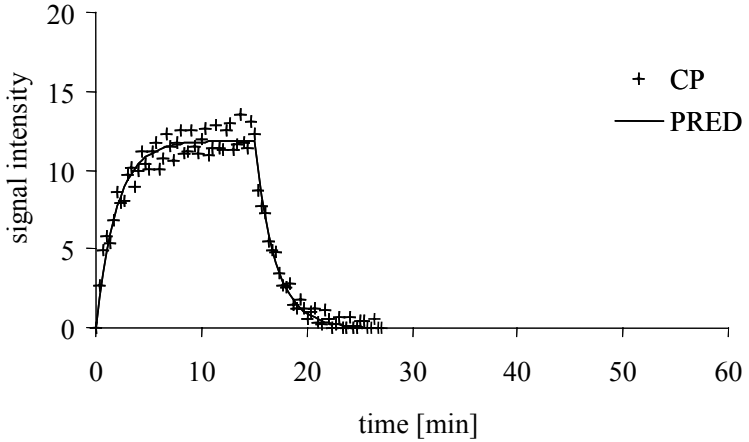

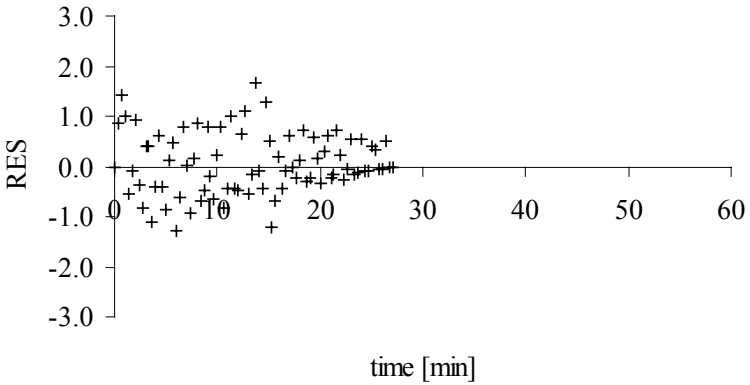

Figure 7.7: SI-time curves of Gd-BOPTA and Gd-DTPA after normalization with reference vials and correction for the baseline together with the predicted curves resulting from the pharmacokinetic analysis with a two-, respectively one-compartment model. CP = observations in the whole system, PRED = predictions in the whole system, Y1 = predictions in the central compartment, Y2 = predictions in the peripheral compartment, RES = residuals.

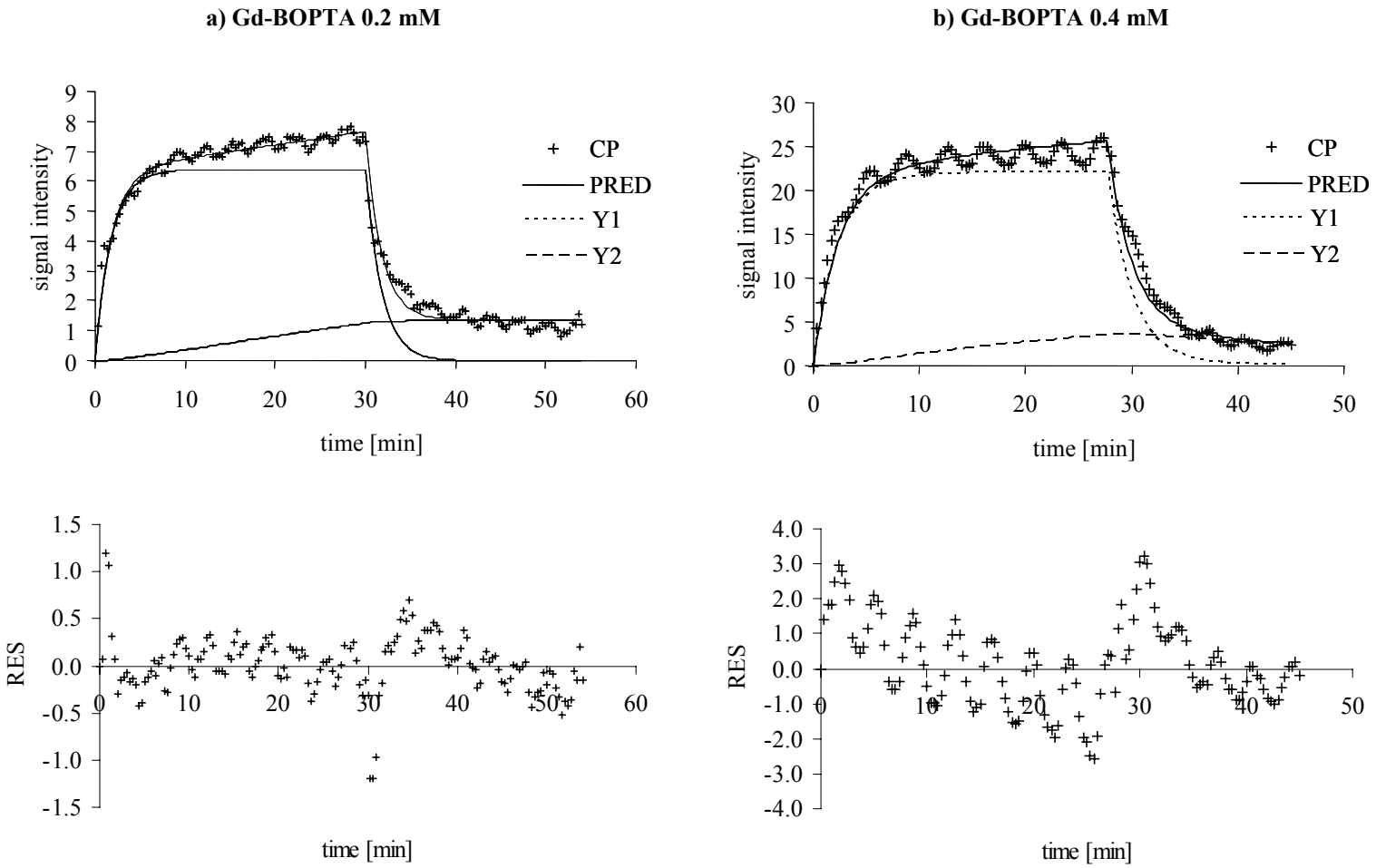

Figure 7.8: SI-time curves of Gd-BOPTA after normalization with reference vials and correction for the baseline together with the predicted curves resulting from the pharmacokinetic analysis with a two-compartment model. Two particular examples are illustrated: a) k_{12} had to be fixed to 0 to fit the experimental data, b) the model was not well adapted to the data. CP = observations in the whole system, PRED = predictions in the whole system, Y1 = predictions in the central compartment, Y2 = predictions in the peripheral compartment, RES = residals.

Table 7.1: Results of the pharmacokinetic analysis of the SI-time curves of Gd-BOPTA with a two-compartment model, and Gd-DTPA with a one-compartment model, after normalization with reference vials and correction for the baseline.

Gd-BOPTA											
concentration [mM]	k_{10} [min^{-1}]	SEE [min^{-1}]	k_{12} [min^{-1}]	SEE [min^{-1}]	k_{21} [min^{-1}]	SEE [min^{-1}]	σ [SI]	α [min^{-1}]	β [min^{-1}]	$t_{1/2}$ (α) [min]	$t_{1/2}$ (β) [min]
0.05	4.24E-01	2.43E-02	1.02E-02	1.25E-03	5.41E-04	4.27E-03	2.21E-01	4.34E-01	5.28E-04	1.60E+00	1.31E+03
	3.89E-01	4.12E-02	1.04E-02	4.58E-03	2.75E-02	1.70E-02	3.39E-01	4.01E-01	2.68E-02	1.73E+00	2.59E+01
0.1	5.60E-01	1.33E-01	7.02E-03	8.63E-04	1.00E-06	k21 fixed	3.02E-01	5.67E-01	9.88E-07	1.22E+00	7.02E+05
	3.44E-01	1.14E-02	1.58E-02	1.44E-03	3.27E-02	3.30E-03	1.80E-01	3.61E-01	3.11E-02	1.92E+00	2.23E+01
0.2	4.20E-01	1.49E-02	8.45E-03	9.85E-04	1.06E-02	4.04E-03	4.53E-01	4.28E-01	1.04E-02	1.62E+00	6.69E+01
	4.79E-01	1.80E-02	9.59E-03	1.01E-03	1.28E-02	3.57E-03	5.14E-01	4.89E-01	1.26E-02	1.42E+00	5.52E+01
0.4	3.02E-01	2.95E-02	8.89E-03	1.90E-03	1.90E-02	7.97E-03	2.49E+00	3.11E-01	1.84E-02	2.23E+00	3.76E+01
	4.21E-01	3.30E-02	9.02E-03	3.02E-03	3.00E-02	1.47E-02	1.23E+00	4.31E-01	2.94E-02	1.61E+00	2.36E+01
mean	4.17E-01		9.92E-03		1.66E-02			4.28E-01	1.62E-02	1.67E+00	8.79E+04
SD	7.90E-02		2.60E-03		1.28E-02			7.75E-02	1.24E-02	3.06E-01	2.48E+05

Gd-DTPA											
concentration [mM]	k_{10} [min^{-1}]	SEE [min^{-1}]					σ [SI]			$t_{1/2}$ (k_{10}) [min]	
0.05	4.21E-01	2.10E-02					2.66E-01			1.65E+00	

0.1	5.28E-01	3.26E-02					2.99E-01			1.31E+00	
	2.75E-01	6.47E-03					3.30E-01			2.52E+00	
0.2	3.87E-01	1.19E-02					6.54E-01			1.79E+00	
	5.20E-01	1.66E-02					6.18E-01			1.33E+00	
0.4	3.70E-01	1.32E-02					1.12E+00			1.87E+00	
mean	4.17E-01									1.75E+00	
SD	9.61E-02									4.45E-01	

SEE: standard error of estimate, SD: standard deviation, σ: standard deviation of the residual error according to equation 7.6

Several comments can be made on the results contained in table 7.1. First, the precision of k_{21} was low for some Gd-BOPTA experiments, showing that estimating this parameter was difficult and suggesting that it might have been adequate to fix it to 0, as done with the first experiment at 0.1 mM. Second, the between-experiment variability was large for k_{21} (1.66E-02 ± 1.28E-02 min^{-1}), because of very low values in some experiments. In particular fixing k_{21} to 1E-06 in one experiment led to an increase in the standard deviation of both k_{21} and β. Although k_{21} (1.66E-02 ± 1.28E-02 min^{-1}) was in general higher than k_{12} (9.92E-03 ± 2.60E-03 min^{-1}), the amount of Gd-BOPTA transferred from the central to the peripheral compartment was much higher than the inverse transfer because the concentration of Gd-BOPTA in the central compartment was much higher than the one in the peripheral compartment. This phenomenon was visible on figures 7.7 and 7.8 where the SI in the peripheral compartment increased over the time of perfusion and only slightly decreased during washing.

Another important point is that there was no difference between the rate constants obtained with different concentrations of Gd-BOPTA. The same remark can be made with Gd-DTPA. Hence, we calculated mean values and standard deviations of all rate constants across all concentrations. The k_{10} were identical for Gd-BOPTA (4.17E-01 ± 0.79E-01 min^{-1}) and Gd-DTPA (4.17E-01 ± 0.96E-01 min^{-1}). In theory, they were expected to be identical. Indeed, k_{10} represented the elimination of the contrast agent from the HFB (central compartment) by the simple washing with a solution free of contrast agent and Gd-BOPTA was not metabolized by hepatocytes but excreted unchanged. The fact that k_{10} were found to be identical indicates that the complex model developed to describe the Gd-BOPTA experimental curves was of good quality. In table 7.1, the $t_{1/2\,(k10)}$ was aligned with the $t_{1/2\,(\alpha)}$. Actually, when changing from a two- to a one-compartment model and setting $k_{12} = k_{21} = 0$ in equations 7.3 and 7.4, the result is that $\alpha = k_{10}$ and $\beta = 0$. The $t_{1/2\,(\alpha)}$ were similar for Gd-BOPTA (1.67 ± 0.31 min) and Gd-DTPA (1.75 ± 0.45 min), showing that the alpha phase of Gd-BOPTA reflected especially the diffusion of the contrast agent in the HFB. Hence, the scheme of figure 7.3 could be adapted to our hepatocyte HFB as seen in figure 7.9.

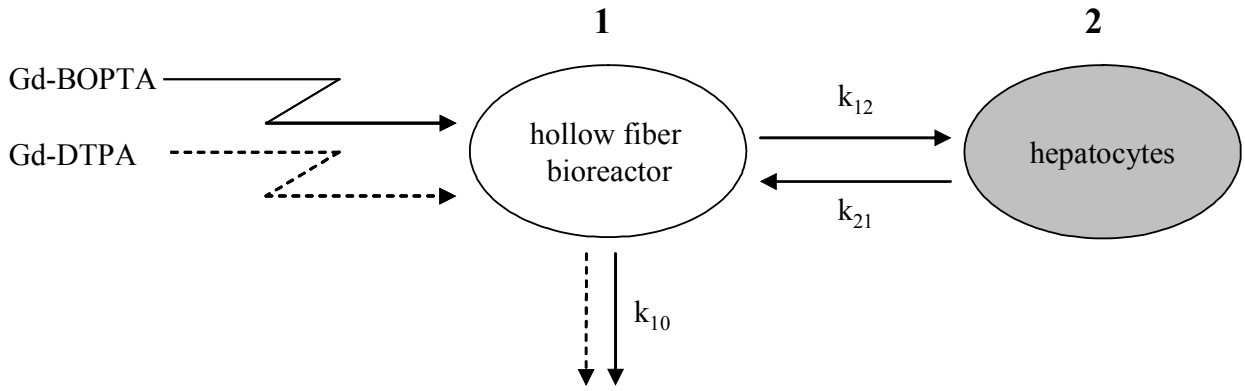

Figure 7.9: Schematic representation of the hepatocyte hollow fiber bioreactor as a two-compartment open model. Contrast agents are administered and eliminated from compartment 1, i.e. the HFB. Gd-BOPTA distributes between compartment 1 and 2, i.e. it enters the hepatocytes, in contrast to the extracellular Gd-DTPA. The rate constants for the processes are indicated, full lines refer to Gd-BOPTA and dashed lines to Gd-DTPA.

In summary, the compartmental models developed permitted to describe well our experimental data. Nevertheless, several suggestions are made to overcome some weaknesses of this modeling procedure. The first problem encountered was linked to the visual and manual determination of the baseline. Actually, as seen in figure 7.6 and as already discussed in chapter 5, the initial SI had a positive value. The curves were first normalized according to reference vials and corrected to 0, in order to be comparable to each other. This manual approximation could induce errors of estimation. A solution to this problem would be the introduction of an additional parameter in the model which would estimate the baseline. A second problem came from the visual and manual determination of the start and end point of

the perfusion which was reflected by high residuals at the times corresponding to the beginning and end of the perfusion. This problem could be solved by the introduction of a parameter which would estimate a lag-time for the beginning of the perfusion and a parameter to estimate its end. The influence of the lag-time on the estimation of concentration-time curves has been studied [31]. Finally, a third problem was linked to the background noise characterized by an oscillatory behavior which increased with the concentration of contrast agent. These fluctuations of SI induced high residual errors and could distort estimations. To solve this problem seems to be more difficult as the origin of these oscillations should be known in order to be able to suppress them.

Most of the data on the pharmacokinetics and tissue distribution of MRI contrast agents have been obtained by dosage of their content in biological samples such as plasma, urine and bile [32]. Nevertheless, some recent pharmacokinetic studies have been based on dynamic contrast enhanced T_1-weighted MRI (DCE-MRI) data. Actually, DCE-MRI has recently emerged as a promising method notably for diagnosis, prognosis and therapy monitoring of cancer [33,34] or for the assessment of blood brain-barrier permeability [35]. The review by Taylor and Reddick [36] gives a good overview of the progresses made in the field of pharmacokinetic MRI. A considerable variation in both the methods of data acquisition and analysis exists between the different research groups. The majority of clinical investigations do not analyze MRI data using a pharmacokinetic model, but rather extract a variety of empirical parameters. These semi-quantitative analyses usually calculate the magnitude or the rate of SI change after injection of contrast agent. Some authors correlated these empirical values with histological diagnosis with relative success. Pharmacokinetic MRI determinations have two advantages over empirical determinations: they can be compared between groups of investigators and patients, and they can yield insight into physiological parameters (e.g. vascular permeability). To convert empirical data to more robust pharmacokinetic parameters, two major steps have to be done. The first step is to convert the dynamic MR SI curve, *SI(t)*, into a concentration curve, *C(t)*. Knowledge of the contrast agent concentration is required to extract as much relevant physiological information as possible from the kinetic data. This

complicates analysis of DCE-MRI data because only the SI is generally measured, and that may not be easily related to the concentration of contrast agent in tissue as already discussed in chapters 3 and 6. The second step is to model the relation of the concentration in the tissue to the concentration-time curve in the central compartment in order to gain insight into the physiological process of exchange of contrast agent between the different compartments. A variety of parameters have been estimated; often the same quantity appears with different names or symbols in different reports, so that a comparison of work from different research groups is almost impossible. Tofts et al. [37] described a standard set of names and symbols related to the estimate of kinetic parameters and proposed to use them as international standards. It was not possible for us to know whether it was trivial or not to use a software which permitted to fix the monitored compartment as being the sum of all compartments present, as done in the present study, since this information was not mentioned in available papers related to MRI pharmacokinetics.

7.3.3.2 Transport studies of Gd-BOPTA with hepatocytes contained in a HFB

To elucidate the transport mechanism of Gd-BOPTA into hepatocytes, the uptake of different concentrations (0.05 - 0.4 mM) of Gd-BOPTA was studied by MRI with the newly developed hepatocyte HFB. After a pharmacokinetic analysis of the perfusion experiments, we plotted the value of the SI in the peripheral compartment at the end of the 30 minutes perfusion with Gd-BOPTA, attributable to the amount of Gd^{3+} inside the hepatocytes, against the concentration of Gd-BOPTA perfused (figure 7.10).

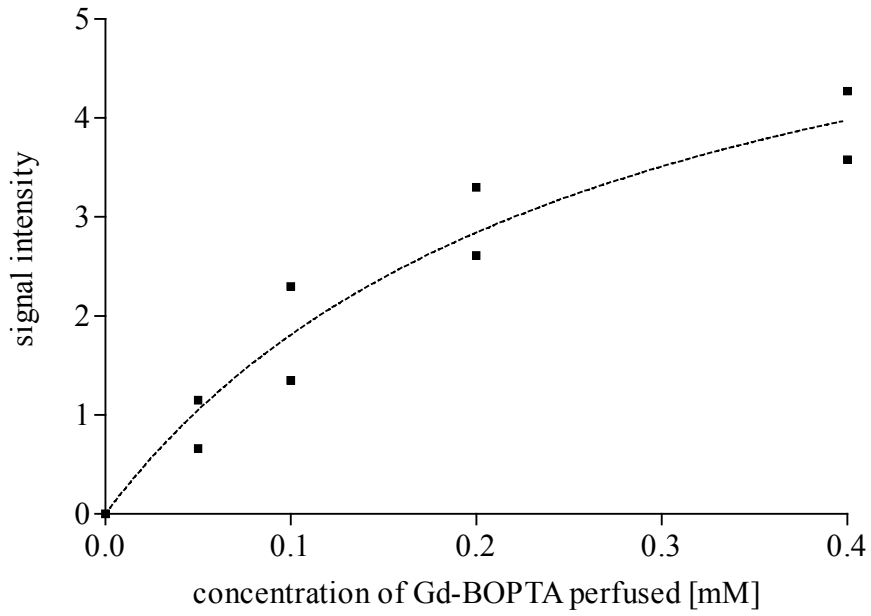

Figure 7.10: Signal intensity in the peripheral compartment, i.e. in the hepatocytes, after 30 minutes of perfusion of the hepatocyte HFB with a solution containing Gd-BOPTA at concentrations ranging from 0.05 to 0.4 mM.

Figure 7.10 shows that the SI due to the Gd^{3+} contained in the hepatocytes after 30 minutes of perfusion with different concentrations of Gd-BOPTA was not linearly correlated to the concentration of Gd-BOPTA perfused. The approximate curve which ran through the points typically described a saturable process. These observations tend to support a receptor-mediated mechanism rather than an uptake mechanism by free diffusion.

After experiments where two solutions of Gd-BOPTA were perfused consecutively in the same hepatocyte HFB, cells were extracted from the HFB, lysed and the residual quantity of Gd^{3+} in the bioreactor was determined by ICP-AES. The study of the relation between the total residual SI and the residual intracellular concentration of Gd^{3+} in the HFB showed that 1 unity of SI corresponded to 15.9 ± 2.1 μM of Gd^{3+} ($n = 4$) for cumulative concentrations of Gd-BOPTA in the solution perfused up to 0.4 mM. We made an approximation of the intracellular content of Gd^{3+} after the perfusion of a solution containing 0.2 mM Gd-BOPTA. The mean of the two points obtained with Gd-BOPTA 0.2 mM was 2.95 SI (figure 7.10),

which could be transformed in an intracellular concentration of Gd^{3+} equal to 46.9 ± 6.2 μM, i.e. 23.5 ± 3.1% of the concentration in the perfusion solution. On the other hand, the intracellular content of Gd^{3+} after the incubation of the freshly isolated hepatocytes in suspensions for 60 minutes with Gd-BOPTA 0.2 mM was 32.6 ± 4.6 μM, i.e. 16.3 ± 2.3% of the concentration in the incubation solution (§7.3.2). Although the calculation of the intracellular content of Gd^{3+} in the HFB was approximate and resulted from a 30 minutes perfusion (compared to 60 minutes for the incubation), the two values were in the same order of magnitude.

Despite these observations, the SI of the peripheral compartment after 30 minutes of perfusion with Gd-BOPTA could not be transformed in an exact intracellular concentration of Gd^{3+}. Actually, the intracellular amount of Gd^{3+}, reflected by the SI in the peripheral compartment, was the consequence of successive perfusions with different concentrations of Gd-BOPTA. And as already discussed in chapter 6, conversion of SI to concentration of contrast agent is not possible yet because the relation between the intracellular concentration of Gd^{3+} and the resulting SI is still not known.

The possible inhibition of the uptake of Gd-BOPTA by BSP was assessed by perfusing the HFB first with a solution containing 0.1 mM Gd-BOPTA alone and then with a solution containing 0.1 mM Gd-BOPTA and 0.1 mM BSP. The same experiment was repeated with concentrations of Gd-BOPTA and BSP of 0.4 mM (figure 7.11). Although SI were slightly lower during the perfusion with Gd-BOPTA + BSP, this difference was not significant considering the fluctuations of SI. The same was observed with the perfusion of Gd-BOPTA + BSP at a concentration of 0.1 mM. Despite their preliminary character (we tested only two concentrations one time), the results reported here seem to indicate that there was no inhibition of the transport of Gd-BOPTA into hepatocytes by BSP.

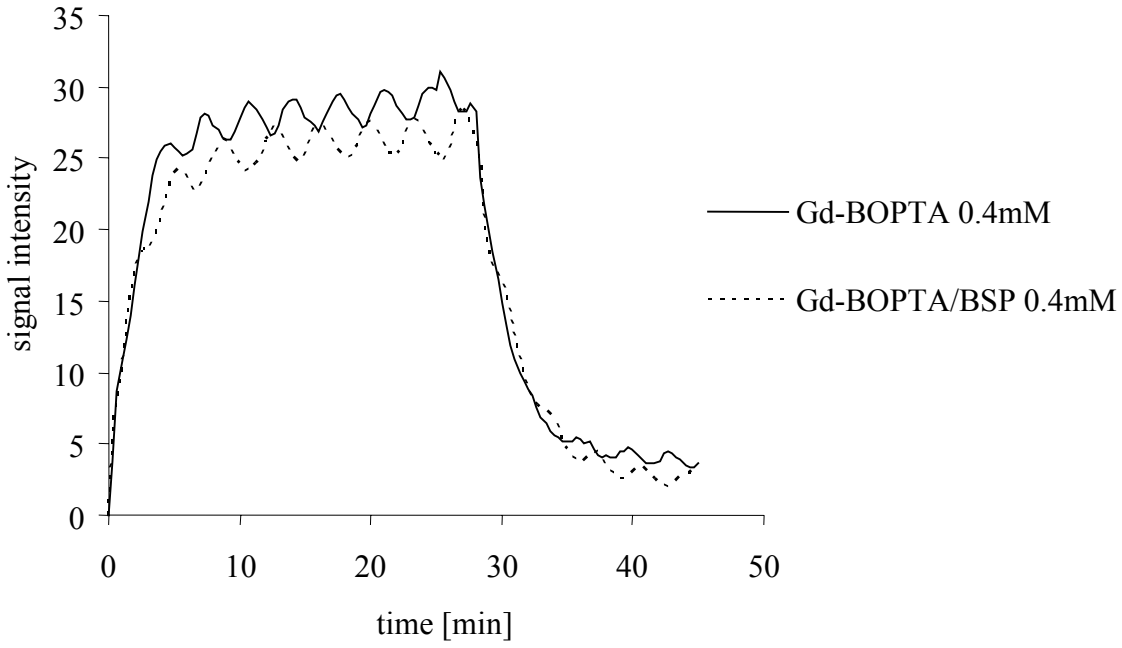

Figure 7.11: Evolution of normalized MR signal intensity with time in a hollow fiber bioreactor containing $4 \cdot 10^7$ hepatocytes/ml. The bioreactor was perfused with a solution containing 0.4 mM Gd-BOPTA for 30 minutes, with a solution exempt of contrast agent for 15 minutes, with a solution containing 0.4 mM Gd-BOPTA + 0.4 mM BSP for 30 minutes, and then with a solution exempt of

contrast agent for 15 minutes. SI were normalized according to the SI of reference vials and corrected to zero. Although the perfusions were consecutive, they were superposed for a better comparison.

Similar experiments of inhibition were performed with perfused rat livers and it was found that an equimolar concentration of BSP totally inhibited the hepatocyte uptake of Gd-BOPTA at concentrations of 0.5 mM [38]. These results are in contradiction with our observations. Such contradictory observations are also found in the literature: De Haën et al. [4] observed a partial inhibition of the Gd-BOPTA uptake by BSP in rats, while Pascolo et al. [2] found that the free diffusion of Gd-BOPTA was not inhibited by BSP in rat sinusoidal membrane vesicles. These findings could indicate that a modification of the transport system occurs during the isolation of the hepatocytes and the sinusoidal membrane vesicles which renders the transport of Gd-BOPTA no longer sensitive to the inhibition of BSP. Indeed, this could be the consequence of the rather aggressive isolation procedure or of the loss of the membrane polarity, as already discussed in paragraph 7.3.1.

The excretion of Gd-BOPTA is known to occur via the active transporter mrp2 [5-7]. Although mrp2 was expressed in freshly isolated hepatocytes as shown on Western blots (figure 7.4), the SI due to Gd-BOPTA in the peripheral compartment, meant to represent the hepatocytes, only slightly decreased over 30 minutes washing (figure 7.7a). Several hypotheses can be proposed to explain these observations. The slow excretion observed *in vitro* can be of the same magnitude as *in vivo*, where the excretion of Gd-BOPTA by mrp2 into the bile is known to be a rate-limiting step [7], or it can be slower, due for instance to a) a change of the transporter during the hepatocyte isolation, b) an unfavorable energetic state of the cells, or c) binding of Gd-BOPTA anywhere in the hepatocytes. Moreover, these results do not allow to make comments on the possible reversibility of the uptake transport mechanisms as it cannot be excluded that the slow release of Gd-BOPTA occurred through this mechanism.

7.4 Conclusion

The goal of this work was to study the transport of the hepatobiliary MRI contrast agent Gd-BOPTA in freshly isolated rat hepatocytes. First, the expression of the transporters known or suspected to be involved in the transport of Gd-BOPTA in isolated hepatocytes, i.e. oatp1, oatp2, oatp4 and mrp2, was verified. Western blotting indicated that all of them, except oatp4, were expressed similarly in isolated hepatocytes and in a control sample of an entire liver. Then, the uptake of Gd-BOPTA by freshly isolated hepatocytes in suspension was evaluated by ICP-AES to check the functionality of the uptake mechanisms. After 1 hour of incubation with Gd-BOPTA 0.2 mM, the intracellular content of Gd^{3+} represented 16% of the concentration of Gd-BOPTA in the incubation solution. The results of these two experiments ensured that freshly isolated hepatocytes offer a suitable cellular model for the investigation of Gd-BOPTA uptake.

We pursued the study of the uptake mechanisms of Gd-BOPTA by MRI with our newly developed MRI compatible hepatocyte HFB. This cellular model was shown to reproducibly differentiate the behavior of the intracellular contrast agent Gd-BOPTA and the extracellular contrast agent Gd-DTPA, while ensuring a functional stability and an intact cellular morphology. Concentrations of Gd-BOPTA ranging from 0.05 to 0.4 mM were perfused through the HFB and the resulting SI-time curves were submitted to compartmental pharmacokinetic modeling. The software NONMEM was used for this purpose as it permitted to take into account the particularity of the MRI data, i.e. it allowed to consider the compartment of measure as being the sum of all the compartments present (the central and the peripheral compartments), in contrast to most of the usual pharmacokinetic software. Gd-BOPTA curves were fitted successfully with a two-compartment model while a one-compartment model described well the ones with Gd-DTPA. The estimated parameters (k_{10}, k_{12}, k_{21}) were the same for all concentrations of Gd-BOPTA perfused through the HFB. The means of the elimination rate constants k_{10} were identical for Gd-BOPTA

(4.17E-01 ± 0.79E-01) and Gd-DTPA (4.17E-01 ± 0.96E-01). Considering that Gd-BOPTA underwent no biotransformation and that the HFB were identical, the elimination rate constants k_{10} were theoretically the same. The fact that estimates were indeed identical thus indicated that the proposed model adequately described the system under study. Expressing the data in terms of compartmental models and associated parameters permitted a better interpretation of the data. Actually, the additional compartment present with Gd-BOPTA, as compared to Gd-DTPA, could be associated to the hepatocytes, into which Gd-BOPTA distributed. The relation between the SI in the peripheral compartment, i.e. the hepatocytes, after 30 minutes of perfusion and the concentration of Gd-BOPTA perfused was nonlinear. This indicated that the uptake of Gd-BOPTA seemed to follow a saturable mechanism, which is in agreement with a carrier mediated transport.

References

[1] Moncelli MR, Becucci L, De Haën C, and Tirone P, Interactions between magnetic resonance imaging contrast agents and phospholipid monolayers, *Bioelectrochem Bioenerg*, 1998, **46**, 205-213.

[2] Pascolo L, Cupelli F, Anelli PL, Lorusso V, Visigalli M, Uggeri F, and Tiribelli C, Molecular mechanisms for the hepatic uptake of magnetic resonance imaging contrast agents, *Biochem Biophys Res Commun*, 1999, **257**, 746-752.

[3] Van Montfoort JE, Stieger B, Meijer DKF, Weinmann H-J, Meier PJ, and Fattinger KE, Hepatic uptake of the magnetic resonance imaging contrast agent gadoxetate by the organic anion transporting polypeptide Oatp1, *J Pharmacol Exp Ther*, 1999, **290**, 153-157.

[4] Freshney RI, Specialized cells, In 'Culture of Animal Cells', Ed. Freshney RI, Wiley-Liss, New York, 2000, pp. 345-384.

[5] Pascolo L, Petrovic S, Cupelli F, Bruschi CV, Anelli PL, Lorusso V, Visigalli M, Uggeri F, and Tiribelli C, ABC protein transport of MRI contrast agents in canalicular rat liver plasma vesicles and yeast vacuoles, *Biochem Biophys Res Commun*, 2001, **282**, 60-66.

[6] De Haën C, Lorusso V, and Tirone P, Hepatic transport of gadobenate dimeglumine in TR- rats, *Acad Radiol*, 1996, **3**, 452-454.

[7] De Haën C, La Ferla R, and Maggioni F, Gadobenate dimeglumine 0.5 M solution for injection (Multihence) as contrast agent for magnetic resonance imaging of the liver: mechanistic studies in animals, *J Comput Assist Tomogr*, 1999, **23 (Suppl. 1)**, S169-S179.

[8] Groothuis GMM and Meijer DKF, Drug traffic in the hepatobiliary system, *J Hepatol*, 2001, **24**, S3-S28.

[9] Miyauchu S, Sawada Y, Iga T, Hanano M, and Sugiyama Y, Comparison of the hepatic uptake clearences of fifteen drugs with a wide range of membrane permeabilities in isolated rat hepatocytes and perfused rat livers, *Pharm Res*, 1993, **10**, 434-440.

[10] Petzinger E and Frimmer M, Comparative investigations on the uptake of phallotoxins, bile acids, bovine lactoperoxidase and horseradish perodidase into rat hepatocytes in suspensions and in cell cultures, *Biochim Biophys Acta*, 1988, **937**, 135-144.

[11] Eckhardt U, Schroeder A, Stieger B, Höchli M, Landmann L, Tynes R, Meier PJ, and Hagenbuch B, Polyspecific substrate uptake by the hepatic organic anion transporter Oatp1 in stably transfected CHO cells., *Am J Physiol*, 1999, **276**, G1037-G1042.

[12] Reichel C, Gao B, Van Montfoort JE, Cattori V, Rahner C, Hagenbuch B, Stieger B, Kamisako T, and Meier PJ, Localization and function of the organic anion-transporting polypeptide Oatp2 in rat liver, *Gastroenterology*, 1999, **117**, 688-695.

[13] Dumont M, Jacquemin E, D'Hont C, Descout C, Cresteil D, Haouzi D, Desrochers M, Stieger B, Hadchouel M, and Erlinger S, Expression of the liver Na+-independent organic anion transporting polypeptide (oatp-1) in rats with bile duct ligation, *J Hepatol*, 1997, **27**, 1051-1056.

[14] Madon J, Hagenbuch B, Landmann L, Meier PJ, and Stieger B, Transport function and hepatocellular localization of mrp6 in rat liver, *Mol Pharmacol*, 2000, **57**, 634-641.

[15] Cattori V, Van Montfoort JE, Stieger B, Landmann L, Meijer DKF, Winterhalter KH, Meier PJ, and Hagenbuch B, Localization of organic anion transporting polypeptide 4 (Oatp4) in rat liver and comparison of its substrate specificity with Oatp1, Oatp2 and Oatp3, *Pflugers Arch*, 2001, **443**, 188-195.

[16] Seglen O, Preparation of isolated rat liver cells, In 'Methods in Cell Biology', Ed. Prescott DM, Academic Press, New York, 1976, Vol. 13, pp. 29-83.

[17] Shah V, Cao S, Hendrickson H, Yao J, and Katusic ZS, Regulation of hepatic eNOS by caveolin and calmodulin after bile duct ligation in rats, *Am J Physiol Gastrointest Liver Physiol*, 2001, **280**, G1209-G1216.

[18] Bradford MM, A rapid and sensitive method of quantification of microgram quantities of protein utilizing the principle of protein-dye binding, *Anal Biochem*, 1976, **72**, 248-254.

[19] Laemmli UK, Cleavage of structural proteins during the assembly of the head of bacteriophage T4, *Nature*, 1970, **227**, 680-685.

[20] Towbin H, Staehelin T, and Gordon J, Electrophoretic transfer of proteins from polyacrylamide gels to nitrocellulose sheets: procedure and some applications, *Proc Natl Acad Sci USA*, 1979, **76**, 4350-4354.

[21] Roman LM and Hubbard AL, A domain-specific marker for the hepatocyte plasma membrane: localization of leucine aminopeptidase to the bile canalicular domain, *J Cell Biol*, 1983, **96**, 1548-1558.

[22] Greengard O, Federman M, and Knox WE, Cytomorphology of developing rat liver and its application to enzyme differentiation, *J Cell Biol*, 1972, **52**, 261-272.

[23] Sasse D, Spornitz UM, and Maly IP, Liver architecture, *Enzyme*, 1992, **46**, 8-32.

[24] Weibel ER, Staubli W, Gnagi HR, and Hess FA, Correlated morphometric and biochemical studies on the liver cell, *J Cell Biol*, 1969, **42**, 68-91.

[25] Wagner JG, Integrated Equations for Several Pharmacokinetic Models, In 'Biopharmaceutics and Relevant Pharmacokinetics', Drug Intelligence Publications, Hamilton, 1971, pp. 292-296.

[26] Lewin M, Clément O, Belguise-Valladier P, Tran L, Cuénod C-A, Siauve N, and Frija G, Hepatocyte targeting with Gd-EOB-DTPA, *Invest Radiol*, 2001, **36**, 9-14.

[27] Jauregui HO, and Gann KL, Mammalian hepatocytes as a foundation for treatment in human liver failure, *J Cell Biochem*, 1991, **45**, 359-365.

[28] Bader A, Reimer P, Knop E, Böker K, Christians U, Weissleder R, and Sewing K-F, An organotypical *in vitro* model of the liver parenchyma for uptake studies of diagnostic MR receptor agents, *Magn Reson Imaging*, 1995, **13**, 991-1002.

[29] Ishigami M, Tokui T, Komai T, Tsukahara K, Yamazaki M, and Sugiyama Y, Evaluation of the uptake of pravastatin by perfused rat liver and primary cultured rat hepatocytes, *Pharm Res*, 1995, **12**, 1741-1745.

[30] Thorstensen K and Romslo I, The interaction of gadolinium complexes with isolated rat hepatocytes, *BioMetals*, 1995, **8**, 65-69.

[31] Balant L, Revillard C, and Venturas K, Absorption gastro-intestinale et analyse multicompartimentale sur ordinateur, *Pharm Acta Helv*, 1977, **52**, 89-95.

[32] Lorusso V, Arbughi T, Tirone P, and De Haën C, Pharmacokinetics and tissue distribution in animals of gadobenate ion, the magnetic resonance imaging contrast enhancing component of gadobenate dimeglumine 0.5 M solution for injection (MultiHance), *J Comput Assist Tomogr*, 1999, **23 (Suppl. 1)**, 181-194.

[33] Hawighorst H, Knapstein PG, Weikel W, Knopp MV, Zuna I, Knof A, Brix G, Schaeffer U, Wilkens C, Schoenberg SO, Essig M, Vaupel P, and Van Kaick G, Angiogenesis of uterine cervical carcinoma: characteriztion by pharmacokinetic

resonance parameters and histological microvessel density with correlation to lymphatic involvement, *Cancer Res*, 1997, **57**, 4777-4786.

[34] Evelhoch JL, Key factors in the aquisition of contrast kinetic data for oncology, *J Magn Reson Imag*, 1999, **10**, 254-259.

[35] Port MD, Knopp MV, Hoffmann U, Milker-Zabel S, and Brix G, Multicompartment analysis of gadolinium chelate kinetics: Blood-tissue exchange in mammary tumors as monitored by dynamic MR imaging, *J Magn Reson Imag*, 1999, **10**, 233-241.

[36] Taylor JS and Reddick WE, Evolution from empirical dynamic contrast-enhanced magnetic resonance imaging to pharmacokinetic MRI, *Adv Drug Deliv Rev*, 2000, **41**, 91-110.

[37] Tofts PS, Brix G, Buckley DL, Evelhoch JL, Henderson E, Knopp MV, Larsson HBV, Lee TY, Mayr NA, Parker GJM, Port RE, Taylor J, and Weisskoff RM, Estimating kinetic parameters from dynamic contrast-enhanced T1-weighted MRI of a diffusable tracer: standardized quantities and symbols, *J Magn Reson Imag*, 1999, **10**, 223-232.

[38] Pastor CM, Planchamp C, Pochon S, Lorusso V, Montet X, Mayer JM, Terrier F, and Vallée JP, Bromosulfophtalein inhibits the entry of Gd-BOPTA/Dimeg in hepatocytes. Hepatic kinetics by magnetic resonance imaging in the isolated perfused rat liver, *Radiology*, 2002, In press.

Chapter 8
General conclusion and perspectives

Magnetic resonance imaging (MRI) plays an important role in the diagnosis of several hepatic diseases. The use of contrast agents, and in particular hepatobiliary contrast agents such as Gd-BOPTA, allows to improve the detection of such diseases. Actually, hepatobiliary contrast agents are able to enter hepatocytes by a mechanism which is not yet fully elucidated and are partially excreted into the bile. The aim of this work was thus to develop a MRI compatible *in vitro* model to study the transport of hepatobiliary contrast agents into hepatocytes.

The cellular device chosen consisted of a hollow fiber bioreactor (HFB), a structure particularly well suited for our expectations. First, its plastic composition made it MRI compatible. Second, it was included in a dynamic system which has the advantage that hepatocytes contained in the HFB were continually fed with a thermoregulated solution containing oxygen and nutrients which allowed to use high cellular densities without loss of viability. Finally, the dynamic aspect of the culture system permitted to change the solutions perfused in the HFB and thus to study different conditions during a single experiment.

The HFB perfusion system was also built in order to be compatible with the magnetic field, i.e. all the elements situated inside the magnet were made of plastic or glass, while the elements containing metal were set in a room adjacent to the magnet. The sensible choice of the heating system, oxygenation, HFB device, flow rate and hepatocyte density in the HFB assured optimal experimental conditions. The preservation at 4°C of the hepatocytes in the University of Wisconsin solution permitted to keep them viable and functional during the period of time between their isolation and the MRI experiment. A good viability was also obtained during the MRI experiments as assessed by oxygen consumption and release of intracellular enzymes.

First, we demonstrated that the hepatocyte HFB is able to distinguish in a reproducible manner between the hepatobiliary contrast agent Gd-BOPTA and the extracellular contrast agent Gd-DTPA. The results were expressed as the variation of the mean signal intensity (SI) of a cross-section of the HFB with time. Although the SI was linearly correlated with the concentration of contrast agent, SI-time curves obtained with the hepatocyte HFB were not converted to concentration-time curves, mainly because the relaxivity of Gd-BOPTA is not identical in the intracellular fluid and in the perfusion solution. The SI-time curves were submitted to compartmental pharmacokinetic analysis. The curves of Gd-DTPA and Gd-BOPTA were fitted successfully with a one- respectively two-compartment model, where the peripheral compartment is meant to represent the hepatocytes in which Gd-BOPTA distributed. In a second step, the effect of the concentration of Gd-BOPTA on its uptake into hepatocytes was studied to elucidate the transport mechanism involved. The results showed that Gd-BOPTA seemed to be taken up into hepatocytes by a saturable mechanism indicating that the transport of Gd-BOPTA was mediated by a specific transporter rather than by free diffusion.

Additional experiments should be carried out to confirm this hypothesis, such as the inhibition of the transport of Gd-BOPTA with specific substances. Another interesting approach would be to replace the hepatocytes in the HFB by oocytes transfected with cRNA encoding for different transporters to study the selectivity of Gd-BOPTA transport into the cells. Our newly developed hepatocyte HFB could be further used to study other hepatobiliary contrast agents to get a better understanding of their uptake and excretion mechanisms in hepatocytes. Healthy rat hepatocytes in the HFB could be replaced by healthy human hepatocytes or by diseased rat or human hepatocytes to see how or if the transport mechanisms of hepatobiliary contrast agents are disturbed. Finally, the pharmacokinetic compartment model developed should be applied to other MRI data. As it would be more appropriate to process concentration-time curves rather than SI-time curves, further studies are needed convert SI into contrast agent concentration.

In summary, we developed a useful tool to study the hepatic transport of hepatobiliary contrast agents directly by MRI. The challenge for future work is now to extend its use to allow the extrapolation of the findings to humans and to use the assessment of the transport of MRI hepatobiliary contrast agents as a means to diagnose liver diseases.

Development of a hepatocyte hollow fiber bioreactor for the study of contrast agents by magnetic resonance imaging

Magnetic resonance imaging (MRI) is a powerful tool of medical diagnosis notably because of the remarkably good resolution of its images. Contrast agents, in particular gadolinium (Gd^{3+}) chelates, allow to further improve the detection of diseases. One can distinguish between extracellular gadolinium chelates such as Gd-DTPA, and hepatobiliary gadolinium chelates such as Gd-BOPTA. The latter are able to enter hepatocytes from which they are partially excreted into the bile. Due to these properties, hepatobiliary contrast agents are particularly interesting for the MRI of the liver. It is conceivable that a diseased liver has a modified transport of hepatobiliary contrast agents in hepatocytes which would be reflected in a change of the signal intensity. However, these mechanisms and their possible modifications due to hepatic diseases are not completely understood.

The aim of this thesis was to develop an *in vitro* model to study the transport of hepatobiliary contrast agents in hepatocytes directly by MRI. A dynamic system including a hollow fiber bioreactor (HFB) containing a high density of freshly isolated rat hepatocytes was built in order to be compatible with the magnetic field, which implied in particular the absence of metal in the elements placed in the magnet. Despite this technical difficulty, a sensible choice of the HFB, the constituents of the perfusion system and the experimental conditions permitted to maintain good cellular viability and to distinguish in a reproducible manner between Gd-BOPTA and Gd-DTPA. The data obtained, expressed as signal intensity (SI) versus time, were analyzed with a compartmental pharmacokinetic model. The SI-time curves of Gd-DTPA and Gd-BOPTA were fitted successfully with a one- respectively two-compartment model, where the peripheral compartment is meant to represent the hepatocytes into which Gd-BOPTA distributed. The results obtained showed that Gd-BOPTA seemed to be taken up into hepatocytes by a saturable mechanism, indicating the presence of a specific transporter.

The HFB developed here offers an interesting tool to study the transport mechanisms of hepatobiliary contrast agents. A better understanding of these mechanisms could allow to use the kinetics of hepatobiliary contrast agents as an efficient diagnostic method of hepatic diseases.

Développement d'un bioréacteur à réseaux capillaires contenant des hépatocytes pour l'étude d'agents de contraste par imagerie par résonance magnétique

L'imagerie par résonance magnétique (IRM) est un outil diagnostique très puissant notamment grâce à la remarquable précision de ses images. L'IRM peut faire appel à des agents de contraste, les plus utilisés étant ceux à base de gadolinium (Gd^{3+}). On distingue les agents extracellulaires comme le Gd-DTPA, des agents hépatobiliaires comme le Gd-BOPTA qui sont capables d'entrer spécifiquement dans les hépatocytes et qui sont ensuite partiellement excrétés dans la bile. Cette propriété les rend particulièrement intéressants pour l'imagerie du foie, où une atteinte peut se manifester par un changement dans l'intensité du signal IRM dû à une modification du transport du produit de contraste dans les hépatocytes. Or ces mécanismes de transport et leurs modifications possibles en cas de maladie ne sont toujours pas entièrement élucidés à l'heure actuelle.

Le but de cette thèse était donc de mettre au point un modèle *in vitro* permettant d'étudier directement par IRM le transport des agents de contraste hépatobiliaires dans les hépatocytes. Un système dynamique comprenant un bioréacteur à réseaux capillaires contenant une haute densité d'hépatocytes de rat fraîchement isolés a été construit de façon à être compatible avec le champ magnétique, ce qui impliquait surtout l'absence de métal dans les éléments se trouvant dans l'aimant. Malgré cette difficulté technique, le choix judicieux du bioréacteur, des constituants du système de perfusion et des conditions expérimentales a permis de maintenir une bonne viabilité cellulaire et de pouvoir distinguer de façon reproductible les comportements du Gd-BOPTA et du Gd-DTPA. Les données obtenues, exprimées en intensité de signal en fonction du temps, ont été analysées par un modèle pharmacocinétique compartimental. Les données du Gd-DTPA et du Gd-BOPTA ont pu être modélisées avec succès par un modèle mono- respectivement bi-compartimental, où le compartiment périphérique supplémentaire dans le deuxième cas est sensé représenter les hépatocytes dans

lesquels le Gd-BOPTA est capable de pénétrer. Les résultats ont montré que le Gd-BOPTA semble entrer dans les hépatocytes selon un mécanisme saturable indiquant la présence d'un transporteur spécifique.

Le bioréacteur développé représente un outil intéressant pour l'étude des mécanismes de transport cellulaire des agents de contraste hépatobiliaires. Une meilleure connaissance de ces mécanismes pourrait permettre d'utiliser par la suite la cinétique des agents de contraste hépatobiliaires comme méthode de diagnostic de maladies hépatiques.

Résumé large public

Les produits de contraste pour l'imagerie par résonance magnétique (IRM) sont utilisés pour améliorer la différentiation entre les divers tissus imagés. Les agents de contraste les plus utilisés sont ceux à base de gadolinium (Gd^{3+}). On distingue les agents extracellulaires, comme le Gd-DTPA, des agents hépatobiliaires, comme le Gd-BOPTA, qui sont capables d'entrer spécifiquement dans les cellules hépatiques (hépatocytes) et qui sont ensuite partiellement excrétés dans la bile. Les mécanismes de transport des agents hépatobiliaires dans les hépatocytes ainsi que la façon dont ces mécanismes de transport sont modifiés en cas de maladie hépatique ne sont pas entièrement élucidés à l'heure actuelle.

Le but de cette thèse était donc de mettre au point une méthode de culture cellulaire permettant d'étudier le transport des agents de contraste hépatobiliaires dans les hépatocytes. Nous avons construit un bioréacteur contenant des hépatocytes de rat fraîchement isolés de manière à ce qu'il soit compatible avec le champ magnétique, ceci afin de pouvoir faire les mesures directement avec l'appareil d'IRM utilisé pour les patients (voir la figure ci-dessous). Les résultats obtenus ont montré que le Gd-BOPTA semble entrer dans les hépatocytes selon un mécanisme saturable indiquant la présence d'un transporteur spécifique.

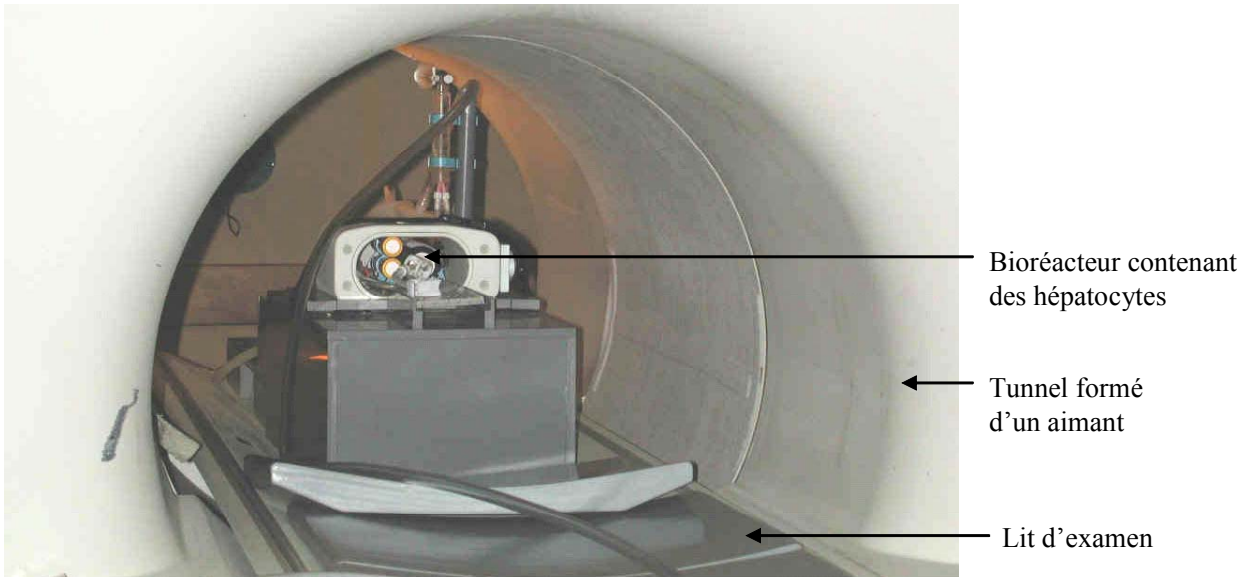

Dans le futur, l'utilisation du bioréacteur pourrait être étendue à l'étude d'autres agents de contraste pour IRM. On pourrait également introduire d'autres cellules dans le bioréacteur, comme par exemple des hépatocytes de rat malades, ou des hépatocytes humains, sains ou non. Ceci permettrait de disposer de suffisamment de données pour envisager une extrapolation des résultats à l'homme afin d'utiliser le transport des agents de contraste hépatobiliaires comme outil de diagnostic de maladies hépatiques.

Abbreviations

The following abbreviations are currently used throughout the document:

- A -

AEBSF:	4-(2-aminoethyl) benzenesulfonyl fluoride hydrochloride
ALF:	acute liver failure
ALT:	alanine aminotransferase
AST:	aspartate aminotransferase

- B -

BAL:	bioartificial liver
BBB:	blood-brain barrier
BSA:	bovine serum albumin
BSP:	bromosulfophtalein
BSS:	balanced salt solution

- C -

CT:	computed tomography

- D -

DCE-MRI:	dynamic contrast enhanced T_1-weighted MRI
DMSO:	dimethylsulfoxide

- E -

E-64:	N-(trans-epoxysuccinyl)-L-leucine 4-guanidinobutylamide
7-EC:	7-ethoxycoumarin
ECS:	extracapillary space of the hollow fiber bioreactor
EDTA:	ethylenedinitrilo tetraacetic acid
EGTA:	ethyleneglycol-O,O'-bis(2-aminoethyl)-N,N,N',N'-tetraacetic acid
EHBR:	Eisai hyperbilirubinaemic rat

- F -

FA:	flip angle
FCS:	fetal calf serum
FOV:	field of view
FSA:	fiber surface area of the HFB

- G -

GGT:	γ-glutamyl transpeptidase
GLDH:	glutamate dehydrogenase
GPT:	glutamic pyruvic transaminase
GRE:	gradient echo
GSH:	glutahthione

- H -

HF:	hollow fiber
HFB:	hollow fiber bioreactor

7-HC: 7-hydroxycoumarin

- I -

ICP-AES: inductively coupled plasma atomic emission spectrometry
ICS: intracapillary space of the hollow fiber bioreactor
IR: inversion recovery

- L -

LDH: lactate dehydrogenase

- M -

MRI: magnetic resonance imaging
MRP: multidrug resistance-associated protein

- N -

NMR: nuclear magnetic resonance

- O -

OATP: organic anion transporting polypeptide

- P -

PEG: polyethyleneglycol
PET: positron emission tomography

- R -

RES: reticuloendothelial system
RF: radiofrequency
ROI: region of interest

- S -

SE: spin echo
SI: signal intensity
SR: total or partial saturation recovery

- T -

T_1: longitudinal relaxation time
T_2: transversal relaxation time
TE: echo delay time
TI: inversion time
TMZ: trimetazidine
TR: repetition time

- U -

US: ultrasound
UW solution: University of Wisconsin solution